Physics Lib.

AUG 19 1935

DO NOT TAKE FROM LIBRARY

copy 2

THE PHYSICAL REVIEW

VOLUME 48 *Second Series* NUMBER 4

AUGUST 15, 1935

Published for the

AMERICAN PHYSICAL SOCIETY

by the

AMERICAN INSTITUTE OF PHYSICS
Incorporated

LANCASTER, PA., AND NEW YORK, N. Y.

THE AMERICAN PHYSICAL SOCIETY

OFFICERS OF THE SOCIETY

R. W. WOOD, *President*
The Johns Hopkins University
Baltimore, Maryland

F. K. RICHTMYER, *Vice President*
Cornell University
Ithaca, New York

W. L. SEVERINGHAUS, *Secretary*
Columbia University
New York, New York

G. B. PEGRAM, *Treasurer*
Columbia University
New York, New York

JOHN T. TATE, *Editor*
University of Minnesota
Minneapolis, Minnesota

L. B. LOEB, *Local Secretary for the Pacific Coast*
University of California
Berkeley, California

THE PHYSICAL REVIEW

BOARD OF EDITORS

JOHN T. TATE, *Editor*

J. W. BUCHTA, *Assistant Editor*

Associate Editors

K. K. DARROW
J. C. HUBBARD
A. E. RUARK
A. ELLETT
L. A. TURNER
G. E. UHLENBECK
W. V. HOUSTON
R. S. MULLIKEN
I. I. RABI

THE PHYSICAL REVIEW, which was established in 1893, is a journal of experimental and theoretical physics. It is published for the American Physical Society by the American Institute of Physics Incorporated. There are two volumes annually with twelve issues in each volume.

Manuscripts for publication should be submitted to John T. Tate, University of Minnesota, Minneapolis, Minnesota.

Proof and all correspondence concerning papers in the process of publication, should be addressed to the Editorial Secretary, American Institute of Physics, 11 East 38th Street, New York, New York.

Subscription price: United States and Possessions and Canada, $15.00; Foreign, $16.50. Subscriptions and orders for back numbers should be addressed to Prince and Lemon Streets, Lancaster, Pennsylvania, or to the American Institute of Physics, 11 East 38th Street, New York, New York.

Advertising is not accepted for the *Physical Review* but attention is called to the *Review of Scientific Instruments with Physics News and Views*, a companion publication of the Institute, and a medium through which the field of physics can be reached most effectively. Rates and other information will be furnished on request to the Editorial Secretary.

Changes of address and complaints of failure to receive the *Physical Review*, in the case of members of the American Physical Society, should be addressed to the Treasurer; in the case of other subscribers, to the Editorial Secretary. New copies can be sent free in response to complaints of non-delivery only if notice of non-delivery is received within three months of date of issue.

The Physical Review is published semi-monthly at Prince and Lemon Streets, Lancaster, Pennsylvania.

Entered at the Post Office at Lancaster, Pennsylvania, as second class matter.

Acceptance for mailing at special rate of postage provided for in section 1103, Act of October 3, 1917, authorized September 6, 1926.

THE
PHYSICAL REVIEW
A Journal of Experimental and Theoretical Physics
VOL. 48. NO. 4 AUGUST 15, 1935 SECOND SERIES

Progress of the Directional Survey of Cosmic-Ray Intensities and Its Application to the Analysis of the Primary Cosmic Radiation

THOMAS H. JOHNSON, *Bartol Research Foundation of the Franklin Institute*
(Received June 17, 1935)

Since the 1934 report, asymmetries have been studied by the coincidence counter method at several stations in Mexico and in Colorado so that the completed survey now includes data at high (4300 m), low (sea level) and intermediate elevations at the geomagnetic equator, in the intermediate latitudes λ29°, and in the high latitude λ50° besides additional data at an intermediate elevation in latitude λ36°. For the measurements an automatic multi-directional intensity comparator has been developed. Using the results of the theoretical investigations of Lemaitre, Vallarta and Bouckaert the measured asymmetries have been reduced to relative specific intensities (per unit range of x) of the unbalanced positive component and it is found that this varies with the atmospheric path length $h \sec z$, according to an exponential law. The observed intensities, taking account of absorption, have been used in conjunction with the results of LVB to compute the longitude and latitude effects to be expected from the positives alone. The latitude effect thus computed is greater than that observed between Peru and Panama but the computed longitude effect is, in general, too small. It is possible that the anomaly is to be explained by the departures of the horizontal intensity from the values which would pertain if the earth's field were accurately that of a simple doublet. The work has been done under grants from the Carnegie Institution of Washington, administered by its Cosmic-Ray Committee.

INTRODUCTION

THE survey, undertaken in 1933 for the study of directional distributions of the cosmic radiation in various latitudes and elevations, resulted[1] in reasonably accurate values of the east-west asymmetries for the elevations 3340 m and 4300 m in Peru on the geomagnetic equator, at sea level in Panama, and at sea level in the United States. Less accurate results were also obtained at sea level in Peru, at three elevations in Mexico ranging from sea level to 3300 m, and at 3300 m in Colorado. Asymmetries in these and in other locations have also been measured by other investigators, confirming these results and adding to the comprehensiveness of the general survey.

Because of the importance of the asymmetry measurements for the analysis of the primary cosmic radiation, further studies were undertaken in 1934 with the view to improving the accuracy and to extending the range of elevations of the measurements in and between the latitudes λ29° and λ50° where most of the change of intensity takes place. For the earth-magnetic analysis of the cosmic radiation, measurements of the intensities and east-west asymmetries as functions of the latitude determine the distribution with respect to the magnetic rigidity, $H\rho$, of both positive and negative components but the earth-magnetic mass spectrograph has not been provided with the customary electric field by which it would have been possible to separate the velocity and e/m factors in the expression $H\rho = mv/e$. For the final identification of the particles, therefore, it is necessary to rely upon absorption measure-

[1] T. H. Johnson, Phys. Rev. **45**, 569 (1934).

ments. In order to provide data for this purpose, as high an accuracy as possible was desired in regard to the variation of the asymmetry with elevation and zenith angle.

During the survey several other related investigations were made, some of which have already been reported. For further estimates of the role of the soft secondary radiations in relation to the asymmetry, east and west intensities were compared at the high elevation station in Mexico with an absorbing block of lead between the counters. Further studies were also made of the north-south asymmetries[2] at two stations in Mexico. Shower intensities were measured, in relation to the vertical cosmic-ray intensity as a standard, at all of the 1934 stations. At the high elevation station in Mexico the east-west asymmetry of the shower-producing radiation was studied.[3]

Apparatus for Determination of the Directional Distribution of the Rays which Produce Coincidence Discharges of Collinear Counters

Considerable experience with coincidence counter measurements has shown that cosmic-ray intensities from two directions can be compared with an accuracy depending only upon the statistical fluctuations of the total number of rays counted, provided the apparatus is shifted back and forth between the two directions at frequent intervals. In the present apparatus this shifting of direction, as well as the taking of readings at the end of each interval, were wholly automatic. In order to count a large number of rays in limited time, seven independent trains of counters were mounted on a single cylindrical chassis, Figs. 1 and 2. Around its periphery 42 Geiger-Müller tube counters, with cylinders 1.6 cm in diameter and 15 cm long, were densely spaced and were parallel connected, as indicated in a typical case by the brackets of Fig. 1, in fourteen groups of three each. These constituted the outside members of the seven triple-coincidence trains. The central member of each train was a common, axial group of five counters. Each group was connected to the grid of a type 77 vacuum tube and the amplified pulses from diametrically opposite groups were combined with those from the central group for the selection and recording of the coincidences. The circuit for this purpose embodied the principles outlined by Fussell and Johnson[4] and is shown diagrammatically in Fig. 3. The distance between the outside groups of each train was 28 cm and the solid angle for which half or more of the

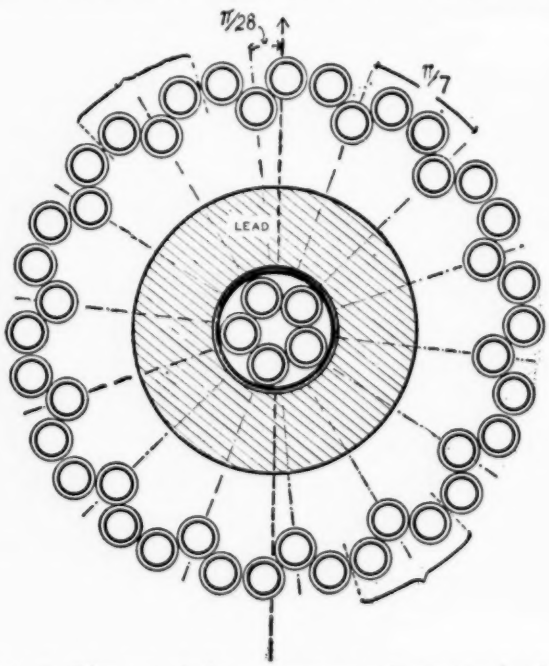

Fig. 1. Diagram of the arrangement of counters in the multidirectional cosmic-ray intensity comparator.

Fig. 2. The multidirectional cosmic-ray intensity comparator and its recording equipment.

[2] T. H. Johnson, Phys. Rev. **47**, 91 (1935).
[3] T. H. Johnson, Phys. Rev. **47**, 318 (1935).
[4] L. Fussel, Jr. and T. H. Johnson, J. Frank. Inst. **217**, 517 (1934).

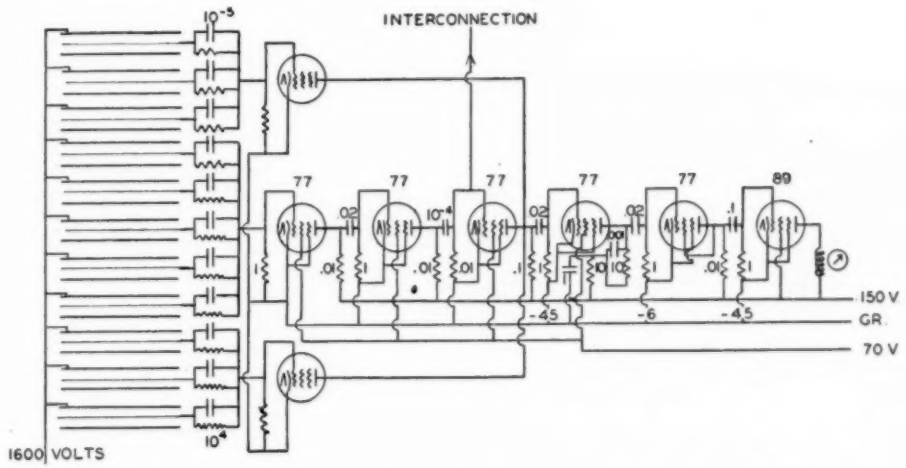

FIG. 3. The circuit for selecting and recording coincidences. Resistances in megohms, capacities in microfarads, and potentials in volts.

counter areas were effective extended to 4.5° in zenith angle and to 14° measured in the plane of the counter wires on both sides of the midline of the train. The central counters were inside a steel tube of 3.2 mm wall thickness and, when additional absorbing material was desired, lead rings were slipped over this as indicated in Fig. 1. Thicknesses up to 10 cm could thus be introduced into the paths of the coincidence producing rays. The elements of each of the coincidence-selecting circuits were mounted on the chassis but the out-put pulses from the last stage amplifiers were led out on a cable running through the axis of the chassis to an auxiliary box containing the seven recording dials and a photographic device. The dials, a watch for time records, and a series of lamp bulbs, certain of which flashed at the instant of photographing to indicate the position of the chassis, were all mounted together on a panel and this was photographed at regular intervals with a Simplex Pockette 16-mm movie camera. The exposures were timed by weight-driven clock works and during the field work they were made at fifteen minute intervals. Simultaneously with the operation of the camera, small motors geared to the chassis were set in operation and these continued to run until a determined shift in position had been effected. On the even intervals, shifts in azimuth were made by rotation about a vertical axis and on the odd intervals the chassis was rotated in zenith angle about a horizontal axis. The two fixed azimuth positions were adjustable by a pair of stops clamped to a circle but the successive zenith angle positions were spaced at fixed angles, $\pi/7$ apart, and at these positions the midlines of the counter trains pointed at angles 6.4°, 32.1°, 57.9° and 83.5° from the zenith on one side and at 19.3°, 45° and 70.7° on the other side. A shift in zenith angle carried each counter train from one of these positions to the next in the order of rotation. The sequence of readings from a particular train thus contained pairs of successive data at each zenith angle with one datum for each of two azimuths. Each pair of data resulted in a value of the azimuthal asymmetry, α, defined below, which was independent of long time variations of counter sensitivity or of relative sensitivities of different trains.

In the determination of asymmetries by this method it is essential that the axis of azimuthal rotation be exactly vertical. If the axis is out of vertical by an angle δ an apparent asymmetry at zenith angle z can be introduced of maximum amount $\Delta j/j = 4\delta \tan z$. To guard against an error of this nature the carriage supporting the chassis was mounted on leveling screws at the top of an iron tripod and the legs of the tripod were usually set in concrete on a stone pier or other firm foundation. An 8-inch level, reading to one minute of arc, was fixed to the carriage and constant checking during each run showed variations due to varying tensions on the cable

TABLE I. *East-west asymmetry measurements of the 1933, 1934 surveys.*

ZENITH ANGLE z	ASYMMETRY A	NO. OF DATA N	TOTAL COUNTS WEST C_w	TOTAL COUNTS EAST C_e	PROBABLE ERROR OF A R
Cerro de Pasco, Peru; λ0°; mean barometer, b, 46 cm.; atmospheric depth, h, 6.24 m of water; elevation 4300 m					
15°	0.084	183	59,295	55,049	0.0042
30°	.125	160	39,601	35,418	.0054
45°	.139	72	11,024	9,764	.0085
60°	.174	98	6,760	6,028	.015
*45°	.188	46	4,260	3,595	.019
* 3.8 cm lead between counters					
Huancayo, Peru; λ0°; b, 51.8 cm; h, 7.03 m; elev. 3340 m					
15°	.063	118	25,866	24,332	.0060
30°	.117	143	24,874	21,963	.0065
45°	.140	218	24,819	21,284	.0061
60°	.156	151	8,039	7,056	.011
75°	.061	87	1,666	1,560	.023
Lima, Peru; λ0°; b, 76 cm; h, 10.3 m; sea level					
15°	.064	94	10,120	9,930	.0093
30°	.092	144	12,358	10,865	.0082
45°	.145	63	3,541	2,937	.016
Barro Colorado Island, Panama Canal Zone; λ20°; b, 76 cm; h, 10.3 m					
15°	.036	157	17,669	17,386	.0077
30°	.047	328	30,758	29,513	.0056
45°	.066	350	23,146	21,190	.0072
60°	.035	195	6,415	6,229	.012
*75°	−.011	155	2,077	2,322	.019
* western horizon possibly obscured by forest					
El Pico Nevado de Toluca; λ29°; b, 64.2 cm; h, 6.25 m; elev. 4300 m					
6.4°	.0304	245	30,175	29,343	.0054
19.3°	.0654	243	23,191	21,814	.0055
32.1°	.1012	242	20,260	18,354	.0074
45.0°	.1162	248	14,911	13,282	.0085
57.8°	.1288	239	7,419	6,564	.0110
70.7°	.051	243	3,834	3,646	.015
*83.5°	−.062	245	1,628	1,736	.025
* western horizon obscured up to 12° by mountain ridge					
El Pico Nevado de Toluca; 8.6 cm of lead between counters					
6.4°	.0092	179	12,122	11,942	.0092
19.3°	.0496	173	11,105	10,564	.0087
32.1°	.084	176	9,016	8,232	.0097
45°	.088	176	7,040	6,445	.0112
57.8°	.081	169	3,684	3,392	.0144
70.7	.030	177	2,322	2,282	.021
*83.5	.116	176	1,368	1,206	.029
* See above.					
Vera Cruz, Mexico; λ28°; b, 76 cm; h, 10.3 m; sea level; 1934					
6.4°	.0149	271	10,331	10,365	.0097
19.3°	.021	269	9,549	9,385	.010
32.1°	.050	270	7,608	7,184	.011
45	.023	266	6,163	6,131	.023
57.8°	.062	237	3,859	3,520	.0123
70.7°	.028	264	2,633	2,611	.021
83.5°	.111	258	1,542	1,475	.032
San Rafael, Mexico; λ29°; b, 50 cm; h, 6.8 m; elev. 3300 m; 1933					
20°	.062	73	14,976	16,181	.0095
30°	.078	54	10,522	11,058	.0099
50°	.081	41	4,763	4,774	.018
Mexico City, Mexico; λ29°; b, 55 cm; h, 7.5 m; 2200 m elev.; 1933					
30°	.048	59	15,702	14,098	.0084
40°	.078	65	21,424	13,621	.008
50°	.086	38	7,080	6,221	.013
*50°	.12	19	2,554	2,505	.019
65°	.037	23	1,533	1,747	.037
* 3.8 cm lead between counters					
Parral, Chihuahua, Mexico; λ36°; b, 62.4 cm; h, 8.45; elev. 1730 m; 1934					
6.4°	.015	376	19,367	19,217	.0073
19.3°	.027	374	18,439	17,973	.0072
32.1°	.053	370	13,862	13,148	.0085
45°	.031	370	10,504	10,218	.0095
57.8°	.027	370	6,072	5,975	.014
70.7°	.006	373	4,089	4,013	.016
83.5°	.011	367	2,322	2,297	.024
*60.0°	.039	139	14,177	13,616	.008
* Large counters used.					
Mt. Evans, Colorado; λ49°; b, 46.2 cm; h, 6.25 m; elevation 4300 m; 1934					
6.4°	−.003	206	62,999	62,761	.0052
19.3°	.016	209	59,563	59,068	.0054
32.1	.020	203	44,599	43,831	.0067
45°	.016	209	38,865	38,387	.0073
57.8°	.005	204	24,511	23,980	.0097
70.7°	.028	208	21,180	20,946	.011
*83.5°	.022	207	17,360	16,788	.014
* western horizon obscured by mountain ridge up to 8°					
Echo Lake, Colorado; λ49°; b, 52.4 cm; h, 7.10 m; elev. 3180 m; 1934					
6.4°	.021	240	36,520	35,977	.0054
19.3°	−.007	240	31,924	32,759	.0061
32.1	.023	237	25,493	25,105	.0073
45°	.019	232	18,293	17,870	.0076
57.8°	.035	229	11,323	11,069	.012
70.7°	.044	237	7,341	6,962	.016
83.5°	.015	237	4,897	4,759	.022
Swarthmore, Pennsylvania; λ51° 27′; b, 76 cm; h, 10.3 m; elev. 100 m 1934					
6.4°	.021	563	37,343	36,620	.0052
19.3°	.004	563	35,176	34,927	.0050
32.1°	.005	562	27,331	27,156	.0057
45°	−.005	563	19,660	19,814	.0082
57.8°	.022	557	12,307	12,054	.0089
70.7°	.059	558	7,585	7,354	.0129
83.5°	.049	453	3,670	3,517	.016

of not more than five minutes. The average error in leveling could not have exceeded two minutes and the false asymmetry from this source could not have been over a tenth of a percent.

Sites for the measurements were always selected for open horizons and the apparatus was covered only by a canvas tent for weather protection. Azimuthal orientations were made with respect to the local magnetic fields as determined by compass readings at several nearby points.

The apparatus operated on 110 volts 60 cycles, supplied either from commercial lines or from a Cushman gasoline-electric generator of 500 watts capacity. For the shower studies, supplementary equipment consisting of three parallel groups of large counters was also used.

In the period from August first to November tenth, 1934, the instruments were operated at the following stations in the order given, Echo Lake (Colorado), Mt. Evans (Colorado), Copilco (Mexico), El Pico Nevado de Toluca (Mexico), Vera Cruz (Mexico), Parral (Mexico). Following these an extensive run was made on the roof of the Bartol Laboratory in Swarthmore, Pa. These stations as well as those of the 1933 survey are indicated on the map of Fig. 4.

Results of the East-West Asymmetry Measurements

The results of the east-west asymmetry measurements of the 1933 and 1934 surveys are contained in Table I. In the previous reports the 1933 measurements had been computed in terms of the ratio of the east and west counts, j_w/j_e. The statistical fluctuations of this quantity are not symmetric with respect to the value unity when $\bar{j}_w=\bar{j}_e$ and in the case of low counting rates and short time intervals, an appreciable false asymmetry favoring the west can be introduced in the computation. For this reason the 1933 data have been recomputed and the 1934 data computed in terms of the quantity $\alpha=2(j_w-j_e)/(j_w+j_e)$, (1), for which the fluctuations are symmetric with respect to the value zero when $\bar{j}_w=\bar{j}_e$. Table I therefore supersedes Table I, reference (1). The asymmetry, A, listed in the second column is the average of the individual determinations of α. $A=\Sigma\alpha/N$, (2), where N is the total number of pairs of data, given in the third column. The total number of rays counted in the east and west directions are also listed under C_e and C_w. The probable error of A has been computed from the dispersion of the α's and is listed under R. Instead of the usual method of averaging the squares of the deviations, R has been computed by a shorter method avoiding the extra summations. The short method agrees with the usual method if the dispersion follows a Gaussian distribution and an approximate check on this condition was made in each case by plotting the frequency curves for α. If S^+ and S^- represent the sums of the positive and negative values of α, respectively, then $A=(S^+-S^-)/N$ and, in the case of the Gaussian distribution, is easy to show that the standard deviation of α is

$$\sigma=(\pi/2)^{\frac{1}{2}}[(S^++S^-)/N-A\phi(A/\sigma)]\times\exp(A^2/2\sigma^2), \quad (3)$$

where $\phi(x)=(2/\pi^{\frac{1}{2}})\int_0^x\exp(-x^2)dx$. Usually $A\ll\sigma$ and it was easy to solve (3) for σ by successive approximations. The standard deviation of the average asymmetry A is $\Sigma=\sigma/(N)^{\frac{1}{2}}$ and the probable error of A is $R=0.6745\Sigma$.

The only systematic error which merits discussion is that due to accidental counts. Since each counter train was periodically pointed at the low angle of 83.5°, the counting rate in that direction gave frequent check on the possible number of counts due to this cause. Except for some of the readings on Mt. Evans, where it was discovered that the selecting bias had been adjusted too closely, the horizontal rate was less than 10 percent of the vertical rate and since most of these counts must have been due to cosmic rays, no correction for accidentals was needed. At higher zenith angles where natural double coincidences are more frequent, the accidental triple coincidences would also be more frequent, but these would be proportional to the double coincidence rates and hence subject to the directional asymmetries. Correction for this effect would be of a second order and would involve only the lower angular resolution of the double coincidences. In the case of the Mt. Evans data accidental counts uninfluenced by the direction of the instrument were not more than twenty percent of the vertical counting rate and this would call for a correction to be added to the tabulated values of A, not to exceed 40 percent at $z=45°$.

The results of the two surveys as well as those of all other observers who have reported quanti-

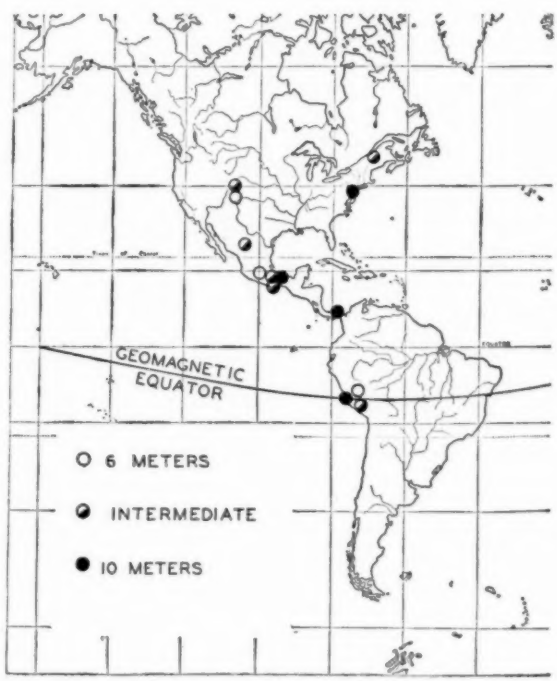

Fig. 4. Map indicating the scope of the directional survey.

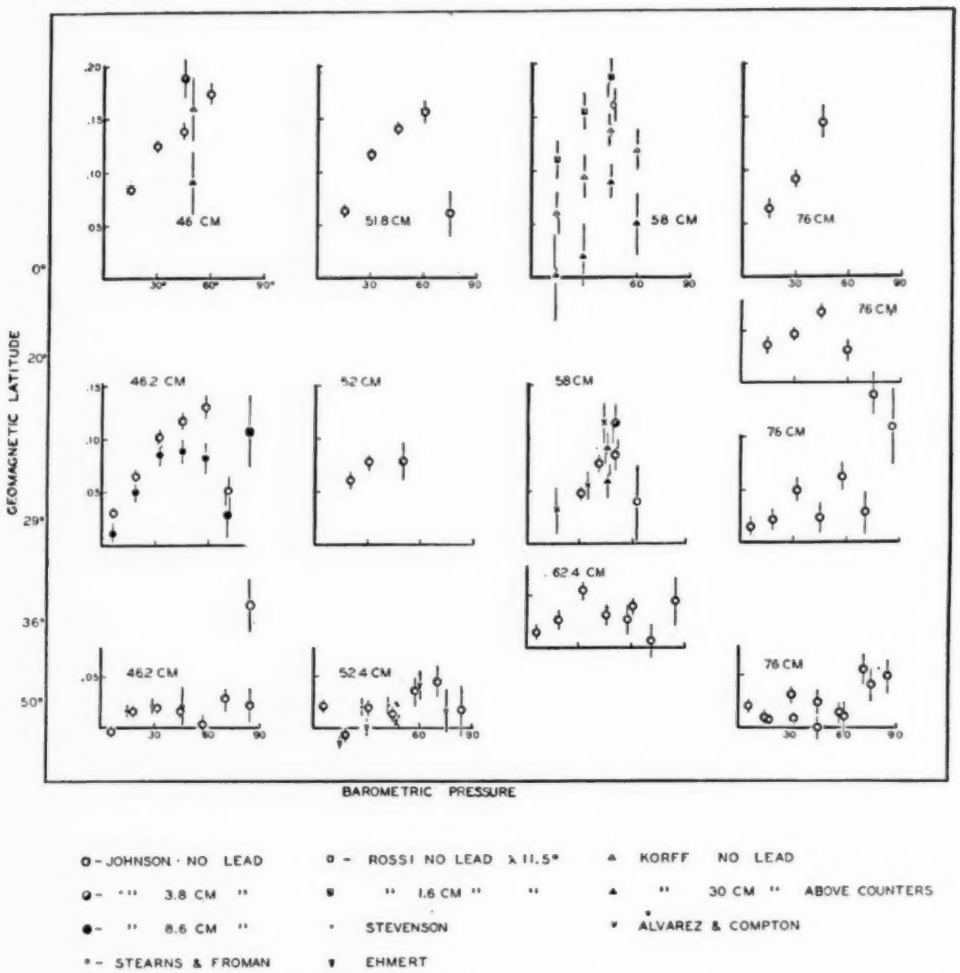

FIG. 5. Compilation of east-west asymmetry measurements. For each station the asymmetry, A, is plotted against zenith angle.

tative measurements which have come to the writer's attention are plotted in Fig. 5. The probable errors are indicated by the vertical lines. Data obtained with lead absorbers are represented by shaded points as noted. Rossi and the writer have placed the lead between the counters whereas Korff placed his lead above the train.

The new data have not changed the salient features of the asymmetry effect but serve to bring out more strongly than before the increase of the asymmetry at the equator over that of higher latitudes. The new results for high and low elevations in Mexico confirm very definitely the effect reported in reference (1) that the asymmetry increases with elevation. In the latitude λ50° the Mt. Evans asymmetries agree with those found at the same location by Stearns and Froman[5] whereas the new Swarthmore asymmetries are in general lower than those found previously by Johnson and Stevenson.[6] It is also noted that for many of the stations the low angles of 70.7° and 83.5° seem to show consistently higher asymmetries than would have been expected from simple extrapolation of the higher angle values. This effect does not appear in the Nevado de Toluca and Mt. Evans results at the 83.5° angle, possibly because of shielding on the west by mountain ridges but of the data for 70.7° and 83.5° at Vera Cruz, Parral, Echo

[5] J. C. Stearns and D. K. Froman, Phys. Rev. **46**, 535 (1934).
[6] T. H. Johnson and E. C. Stevenson, Phys. Rev. **44**, 125 (1933).

Lake and Swarthmore and for 70.7° on Mt. Evans and Nevado de Toluca, eight show asymmetries greater than three percent compared with three showing asymmetries less than three percent. Since the high angle data seem to extrapolate to a zero effect at the horizon, there thus seems to be indication for abnormal asymmetries at low angles. These could possibly be explained by the deflection of primary positive rays after they have been slowed down by atmospheric energy losses.

It is again noted that no significant part of the observed asymmetry can be accounted for by the deflection of secondaries generated in the atmosphere. This is clearly brought out by the theory of the secondary effect given by Bowen[7] and was simply demonstrated from the experimental point of view by the reasoning given in reference (1). It may be, and probably is, true that most of the rays actually counted, whether they belong to the field sensitive component or not, are secondaries, but these, in general, should have very nearly the same direction as the primaries which produced them. Conservation of direction during the production process is insured, in the case of energies large compared with the rest mass energy, by the conservation of energy and momentum, and the magnetic deflection by the earth's field, before the ray has lost too much energy to allow it to pass through the instrument, cannot exceed a few degrees at the elevations included in the survey. Since the evidence of Anderson[8] and others indicates equal numbers of positive and negative secondaries such magnetic deflections, even if of significant magnitude, could produce no asymmetries.

The observations made with lead absorbing screens are of interest in this connection. Those of the writer in Peru[1] and of Rossi[9] in Asmara showed an increase of asymmetry due to the effect of the lead. Later measurements by Korff[10] with lead placed above, instead of between, the counters and with thicknesses up to 30 cm, showed a reverse effect. The present measurements on Nevado de Toluca with 8.6 cm of lead between the counters also show a reduction in the asymmetry, agreeing with Korff. The results of all observers made at a zenith angle of 45° are compiled in Fig. 6. Although the three points showing an increase due to lead are accompanied by rather high probable errors, the combined evidence seems sufficient to show that the effect of lead placed between counters is of the character indicated by the curve. The negative result of Korff for two centimeters of lead can possibly be explained by the increased count due to poorly directed showers generated in the lead above. Any undirected background of this character would tend to reduce the percentage asymmetry. For lead between counters, the first thicknesses reduce the diffuse background of softest radiations but further thicknesses cut into the asymmetric component more than into the average radiation. This accords with the view that the background radiation consists of higher energy corpuscles. Present indications are that a slight correction should be added to the measured asymmetries to take account of the diffusion of softest secondaries, though it is felt that the effects should be studied further before such corrections can be applied with certainty.

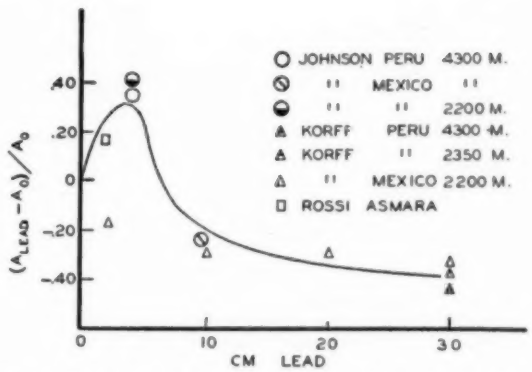

FIG. 6. Effect of lead absorbing screens of varying thickness on the east-west asymmetry at a zenith angle of 45°.

SIGNIFICANCE OF EAST-WEST ASYMMETRIES

The theory of Størmer,[11] as was first clearly stated by Rossi,[12] gives a simple interpretation

[7] I. S. Bowen, Phys. Rev. **45**, 349 (1934).
[8] C. D. Anderson and S. H. Neddermeyer Report at the Int. Cong. on Physics, London (1934).
[9] B. Rossi, Ricerca Scient. **5**, 594 (1934).
[10] S. A. Korff, Phys. Rev. **46**, 74 (1934).

[11] C. Størmer, University Observatory, Oslo, Pub. No. 10 (1934); Ergebnisse der Kosmischen Physik **1**, 1 (1931). Størmer has also made estimates of the cones for infinite orbits but for convenience his basic first approximation will be referred to as the Størmer theory.
[12] B. Rossi, Nuovo Cimento (3) **8**, 3 (1931); Rend. Lencei **13**, 47 (1931).

to the east-west asymmetry. Positive rays must have a higher rigidity if they are to reach an observer on the surface of the earth from an eastern direction than is required from the same zenith angle to the west. Rays of rigidity between the two limiting values corresponding to eastern and western directions will illuminate the western but not the eastern direction. In the case of negative rays the directions are reversed, but if there is an excess of positives, unbalanced in this sense by an equal intensity of negatives in the same range of rigidity, the western intensity will be the greater. The difference of the western and eastern intensities gives a measure of the unbalanced positives included within the range of rigidity between the minimum values for the two directions. In the Störmer theory the value of the rigidity, $H\rho$, of rays incident in latitude λ from meridan angle θ (between the vertical plane of the magnetic meridian and the direction from which the ray has come, measured positively towards the west if the rays are positive) is given by

$$H\rho = Mx^2/r^2, \tag{4}$$

where M is the magnetic moment of the earth (8.04×10^{25} e.m.u.), r is the radius of the earth (6.37×10^{8} cm) and

$$1/x = -\gamma/\cos^2\lambda + (\gamma^2/\cos^4\lambda + \sin\theta/\cos\lambda)^{\frac{1}{2}}. \tag{5}$$

Henceforth for convenience the term *rigidity** will apply to the quantity x instead of to $H\rho$.

In the east-west plane at the equator the orbits for which the constant γ has the value -1 are those along which rays of lowest rigidity reach the earth from infinity. At higher latitudes and from other directions at the equator the values of γ for infinite orbits of minimum rigidity are greater than -1 and depend upon the direction. This question has been extensively investigated by Lemaitre and Vallarta (LV)[13] and by Lemaitre, Vallarta and Bouckaert (LVB)[14] who have made precise determinations of the minimum rigidities of orbits from infinity as a function of the angle of incidence in latitudes $\lambda0°$, $\lambda10°$ and $\lambda20°$, but for the higher latitudes the theory is not yet completed. The application of Liouville's theorem, as shown by LV and by Swann[15] assures that all positions and directions will be illuminated with uniform intensity (except for the effect of atmospheric absorption) by radiation whose rigidity is above the minimum value corresponding to those positions and directions. Hence the intensity of corpuscular radiation from any direction can be expressed as the sum of two integrals, one for the positive the other for the negative radiation, the integrands of which are the specific intensities (per unit range of x) at the point and from the direction of observation, and the integrations extend to infinity from the minimum values of x corresponding to the latitude, the direction, and the sign of charge. The observed specific intensity is determined by the specific intensity in external space and by absorption along the atmospheric path $h\sec z$. The difference of eastern and western intensities at the same zenith angle is the difference of the same two integrals, or, since the lower limit of x for negative rays from the east is the same as that for positive rays at the same zenith angle from the west, these reduce to a single integral whose integrand is the specific intensity of unbalanced positives, $k(x)$, and the limits are the minimum values of x for positive rays from the two directions. Thus the asymmetry, defined as in (1) and (2) is

$$A(\lambda, h\sec z) = [1/j_\lambda(h\sec z)]\int_{x_w(\lambda,\ z)}^{x_e(\lambda,\ z)} k(x, h\sec z)dx. \tag{7}$$

Over small ranges of x corresponding to the minimum values for eastern and western directions near the zenith a uniform distribution with respect to x of the specific intensity, k_λ, may be assumed and to this approximation (7) reduces to

$$(k/j)_\lambda(h\sec z) = A/(x_e - x_w). \tag{8}$$

(k/j) may be called the specific relative intensity of unbalanced positive radiation after filtering

* x is the quantity sometimes loosely referred to as the energy. The energy in electron volts is given by

$$v = (300\, m_0c^2/e)[(Z^2e^2M^2x^4/m_0^2c^4r^4+1)^{\frac{1}{2}}-1], \tag{6}$$

where m_0 and Ze are rest mass and charge of the ray and c is the velocity of light.

[13] G. Lemaitre and M. S. Vallarta, Phys. Rev. **43**, 87 (1933).

[14] G. Lemaitre, M. S. Vallarta and L. Bouckaert, Phys. Rev. **47**, 434 (1935).

[15] W. F. G. Swann, Phys. Rev. **44**, 224 (1933).

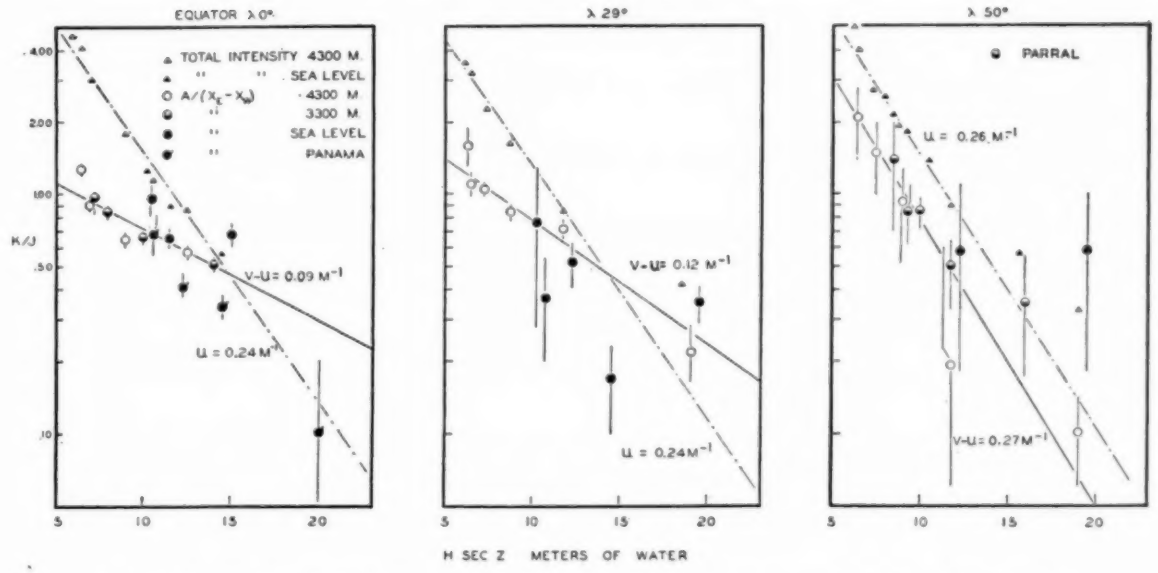

FIG. 7. The specific relative intensity of unbalanced positive radiation, and total intensity plotted against the atmospheric path length, h sec z.

through atmospheric path length h sec z. Values of $x_e - x_w$ are given by the theories and the values chosen are listed in the Table II. In this way each asymmetry value has been reduced to specific relative intensity of unbalanced positives and the results are plotted on logarithmic scale against h sec z in the three diagrams of Fig. 7 corresponding to the three latitudes λ0°, λ29° and λ50°. In each case the values deduced from measurements at 4300 meters are represented by the open circles, those from sea level measurements by solid circles and those from intermediate elevations by partially shaded circles. Since the energy values for λ20° are not appreciably different from those for the equator, the Panama results have been included in the plot for λ0° and with less justification the Parral data have been represented by the partially shaded circles in the λ50° plot. Data for zenith angles greater than 60° are not included in the range of the plots and if they were, the points would be somewhat erratic. In the case of the λ50° plot some of the small angle points for sea level are also erratic and fall off the vertical range. Therefore the analysis of the λ50° data cannot be given undue weight.

TABLE II. $(x_e - x_w)$ *for various values of* z *measured in the vertical east-west plane.*

GEOMAGNETIC LATITUDE	$z = 15°$	30°	45°	60°	THEORY
0°	0.068	0.139	0.216	0.305	LVB, Størmer
20°	.052	.112	.193	.300	LVB
29°	.020	.056	.095	.136	LV
36°	.025	.047	.064	.079	Størmer
50°	.006	.012	.018	.024	Størmer

Since the asymmetric component extends over but a short range of x it affords opportunity for the study of intensity variations in the atmosphere due to primaries of definite energy. It has been customary to think of the absorption of corpuscular radiation in terms of a definite range, R, depending upon the energy. If corpuscular rays of definite energy were characterized by a definite range, R, the absolute specific intensity of the unbalanced positive component would be uniform within path lengths from the top of the atmosphere h sec $z < R$ and zero for h sec $z > R$. Since the total intensity follows closely the exponential law, a logarithmic plot of k/j *vs.* h sec z would resemble Curve I Fig. 8. The upward slope of the first part of the curve is the positive value of the absorption coefficient u of the total radiation. Another type of absorption to be considered corresponds to processes of energy loss whereby the rays give up all of their energy at once, but the depth at which this happens is a matter of probability. This type is characterized by the exponential law. In this case the relative specific intensity

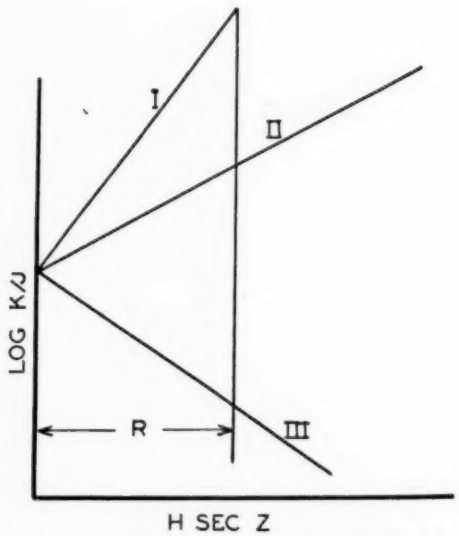

FIG. 8. Log k/j *vs.* h sec z. (I), assuming the positives are characterized by a definite range R; (II), assuming the positives are characterized by an exponential absorption coefficient $v<u$; and (III), assuming the positives are characterized by a coefficient $v>u$.

of unbalanced positives is represented by lines II or III accordingly as the positives are more or less penetrating than the average radiation. The slopes of II and III are the differences, $u-v$, of the absorption coefficients of the average and positive radiations, a quantity which may be called the filtering coefficient.

Although the probable errors are still high, it is evident from Fig. 7 that the results are best represented by curves of type III, Fig. 8, corresponding to exponential absorption with $v>u$. There is no indication of a range type of absorption such as has been usually assumed. It is also worthy of note that the intensity of the positives, within the present accuracy, is a single valued function of h sec z, regardless of the elevation, as must be expected for all types of absorption unless there is an appreciable scattering.

TABLE III. *Results of graphical analyses of the specific intensity of positives and of the average total intensity.*

Geomagnetic latitude, λ	0°	29°	50°
Filtering coefficient, $(v-u)$ per m of water	0.09	0.12	0.27
Absorption coefficient of the average radiation, u, per m of water	.24	.24	.26
Absorption coefficient of the positives, v, per m of water	.33	.36	.53
Specific relative intensity of positives, k_0/j_0	1.73	2.5	12.5
Average x	.50	.43	.21
Average electron energy, 10^9 v	15	10.8	2.5
Average proton energy, 10^9 v	14.1	9.9	1.9

Though the x differences as derived from the LV and Størmer theories are admittedly inaccurate, such inaccuracies should not affect the slopes of the lines representing the data as long as the x_0 differences are approximately linear functions of zenith angle over the short range near the zenith. The vertical displacements, however, would be so affected. There is an indication of a relative hardening of the positives with respect to the average radiation in the higher energy ranges occurring near the equator though the effect is by no means as great as would be expected if ranges $(1/v)$ were proportional to energies. In this connection the actual absorption coefficients of the positives have been derived from the filtering coefficients by adding the coefficients of the average radiation. The latter have been determined graphically in Fig. 7 from the coincidence counter measurements of average intensity *vs.* zenith angle. For the equator these were made in the north azimuth at two elevations, sea level and 4300 meters.[1] In the other latitudes east-west averages of the same data from which asymmetries have been derived have been used. In the case of the Mt. Evans data a somewhat uncertain correction has been made for the unusually high accidental rates experienced at that station. The results of these graphical analyses and data regarding the energies of the rays are collected in Table III.

By making use of the above results and of the values of the cone openings given by LVB the intensity of the unbalanced positive component can be integrated over all directions and over the ranges of x included in the asymmetrical components up to that which comes in with full intensity from the eastern horizon at the equator. A similar integration was made in reference (1) using the values of the cones published in 1933 by Vallarta.[16] Vallarta[17] has also made a somewhat similar calculation in his paper on the longitude effect, using an arbitrarily chosen energy distribution function and without considering the effect of atmospheric absorption. In the following calculations the observed intensity of the unbalanced positives and its variation with atmospheric path are used, so that a comparison of the calculated and observed

[16] M. S. Vallarta, Phys. Rev. **44**, 1 (1933).
[17] M. S. Vallarta, Phys. Rev. **47**, 647 (1935).

latitude and longitude effects may be regarded as a criterion for the existence or nonexistence of an additional mixed component, and as a test of the underlying assumptions. According to Fig. 7 the specific relative intensity of unbalanced positives in the range of x corresponding to the asymmetry in latitude λ may be expressed by

$$(k/j)=(k_0/j_0)_\lambda \exp\left[-(v-u)h \sec z\right] \quad (9)$$

and the total or average intensity by

$$j=j_0 \exp\left[-uh \sec z\right], \quad (10)$$

where, in both cases, the constants are given in Table III. If $f(x,z)$ is the fraction of the elementary solid angle $2\pi \sin z dz$, illuminated by rays of rigidity x, then the total intensity at depth h due to unbalanced positives of rigidity in the range dx, integrated over all angles is

$$\bar{k}(x)dx=2\pi dx\int_0^{\pi/2} k(x, h \sec z) f \sin z dz \quad (11)$$

and the fraction of the total intensity, J, due to rays of rigidity within the observable range below x_{0e} which cuts off at the eastern equatorial horizon is

$$K/J=1/J\int_{x_w}^{x_{0e}} \bar{k}dx, \quad \text{where}$$

$$J=2\pi\int_0^{\pi/2} j_0 \exp\left(-uh \sec z\right) \sin z dz. \quad (12)$$

It is noted that for $x>x_e$, $f(x,z)=1$ and for $x<x_w$, $f=0$. For $x_w<x<x_e$, the values of f are obtained from the results of LVB and are reproduced for $\lambda 0°$ and $\lambda 20°$ in Fig. 9. The integration of (11) and (12) has been made graphically, and with $x_{0e}=0.7$ as an upper limit it is found that at the equator $K/J=10.4$ percent at sea level and 14.2 percent at 4300 meters. Since the edge of the cone for $x=0.7$ is 55° below the zenith, the corpuscular intensity having this rigidity is greatly reduced by absorption and the experiments are somewhat insensitive for determining k/j values out to this limit. A more conservative estimate based upon integrations extending to the limit $x_{0e}=0.6$, which cuts off 30° below the zenith towards the east, is that at the equator at least 4.9 percent

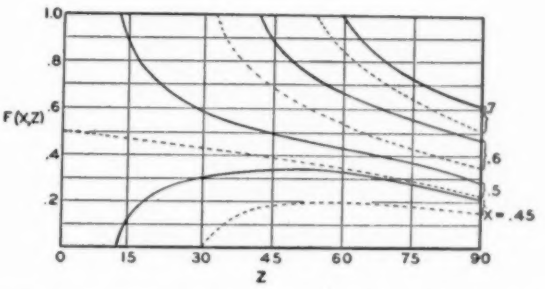

FIG. 9. $f(x, z)$ *vs.* z for various values of x taken from LVB theory. Dotted curves are for $\lambda 0°$ and solid curves for $\lambda 20°$.

at sea level and 6.8 percent at 4300 meters is unbalanced positive radiation.

Since this component is over and above the corpuscular intensity coming into the latitude effect, it may be added to the latter to give the lower limit of the total known corpuscular intensity in high latitudes. Using the results of Compton[18] and the above values corresponding to integration to $x_{0e}=0.6$, it appears that at least 30 percent of the high latitude intensity at 4300 meters and 16.6 percent of the intensity at sea level is due to corpuscular primaries of both signs of charge.

At the latitude $\lambda 20°$ for which f values are also given by LVB the integration of (12) to the upper limit 0.7 gives the values $K/J=12.0$ percent at sea level and 16.9 percent at 4300 meters. Thus the latitude effect between Panama and Peru, accountable by positives alone, is $12.0-10.4=1.6$ percent at sea level and $16.9-14.2=2.7$ percent at 4300 meters. If the values for $x_{0e}=0.6$ are used the predicted latitude effects are 1.4 percent at sea level and 2.0 percent at 4300 meters. Comparing these figures with the sea-level measurements of Millikan and Neher[19] and the airplane measurements of Bowen, Millikan and Neher[20] it appears, anomalously, that the unbalanced positives are more than enough to account for the whole of the latitude effect between these two latitudes. The observed effect at sea level is only 0.5 percent and at 4300 meters no effect was found within an uncertainty which may be estimated at about three percent. In the case of the sea-level

[18] A. H. Compton, Phys. Rev. **43**, 387 (1933).
[19] R. A. Millikan and H. V. Neher, Phys. Rev. **47**, 205 (1935).
[20] I. S. Bowen, R. A. Millikan and H. V. Neher, Phys. Rev. **46**, 641 (1934).

data there thus seems to be a definite discrepancy between the theory and the observations and there is a probable discrepancy at the higher elevations.

A criterion for the existence of a mixed component which should be more satisfactory from the theoretical standpoint is the comparison of observed longitude effects with those to be expected from the unbalanced positive intensity. This calculation involves only the cone openings at the equator. Following the method of Vallarta, it is assumed that the longitude effect is caused by the displacement of the magnetic center of the earth from its geometric center. Distances from the magnetic center of several points on the earth's surface and a compilation of observed intensities have been copied directly from Vallarta's paper.

To determine the longitude effect expected from a given intensity of corpuscular radiation integrations similar to (12) must be performed between limits chosen to correspond with the different magnetic radii. Since the curves of LVB, analogously with Eq. (5), fix the values of x as a function of λ and the direction, independently of r, the limits of integration expressed as x values are also fixed independently of r although the absolute rigidity $H\rho$, corresponding to a given value of x varies with r according to (4). It is therefore convenient to define $x=r(H\rho/M)^{\frac{1}{2}}$ as the value of x corresponding to a given $H\rho$ at a distance from the magnetic center equal to the standard earth radius, $r=6370$ km, and to define $x'=r'(H\rho/M)^{\frac{1}{2}}$ as the value of x corresponding to the same value of $H\rho$ at a point where the magnetic radius is r'. The LVB theory then defines the same cone openings at all points on the magnetic equator for the same values of x' though for a particular value of x the cones vary from place to place with r'. To integrate (12) over a definite band of radiation the limits must correspond to fixed values of x. Thus to determine the intensity due to rays of rigidity less than x_e, the integration must extend to $x'=x_e'r/r'$. For $x'>x_e'$, $f(x',z)=1$, and it is convenient to separate (12) into two parts

$$K/J=(K/J)_0+\Delta K/J,$$

in which the longitude effect is (13)

$$\Delta K/J=1/J\int_{x_e'}^{x_e'r/r'} k(x')\sin z dz \quad (14)$$

and $(K/J)_0$ is the relative corpuscular intensity at the standard earth radius, r.

To an approximation consistent with present experimental accuracies it appears unnecessary to take account of a possible functional relation between k and x either for the range of x included in any particular asymmetrical component or, even less so, for ranges involved in the longitude effect. Thus the second term of (13) reduces to the simple form

$$\Delta K/J=x_e'k_0(r'-r)G(vh)/j_0rG(uh), \quad (15)$$

where the Gold integral,

$$G(y)=2\pi\int_0^{\pi/2}\exp(-y\sec z)\sin z dz.$$

With the values of the constants given in Table III and with $x_{0e}'=0.7$, (15) reduces, for sea level at the equator to

$$\Delta K/J=0.35(r'-r)/r. \quad (16)$$

Values of the longitude effect calculated from (16) are given in Table IV where they are compared with the observed values, $\Delta I/I$. The agreement is not as good as could be hoped for, and in general, the positive component seems insufficient to account for as large a variation with longitude as is observed. Since this same component was more than sufficient to account for the latitude effect, it seems impossible to reconcile the two conclusions, except through

TABLE IV. *Comparison of observed longitude effect with that expected from the unbalanced positive intensity at the equator. All points are on the geomagnetic equator.*

LOCATION	LONGITUDE	$(r'-r)/r$	$\Delta K/J$ CALC.	$\Delta I/I$ OBS.
Lima, Peru	76W	0.023	0.008	0.012
SS Lane, Honolulu to Sydney	160W	−.039	−.014	.008
SS Lane, Bombay to Colombo	75E	.0031	.001	.000
SS Lane, S. Hampton to Cape Town	15W	.044	.015	.042
SS Lane, Hong Kong to Singapore	110E	−.0236	−.008	−.038

some modification of the theory. Possibly consideration of the real field of the earth would provide a satisfactory interpretation of the situation. It may be noted that the latitude effect between the equator and 20°N for the voyage of the Millikan-Neher electroscope between Los Angeles and Melbourne was about 2.5 percent and if this is taken as a better value for comparison with the calculations based upon the equatorial asymmetry, both latitude and longitude effects demand the existence of an additional mixed component. On the other hand it must be borne in mind that certain corrections for diffusion of secondary radiations and for accidental counts are suggested as being applicable to the asymmetry measurements and these tend to raise the calculated latitude and longitude effects, so that it is quite possible that the positives alone can account for the whole of the field sensitive component.

ACKNOWLEDGMENTS

The work has been carried out by means of a grant from the Carnegie Institution of Washington, administered by its Cosmic-Ray Committee. Facilities on Mt. Evans were generously provided by the City of Denver through the courtesy of D. D. Keim. In this connection the cooperation of Professor J. C. Stearns is also acknowledged. Professor M. S. Vallarta and Dr. C. R. Margain cooperated extensively in providing facilities in Mexico for the work at Copilco and Nevado de Toluca. Acknowledgment is also made of the courtesy and very generous support given the work by many officials of the Federal Government of Mexico and by Governor Solárzano of the State of Mexico. Mr. Lewis Fussell, Jr., cooperated in the field work and in the reduction of data and Dr. E. C. Stevenson helped with the construction and design of the apparatus.

AUGUST 15, 1935 PHYSICAL REVIEW VOLUME 48

The Infrared Absorption Spectrum of Solid Hydrogen Chloride

PAUL E. SHEARIN, *Mendenhall Laboratory of Physics, Ohio State University*

(Received June 19, 1935)

The infrared absorption spectrum of solid hydrogen chloride has been studied in the region of 3.7 μ with the aid of an echellette grating. The band is composed of a series of fairly broad lines, and if the center is taken to be the line at 2669 cm^{-1} the remaining lines taken in pairs can be grouped about this line with approximately equal spacings. Thus it appears that the band differs from the band in gaseous hydrogen chloride in that it has a zero line.

THE study of the absorption bands in the infrared of gas molecules under high dispersion has revealed many facts enabling one quite clearly to understand their behavior and structure. Many crystals show fully as well-developed bands as do gas molecules when measured with prism spectrometers, but only in few cases have measurements under high dispersion been made. Hardy and Silverman[1] and Silverman[2] have made measurements on quartz crystals and on the carbonates using an echellette grating and have found these bands to have a fine structure far more complex than that of gas molecules. The bands may as in gas molecules be ascribed to vibrations of the atoms comprising the ionic configurations in the crystal lattice, but no mechanism adequately serves to explain the fine structure. Of the proposed explanations perhaps the most plausible is the theory that the ionic configurations may be thought of as rotating under certain constraints. Such theories have been advanced by chemists to explain specific heat curves for crystals. Attempts quantitatively to describe these phenomena have been made by Pauling,[3] Stern[4] and recently more

[1] Hardy and Silverman, Phys. Rev. **37**, 176 (1931).
[2] Silverman, Phys. Rev. **39**, 72 (1932); Phys. Rev. **45**, 158 (1934).
[3] L. Pauling, Phys. Rev. **A36**, 430 (1930).
[4] Stern, Proc. Roy. Soc. **130**, 551 (1930).

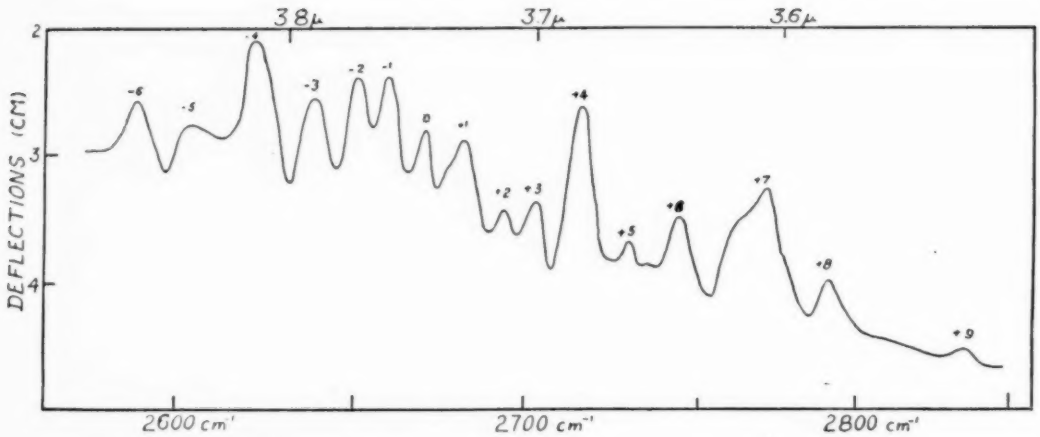

FIG. 1. Transmission curve of solid HCl—a composite of several runs.

completely by Nielsen.[5] From the latter's work one sees that the rotational energy level scheme for a polyatomic configuration is so extremely complex that a theory of rotation might well account for the intricate absorption pattern found in quartz and in the carbonates.

In view of the extreme complexity of the energy level scheme for polyatomic molecules in crystals, it seems important to study the spectrum of a diatomic configuration where the scheme is much simpler. Hydrogen chloride in the solid form was chosen to work on since it had been pointed out by Pauling that rotation was here apt to take place; moreover, the preliminary work by Hettner[6] on this substance had shown that the absorption at 3.7μ exhibited at least a doublet structure and gave a suggestion of a more complex structure.

For this experiment a vacuum system for manipulating the hydrogen chloride, equivalent except for unessential details to that used by Hettner, was constructed. To this system was sealed a Dewar flask of clear fused quartz from which the tip had been removed, so that by putting liquid air in the flask a thin layer of HCl could be frozen to the inside wall. The radiation was passed directly through the flask since liquid air is transparent to the spectral range here under investigation. The spectrograph was of a well-known design, fitted with a grating ruled with 800 lines per inch and used in fourth order. To eliminate higher order radiation, a monochromatic device was inserted before the slit of the grating spectrometer. As experienced by Hettner, it was necessary to put the absorbing medium in the energy beam after dispersion rather than in the undispersed beam as is customary, since the total radiation absorbed by the 3.7μ region was sufficient to cause the absorbing layer to sublime to cooler regions of the flask.

TABLE I. *Wavelengths and frequencies of the lines in the 3.7μ band of solid HCl.*

LINE NUMBER	FREQUENCY (cm^{-1})	WAVELENGTH IN μ	LINE NUMBER	FREQUENCY (cm^{-1})	WAVELENGTH IN μ
−6	2588	3.863	1	2681	3.729
−5	2606	3.837	2	2693	3.713
−4	2622	3.813	3	2703	3.700
−3	2639	3.791	4	2718	3.681
−2	2650	3.772	5	2729	3.664
−1	2660	3.760	6	2747	3.640
0	2669	3.746			

The data were recorded in terms of galvanometer deflections for each circle setting. This seemed satisfactory since this region is quite free from atmospheric bands. The transmission curve, which is a composite over several runs, is shown in Fig. 1, circle settings having been replaced by a wavelength scale in μ and a frequency scale in cm^{-1}. As shown in Fig. 1, the absorption by solid hydrogen chloride is of a complex nature which has here been partly resolved. No claim of complete resolution is made since many of the lines appear broad and unsymmetrical and, moreover, because of considerable dissipation of

[5] H. H. Nielsen, J. Chem. Phys. **3**, 189 (1935).
[6] G. Hettner, Zeits. f. Physik **78**, 14 (1932).

light energy by scattering through the absorption chamber, rather wide spectrometer slits were necessary. Due to the constant boiling of the liquid air in the flask, the transmission of the light energy was not quite constant for a given setting so that the galvanometer deflections would fluctuate about some mean value determined by averaging over about ten readings. Consequently the actual relative intensities of the lines in the band must be considered doubtful. Because of rapidly increasing absorption toward longer wavelengths, the measurements were not carried beyond 3.9μ. In Table I are given the wavelengths and frequency positions of the lines as observed in the band.

It is here rather difficult to determine what is the center of the band. This can probably only be accomplished when an analysis of the line structure can be made, and it seems wiser to leave this to a later date when it is hoped more exact measurements can be completed. The line marked 0 is, however, chosen as the center because the other lines in the band, $+1$, -1, $+2$, -2, etc., taken in pairs occur almost equally spaced about it. If one adheres to a theory of rotation of the molecules, the rotation lines should form $+$ and $-$ branches and one would then expect corresponding lines in these branches to lie approximately the same distance from the center.

If this identification is assumed to be correct, this band in contrast to that of gaseous HCl has a 0 line. If the HCl molecule in the solid is assumed to be rotating under constraints, this is, however, not surprising, for if the molecule were completely clamped one can see from purely classical considerations that only the 0 line should occur. This may also be seen from Nielsen's work where for the electric moment along the axis of symmetry the selection rules are seen to be $\Delta v = \Delta k = \Delta n = 0$.

These measurements, which are really to be looked at as of a preliminary character, suggest very strongly that actual rotation of the HCl molecule in the solid state under certain constraints does take place. A new cell has been designed to eliminate the scattering of the light energy completely and where the light beam will not have to traverse the liquid-air medium. With it, it is hoped to repeat these readings with narrower slits and under more favorable conditions of observation.

The writer wishes to express his appreciation to Dr. W. H. Bennett and to Dr. R. V. Zumstein for many helpful suggestions throughout this experiment. The writer is indebted to Dr. Harald H. Nielsen for suggesting the problem and for help in the interpretation of the results. A grant-in-aid given by the National Research Council is also acknowledged with gratefulness.

Inelastic Scattering of Quanta with Production of Pairs

MILTON S. PLESSET AND JOHN A. WHEELER,* *Institute for Theoretical Physics, Copenhagen*

(Received June 12, 1935)

The problem of accounting for the anomalous scattering of gamma-rays suggests the importance of investigating the probability of processes in which an incoming quantum produces an electron-positron pair in the field of a nucleus, going on in a new direction with diminished energy. To determine the cross section in the general case is difficult, but an estimate of the total magnitude of the effect in the energy range of interest is obtained by a calculation of the cross section as a function of the energies of the incident and scattered quanta and the angle between them in the limit where the electron-positron pair is produced with small kinetic energy.

While there exists a possibility of observing the process under suitable experimental conditions, the cross section is found to be too small to contribute appreciably to the production of the hard component in the radiation from heavy elements exposed to penetrating gamma-rays.

I

THE inelastic scattering of gamma-rays at a nucleus with the production of an electron-positron pair has an interest as a possible contribution to the anomalous scattering which is observed in heavy elements. In the effect considered here, the incident quantum produces a pair in the field of the nucleus and goes on in a new direction with diminished energy. This process involves a second order interaction with the radiation field, and is closely related to the type of radiative effect in which an electron emits two quanta on colliding with a nucleus. The quantitative relation between the two processes is given below. The connection between the inelastic scattering and the related double radiation is of the same kind as that between the photoelectric production of pairs and the production of a single quantum by an electron in the field of a nucleus.[1]

The calculation here uses the Born approximation for the wave functions of the electron and the positron in the Coulomb field of the nucleus. In the Born expansion of the wave functions in plane waves, only the terms up to the first order in Z are needed to give the inelastic scattering. Since the process is of the second order in the interaction with the radiation field, it requires a perturbation calculation altogether of the third order. For this reason the cross section involves many more terms than that for the photoelectric production of pairs, which is likewise first order in Z, but only of the first order in the interaction with the radiation field.

In the region of the high quantum energies it is in theory possible to treat the problem by the method (Williams[2] and Weizsäcker[3]) of replacing the nuclear field by an equivalent radiation field, and considering the interaction of the virtual quanta in this field with the incident quantum. Knowledge of the cross section for the collision of two quanta in field-free space with the production of a pair and a new quantum would then make possible a calculation in the region of high energies of the probability of the process considered here. As this cross section has not yet been calculated, it is simpler, as well as more accurate, to proceed directly as below.

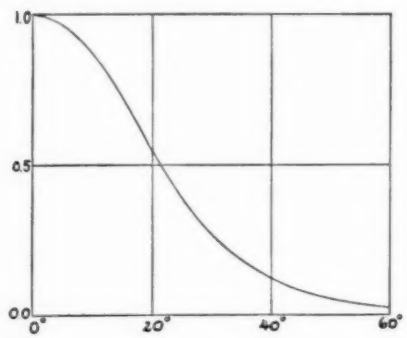

FIG. 1. Distribution in angle of the scattered quanta for $\nu=5$, $\sigma=3$.

* National Research Fellow.

[1] H. Bethe and W. Heitler, Proc. Roy. Soc. **A146**, 83 (1934).

[2] E. J. Williams, Kgl. Danske Vid. Math.-fys. Medd. **13**, 4 (1935).

[3] C. V. Weizsäcker, Zeits. f. Physik **88**, 612 (1934).

II

Calculations concerned with electrons of relativistic energies take a simple and convenient form when the quantities entering are expressed in natural units.[4] These units are: for length, $\hbar/mc$; time, $\hbar/mc^2$; action, $\hbar$; energy, mc^2; momentum, mc; charge, e; potential, $emc/\hbar$. In these units, the potential energy of two electrons at a distance r is α/r, where $\alpha=e^2/\hbar c$, and the energy of the electromagnetic field is $(\alpha/8\pi)\int(E^2+H^2)dv$. The operators p_x and H go over into $-i\partial/\partial x$ and $i\partial/\partial t$, and Dirac's equation, including the electromagnetic field, becomes (following the usual derivation)

$$\{i\partial/\partial t+\boldsymbol{\alpha}\cdot\mathbf{p}+\alpha V+\beta-\sum_k N\nu+\sum_k(2\pi\alpha/\nu V)^{\frac{1}{2}}(b\boldsymbol{\alpha}\cdot\mathbf{f}\exp i\boldsymbol{\nu}\cdot\mathbf{x}+b^*\boldsymbol{\alpha}\cdot\mathbf{f}\exp -i\boldsymbol{\nu}\cdot\mathbf{x})\}\varphi=0. \tag{1}$$

The summations are extended over all quantum frequencies $\boldsymbol{\nu}_K$ and polarizations $\mathbf{f}_K$; in (1) b_K and N_K have the matrix elements $b_{ij}=\sqrt{j}\delta_{i+1,\,j}$, $N_{ij}=j\delta_{ij}$. N_K is the operator for the number of quanta of type K.

The term in (1) involving the b's represents the interaction between the electron and the radiation field. To the first order in this interaction, scattering does not occur. A perturbation calculation to the second order gives for the general scattering cross section the expression

$$d\varphi_i=\alpha^2(\sigma/\nu)\,|\sum_j\{B_{ij}A_{j0}/(E_0-E_j+\nu)+A_{ij}B_{j0}/(E_0-E_j-\sigma)\}|^2d\Omega. \tag{2}$$

$d\varphi_i/d\Omega$ is the cross section per unit solid angle of emission of the scattered quantum $\boldsymbol{\sigma}$ for a transition in which the incident quantum $\boldsymbol{\nu}$ disappears and the electron is raised from the initial state ψ_0 of energy E_0 to the final state ψ_i of energy $E_i=E_0+\nu-\sigma$. The summation Σ_j is to be extended over all electron states ψ_j. The A's and B's are the matrix elements for the interaction with the radiation field:

$$A_{ij}=\int\psi_i^*\mathbf{a}\cdot\boldsymbol{\alpha}\exp i(\boldsymbol{\nu}\mathbf{x})\psi_j dv;\quad B_{ij}=\int\psi_i^*\mathbf{b}\cdot\boldsymbol{\alpha}\exp(-i\boldsymbol{\sigma}\mathbf{x})\psi_j dv. \tag{3}$$

$\mathbf{a}=\mathbf{f}_\nu$ and $\mathbf{b}=\mathbf{f}_\sigma$ are the polarization vectors of the incident and scattered quanta.

In the present problem of the inelastic scattering by the negative energy electrons in a nuclear field, ψ_0 is a state of negative energy and ψ_i one of positive energy, these two states, respectively, corresponding to the positron and electron produced in the process. To determine the total cross section for the production of a scattered quantum in the energy range $d\sigma$ and in the solid angle $d\Omega$, summation of $d\varphi_i$ is made first over all states ψ_i of energy between $E_i-dE_i=E_0+\nu-(\sigma+d\sigma)$ and $E_i=E_0+\nu-\sigma$, keeping E_0 fixed; a sum is then carried out over all negative energy states ψ_0 between the two limits $E_0=-(\nu-\sigma-1)$ and $E_0=-1$. Finally the result is summed over both polarization directions of the scattered quantum and averaged over both polarizations of the incident quantum to give the cross sections desired:

$$\frac{d^2\varphi}{d\Omega d\sigma}=\alpha^2\frac{\sigma}{\nu}\frac{1}{2}\sum_a\sum_b\int dE_0\sum_{s_0}\int d\Omega_0\left(\frac{L}{2\pi}\right)^3 p_0|E_0|\sum_{s_i}\int d\Omega_i\left(\frac{L}{2\pi}\right)^3 p_iE_i|\sum_j\{\cdots\}|^2. \tag{4}$$

In (4) the wave functions are considered normalized over a cube of volume L^3, so that the number of states, having a given spin s_0 and a momentum at a large distance from the nucleus in the range dp_0 and the solid angle $d\Omega_0$, is $(L/2\pi)^3p_0^2dp_0d\Omega_0=(L/2\pi)^3p_0E_0dE_0d\Omega_0$.

In an accurate evaluation of (4) the wave functions satisfy the equation

$$(E-i\boldsymbol{\alpha}\cdot\nabla+\beta+\alpha Z(r)/r)\psi=0; \tag{5}$$

$Z(r)$ determines the potential for an electron in the field of a screened nucleus of charge $Z=Z(0)$. The normalized solution of (5) to the first Born approximation is

[4] A. E. Ruark, Phys. Rev. **38**, 2240 (1931).

$$\psi = L^{-\frac{3}{2}}\left\{\exp(i\mathbf{p}\cdot\mathbf{x}) - (\alpha/2\pi^2)\int \frac{Z-F(|\mathbf{p}-\mathbf{p}'|)}{|\mathbf{p}-\mathbf{p}'|^2}\,\frac{E-\boldsymbol{\alpha}\cdot\mathbf{p}'-\beta}{E^2-p'^2-1}\exp(i\mathbf{p}'\cdot\mathbf{x})dp_x'dp_y'dp_z'\right\}S. \tag{6}$$

F is the usual atomic form factor; S is the normalized spin vector for free electron waves of momentum $\mathbf{p}$ and energy E. The wave functions ψ_0, ψ_j and ψ_i entering in (4) are approximated by taking the solution (6) with appropriate values E and $\mathbf{p}$; with this form for the wave functions the integrations over the coordinates and momenta entering into the A's and B's are easily carried out. Owing to the appearance of δ functions in the matrix elements only four values of $\mathbf{p}_j$ contribute to the sum over intermediate states. The summation over spins is simplified by the relation holding for the two independent spin functions corresponding to the same energy, E, and momentum, $\mathbf{p}$:

$$\sum_{\text{Spin}} SS^* = (E-\boldsymbol{\alpha}\cdot\mathbf{p}-\beta)/2E.$$

The additional relation that

$$\sum_{S_0}\sum_{S_i}|M_{i0}|^2 = \text{Spur}\,\frac{E_i-\boldsymbol{\alpha}\cdot\mathbf{p}_i-\beta}{2E_i}M\frac{E_0-\boldsymbol{\alpha}\cdot\mathbf{p}_0-\beta}{2E_0}M^*,$$

which holds for any matrix element M_{i0} of the form $(S_i^*MS_0)$, reduces the expression (4) for the inelastic cross section to

$$\frac{d^2\varphi}{d\Omega d\sigma} = \frac{\alpha^4}{2^9\pi^4}\frac{\sigma}{\nu}\sum_a\sum_b\int dE_0\int d\Omega_0\int d\Omega_i\frac{p_0p_i}{\tau^4}(Z-F(\tau))^2\,\text{Spur}\,(E_i-\boldsymbol{\alpha}\cdot\mathbf{p}_i-\beta)N(E_0-\boldsymbol{\alpha}\cdot\mathbf{p}_0-\beta)N^*. \tag{7}$$

Here $\boldsymbol{\tau}$ is the momentum transfer to the nucleus, $\boldsymbol{\nu}-\boldsymbol{\sigma}+\mathbf{p}_0-\mathbf{p}_i$; and the matrix $N=N_1+N_2$, where

$$N_1 = \frac{\mathbf{b}\cdot\boldsymbol{\alpha}[E_0+\nu-\boldsymbol{\alpha}\cdot(\mathbf{p}_i+\boldsymbol{\sigma})-\beta][E_0+\nu-\boldsymbol{\alpha}\cdot(\mathbf{p}_0+\boldsymbol{\nu})-\beta]\mathbf{a}\cdot\boldsymbol{\alpha}}{[E_i\sigma+\mathbf{p}_i\cdot\boldsymbol{\sigma}][E_0\nu-\mathbf{p}_0\cdot\boldsymbol{\nu}]}$$

$$+\frac{2\mathbf{b}\cdot\boldsymbol{\alpha}[E_0+\nu-\boldsymbol{\alpha}\cdot(\mathbf{p}_i+\boldsymbol{\sigma})-\beta]\mathbf{a}\cdot\boldsymbol{\alpha}[E_0-\boldsymbol{\alpha}\cdot(\mathbf{p}_i+\boldsymbol{\sigma}-\boldsymbol{\nu})-\beta]}{[E_i\sigma-\mathbf{p}_i\cdot\boldsymbol{\sigma}][p_0^2-(\mathbf{p}_i+\boldsymbol{\sigma}-\boldsymbol{\nu})^2]}$$

$$+\frac{2[E_i-\boldsymbol{\alpha}\cdot(\mathbf{p}_0+\boldsymbol{\nu}-\boldsymbol{\sigma})-\beta]\mathbf{b}\cdot\boldsymbol{\alpha}[E_0+\nu-\boldsymbol{\alpha}\cdot(\mathbf{p}_0+\boldsymbol{\nu})-\beta]\mathbf{a}\cdot\boldsymbol{\alpha}}{[E_0\nu-\mathbf{p}_0\cdot\boldsymbol{\nu}][p_i^2-(\mathbf{p}_0+\boldsymbol{\nu}-\boldsymbol{\sigma})^2]}; \tag{8}$$

and

$$N_2(\boldsymbol{\nu},\mathbf{a};\boldsymbol{\sigma},\mathbf{b}) = N_1(-\boldsymbol{\sigma},\mathbf{b};-\boldsymbol{\nu},\mathbf{a}). \tag{9}$$

The elementary cross section for the production of a scattered quantum in the solid angle $d\Omega$ with the appearance of a positron in the cube $dp_0dq_0dr_0$ of momentum space at $-\mathbf{p}_0$ and an electron in $dp_idq_idr_i$ at $\mathbf{p}_i$ is

$$d^7\varphi = (Z-F(\tau))^2\alpha^4 2^{-9}\pi^{-4}\sigma\nu^{-1}\tau^{-4}E_0^{-1}E_i^{-1}\sum_a\sum_b\text{Spur}\,(E_i-\boldsymbol{\alpha}\cdot\mathbf{p}_i-\beta)N(E_0-\boldsymbol{\alpha}\cdot\mathbf{p}_0-\beta)N^*$$
$$\times d\Omega dp_0dq_0dr_0dp_idq_idr_i. \tag{10}$$

The elementary cross section for the radiation of two quanta when an electron passes through the field of a nucleus is simply related to (10).

$$d^7\Phi = (Z-F(\tau))^2\alpha^4 2^{-9}\pi^{-4}\sigma^{-1}\nu^{-1}p_0p_i^{-1}\tau'^{-4}\sum_a\sum_b\text{Spur}\,(E_i-\boldsymbol{\alpha}\cdot\mathbf{p}_i-\beta)N'(E_0-\boldsymbol{\alpha}\cdot\mathbf{p}_0-\beta)N'^*$$
$$\times d\Omega_0d\nu_xd\nu_yd\nu_zd\sigma_xd\sigma_yd\sigma_z \tag{11}$$

is the cross section for the emission of two quanta of energies ν and σ in the ranges $d\nu_xd\nu_yd\nu_z$ and

$d\sigma_x d\sigma_y d\sigma_z$ by an electron of initial momentum $\mathbf{p}_i$ and of final momentum $\mathbf{p}_0$ in the solid angle $d\Omega_0$. In (11), $\tau'(\nu, \sigma)=\tau(\nu, -\sigma)$; and $N'(\nu, \sigma)=N(\nu, -\sigma)$, where τ and N are the quantities occurring in (10).

For given ν, in the case of the inelastic scattering of quanta with pair production, the momentum transfer, τ, to the nucleus has its minimum value when $\sigma=0$ and the pair particles divide the energy ν equally and go in the forward direction. In this case, $\tau=\nu-(\nu^2-4)^{\frac{1}{2}}$. The screening effect of the atomic electrons enters in $F(\tau)$, and is negligible for values of $\tau>Z^{\frac{1}{2}}/137(=0.032$ for Pb). Thus for incident quantum energies less than $50mc^2$ screening can be neglected for Pb and all lighter elements, and $Z-F$ in (7) may be replaced by Z. With this limitation on the energy range, the cross section may be written in ordinary units of length as $d^2\varphi/d\Omega d\sigma=\alpha^2Z^2(e^2/mc^2)^2f(\nu, \sigma, \theta)$ where f is a function only of the energies of the incident and scattered quanta and the angle between them.

The large number of terms entering into the spur when the spin reductions are carried out greatly complicates the evaluation of the cross section (7) in the general case. It is sufficient, however, to obtain an estimate and upper limit for the total cross section in order to determine how much the inelastic scattering with pair production can contribute to the intensity of the radiation observed experimentally from heavy elements exposed to hard gamma-rays. The calculations are much simplified in the limiting case in which the pair particles have small kinetic energy. This fact suggests the procedure of evaluating the cross section accurately in this limit, and using the result to estimate the total cross section. In this limit the integrations over the directions of the pair particles may be directly performed, and the cross section reduces to

$$\frac{d^2\varphi}{d\Omega d\sigma}=\frac{Z^2\alpha^4}{2^7\pi}\frac{\sigma}{\nu}\frac{(\nu-\sigma-2)^2}{(\nu-\sigma)^4}\sum_a\sum_b \text{Spur}\,(1-\beta)N(1+\beta)N^*. \tag{12}$$

N here is taken from Eqs. (8) and (9) with $p_0=0$, $E_0=-1$; $p_i=0$, $E_i=1$. In general the spur of $(1-\beta)M(1+\beta)M^*$ has the value $8\{(\mathbf{B}+\mathbf{E})\cdot(\mathbf{B}^*+\mathbf{E}^*)+(G+H)(G^*+H^*)$ for any spin matrix M,

$$M=A+\mathbf{B}\cdot\boldsymbol{\alpha}+C\beta+\mathbf{D}\cdot\mathbf{S}+\mathbf{E}\cdot\boldsymbol{\alpha}\beta+\mathbf{F}\cdot\mathbf{S}\beta+G\alpha_1\alpha_2\alpha_3+H\alpha_1\alpha_2\alpha_3\beta.$$

Accordingly the cross section depends only on the coefficients of $\boldsymbol{\alpha}$ and β in $N(1+\beta)$. In this way the cross section for inelastic scattering with pair production near the limit $\sigma=\nu-2$ is found to be

$$\frac{d^2\varphi}{d\Omega d\sigma}=\frac{Z^2\alpha^4}{\pi}\frac{\sigma}{\nu}\frac{(\nu-\sigma-2)^2}{(\nu-\sigma)^8}[(1+\mu^2)+\nu\sigma(1-\mu^3)+\nu^2\sigma^2(1+\mu)(1-\mu)^2(3-\mu)/8], \tag{13}$$

where $\mu=\mathbf{v}\cdot\boldsymbol{\sigma}/\nu\sigma$.

Eq. (13) shows that, as the energy of the scattered quantum increases, the cross section falls off as the square of the energy difference, $(\nu-\sigma-2)^2$. If (13) is extrapolated from the limit $\sigma=\nu-2$ toward the limit $\sigma=0$, it gives a rapidly increasing cross section; since it is clear for physical reasons that the cross section remains finite for all σ, Eq. (13) may reasonably be used to give an upper bound for total cross section. In this way, the following upper limit is found for the total cross section in the special case $\nu=5$ by integrating over all angles Ω and all scattered frequencies σ:

$$\varphi<0.011\alpha^2Z^2(e^2/mc^2)^2. \quad (\nu=5.) \tag{14}$$

The most important contribution to the total cross section (14) integrated over σ comes from values of σ not near the limit $\nu-2$. Thus when $\nu=5$, for most of the pairs produced, the kinetic energy $\nu-2-\sigma$ of the two particles is considerable. Analogy with calculations on the photoelectric production of pairs would indicate that also in the present problem the most probable situation is that in which the energy is divided fairly equally. Accordingly the main contribution to the total cross section comes from processes in which both the pair particles produced will have sufficiently large momenta for the Born approximation to be valid ($p_0, p_i>\alpha Z$). Eq. (7) is therefore accurate

in the most important region of energies of the scattered quanta. Any errors due to failure of the Born approximation will be in the direction to make (14) an overestimate. The approximation to (7) by the use of (13) must be regarded as the first term in a purely analytical development not involving the question of the validity of the Born approximation in the limit $\sigma=\nu-2$.

For the Th C″ radiation with $\nu=5.15$, the inelastically scattered radiation ranges from $\sigma=0$ to $\sigma=3.15$, with the intensity falling rapidly towards the high energy side. The more energetic scattered quanta are strongly concentrated within a small angle $\sim 1/\nu$ (see Fig. 1), as is evident from the presence of the denominator $(\nu-\sigma)^8$ in (13).

The estimate (14) shows that in pair production the ratio of the cross section with inelastic scattering to that with simple photoelectric absorption ($\varphi=0.67\alpha Z^2(e^2/mc^2)^2$) is less than 1.2×10^{-4} for Th C″ gamma-rays; the contribution of the inelastic scattering is clearly negligible, both to absorption, and to the production of the gamma-radiation observed to come from heavy elements exposed to high energy quanta. The only simple possibility for observing the effect discussed here would be in a cloud chamber containing a heavy gas, or a thin metallic foil, exposed to hard monochromatic gamma-rays. With this arrangement the appearance of pairs with total energies less than the incident energy would be attributable to the inelastic scattering.

AUGUST 15, 1935 PHYSICAL REVIEW VOLUME 48

Carbon Radioactivity and Other Resonance Transmutations by Protons

L. R. HAFSTAD AND M. A. TUVE, *Department of Terrestrial Magnetism, Carnegie Institution of Washington*

(Received June 10, 1935)

By observations with direct-current potentials of from 200 to 900 kv and currents of protons and deuterons up to 10 microamperes, it is shown that: (1) The induced radioactivity from the reaction ($C+H^1$) is produced by a resonance process with two resonance lines at about 400 and 480 kv indicated, whereas the efficiency of the corresponding process for ($C+D^2$) increases approximately exponentially throughout the voltage range covered; (2) the gamma-rays emitted in the reaction ($Li+H^1$) show resonances at 450 kv and 850 kv; (3) the gamma-rays from ($F+H^1$) suggest resonances at 320, 700 and 800 kv; (4) the gamma-rays from ($Be+H^1$) do not appear to be produced by a resonance process.

INTRODUCTION

THIS paper gives a more detailed report of the experiments on which recent Letters to the Editor[1] from the Department of Terrestrial Magnetism of the Carnegie Institution of Washington were based.

I. EXPERIMENTAL TECHNIQUE

High voltage equipment

The concentric one- and two-meter Van de Graaff installation at the Department, shown schematically in Fig. 1, was used in this work.

A maximum of 1300 kv is available with this apparatus, but it was limited to about 900 kv in this work by sparking to ground along the paper charging belt which had been in use nearly eight months and was in bad condition. While replacement of the belt is a relatively minor operation, it was postponed until the present work was finished to avoid possible extraneous delays.

Charging currents

Under best conditions a charging current of 750 microamperes has been obtained with this department's equipment, but all the work reported here was done with reduced belt speed and with charging currents of about 300 microamperes. Some of the observations reported were made in August 1934 with the relative humidity as high as 71 percent.

Voltage calibration

At the higher voltages it was possible to obtain range measurements on the primary beam, but

[1] Hafstad and Tuve, Phys. Rev. **47**, 506 (1935).

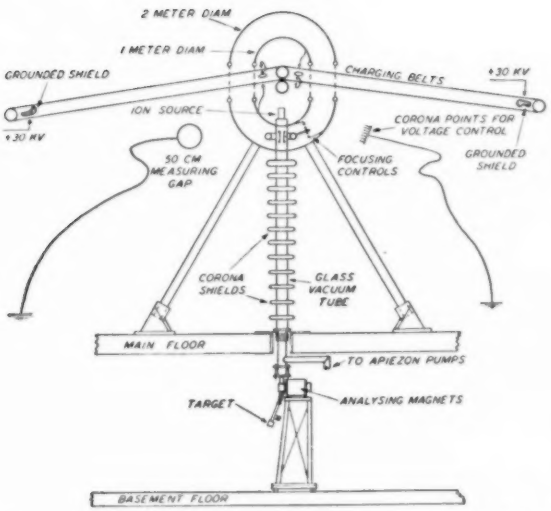

FIG. 1. Schematic diagram of concentric Van de Graaff generator.

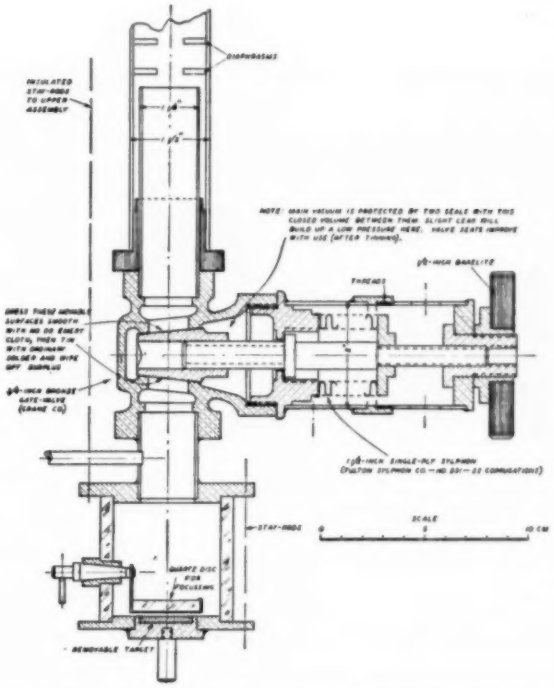

FIG. 2. Sylphon gate value and target assembly with Faraday cage.

below 500 kv (thinnest available metal window) it was necessary to resort to sphere gap voltage indications. The problem was further complicated by the concentric sphere design, since the gap responds only to the voltage on the outside sphere, so that the voltage between spheres must be added separately. However, by taking direct range measurements on the primary beam at 750, 700, 600 and 525 kv, and by measuring (with 25-cm sphere gap) the voltage between the spheres for the focusing voltage settings used in the present work, enough points were obtained on the absolute voltage curve so that intermediate points could be obtained by interpolations without large errors. The greatest uncertainty lies in the range *versus* energy relation for low energy protons which as yet is not definitely established.[2] We have assumed as a compromise value a range of 10 mm for 500 kv protons [36 mm for 1200 kv].

Voltage variation

Voltage variation during most of this work was obtained by setting the sphere gap for some desired voltage and then adjusting the position of grounded corona points until the gap just failed to spark. This index was chosen because the sphere gap response is sharp and reasonably repeatable over many trials. In the latter part of the work when very exact voltage settings had been shown to be necessary, a different method of holding the voltage at the sphere gap setting was used which will be described below.

Ion source

The ion source used was the old low voltage arc previously used at the Department of Terrestrial Magnetism but modified by the use of an oxide coated filament of platinum and the use of picein instead of Apiezon "Q" for all joints, thus eliminating slow leaks and permitting the hydrogen or deuterium to be kept relatively free of air or foreign vapors. This purity is apparently an important requirement, for with a small amount of air in the arc not over 0.2 microampere could be obtained in the magnetically resolved proton beam whereas with pure H_2 (or mixed with He) up to 12 microamperes has been obtained, though this required a large gas flow. Most of the work here reported was done with target currents of 5 to 10 microamperes, measured in a deep Faraday cage at the target.

The use of a low voltage arc in this work has proved to be a distinct advantage for the velocity spread in the beam is very small even compared to voltage increments used in investigating the voltage variation near points of resonance.

[2] Cockcroft and Walton, Nature **129**, 242 (1932); Blackett and Lees, Proc. Roy. Soc. **A134**, 665 (1932).

Most of the data on which this paper is based were obtained on a single oxide coated filament of platinum installed December 17, 1934, and burned out by accident on February 14, 1935.

Target assembly

In order to permit the removal of activated targets, the target assembly shown in Fig. 2 was used. The valve and target holder, being insulated from the rest of the system, form an excellent Faraday cage, and, since the beam is limited by the diaphragms above the valve, one can be certain that all current measured actually strikes the target. The movable quartz disk just above the removable target permits the beam to be brought into a stable focus before the target is actually exposed. Any wandering of the spot thereafter makes itself evident by a decrease in the measured target current, which was continuously observed throughout the time of bombardment.

A magnetic field sufficient to give a separation of about 5 cm between the mass one and mass two spots at the target was used in these experiments. When sharply focused, the spots were 5 mm or less in diameter. In practice the spots were deliberately defocused slightly in order to cover the targets more uniformly.

Measuring instruments

The present investigation was undertaken in order to clarify discrepancies between the observations obtained at Washington and Pasadena on the radioactivity produced in carbon by protons and deuterons. By the use of one of Professor Lauritsen's own electroscopes, kindly loaned to us at our request, for most of these observations, we were able to eliminate one important experimental variable and to make our later measurements entirely comparable to his. Our earlier measurements had been made using a Geiger point counter and an ionization chamber connected to a vacuum tube electrometer (FP-54), so a series of intercomparisons was made between these instruments and the Lauritsen electroscope and Geiger tube counters as used by other workers. These comparisons will be discussed in connection with the question of absolute yield.

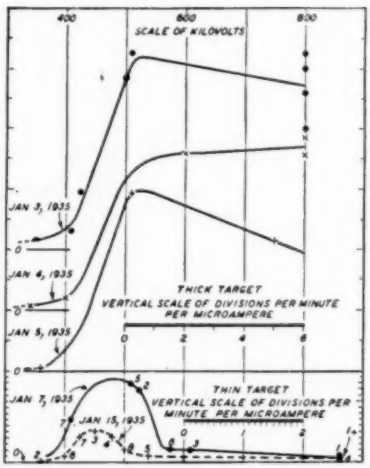

FIG. 3. Excitation functions for induced radioactivity from carbon (thin and thick targets).

II. CARBON RADIOACTIVITY

Excitation function for $(C+H^1)$

The upper two curves shown in Fig. 3 for thick Acheson graphite disks were taken with relatively small target currents and imperfect voltage control, but both suggested strongly an abrupt rise between 400 and 600 kv and no great change at higher voltages as might be expected only from a resonance effect. The points for January 5, 1935, were taken with improved voltage control and target currents raised to 7 to 10 microamperes in preparation for the verifying thin target observations to follow.

The thin targets used for the observations on January 7 were prepared by smoking clean copper disks over a candle flame. The points are numbered in the order of the observations, a separate target being used for each point, and, as will be surmised, point 7 was taken with every expectation of finding it well below the resonance point. The high value of point 7 was the first hint of a peculiarly broad resonance. The total intensity observed being only one-fifth of that for a solid target, it appeared difficult to ascribe this width to target thickness but equally difficult to account for it in any other way.

After considerable experimentation a new set of thin targets was made by slowly evaporating a suspension of colloidal carbon in water (aquadag) onto a set of clean copper disks which had been washed in alcohol just before being dropped into the carbon suspension. This process gave an

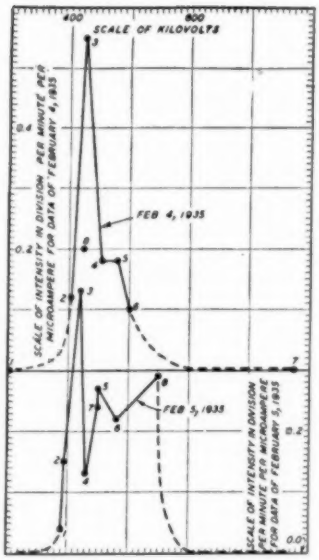
400
600
SCALE OF KILOVOLTS
SCALE OF INTENSITY IN DIVISION PER MINUTE PER MICROAMPERE FOR DATA OF FEBRUARY 4, 1935
FEB 4, 1935
FEB 5, 1935
SCALE OF INTENSITY IN DIVISION PER MINUTE PER MICROAMPERE FOR DATA OF FEBRUARY 5, 1935

FIG. 4. Excitation function for induced radioactivity from carbon (thin target).

extremely thin and fairly uniform layer of carbon. The results of observations made on these targets are shown in the curve for January 15, 1935. It will be noted that the intensity of the effect was still further reduced so that the total stopping power of the film might be estimated, by comparison with the thick target intensity, as about one-twentieth of the resonance width. From these curves it seemed safe to conclude that a resonance "half-width" of about 50 kv must be assigned to the nucleus.

After correspondence with Professor Breit regarding the above results it appeared highly desirable to obtain some indication as to the exact shape of the resonance curve, and it seemed, in view of the consistency of the points obtained January 15, that with special care this might be barely possible. A new set of thin targets was prepared with even more care than before. A weighed quantity of aquadag was used in the suspension, and from the area covered on evaporation the weight of carbon per square centimeter could be determined and a corresponding average stopping power estimated. This was approximately one-tenth millimeter (air equivalent) for the targets used.

With the new set of targets the curves shown in Fig. 4 were obtained. While one might expect a "tailing" on the high voltage side of a resonance peak produced by thick spots in the targets, a second maximum as suggested in these curves hardly can be dismissed as being produced in this way. On the other hand, to prove the existence of a double maximum from thin target observations is also very difficult. Either a set of targets must be first proved to be of uniform thickness at *all* points in some way, or else one single target must be used throughout the investigation, allowing ample time for decay between activations. Unless voltage settings are reproducible with great accuracy, the latter method is impracticable. In either case it would also have to be demonstrated that the ion beam was truly homogeneous and free of appreciable "tailing" of ions with velocities below the maximum. We consequently chose to return to thick target observations to test for the existence of a step or steps in the excitation curve, which must exist if the multiple resonances were real. In a series of three curves strong indications were obtained for such an effect, but the observed points failed to repeat sufficiently well to permit a definite conclusion to be drawn. Finally, however, by arranging a convenient control for the charging current we were able to force the gap to spark approximately every 30 seconds and thus hold the voltage "up against the sphere gap limit" with assurance that voltage could be neither high nor low for any appreciable period. The two final curves obtained under these conditions are shown in Fig. 5. It is felt this evidence forces us to conclude that this proton resonance on carbon is not due to a single resonance line but to a doublet or to a multiplet of which two components are clearly indicated between 400 and 500 kv.

This conclusion does not appear to us to contradict the results of Cockcroft, Gilbert and Walton,[3] for the existence of two close resonance peaks, plus the possible spread in energy among the ions of their beam produced by a 20-kv canal-ray source, would tend to give a slowly rising curve such as they observed.

Absolute yields

Our values for absolute yields for the $(C+H^1)$ reaction have now been obtained by several methods which show a reasonable agreement with each other as well as with the recent quantitative

[3] Cockcroft, Gilbert and Walton, Proc. Roy. Soc. **A148**, 225 (1935).

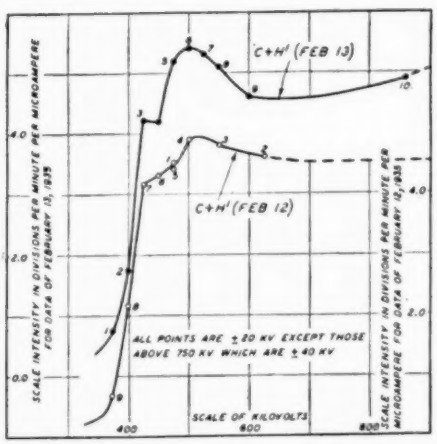
C+H¹ (FEB 13)
C+H¹ (FEB 12)
ALL POINTS ARE ± 20 KV EXCEPT THOSE ABOVE 750 KV WHICH ARE ± 40 KV
SCALE OF KILOVOLTS
SCALE INTENSITY IN DIVISIONS PER MINUTE PER MICROAMPERE FOR DATA OF FEBRUARY 13, 1935
SCALE INTENSITY IN DIVISIONS PER MINUTE PER MICROAMPERE FOR DATA OF FEBRUARY 12, 1935

FIG. 5. Excitation function for induced radioactivity from carbon (thick target).

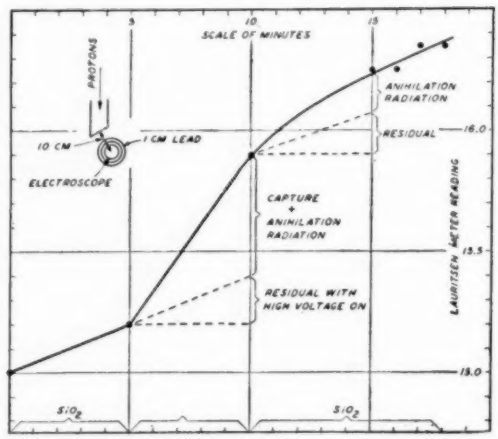

FIG. 6. Gamma-rays from C+H¹, January 16, 1935.

measurements on this point by Cockcroft, Gilbert and Walton.

Our first observations on induced radioactivity were made with a point counter, but this was used only as an indicator, being discarded for the more convenient as well as more quantitative measurements with a vacuum tube electrometer after it had been found repeatedly that a counting rate of about two counts per minute on the point counter corresponded to a 1-cm deflection of the galvanometer spot. Since in our early observations we failed to observe a (C+H¹) effect with this apparatus but later (after being informed by Cockcroft that a proton effect persisted even after magnetic analysis had been introduced in their experiments) measured the effect with the same apparatus, it is important to record that in the original experiments a disk of graphite was bombarded through a valve with a relatively long and small bore so that an unknown part of the current was lost to the walls. Since this effect should be about the same for either proton or deuteron beams, no correction was made for this effect in our *ratio* determinations. As soon as it was apparent that the discrepancy between different laboratories involved the absolute magnitude of the effect, the smaller cock was replaced with the one shown in Fig. 2 after which the magnitude of *both* the proton and deuteron effects was considerably increased.

From a measurement made in August 1934 with the vacuum tube electrometer, we estimated the absolute yield of the (C+H¹) reaction to be of the order of one disintegration per 10^{10} incident protons. This value might vary by a factor of 3 or 4 because of uncertainties in the estimates of solid angles and the average number of ions produced by each positron entering the ionization chamber from the activated target.

In measurements made recently using Lauritsen's electroscope we have consistently found a discharge rate of about 4 divisions per minute per microampere. Assuming 2×10^6 ions per division, 500 ions per positive electron, and a solid angle of $4\pi/4$, we get a yield of 1 per 2×10^{10} incident deuterons. The probable error is, however, greater than for the electrometer measurement above since in the latter case the absolute sensitivity of the instrument is accurately known.

Finally using a tube counter with a 6-mm diameter window covered with cellophane on a 50 percent gauze, we observed 16, 33 and 43 counts per minute per microampere, with the activated carbon disk at 10, 4 and 2 cm, respectively, from the window. At the closest position our amplifier was obviously paralyzed (improvised output circuit), but the 10- and 4-cm positions give yields of 1 per 3×10^9 and 1 per 5×10^9, respectively, in rough agreement with the above observations as well as those of the Cavendish Laboratory. However, since in our counter observations the inverse square law is clearly not obeyed, and an indefinite but considerable fraction of the counts was produced by annihilation radiation, which was not corrected for, they are probably no more accurate than the

other determinations, so the original yield of 1 per 10^{10} will be retained as our value until a more quantitative estimate can be made.

Capture radiation

An important question in connection with the reaction $C^{12}+H^1 \rightarrow N^{13}+h\nu$ which is the most probable in this case is the detection of the gamma-rays indicated. Observations on this radiation, which we had assumed would be too weak to measure, were obtained in a control run during $(Li+H^1)$ observations. To insure that the resonance gamma-rays from lithium, occurring at nearly the same voltage as the carbon resonance, were not due to carbon contamination, the thin lithium target was replaced by a solid graphite target, with the result for thick targets of C and SiO_2 bombarded with 4.4 microamperes of protons as shown in Fig. 6. From these observations it appears that there is a very small effect of less than 0.1 division per minute which may be ascribed to the "capture" radiation. Since there should be one quantum emitted per capture, and the number of captures is fairly well established as of the order of one capture per 10^{10} incident protons, it should be possible to obtain a check on this process. For a current of 4.4 microamperes of protons to a solid carbon target we should expect, therefore, approximately 3000 quanta per second. A comparison of this expectation with the observed discharge rate of 0.1 division per minute can be obtained by the following crude but plausible assumptions:

(1) That the capture radiation is predominantly of high energy as deduced from the energy balance of the equation, giving essentially the same discharge rate through 1 cm of lead as through 3 cm, and that it has an ionizing power equal to that of the hard quanta from radium.

(2) That for radium the ratio of hard quanta to the total number is given approximately by the ratio of the measured discharge rates through 3 cm of lead and through about 3 mm of glass, respectively.

(3) That a measurement for radium at 25 cm can be adjusted to a target distance 10 cm by the inverse square law without introducing appreciable errors.

By assumption (3) we get a value of 15 divisions per minute for 1 mg radium at target distance through 3 cm of lead. By assumption (2) we obtain a ratio less than 1/23 for hard to total quanta under the conditions of our experiment. Finally, taking 7×10^7 as the total number of quanta emitted from 1 mg of radium, we get 0.1 division per minute $\leq$20,000 quanta per second, to be compared with the 3000 quanta per second which was to be expected. There is thus a fair agreement as to the order of magnitude of the effect and we believe this can be taken as further evidence for the reality of the capture-process. The effect here observed is too small to justify attempts to improve the measurements, especially since much more intense ion beams will soon be available.

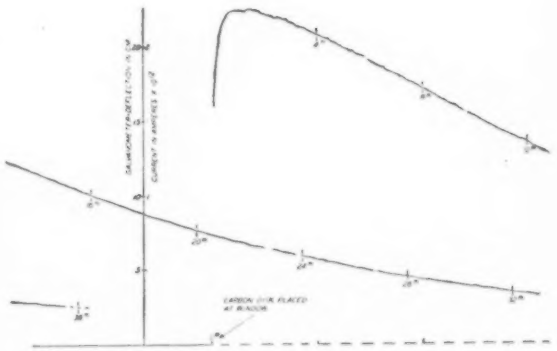

FIG. 7. Decay curve for $(C+D)$ radioactivity.

Decay periods

Numerous measurements have been made of the decay periods of both the $(C+H^1)$ and $(C+D^2)$ effects, but the values obtained fluctuate too much to permit any accurate value to be given. In our experience tube counters are found to show an apparently increased sensitivity after short periods of fast counting which gradually settles down to the normal value, thus giving a spurious decay even for sources presumably constant. Our best values are those obtained from photographic records taken with the vacuum tube electrometer of which an example is given in Fig. 7. This curve for $(C+D^2)$, which was started within three minutes after activation, gives a half-period of 10.2 ± 0.5 minutes by a least-square adjustment.

Equally good determinations have been obtained from other records, but the values often fell outside the limit of errors for previous measurements. For example, from a record on

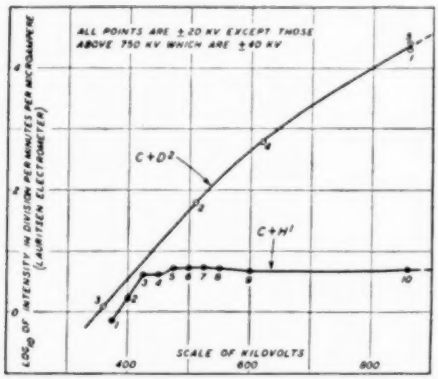

FIG. 8. Excitation function for induced radioactivity from carbon.

another target begun an hour after activation a value of 11.1 ± 0.3 minutes was obtained. This value is the highest we have observed, all of the others falling between 10 and 11 minutes, so that on the basis of all of our measurements we would give 10.5 ± 0.5 minutes as a present estimate of the decay period for the radioactive substance produced in this reaction. The reason for the fluctuations is not known, but may be connected either with a slow escape of the radioactive gas or with the presence of some contamination with a longer period.

The $(C+H^1)$ period appears to be the same as that for deuterons within the limits of accuracy of our measurements.

These results are in agreement with the values for the decay period of radio-nitrogen produced from boron by alpha-particle bombardment as given by recent work.[4]

Excitation function for $(C+D^2)$

The results obtained for $(C+D^2)$ are shown, compared to the $(C+H^1)$ effect, in Fig. 8. As in the case of $(C+H^1)$, the intensity was measured by means of the Lauritsen electroscope, waiting for the activity to decay until a convenient discharge rate was obtained, and then calculating the initial activity using a half-period of 10.5 minutes, as determined above.

The curve for $(C+D^2)$ shows a continuous rise which is approximately exponential throughout the voltage-range covered, in contrast to the resonance for $(C+H^1)$. This difference may

[4] C. D. Ellis and W. J. Henderson, Nature **135**, 429 (1935); H. Fahlenbrach, Zeits. f. Physik **94**, 607 (1935).

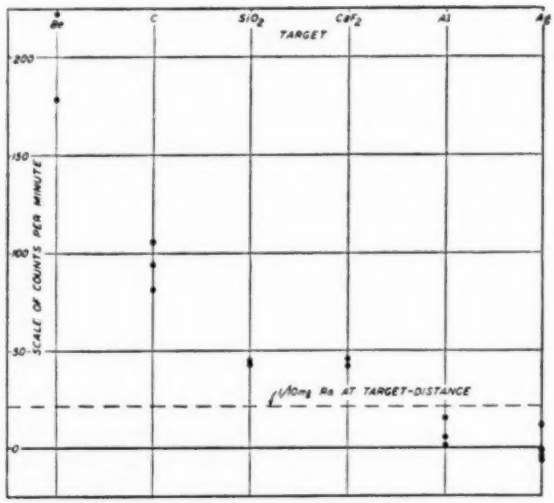

FIG. 9. Gamma-rays by $\sim 0.5\mu$A of $\sim$1200-kv deuterons with 1/2-inch lead shielding (April 1934).

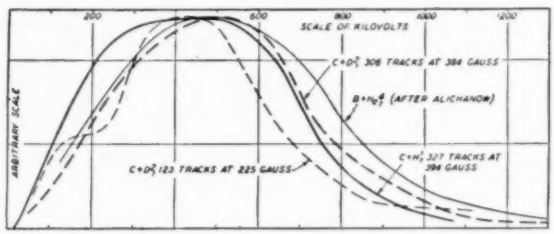
SCALE OF KILOVOLTS
ARBITRARY SCALE
C+D² 306 TRACKS AT 394 GAUSS
B+H² (AFTER ALICHANOW)
C+D² 123 TRACKS AT 225 GAUSS
C+H² 327 TRACKS AT 394 GAUSS

FIG. 10. Energy distribution of positrons.

account for the observation reported by Cockcroft, Gilbert and Walton[3] that a carefully cleaned target (therefore, thin film of contamination) bombarded at 550 kv gave 300 counts per minute for deuterons but no observable effect for protons of this energy which is above that for resonance.

From the ratio of the two effects at 900 kv and the known yield for protons one gets immediately an efficiency of about 5 in 10^7 for the deuteron reaction involving the production of N^{13}.

Gamma-rays from $(C+D^2)$

By a comparison of the intensity of the radiation from $(C+D^2)$ with that from radium as measured by the Lauritsen electroscope through one-half inch of lead, we obtained a value of about 2 mg radium equivalent per microampere of deuterons at 900 kv. This agrees well with the high value we reported at the Washington meeting of the American Physical Society in April 1934, based on Geiger tube counter obser-

vations as shown in Fig. 9. A rough estimate of the yield from these observations is of the order of one disintegration per 10^6 incident deuterons. Accurate estimates are difficult due to the presence of neutrons.

Energy distribution of positive electrons

Measurements on the energy distribution of the positrons emitted from an activated disk have proved to be time consuming, for relatively few of the tracks photographed are measurable. By measuring only the best tracks, different observers here were able to get repeatable results on any single run, but so few tracks were obtained that the statistical fluctuations were very large and successive runs would give contradictory results. Pending the acquisition of a sufficiently large number of measured tracks to eliminate statistical "humps," the best representation of our present results is perhaps given by a summation of all of our observations on all measurable tracks, smoothed by the usual formula $(a+2b+c)/4$. Such curves are given in Fig. 10 in which the curve of Alichanow[5] for radio-nitrogen is included for convenient comparison.

III. Other Resonance Transmutations Under Proton Bombardment

Gamma-rays from (Li+H¹)

The existence of resonance in the (C+H¹) reaction suggested that a similar behavior might be expected in other proton reactions. The (Li+H) reaction was particularly interesting in view of the failure of Oliphant and Westcott[6] to observe gamma-rays at 400 kv where the workers at the California Institute of Technology at Pasadena had found an easily observable effect at 600 kv. The probable existence of a resonance for this reaction had been suggested by Lauritsen at the Berkeley meeting.

In order that direct comparisons with results of both the Cambridge and Pasadena investigators might be possible, preparations were made to observe simultaneously with the Lauritsen electroscope and a Geiger-Müller tube counter

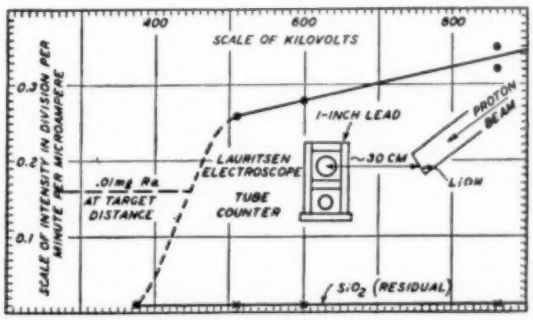

FIG. 11. Excitation function for gamma-rays from Li+H¹, January 11, 1935.

(2×10 cm), as shown in the sketch in Fig. 11. After parallel observations had been obtained at the two lowest points on the curve, a breakdown occurred in the tube counter amplifier so that a complete comparison could not be obtained. However, the following figures for 510 kv will give an indication of the relative sensitivities. For 5.5 microamperes of protons on SiO_2 the electrometer gave 0.1 division per minute and the counter 30 impulses per minute. For the same current on LiOH, the electrometer gave 1.4 divisions per minute compared to 210 for the counter. The residuals with the high voltage cut off were 0.05 division per minute and 10 counts per minute for the electroscope and counter, respectively. The effect was therefore easily observable with either detecting instrument. As may be seen from Fig. 11, the magnitude of the effect is roughly 0.02 mg radium equivalent per microampere of incident protons, which is within a factor of two of that reported by Lauritsen in his original observations.

A thin target curve for the gamma-rays from (Li+H¹) was given in our letter showing a sharp resonance at 450 kv and a suggestion of a second resonance at a higher voltage. A more complete curve verifying the existence of the second resonance at about 850 kv has now been obtained and is shown in Fig. 12.

Alpha-particles from (Li+H¹)

If the energy of the gamma-rays is deducted from total energy available in the (Li+H¹) reaction, the remainder should give the energy of any alpha-particles which might be emitted. Two strong gamma-ray components have been reported from Pasadena for the (Li+H¹) reac-

[5] Alichanow, Zeits. f. Physik **93**, 350 (1935).
[6] Oliphant and Westcott, Int. Conf. Phys., London, 1934, p. 144.

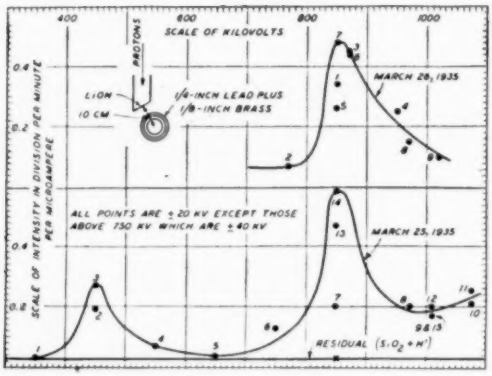
SCALE OF KILOVOLTS
PROTONS
LION
10 CM
1/4-INCH LEAD PLUS
1/8-INCH BRASS
MARCH 28, 1935
MARCH 25, 1935
ALL POINTS ARE ± 20 KV EXCEPT THOSE ABOVE 750 KV WHICH ARE ± 40 KV
RESIDUAL (S, O2 + H1)
SCALE OF INTENSITY IN DIVISION PER MINUTE PER MICROAMPERE

FIG. 12. Excitation function for gamma-rays from $Li+H^1$.

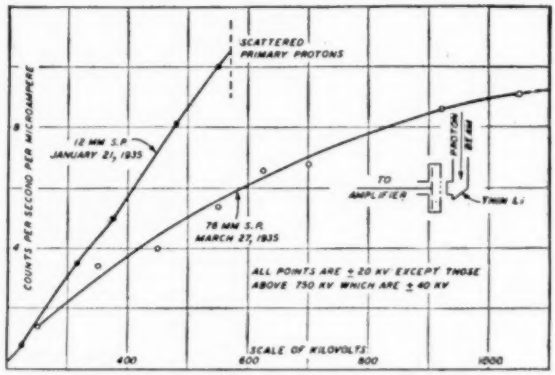
SCATTERED PRIMARY PROTONS
18 MM S.R. JANUARY 21, 1935
76 MM S.R. MARCH 27, 1935
TO AMPLIFIER
PROTON BEAM
THIN Li
ALL POINTS ARE ± 20 KV EXCEPT THOSE ABOVE 750 KV WHICH ARE ± 40 KV
SCALE OF KILOVOLTS
COUNTS PER SECOND PER MICROAMPERE

FIG. 13. Excitation function for alpha-particles from very thin $Li+H^1$.

tion,[7] either of which might be associated with the 450-kv resonance. Efforts to find either of the two predicted alpha-particle groups were unsuccessful, as were efforts to detect the emission of beta-particles either during or subsequent to the bombardment. From these observations we must conclude that if alpha-particles are emitted, their range must be less than 9 mm and the gamma-radiation therefore must be of greater energy than 14 MEV. This is in agreement with later observations by Crane and Lauritsen.[8] Corresponding observations have not yet been made at the 850-kv resonance point.

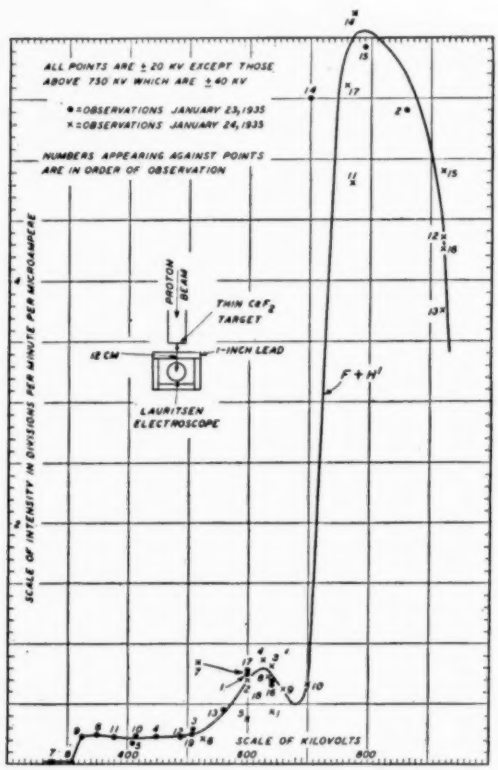
ALL POINTS ARE ± 20 KV EXCEPT THOSE ABOVE 750 KV WHICH ARE ± 40 KV
●=OBSERVATIONS JANUARY 23, 1935
×=OBSERVATIONS JANUARY 24, 1935
NUMBERS APPEARING AGAINST POINTS ARE IN ORDER OF OBSERVATION
PROTON BEAM
THIN CaF2 TARGET
12 CM
1-INCH LEAD
LAURITSEN ELECTROSCOPE
F + H1
SCALE OF KILOVOLTS
SCALE OF INTENSITY IN DIVISIONS PER MINUTE PER MICROAMPERE

FIG. 14. Excitation function for gamma-rays from fluorine (moderately thin target).

Having satisfied ourselves that no new alpha-particle group appeared at the 450-kv resonance, we investigated the variation of the known groups with voltage. Fig. 13 shows the curves obtained for the very thin LiOH target previously used in the gamma-ray resonance observations. It will be noted that neither of these curves shows any discontinuity at the resonance voltages, so that the corresponding alpha-particle groups must be due to completely independent processes.

It is also of interest to remark that for this very thin lithium target the yield for the long range particles is still rising at 1000 kv, in disagreement with the early results reported by Henderson[9] which indicated that the top of the potential barrier for this process was about 400 kv.

Gamma-rays from $(F+H^1)$

Observations were made on two days only on the $(F+H^1)$ reaction, but the results are sufficiently significant to report at this time. In Fig. 14 the readings obtained on a Lauritsen electroscope placed 12 cm from the target and shielded with one inch of lead are plotted against the accelerating voltage. The most correct interpretation will be obtained by noting the sequence of points, for, while small increments of voltage in a

[7] Crane, Delsasso, Fowler and Lauritsen, Phys. Rev. **46**, 531 (1934).

[8] Crane and Lauritsen, Phys. Rev. **47**, 420 (1935).

[9] Henderson, Phys. Rev. **43**, 98 (1933).

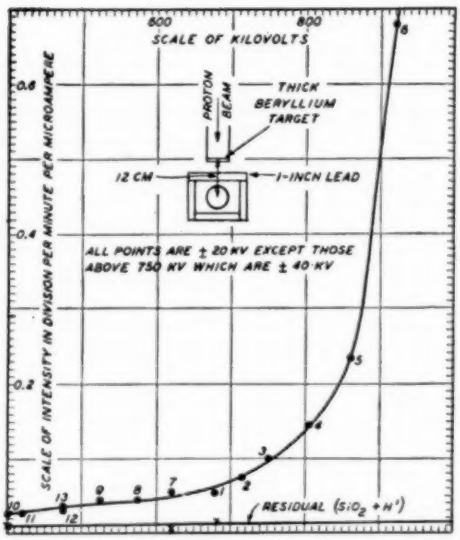

FIG. 15. Excitation function for gamma-rays from $Be+H^1$.

single sequence have proved to be dependable, any large changes in voltage depend on the absolute voltage scale and are less accurate. Thus several resonance voltages are clearly shown, although the absolute voltages for the resonance lines are not well determined.

A rough indication of the intensity can be obtained from the radium calibration cited above, namely, one mg radium at 10 cm gives 15 divisions per minute through 3 cm of lead. Note, however, that the points plotted are for a "moderately thin target," which is thick for 500-kv protons, but thin for 900-kv particles as shown by the curves.

Gamma-rays from ($Be+H^1$)

While this does not appear to be a resonance process, such observations as we have made may well be reported at this time. These are given in Fig. 15. The experimental conditions were the same as for the fluorine observations, except that a thick target was used. The beryllium was known to contain one percent iron, with other impurities under 0.05 percent.

ACKNOWLEDGMENT

We are grateful to Professor Lauritsen for the electroscope he very kindly sent us, which has proved to be exceedingly convenient in this work. We also wish to thank Professors Breit and Gamow for their enthusiastic interest in the problem of radiative capture, and Messrs. Brown and Dahl for invaluable technical assistance.

AUGUST 15, 1935 PHYSICAL REVIEW VOLUME 48

High Voltage Technique for Nuclear Physics Studies

M. A. TUVE, L. R. HAFSTAD AND O. DAHL, *Department of Terrestrial Magnetism, Carnegie Institution of Washington*

(Received June 10, 1935)

A description is given of experiments at the Department of Terrestrial Magnetism, Carnegie Institution of Washington, during four years in which two electrostatic generators and several multiple-section high voltage tubes have been used for the production of high speed protons and deuterons, as required for studies of nuclear transmutations. A 1-meter diameter generator of the type designed by Van de Graaff reaches usable steady potentials up to 600 kilovolts (positive). A generator comprising concentric 1-meter and 2-meter shells, charging current 0.75 milliampere, reaches practical limitations at 1300 kilovolts (positive) in a special room of large size. Voltages below the maximum are steady to within several percent. Details of design and operation are discussed.

Multiple-section high voltage tubes of the Coolidge "cascade" type, giving complete focusing of positive ion currents of 20 microamperes at voltages up to 1200 kilovolts, offer no difficulties in construction or operation. No reasons have yet appeared for expecting any special troubles if this technique were to be extended to much higher voltages and currents.

A. INTRODUCTION

IN response to numerous requests for a comprehensive description of the high voltage technique which has been developed during a period of years in the Department of Terrestrial Magnetism of the Carnegie Institution of Washington[1] and which has been used for studies of

[1] The development of these experiments is described chiefly in the Annual Reports of the Department of Terrestrial Magnetism of the Carnegie Institution of Washington, 1926 to date. Early work is covered by: G. Breit, M. A.

atomic nuclei, this paper presents the more important features of our past experience and the details of our present technique. Although the latter is in many ways imperfect and in process of refinement, it has proved effective and useful, and it is hoped that the concrete presentation of our experiments may be of assistance to other laboratories now initiating similar researches in this field.

With the discovery by Cockcroft and Walton[2] that various transmutation effects actually occur when particle-energies well below one million electron volts are used, the early high voltage objective here and elsewhere of obtaining true nuclear transmutations by artificial means, without special regard to the processes involved, was superseded by an increasing necessity for care in obtaining and interpreting such observations. This is particularly true in view of the importance of impurities, the complexities introduced by the discoveries of neutrons, positrons, and induced radioactivity, and the complications which result from marked differences in the excitation functions for various effects as the energy of the primary particles is altered. We feel that it is desirable, and perhaps even necessary, to work out in fair detail the nuclear reactions of a few light elements, accessible to investigation with moderate particle energies, before the more complex studies using very high voltages may safely be attempted, especially in view of the numerous reaction equations which may be written and the general failure of these to balance when using the accepted mass values.* This mitigates somewhat our initial disappointment over the failure of our equipment to actually attain the voltages indicated in our preliminary tests.

Although our equipment in its present form does not give an extremely high and steady peak voltage, it has many excellent characteristics in the voltage range up to 1000 kilovolts, and constitutes at least one approach toward the ideal of an artificial source of high energy ions, uniform in speed, direction and kind, and under control as to energy and intensity between wide limits. The ultimate desirability of such a source cannot be questioned. The initial adoption of a highly analytical experimental technique, avoiding various averaging effects which tend to obliterate critical features of the data, has led almost immediately in most of our observations to the recognition that the effects are complex and that detailed examination is required.

By reason of the exponential importance of ion velocity and of atomic numbers, and because of the great variety of processes which can and do occur, thin target results with "monochromatic" ion beams seem almost essential for the correct interpretation of thick target observations, especially if the latter are obtained with ion beams heterogeneous in speed and kind. The combination of a constant potential source and a focusing type high voltage tube with magnetic analysis at the target therefore has important advantages over some other types of equipment for this work. We can well testify to the practical aspects of the question from our experience with spark excited Tesla coils.[3] The fluctuating voltage output of the latter, and especially the extreme requirements placed on the ion source and on the time resolution of the detecting instruments (for quantitative results) by the short duration of its peak voltage caused us to abandon the Tesla coil after it had served inexpensively for the development of tubes withstanding extreme voltages and for the demonstration of artificial beta, gamma, proton and deuteron "rays" of energies above one million volts.[4] Its application to transmutation-studies was not seriously attempted, because of the obvious dangers of being misled when using such an unsuitable and erratic voltage-source, and the cost of modifying the Tesla-coil method to minimize these objections.[5] The equipment here described avoided

Tuve and O. Dahl, Phys. Rev. **35**, 51 (1930); M. A. Tuve, G. Breit and L. R. Hafstad, Phys. Rev. **35**, 66 (1930). Subsequent experiments are described in the columns of Letters to Editor of Phys. Rev., 1930, 1931, 1932, 1933 and 1934, and in the following: J. A. Fleming, Science **77**, 298 (1933); M. A. Tuve, Proc. Internat. Elec. Cong., Paris **2**, 915 (1933); M. A. Tuve, J. Frank. Inst. **216**, 1 (1933).

[2] Cockcroft and Walton, Nature **129**, 649 (1932); Proc. Roy Soc. **A137**, 229 (1932).

* The situation is now much more satisfactory as a result of the adjustment of the mass scale made by H. A. Bethe (see Phys. Rev. **47**, 633 (1935); also M. L. E. Oliphant, A. E. Kempton, and Lord Rutherford, Proc. Roy. Soc. **A150**, 241 (1935)).

[3] Tuve, Hafstad and Dahl, Phys. Rev. **39**, 384 (1932).

[4] Carnegie Inst. Wash., Year Books, No. 28, 214 (1929); No. 29, 256–259 (1930); No. 30, 290 (1931); No. 31, 229–233 (1932); M. A. Tuve, L. R. Hafstad and O. Dahl, Phys. Rev. **37**, 469 (1931); **38**, 580 (1931).

[5] D. H. Sloan, Phys. Rev. **47**, 62 (1935).

these difficulties and was built and installed at a moderate cost. It has its limitations, some of them both troublesome and disappointing, and we would be glad to embrace the unquestioned advantages obtainable with a well-designed and expensive constant-potential source of voltage more conventional type for the rather limited range available with our present equipment, but many investigators undoubtedly will be encouraged by the fact that this type of nuclear-physics work is possible, to a voltage limit chiefly determined by the space available, at relatively small expenditure.

B. Electrostatic Generators

(a) Preliminary tests

The limitations of the spark excited Tesla coil had been recognized from the first, but its use in this laboratory was continued until 1931 because no other form of voltage source for potentials of the order of a million volts was accessible to us on the funds available for this work. However, immediately following the construction by Dr. R. J. Van de Graaff of the first example of his simplified form of electrostatic generator,[6] cooperative tests were made in this laboratory in which his original 2-foot generators were used[7] to ascertain that a very high constant potential could be applied without difficulty to the multiple-section tubes we had been using with the Tesla coils. We then undertook here to test the prediction that the attainable voltage with such a generator should be proportional to the diameter of the conducting sphere or shell, by constructing a two-meter generator and observing its performance by means of a generating voltmeter,[8] as the next step in the development of such generators. No suitable housing was available, and the tests were carried on outdoors.[7] Because of flying bugs, lint and other debris electrostatically attracted to the sphere, difficulty was encountered in obtaining a trustworthy measure of the peak voltage and voltage steadiness attainable, but during short periods after cleaning the sphere steady potentials (±3 percent) well in excess of 2000 kilovolts were indicated by the generating voltmeter. The latter was calibrated *in situ* by the application of a known voltage (60 kv) to the generator shell. Since the theoretical voltage limit for this two-meter sphere (giving a field strength of 30 kv per cm at the surface) is about 3300 kilovolts, these observations apparently verified the spark-gap measurements made with the original (2-foot) generators, which had indicated that 60 percent of the theoretical limiting voltage could be attained. We now know this result to be in error, as described below, because the presence of corona makes both the generating voltmeter and the spark-gap indicate higher than the true voltage, the highest actual voltage attainable in practice, according to our subsequent experience with both one-meter and two-meter generators, being only about 35 percent of the theoretical maximum when the sphere potential is positive in sign. In these outdoor experiments most of the measurements were made with the sphere potential negative, since this sign gave less trouble from unsteadiness and the peak voltage appeared to be about the same for either sign of charge. A charging current of 90 microamperes was obtained with a silk and rayon belt 6 inches wide, traveling 6000 feet per minute inside the 20-inch diameter Textolite cylinder used for support. This arrangement protected the belt from deflection by winds, and allowed humidity control by heating, as was necessary on several occasions for good belt insulation. Charge was sprayed on the belt by the corona from a 5-mil tungsten wire connected to a 40-kilovolt kenotron rectifier, and a current doubling arrangement[6] was used inside the sphere. It was interesting to find that after the Textolite support had been baked and coated with paraffin (it was supplied at our request without this customary protection) an indicated potential exceeding 1000 kilovolts was obtainable when the belt was manually operated at about 20 feet per minute. The maximum voltage attainable with this set-up was usually limited by heavy sparks down the Textolite cylinder to ground. These "lightning bolts" splintered the redwood base parts in impressive fashion. Various efforts to adjust the voltage gradient and thus prevent the violent sparking, by means of high resistance leaks

[6] Van de Graaff, Phys. Rev. **38**, 1919 (1931); Van de Graaff, Compton, Van Atta, **43**, 149 (1933).

[7] Photographs reproduced in J. Frank. Inst. **216**, 26 (1933).

[8] P. Kirkpatrick and I. Miyake, Rev. Sci. Inst. **3**, 1 (1932); R. Gunn, Phys. Rev. **40**, 307 (1932); J. E. Henderson, W. H. Goss and J. E. Rose, Rev. Sci. Inst. **6**, 63 (1935).

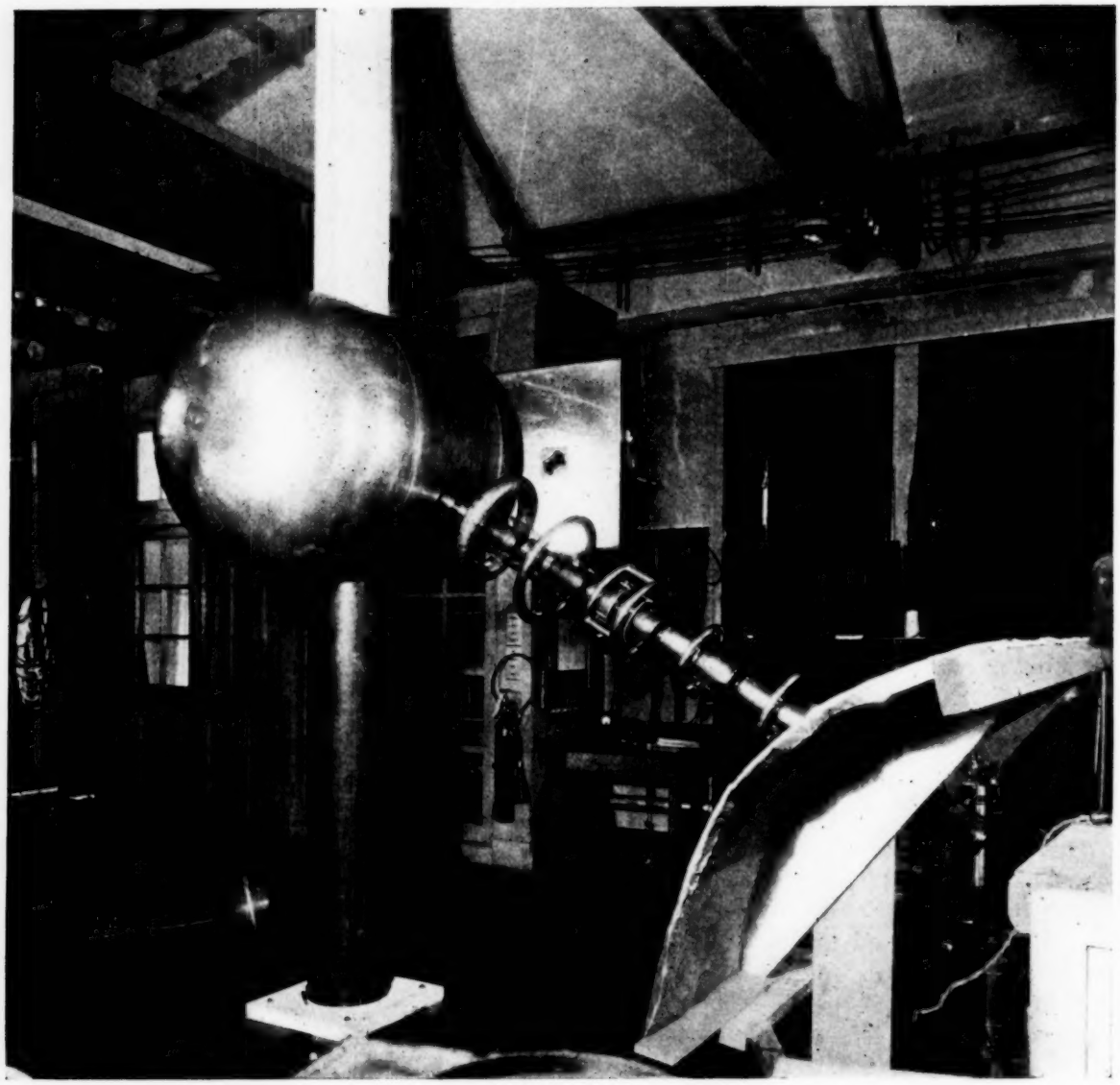

FIG. 1. One-meter electrostatic generator with six-section cascade tube.

applied to the Textolite cylinder, were unsuccessful.

Because of meteorological interference it was not feasible to attempt proton bombardment of targets with this outdoor equipment, although an indicated steady potential of 1000 kilovolts was applied without internal discharge or breakdown to a 34-section tube 9 feet long, comprised of two tubes previously used under oil with the Tesla coils, pumped to a pressure of 1/4 bar.[7]

(b) One-meter generator, construction

Lack of housing prevented further immediate use of the two-meter generator, but after some months the removal of the oil tanks used for the Tesla coil experiments gave us laboratory space for the installation (October 1932) of a smaller generator, as shown on Fig. 1. Because of the practicability of a generator of this size in almost any laboratory, a fairly detailed description of our experience with it will be given here. Two hemispherical shells one meter in diameter (drawn or spun aluminum shells are obtainable in various sizes from the Aluminum Company of America, Pittsburgh, Pennsylvania) are fitted to a short cylindrical section (see Fig. 2) which contains the pulleys, the collector

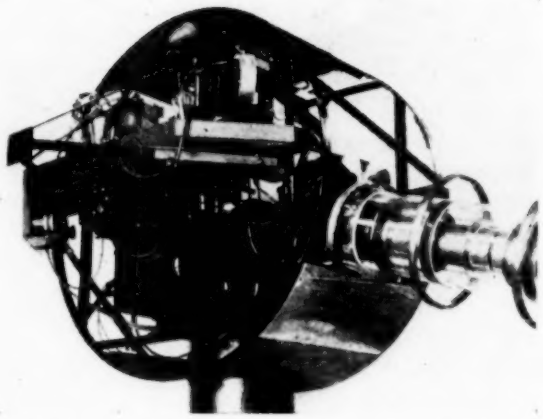

FIG. 2. Construction and interior arrangements of one-meter generator, showing equipment and controls for ion source.

comb and spray wire for current doubling, and the alternating-current and direct-current generators, transformers, controls and hydrogen supply for the ion source which is attached to the high voltage end of the tube (see section C). A 12-inch silk and rayon belt running 4000 feet per minute gives 180 to 200 microamperes charging current and drives the ion source generators. To give maximum clearances with the available space the motor and the charging apparatus for the belt were placed overhead some 12 feet above the concrete floor. The 12-inch Textolite cylinder supports the generator 165 cm above the floor, and other clearances are: Belt length from shell to ground shield 150 cm, tube length 170 cm, minimum distance to grounded shields on rafters 130 cm.

Charging currents. Details of the belt charging arrangements and the shape of the belt openings in the shell are shown in Fig. 3. Numerous efforts were made to increase the charging current, especially when charging the ingoing belt only (for maximum voltage), by means of large and small shield or guard electrodes placed in various positions with respect to the spray wire, and held at either ground or spray wire potential. Temporary improvement apparently was obtained with various positions of shield, but for undetermined reasons the current would revert to the old value in a day or less, after which removing the shield made little change, and it might even appear to be of value in some new position. A theoretical maximum of 660 microamperes would be obtained if the surface

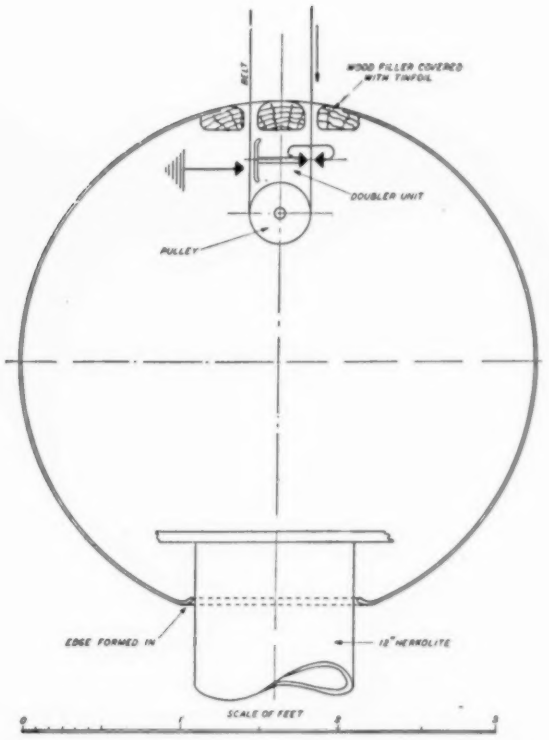

FIG. 3. Detail of openings for charging belt and support column—one-meter generator.

charge on each side of the belt, both when entering and when leaving the sphere (four surfaces), were such as to give an electric field of 30 kilovolts per cm (5.3×10^{-9} coulomb per cm^2, for a belt charged on each side to breakdown value). The charging current was measured with the sphere at ground potential, and may be less when the sphere is at high voltages, especially because of corona to the negatively charged belt leaving the positively charged sphere. When using the "doubler" (negative charge sprayed onto belt leaving the sphere) the charging current measured 170 to 200 microamperes (usually 180), and when charging the ingoing belt only the current was usually about 65 microamperes, although in wet weather it dropped as low as 50 and for short periods (after changing shield-arrangements) it reached 85 microamperes. The fact that the "doubler" always more than doubles the current is an indication that a simple comb fails to discharge the belt completely inside the sphere, so that without the negative spray the belt still carries a small positive surface charge as it leaves.

From measurements made with the generating voltmeter at reduced charging currents (reduced spray voltage) it appears that nearly the same maximum voltage is reached as with full charging current, indicating that most of the charging current is actually available for use on the high voltage tube, except near maximum voltage, where the corona losses increase very rapidly with small changes in voltage.

Voltage limits. Much interest attaches to the maximum voltage attainable with a generator of given dimensions. During the period November 1932 to June 1933 it was found that this one-meter generator reached approximately 500 kilovolts under most weather conditions (400 kv with continued high humidity), 550 kilovolts frequently, and probably as high as 600 kilovolts in dry weather. Maximum voltage was obtainable only when the current doubling device was not used, that is, when charging the ingoing belt only. With the outgoing belt charged negatively (current doubled) very strong corona from the edges of the belt opening in the sphere, due to the increased electric field strength arising from the negative belt charge, reduces the maximum voltage by 50 to 100 kilovolts in spite of the increased charging current. If the positively and negatively charged belts were very close together, this effect should be decreased. In special tests seeking the highest possible voltages (in an effort to demonstrate conclusively the emission of neutrons from helium ions bombarding beryllium) steady potentials as high as 700 kilovolts were apparently obtained for short times, but we regard this figure as too optimistic. For these peak voltage efforts a number of paraffin coated micanite sheets were distributed over various projections and in other positions in the room to reduce the field strength (reduce or eliminate corona) in their vicinity by picking up surface charges and redistributing the field in the direction of greater uniformity. The only item of these tests retained as a permanent feature was a micanite sheet (a paraffin coating is essential) supported on four redwood sticks at the midpoint of the Textolite column. This arrangement eliminates the serious corona (with frequent "lightning bolts") down the column, which is probably due to the large hole (12 inches in diameter) in the conducting shell, and the nearness of the floor.

When the weather was dry and the doubler was not used, the maximum voltage attainable was limited by sparks from the polished spherical surfaces, out into space or toward surrounding objects, indicating that the field at many points on the generator shell reached breakdown value. Whether this was due to the building up of space charge in the vicinity of the sphere or to surface irregularities, which caused local fields three times the average (for a surface having a 1-meter curvature), was undetermined. When the humidity was high, the attainable voltage was limited by heavy sparks up the belt or down the Textolite support. A series of efforts to prevent the latter by providing a high resistance leak to grade the potential down the Textolite was again without success; a close wrapped helix of rubber tubing containing alcohol (adjusted to a leakage of about 10 microamperes at half-voltage) was effective for a few minutes, but on going to full voltage a single heavy spark split the rubber in many places. This type of failure has been true of every effort we have made toward resistance grading of the potential along an insulator; voltage grading by means of corona points between a succession of shields, as on our cascade tubes, appears to be the only reasonable method.

Exact knowledge of the voltage was not essential to the validity of the chief series of experiments for which this generator was used early in 1933 (demonstration that the apparent disintegrations of medium and heavy elements were due to contamination, probably by boron[9]), but the generating voltmeter at 550 kilovolts indicated about 15 percent higher than a rough voltage calibration by magnetic deflection of the high speed protons. Efforts to measure the range of the protons gave values in the same region, but these voltage values were open to question both because of difficulties with foils (metal foils, melted in vacuum, punctured when supported against atmospheric pressure by grids and gave evidence of thin spots; mica windows collected high surface and volume charges and

[9] M. A. Tuve, L. R. Hafstad and O. Dahl, J. Wash. Acad. Sci. **23**, 530 (1933); Phys. Rev. **43**, 942 (1933); **43**, 1055 (1933).

promptly split, etc.) and because of the uncertainty which still exists concerning the range voltage relation for protons near 500 kilovolts. Blackett and Lees[10] give 11.5 mm as the range of a 500-kilovolt proton, whereas Cockcroft and Walton[11] would place this range at about 8.5 mm. Our figures indicated a value between these extremes, and in our work to date we have tentatively the value 10 mm as the range for 500-kilovolt protons (28.5 mm for 1000-kilovolt protons).

It is thus indicated by these experiments, as well as by our later experience with the two-meter generator installation, that positive potentials exceeding 600 kilovolts should not be expected from a generator of this type which approximates a one-meter sphere. The question as to the optimum size of generator for reaching the maximum possible voltage in an available space of given dimensions cannot be answered from our experience. However, we found that this one-meter generator reached practically the same maximum voltage (550 kv) when a flat metal wall (lead foil on Celotex—far from smooth) was placed 50 cm distant from one of the hemispherical ends. This indicates that if sufficient extra length can be obtained, diagonally to a corner or otherwise, for the belts and the insulating supports (which may be cables), it is probably best to use a conducting shell which might at first thought appear too large for the given room size. How far it is profitable to go in this direction can only be determined by experiment.

(c) Two-meter generator

During the summer of 1933 a special laboratory was completed for housing the reconstructed two-meter generator, which was assembled and ready for first voltage tests early in October. A view of the installation (complete with tube) is shown in Fig. 4, and a schematic drawing of the arrangement of the laboratory is shown to scale in Fig. 5. Fig. 6 shows the construction of the generator, with the pulleys, ion source generators and controls. The advantages of a separate belt driving the ion source generators are well worth the slight additional construction involved.

Construction. In order to gain the numerous advantages of a vertical arrangement of the high voltage tube, a tripod support was adopted for this generator, sacrificing the easy control of the humidity of the belt which was a feature of the original outdoor installation, where the belt was run inside the large cylindrical Textolite support. It was also desirable to provide for a high charging current, and the total belt surface was designed on the basis of our experience with the one-meter generator to give 1 milliampere charging current at full speed (8-inch pulleys at 3600 r.p.m.—"four belts" 20 inches wide as in Fig. 5). It has since developed that with paper belts high humidity is a serious obstacle with this equipment, reducing the charging current by a factor of two or more and limiting the maximum voltage to 800 or even 700 kilovolts by "lightning bolts" down the belts. A more unexpected difficulty was the fact that the high lead content glass used for the tube itself (for partial x-ray shielding) adsorbed a layer of surface moisture when the humidity exceeded 50 or 60 percent (May 1934) and constituted almost a short circuit for the generator, its resistance dropping to a few megohms. A large improvement was effected by applying "Victron" varnish to the belt and tube after drying by heat (successive sections of the tube were heated by the blasts from several electric heater hair dryers), but humidity control is highly desirable and almost essential for a satisfactory installation. The whole generator room might be air-conditioned (very expensive) or the belts and tube could be surrounded by thin walled Textolite tubes to limit the volume of air requiring treatment. We have as yet made no provision for humidity control, as the limitations due to humidity are not serious during seven or eight months of the year.

The various clearances from the generator to the walls are shown by the scale drawing of Fig. 5; the ceiling of the high voltage room is 28 feet above the floor; the latter measures 32 by 36 feet and can ultimately be removed without structural alterations if a rectifier equipment or other possible future installation requires additional head room. The generator itself, shown in Fig. 6, comprises concentric one-meter and two-meter shells, with two sections of the

[10] Blackett and Lees, Proc. Roy. Soc. **A134**, 665 (1932).
[11] Cockcroft and Walton, Nature **129**, 242 (1932).

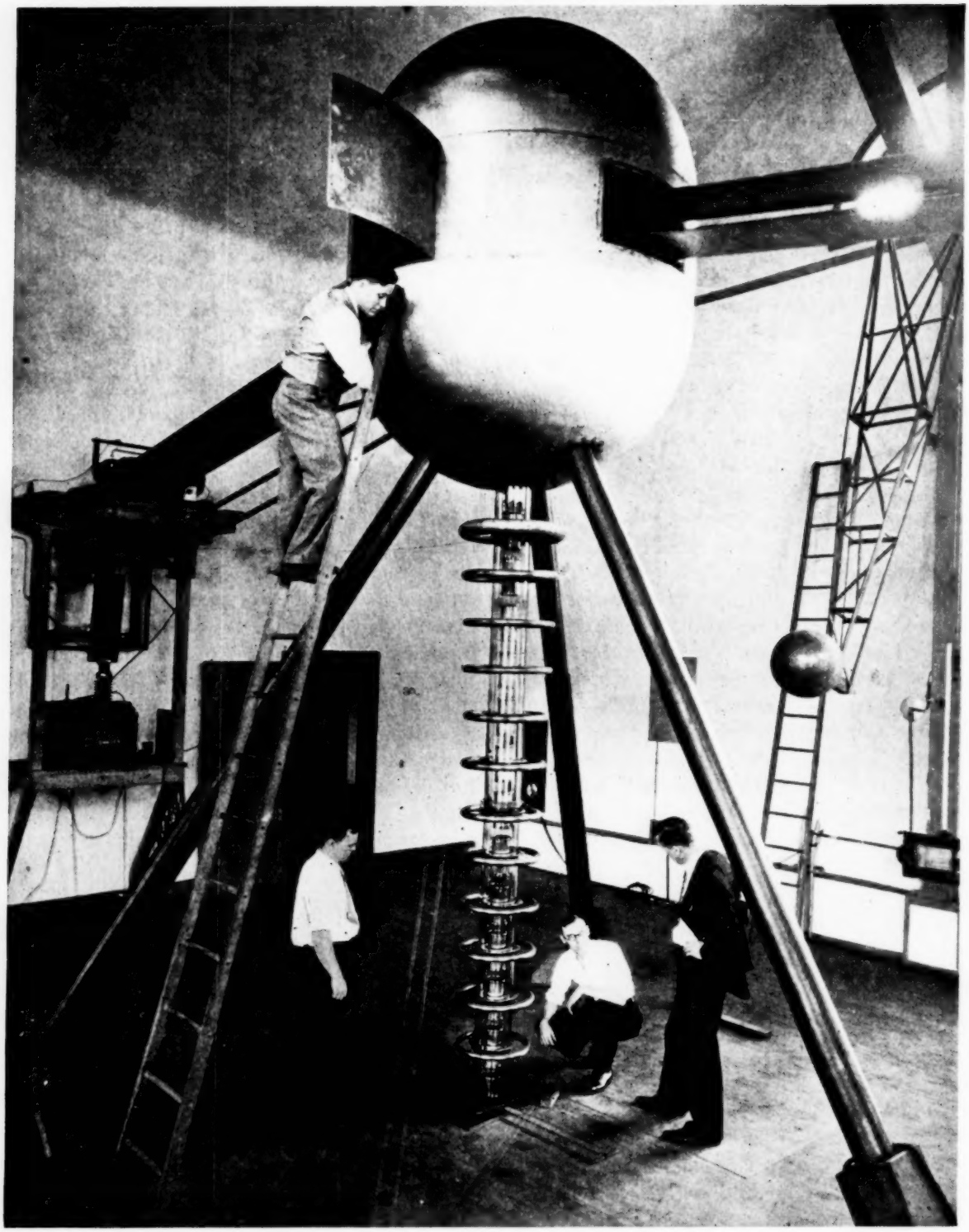

FIG. 4. View of two-meter generator and provisional cascade tube.

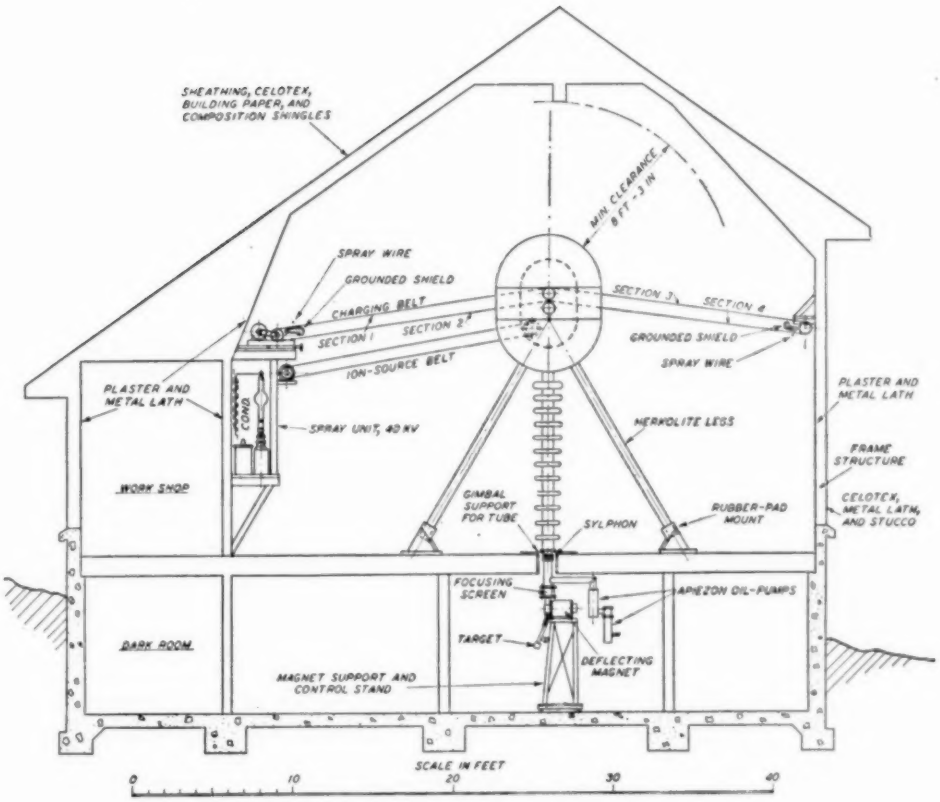

FIG. 5. Section through high voltage laboratory.

high voltage tube installed between the shells, thus giving a total voltage for accelerating the ion-beam which exceeds the maximum voltage of the two-meter shell (above ground) by whatever additional voltage is obtainable between the outer and inner shells. Theoretically, if a constant electric field strength from the outer surface to the center of a system of insulated concentric shells is arranged for by holding the shells at successively higher voltages, one might expect to attain as high a limiting voltage between the center of the system and the outer shell as from the latter to ground (at infinity). As already mentioned, we had failed to observe any large reduction in the maximum voltage on the one-meter generator when a large flat grounded conductor was brought within 50 cm (one radius) of the generator shell. Although trouble due to sparks between outer and inner shells along the belt was anticipated and encountered as a radical limitation with this concentric-shell arrangement, it appeared desirable for at least one interested laboratory to construct such a generator to test its possibilities. The chief value of the inner shell in our experience has been the convenience with which the additional voltage between the shells could be subjected to control by means of variable corona leaks across the two sections of the high voltage tube between the shells, thereby providing control of the electrostatic focusing of the ion beam down the tube and onto the targets. [See section D, below.] We cannot recommend this concentric shell design, however, since the focusing control can be attained inside the larger shell equally well and with much less constructional trouble without the inner shell. The voltage acquired by the collector combs may be utilized, or a transformer and rectifier arrangement could be provided for this purpose.

Voltage limits. The first tests for maximum steady positive potential were made with the generating voltmeter before the tube of this assembly was erected, and gave the surprising result that the outer shell reached a maximum potential of about 1800 kilovolts, steady to 1 or

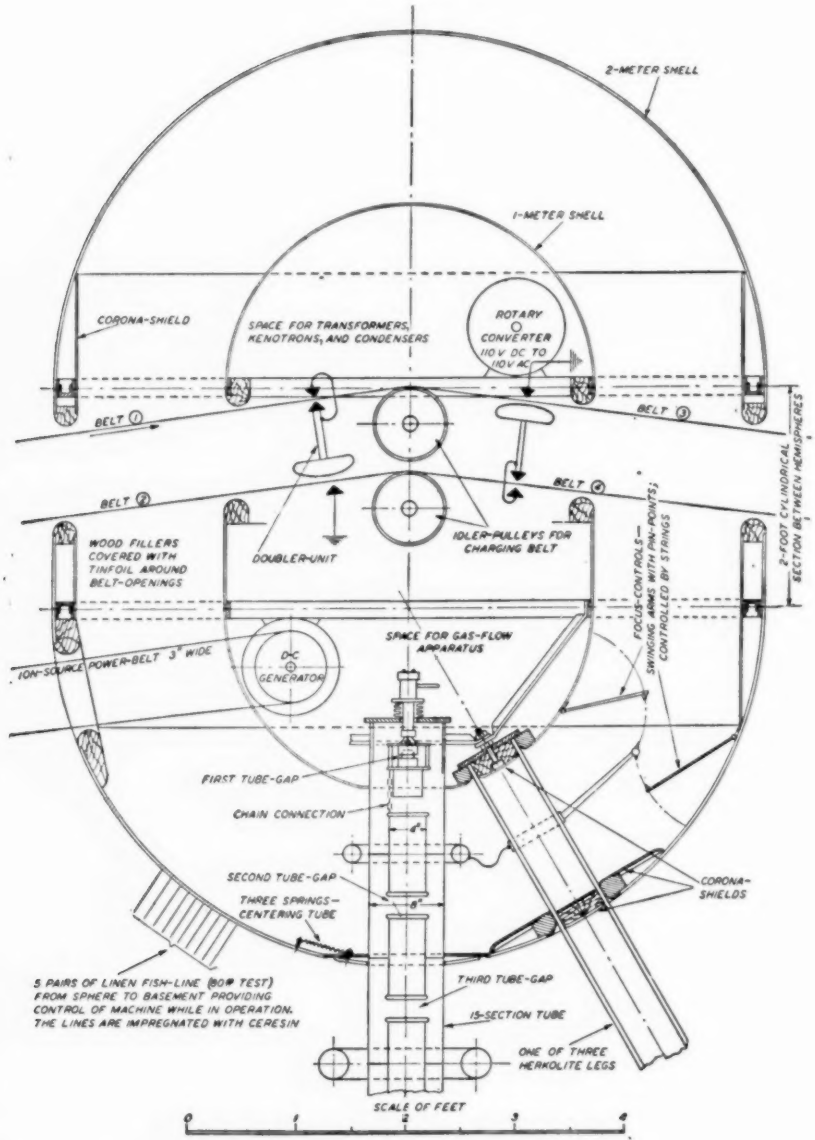
2-METER SHELL
1-METER SHELL
CORONA-SHIELD
SPACE FOR TRANSFORMERS, KENOTRONS, AND CONDENSERS
ROTARY CONVERTER 110 V DC TO 110 V AC
BELT ①
BELT ②
BELT ③
BELT ④
2-FOOT CYLINDRICAL SECTION BETWEEN HEMISPHERES
WOOD FILLERS COVERED WITH TINFOIL AROUND BELT-OPENINGS
DOUBLER-UNIT
IDLER-PULLEYS FOR CHARGING BELT
FOCUS-CONTROLS—SWINGING ARMS WITH PAN-POINTS; CONTROLLED BY STRINGS
ION-SOURCE POWER-BELT 3" WIDE
DC GENERATOR
SPACE FOR GAS-FLOW APPARATUS
FIRST TUBE-GAP
CHAIN CONNECTION
SECOND TUBE-GAP
THREE SPRINGS—CENTERING TUBE
CORONA-SHIELDS
5 PAIRS OF LINEN FISH-LINE (80# TEST) FROM SPHERE TO BASEMENT PROVIDING CONTROL OF MACHINE WHILE IN OPERATION. THE LINES ARE IMPREGNATED WITH CERESIN
THIRD TUBE-GAP
15-SECTION TUBE
ONE OF THREE MERKOLITE LEGS
SCALE OF FEET
0 1 2 3 4

FIG. 6. Details internal arrangements—two-meter generator.

2 percent, instead of the 1200 kilovolts anticipated on the basis of our experience with the one-meter generator. This result prompted a great variety of calibrations and tests, all of which by their internal consistency, especially the proportionality of the generating voltmeter readings to the sphere gap voltages over the range of usefulness of the 50-cm sphere gap, strongly indicated the validity of this not unwelcome result. The high voltage tube was then installed, and, after several weeks spent in obtaining a properly focused and controllable ion spot at the target assembly in the observing room (see Fig. 5), voltage-determinations were made on the high speed ions themselves by their deflection in a calibrated magnetic field and by the range in air (beyond a mica or copper-foil window of measured air equivalent) of the protons in the "mass one spot" (beyond the magnetic analyzer). In spite of the simultaneous indication of a steady potential of 1700 kilovolts according to the generating voltmeter, these two more reliable measures of the voltage indicated a true potential of only about 1000

kilovolts. Since the generating voltmeter is essentially a field strength meter, subject to expected error if used as a voltmeter in the presence of corona and space charge, we accepted the conclusion that our previous measurements with this device were in error, in spite of their internal consistency and our various precautions in the conservative direction. The maximum voltage, measured by proton range, was increased to 1200 kilovolts by the reduction of corona losses and attention to other details, but in spite of prolonged efforts we have never been successful in raising the voltage limit of this two-meter generator above 1300 kilovolts as measured by proton and deuteron ranges at the target assembly. This figure is not an "absolute" upper limit for a generator of this size, but in our installation it is very definitely a practical limit, numerous features reaching their limit at this voltage value, and unless very special efforts are made the maximum voltage is in the vicinity of 1000 kilovolts even in winter.

Under good conditions, compounded of low humidity, good fortune and indefinite other ingredients, the steady voltage reaches a maximum of 1200 kilovolts or slightly higher, and no heavy sparks occur. In darkness heavy corona streamers are seen leaving the rounded edges of the belt holes near the edges of the belts, and other streamers pass between irregularities of the tube shields from section to section, and also out into space. Numerous heavy silk fish lines boiled in paraffin are strung between the controls inside the generator and the operator's position at the targets in the room beneath, and these lines have a tendency to become slightly conducting, with resultant strong corona until the offending lines are boiled again in paraffin or replaced. On a few occasions heavy sparks have passed from the rounded sphere to the slanting ceiling (see Fig. 5), but these sparks are not a major limitation, as are the sparks to the rafter shields and other grounded objects from the one-meter generator (see Fig. 1). Although both generators utilize spun aluminum hemispheres having very smooth outer surfaces, it appears from our experience that great perfection of the generator surfaces is unnecessary and a much rougher sphere can be used if it is cheaper. Decreasing the total charging current from the maximum attainable by a factor of three decreases the maximum voltage only perhaps 200 kilovolts, provided the corona points on the tube are not set so that an unusually large current passes in this way between tube shields, and with the movable "corona control" (see below) removed. Occasionally the 6-inch Textolite (Herkolite) tripod supports have given some trouble at 1200 kilovolts, long "incipient sparks" breaking from the generator shell along their surfaces. Each tripod hole in the shell presents an inward-rounded fillet of 1-inch radius where the support enters, and the metal shell is continued inside the Textolite tube by a metal disk. It appears quite definite that these smaller Textolite supports give much less trouble than the 12-inch and 20-inch holes previously used with similar Textolite supports.

Under poor conditions, which usually appear to be related to high humidity conditions (or a belt which is not thoroughly clean and dry), heavy sparks ("lightning bolts") occur along the positively charged belts to ground. This sparking can usually be reduced or eliminated, with a resultant raising of the maximum attainable voltage (from 800 to 1000 kilovolts, for example) by decreasing the kenotron voltage on the corona spray wires, thus decreasing the charges on the belt. The heavy sparks to ground have nearly always been along the belts, and hence the belt length to ground (12 feet on each side) is evidently too short for high humidity conditions. Minor irregularities in the shell, at the doors and at the joints between hemispherical and cylindrical sections, give no evidence of trouble, as was also found with the smaller generator. It appears, from the relatively infrequent occurrence of sparks over the general surface of the machine, that corona and sparks from the belt openings are the chief limitations of this larger generator, although the generalized limitation by sparks from any point on the shell, observed with the one-meter generator, apparently sets in at about the maximum voltage (1300 kilovolts) which this equipment has been made to give. With the sphere potential *negative*, different behavior obtains; prompt and continuous "lightning bolts" down the high voltage tube (shield to shield—about 5 per second) occur and have deterred us from making voltage

tests with this sign of charge, although if the sphere voltage were reduced by grounded corona points undoubtedly a perfectly satisfactory behavior could be obtained.

Voltage-measurement and control. Measurement of the actual range in air of the protons and deuterons accelerated down the tube was adopted as the most convenient and reliable voltage measure, and has been used in all of our work. This method is extended to the lowest voltages (inconvenient for range measurements) by using a sphere gap as an indicator, calibrated by range measurements over the higher portion of its voltage curve (the corrections are large—the sphere gap indicates about 30 percent too high a voltage, presumably due to the presence of corona and space charges). The arrangement for making range measurements at 500 kilovolts and above is indicated in Fig. 10. A copper-foil window of 9-mm air equivalent (by weight, checked by actual air substitution) is supported by a piece of nickel gauze 100 mesh to the inch over a small hole behind the center of the target, which either can be moved in vacuum or otherwise has a 1-mm hole drilled through it to pass a portion of the bombarding ions through the window. By adjusting the current through the deflecting magnet (magnetic analysis has been used for all of our work) the mass one spot (full speed protons only) or the mass two spot (full speed deuterons and diatomic protium molecular ions) may be brought on the window and the particle ranges measured, either visually or by a shallow ionization chamber (1 mm deep, goldleaf window) connected to a string electrometer. Usually both proton and deuteron ranges are measured as a check on the voltage. A stable hydrogen isotope of mass three was found by similar range measurements[12] and is always observed in the mass three spot with sufficient deuterium flow in the ion source. In the visual range measurements the high speed particles appear as a purple colored beam in air, somewhat divergent, especially toward the end where the ions are slower, and visibly diminishing in intensity over the last couple of millimeters of path. The electrometer usually gives a range about 2 millimeters longer than the visual estimate, probably because of its too great sensitivity (10^{-12} ampere) and the well-known straggling of the particle ranges. Small rapid fluctuations in the voltage, due to corona unsteadiness, could give a similar result. Slightly larger voltage fluctuations, especially when the machine is operated at maximum voltage, show up very clearly by visual observation as a "flicker" of a millimeter or two in the total range length (23 to 35 mm depending on conditions). With high humidity the belt joints become slightly conducting (see below) causing small sparks out into space when the joint enters or leaves the generator. This or other sparking in poor weather causes a range flicker as bad as 4 or 5 millimeters at maximum voltage (voltage fluctuation ± 100 kilovolts or 10 percent), and when the fluctuations reach this we make no attempt to operate at very high voltage.

Adjustment of the generator voltage to any desired value below the maximum is accomplished by moving a grounded "comb" of many corona points (office pins) toward the sphere until the voltage drops to the desired value as indicated by direct range measurement or (at low voltages) by the settings of a 50-cm sphere set for spark over to a smooth portion of the two-meter shell (see Fig. 4). This crude sphere gap is only used as an indicator, being calibrated by range measurements from 500 to 750 kilovolts and the curve extrapolated in obvious fashion below 500 kilovolts. The voltage between the two shells of the generator is held at a fixed value ($\sim$ 90 kv for good focus of the ion beam). This voltage is separately measured and is taken as the zero point for the sphere gap curve (instead of zero voltage) when the extrapolation is made. The voltage calibration curve of Fig. 7 has been used for much of our work. An uncertainty of one millimeter in the range measurements is indicated, and this curve was tentatively adopted last year until a better absolute calibration might become available. The use of a Variac autotransformer in the primary of the 40-kilovolt transformer of the spray voltage unit provides a "vernier control" of the voltage at the operator's position near the targets; by its use the voltage is held "up against" the limit for breakdown of the sphere gap (under 500 kv) or held at the desired value when continuous range measurements

[12] M. A. Tuve, L. R. Hafstad and O. Dahl, Phys. Rev. **45**, 840 (1934).

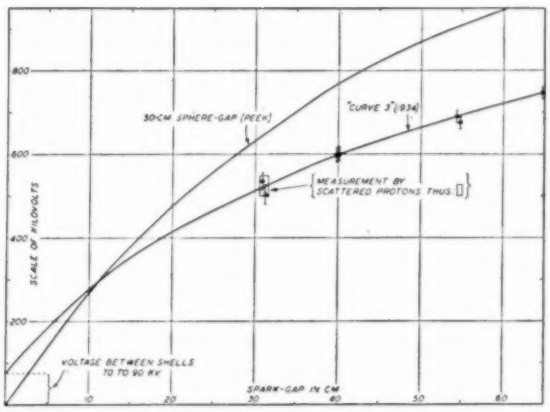

FIG. 7. Voltage scale for spark gap, as calibrated by proton range measurements.

can be made. The inherent "zero percent voltage regulation" of a constant current machine makes it necessary to guard carefully against voltage changes. It is an important characteristic of our technique that most of the ions striking the target have come from the ion source and have the full energy corresponding to the generator voltage as discussed below (sections C and E), so that improvement of the voltage steadiness of the generator is fully reflected in making the ion beam more nearly monochromatic. At voltages below the maximum (corona control in use) the voltage fluctuations of this generator are well under 20 kilovolts, and voltage changes of this amount can be made reliably, although the voltage settings cannot be repeated this closely when large changes are made, or from day to day. Observations on resonance transmutations[13] have demonstrated the steadiness of the generator voltage and will provide calibration points for ultimate intercomparisons and the establishment of an absolute voltage scale.

Belt-materials and treatment. A belt material highly suited to this specialized application still remains to be found, although a surprising degree of satisfaction and serviceability is obtained with rather ordinary materials. Pure silk or silk and rayon ribbons, with sewed joints cemented by airplane "fabric dope," were found satisfactory and long lived on the one-meter generator (also used in outdoor tests of two-meter generator), but such material cannot be obtained in widths between 8 inches and 36 inches. Following Dr. Van de Graaff and his colleagues we have been using on the two-meter generator a special paper belting supplied by the John A. Manning Paper Company, Troy, New York, specified as Electric Belting Paper, thickness 0.017 inch and usually purchased in 80-pound stock rolls 36 inches wide from which we cut both the main belt (20 inches wide, 68½ feet endless length) and the small belt which separately drives the direct-current generator (110 volts, 1 kw, 1800 r.p.m. with belt 3 inches wide and pulleys 8 inches in diameter to prevent slipping under load) located inside the inner shell of the generator, for ion source power.

We feel that we erred in adopting the belt design shown in Fig. 5, in which side stresses on the generator tripod are (unnecessarily) avoided by letting the belt pass over idlers inside the generator, because with this four-pulley arrangement the tracking of the belt is exceedingly sensitive to the requirement that the axes of these central idlers must be accurately perpendicular to the belt motion, as would be rather obvious to a mechanic accustomed to moving heavy objects by placing rollers under them. The tracking of the belt is much less sensitive to the usual adjustments of the axes of the end pulleys. We would install two separate belts instead, if the same belt area and general design were to be duplicated. The pulleys are made from Textolite tubes 8 inches in diameter, 22 inches long, 1/2-inch wall thickness, mounted by Bakelite disks on 1½-inch steel shafts, and they are crowned 1/32 inch over 2 inches at each end. It does not seem that crowning is necessary. A 6-inch silk and rayon ribbon belt runs satisfactorily on these pulleys and stays near the center indefinitely if started there.

Unfortunately no belt material yet tested is electrically satisfactory when subjected to 70 percent humidity at 80°F (Washington summer weather). Although during the winter (October to May) the behavior of the generator does not correlate well with the humidity (below 50 percent), there is no question concerning the ill effect of higher relative humidity on the belt insulation. Passing an unimpregnated paper belt slowly over a 10-kw electric heater for about two hours dries it sufficiently to prevent heavy belt

[13] L. R. Hafstad and M. A. Tuve, Phys. Rev. **47**, 506 (1935).

sparks for days or even weeks in winter, but this treatment lasts only a few minutes in summer humidity. Impregnating the paper with beeswax and rosin or with paraffin removes water which is essential to its mechanical strength, and the belt fails immediately. Coating the hot surface of a dry paper belt with ceresin does not prevent the growth of volume conductivity and gives slippage on the pulleys. However, a dry paper belt thoroughly soaked with Victron varnish (purchased from Dielectric Products Corporation, 63 Park Row, New York City) is relatively, but by no means completely, immune to humidity troubles and has been used to give 900 kilovolts, 750-microampere charging current, in August and behaved satisfactorily for several days after heating with 70 percent humidity at 80° to 85°F. Based on our experience with the silk and rayon belt on the one-meter generator, a charging current of slightly over 1000 microamperes might be expected on this two-meter generator, with a 20-inch belt on 8-inch pulleys at 3600 r.p.m. The theoretical maximum is 3.5 milliamperes. Untreated paper belts gave maximum currents of 620 to 650 microamperes (reduced to full width and full speed), but a Victron coated belt approaches the expected 1 milliampere, as does an untreated belt of light rubberized balloon fabric in the winter (just installed—summer tests have not been made with this material). Yellow varnished canvas, such as is used extensively for transformer insulation and other electrical construction, gives promise of being a satisfactory belt material, although the attainment of a satisfactory joint is yet uncertain; these tests are incomplete.* With the paper belts, various types of joint cements have been tested. Diagonal lap joints with a 3-inch skive are used, one end of the belt being split and the other tapered to give a joint of the same thickness as the belt. Those made with "Casco" casein glue give rise to troublesome sparking; Duco Household Cement has been the most satisfactory although this joint also requires the protection of an outside coat of Victron varnish. After some weeks of use the joint develops cracks, the paper nearest the cement tending to flake away, and after each day's run all such flakes are torn away and the belt reinforced over these areas by the application of silk cloth of light weight soaked in "airplane dope." This cloth cracks in turn, but is readily stripped off and replaced. The cracking at the joints, the collection of surface dirt, and the rough spots produced by heavy sparks are the chief limitations on the life of our Victron coated paper belts. With joint repairs and attention, our paper belts survive more than six months of hard usage (several hundred hours running time); we have used only two belts since beginning observations with this generator (although several belts were destroyed before we learned how to control the four pulley arrangement). Belt tests progress slowly since we consider it unprofitable to cut down a moderately satisfactory belt to test a new and unknown one, and we prefer to keep the generator in use.

C. High Voltage Tubes

Experiments during a period of several years in this laboratory led to the development during 1929–30 of oil immersed multiple-section high voltage tubes[14] which successfully withstood Tesla coil voltages as high as 2,000,000 volts. These tubes incorporated the well-known "cascade" principle of Coolidge,[15] which is an extension of Wien's method of "accelerated canal rays,"[16] and were characterized by the use of a large number of tube sections, each being required to withstand only a relatively small voltage, and each section being provided with external conducting shields to prevent undesired electric fields toward ground and to provide a spark gap between shields for protection against overvoltage. Sketch of a section of a tube of this type is shown in Fig. 8. After adopting in January 1930 the technique of "heat-working"

* Since writing the above the Goodyear rubberized balloon fabric has proved admirable in all respects. It has served from February to June 1935 with no mechanical attention except adjustments for stretching, and with no trace of deterioration. It was coated with Victron varnish (now called Q-Max) as a precaution when humid weather approached, and has continued to give satisfactory results at 900 to 1000 kv even with humidity exceeding 70 percent. This appears to constitute a nearly ideal belt material.

[14] Tuve, Breit and Hafstad, Phys. Rev. **35**, 66 (1930); Carnegie Inst. Wash. Year Book, No. 30, 364 (1931); Tuve, Hafstad and Dahl, Phys. Rev. **37**, 469 (1931).

[15] W. D. Coolidge, J. Frank. Inst. **202**, 693 (1926).

[16] W. Wien, Ann. d. Physik **77**, 313 (1924); **8**, 244 (1902); F. Hoffmann, Ann. d. Physik **77**, 302 (1925).

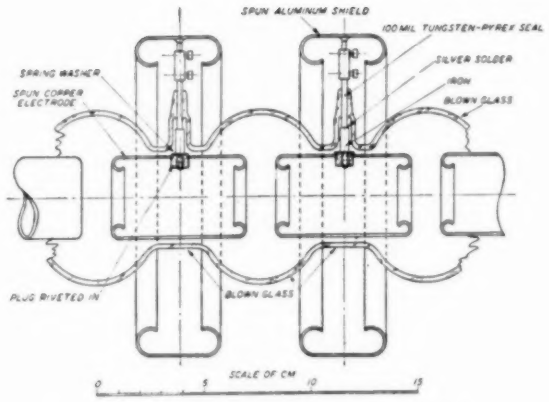

FIG. 8. Details of oil immersed cascade tube.

the Pyrex glass between the bulbs (to eliminate microscopic bubbles), which were blown at 3-inch intervals in ordinary 5-foot lengths of 44-mm Pyrex tubing, we experienced no difficulty with puncturing either on Tesla or direct-current voltages (except twice by the accidental application of grounded wires to the glass bulb of one of the highest voltage sections). These tubes were used successfully under oil with the spark excited Tesla coil for the demonstration of artificial gamma-, beta- and *H*-rays of energies exceeding a million volts,[4, 14] but further attempts to use them were abandoned in May 1931 until a more suitable voltage source of some kind could be obtained. The installation of the one-meter electrostatic generator in October 1932 gave us our first opportunity for a quantitative examination of the focusing properties of a tube of this type and its behavior when carrying appreciable currents.[17] In our work with the widely fluctuating Tesla voltages no estimate of the magnitude of the focusing or defocusing effect on the ion beam due to the curved fields between electrodes had been possible; our tubes had been originally designed solely to withstand high voltages, with the efficiency of transmission of the ions down the tube a secondary matter for later consideration to be met by modifications if necessary. Meanwhile Sloan and Lawrence[18] had found it possible to obtain 10 percent of the initial current on the target of a similar multiple-section tube utilizing high frequency voltages for the acceleration of mercury ions, and Professor Lawrence had kindly predicted to us that our tubes would be proved effective for a large percentage of ion transmission several months before we were able to satisfy ourselves on this point. As soon as we were equipped with a constant potential high voltage generator, it was found that very crude adjustment of the voltages on the several sections of the tube nearest to the generator (by adjustable points giving corona between the shields of these sections) sufficed to give a 1-cm spot on the target at two meters which measured 80 to 150 percent (with secondary emission) of the initial ion current projected from the low voltage arc ion source into the tube, provided this did not exceed 0.2 microampere. For higher currents the pumping speed of the tube itself, originally constructed for oil immersion (Archimedes' principle was our chief experimental obstacle), was too slow to handle the gas evolution and the tube "went soft." This result, that the initial ion beam was completely focused onto the target by the action of the tube itself, was of sufficient interest that it was repeatedly tested and verified; the currents were measured using very deep Faraday cages (50 cm long, 4 cm in diameter); magnetic fields showed that secondaries and slow ions were responsible for less than half of the target-currents, and the main uncertainty (a factor of 2 or less) was caused by irregular variations in the output of the ion source. The reasons why long high voltage tubes having only one or two sections in general give much less satisfactory focusing, unless very careful attention is paid to certain parameters of the problem, will be indicated in another paper, which presents a study of these factors.

To increase the pumping speed, and hence the usable ion current, a six-section tube was constructed using 6-inch moulded Pyrex tubing as shown in Fig. 1. This tube had electrodes made by rolling light gauge sheet brass into $3\frac{1}{2}$-inch cylinders 10 inches long, fitted at each end with a toroidal ring of 1/2-inch copper tubing (with an open crack at the butt joint in the ring). These parts were spot soldered together and the whole supported (in rather bad alignment) by rods passing through holes drilled in the glass wall. Spacing between the electrodes was roughly $1\frac{1}{4}$

[17] A photograph of one of these tubes being used with the one-meter generator for studies of the transmutation of Li and B was reproduced in J. Frank. Inst. **216**, 26 (1933).
[18] Sloan and Lawrence, Phys. Rev. **38**, 2021 (1931).

inches (variable because crooked). Although no parts were outgassed, this tube withstood full voltage (600 kilovolts) with target currents of 0.1 microampere within one-half hour of the first application of voltage immediately after being pumped down. Target currents up to 10 microamperes were obtainable at full voltage within several hours. Due undoubtedly to its faulty electrode alignment, although it gave a marked focusing response to the voltages on the first several sections, this tube did not focus the ions into a small diameter spot but gave an irregular "patchy" distribution over a 5- to 10-cm diameter area on the target. Most of the ions leaving the source reached this area. This tube was utilized for a series of observations on Li, B, Al, Ni and Ag.[19] The emission of rather soft x-rays from this tube in operation with 10 microamperes on the target required shielding for the observers (a pencil electroscope kindly supplied to us by Professor C. C. Lauritsen indicated 0.02 roentgen per minute at 6 feet from the tube, unshielded). This shielding was effected by installing the controls and recording oscillograph and camera in a hut outside the 12-inch concrete walls of the laboratory.

The tube which has been used with the two-meter generator from the time of its initial installation to the present date was first constructed as a temporary expedient, but it has worked well enough to cause postponement of the construction of a more permanent tube. This tube is shown to scale in Figs. 5, 6, 9 and 10, and was constructed from two 64-inch sections and one 32-inch section of moulded lead glass (Corning Glass Works, type 005 glass, 25 percent Pb) 8 inches in diameter. The voltage distribution between the sections of the tube is equalized by corona in air from section to section due to various corners and edges of metal parts inside the ring-shields. Short bent sections of wire have been added inside of each shield, giving corona to the next adjacent section, but these only serve to increase slightly the gradient control and are not essential. Only a moderate corona current passes down the outside of the tube in normal operation, as measured by the current to the bottom ring shield (30 to 110 microamperes as voltage is varied from 250 to 900 kv). At voltages below 900 kilovolts, obtained by moving a set of grounded corona-points toward the sphere, the current to these points nearly equals the total 400-microampere charging current. The corona discharges between tube sections serve the vital function of reestablishing the voltage distribution along the tube if an incipient internal discharge occurs. This safety valve action, together with the relatively low, but by no means negligible, energy which the generator will deliver into a tube flash if breakdown occurs, probably accounts for the very small amount of trouble we have experienced in applying high voltages to our tubes even when carrying the total available ion current from the source (10 to 15 microamperes). The crude type of electrode assembly described for the six-section Pyrex tube was utilized for this initial tube, which will ultimately be replaced by one

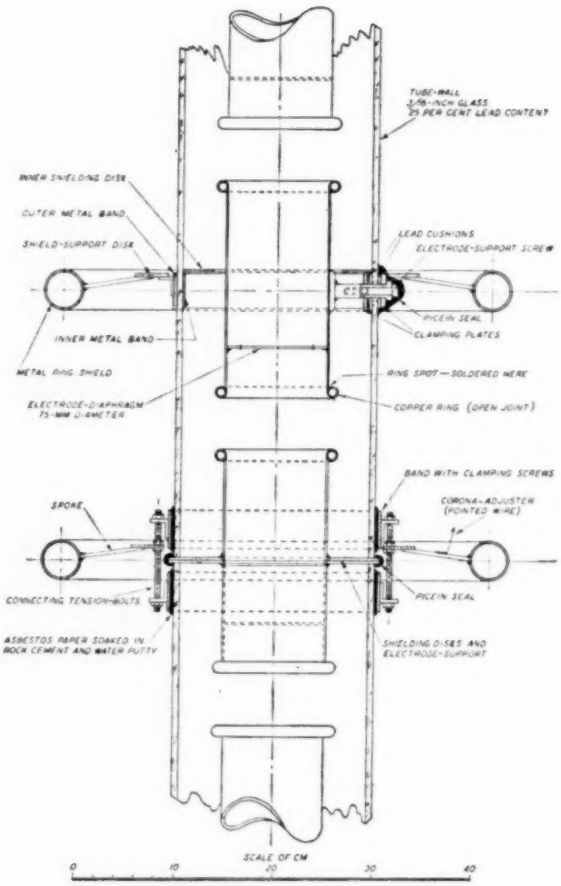

FIG. 9. Detail of tube joint and electrodes.

[19] M. A. Tuve, J. Wash. Acad. Sci. **23**, 530 (1933); Tuve, Hafstad and Dahl, Phys. Rev. **43**, 1055 (1933).

incorporating the following modifications: (a) The electrodes should be axially in alignment; (b) the electrode gaps should be of uniform width (not wedge-shaped or irregular as now) and much narrower to prevent transient deflections of the ion beam by charges on the glass wall of the tube; (c) the pumping speed of the tube itself should be increased by a factor of 10 or more by increase in the diameter of the glass cylinders and improvement (or omission) of the baffles on the outside of the electrodes. As before, no outgassing treatment was given any of the metal parts, and the tube withstood full voltage (above 1000 kv) within three hours of the first application of voltage after eliminating various air leaks. Subsequent exposure to air continues to require a "seasoning" period of the order of one-half hour before the tube will withstand full voltage and current (several microamperes).

The difficulty of applying high voltages to vacuum tubes, for positive ion currents of many microamperes (which are as large as can be used effectively in transmutation experiments at present), is only a matter of superstition if multiple-section tubes are used, as far as we can discover. Constant potentials, instead of being conducive to breakdown, are even more readily withstood than fluctuating Tesla voltages; the crudest kind of un-outgassed electrodes function without breakdown with relatively poor vacua (0.1 bar), and almost any size, shape and number of electrodes and length of tube can be made to focus practically 100 percent of the input ion current onto a relatively small area target if use is made of the focusing-parameters, especially the voltages on the various sections. It thus appears quite unnecessary to make a single section high voltage tube withstand a very high voltage because of the supposed advantage in "solid angle" of the source at the target.

The pumping system for this tube shown in Fig. 5 comprises two Apiezon oil diffusion pumps in series backed by a Hypervac. We changed from mercury to Apiezon pumps only after receiving from Professor E. O. Lawrence the complete designs for these pumps as constructed and used in his laboratory. We are exceedingly grateful to Professor Lawrence and his colleagues for the great saving of time and effort this has meant to us. The speed of the "fine" pump is perhaps 80 liters per second (air) but the overall speed is reduced to about 30 liters per second by the connecting tubes. We have had two experiences with the accidental cracking of the oil in these pumps which probably deserve mention, one of which cost us several weeks of trouble and delay. During April 1934 the pump heaters were left on continuously for two days with a leak in the tube and the Hypervac shut down. The oil in the pumps was hence greatly overheated in the presence of air, cracking to a gummy brown residue and distilling visible quantities of oil into the horizontal pump connection, and onto various surfaces in the lower part of the tube. The pumps were cleaned and refilled, and the visible oil in the pump connection and base of the tube was wiped out with benzol-soaked rags. After running the tube at moderate but increasing voltages and ion currents for a period of about five hours, the remaining oil film in the tube was converted to a noticeable carbon deposit and the tube was again usable, although the focal spot was somewhat unsteady. After several hours of use it was as good as ever.

During the autumn of 1934 we enjoyed a much less fortunate experience, however. Because of an increase in the diameter of the fore-pump connection (to realize an advantage from the "coarse" Apiezon pump) without proper baffles, nearly all of the oil from the "fine" pump diffused over into the "coarse" pump. The remaining few cubic centimeters of oil became overheated and cracked in a high vacuum (not exposed to air as before). Whether due to this cause or to some other, such as the accretion of Apiezon sealing compound Q and picein wax on the inside of the tube, due to numerous removals and repairs of the ion source at the top of the tube, a peculiar phenomenon developed at this time. The tube pressure behaved as though an "unpumpable vapor" was formed when high voltage was applied to the tube. A low pressure (0.005 to 0.01 bar) was readily attained in the tube, increased as usual by the gas flow when operating the ion source to about 0.02 or 0.03 bar, but as soon as the high voltage was applied even with ion currents as small as 0.1 microampere this pressure increased steadily (instead of the usual fixed increase of 5 to 20 percent due to gassing

of tube and targets) at a rate which raised the pressure to the stalling point of the diffusion pumps (about 0.15 bar) in several minutes. If the high voltage was cut off before the pumps stalled, this pressure decreased very slowly, requiring roughly an hour to return to the initial 0.02-bar pressure, although the pumps maintained their usual high speed, as was readily demonstrated by letting in a burst of air or hydrogen. This gas was pumped away in a few seconds, the pressure returning to whatever value (between 0.10 and 0.02) it had been before the burst of gas was admitted. The tube was completely dismantled and all parts cleaned by simple abrasion with steel wool and emery-cloth (solvents uncertain for such a vague surface-impurity), and when reassembled, using picein wax for all joints and seals, all sign of trouble had disappeared. The important convenience of an ionization gauge in locating leaks and other tube troubles is worthy of mention. We use the standard Western Electric gauge, type D-79510, with oxide-coated filament, which withstands unbelievable hard usage, including operation at pressures of many centimeters and repeated "poisoning" by oil vapors. This gauge is attached at the base of the tube for indicating pressures. With 20-milliampere emission a positive ion current of 4 microamperes is taken as 0.01 bar equivalent air pressure. A single gauge has withstood more than a year of rough usage. Minute cracks or holes in picein joints are found by watching the ion current in the gauge while painting the joints successively with 90 percent alcohol, which has the property of adequately "wetting" this wax, closing such holes temporarily, as shown immediately by the gauge. To determine whether a stubborn leak was in the ion source portion of the tube or not, we have repeatedly used the device of filling the generator shells with CO_2 gas, which gives about a 15 percent change in the gauge reading when drawn through the leak in place of air.

The use of heavy lead glass for the walls of this tube has made it possible to operate this unit without any further shielding for the observers although some additional shielding would be desirable (the wooden floor of the high voltage room is negligible protection for the observing room beneath). During the first half-hour of operation after being open to the atmosphere more x-rays are produced, but the usual dosage during a four-hour run of the equipment, recorded by a Lauritsen milli-r-meter (pencil electroscope) suspended in the observing room, amounts to only 10 to 30 scale divisions; the sensitivity is such that 50 scale divisions correspond to about 0.05 roentgen, and cosmic rays give an exposure of about one scale division per day measured by the same instrument. Ten times the daily cosmic-ray exposure is certainly a conservative value to adopt as the safe daily tolerance dosage. Since the equipment is not in operation continuously for many reasons during any period of one week, the total exposure of a single observer is always kept below seven times this very conservative daily dose. The allowable daily tolerance dose for x-rays in medical practice is generally accepted as 0.1 roentgen.

A description of the focusing of this tube and the target-currents attainable will be given in a later section.

D. Ion Sources

A device for supplying high intensity positive ion beams for work of this type with reasonable costs for equipment, power, pumps and gas (deuterium) has been an auxiliary requirement for artificial disintegration experiments which has demanded attention and development in many laboratories. Our earlier work with high speed protons using Tesla coil voltages had been carried out with unsatisfactory source arrangements (various palladium and gas ionization arrangements were tested), and in the summer of 1932 as we began tests of low voltage arc devices Dr. E. S. Lamar suggested the use of a hollow anode arc to obtain high positive ion density. It was immediately found that a hollow anode does not materially increase positive ion density over that of an ordinary low voltage arc discharge, since the space potential rises above that of the anode, but with the filament and hence the discharge near to the probe this type of arrangement (Fig. 11b) gave sufficient ion current (a few microamperes into the tube under operating conditions) for our immediate needs, and in various modifications has been used for nearly all of our experiments to date. At different times during the past two years we have tried

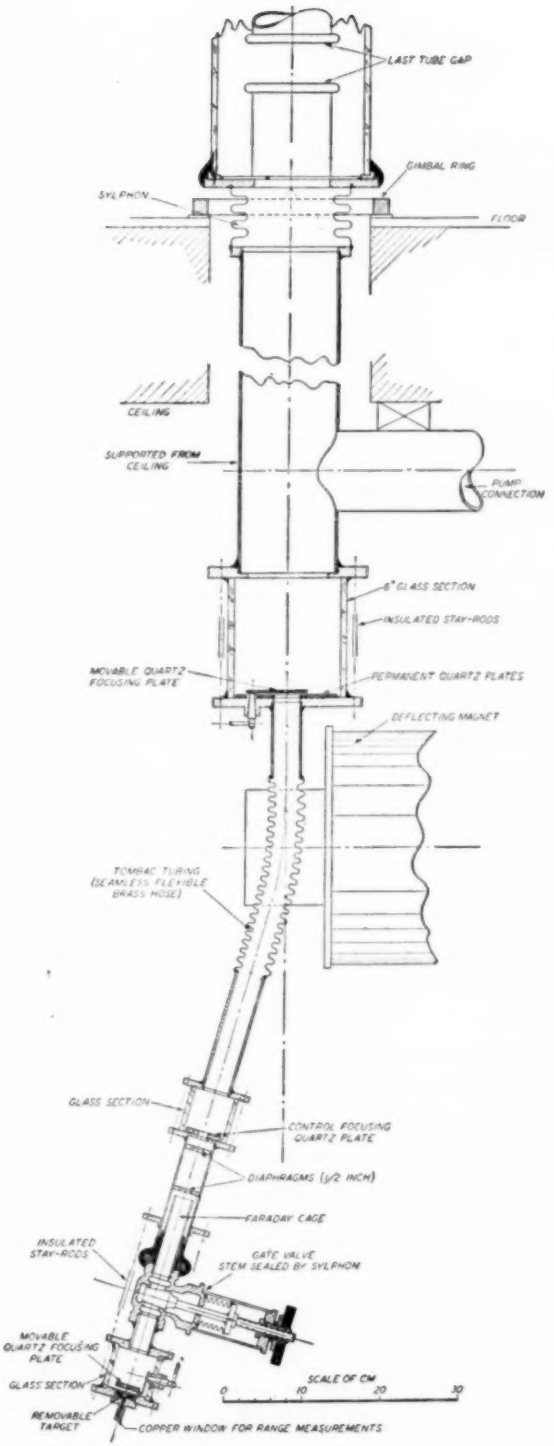

FIG. 10. Details of focus and analysis.

a great many variations of the general type of source which comprises a negative probe electrode (having a canal to pass ions into the high

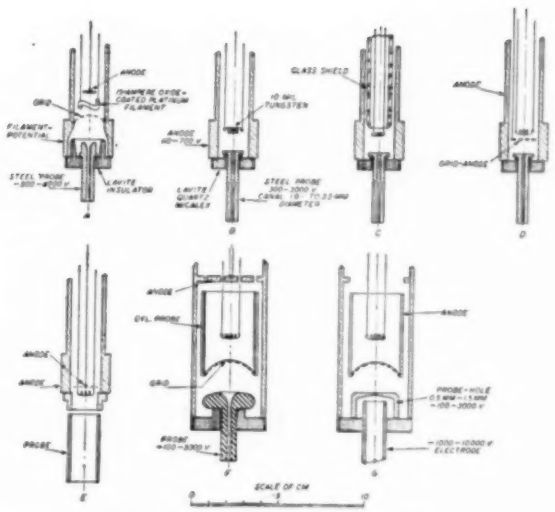

FIG. 11. Ion source arrangements.

voltage tube) immersed in a low voltage arc plasma of considerable volume extent, including the "accommodation coefficient" type (large hollow probe) recently described by Lamar and Luhr,[20] and all types tested were found unsatisfactory except for small ion currents (up to 12 microamperes) under best conditions. A few of the variants tested are illustrated by the diagrams of Fig. 11. Numerous changes of filament and probe positions, and other dimensions, of arc, grid, and probe potentials, and of arc pressure and canal size were made with each type of source design. The primary limitation of all of these arrangements was the fact that the current density to the probe face was consistently too low (10 to 65 microamperes per square mm including secondary electron emission) to counterbalance the requirement that a small area canal or diaphragm hole in the probe is necessary, with gas flowing, to give sufficient pressure for a true arc on one side of the hole and lower pressure in the high voltage tube on the other. With a full area probe hole as in Fig. 11e, ionizing the gas at tube pressure (under 0.1 bar—no true arc), the total tube current was slightly greater, 10 to 30 microamperes, but the focusing was bad or nonexistent with the large source area. This is of course to be expected, since to focus a distributed source places much higher requirements on the "optical" properties of the lens than to focus a point source. Final tests defining the

[20] Lamar and Luhr, Phys. Rev. **46**, 87 (1934).

limitations of this type of source were made with a probe in the form of a thin disk (Fig. 11g). Currents through a hole in this disk could not be space charge limited, as may be the case for a long canal, and yet the maximum ion currents through a 1.5-mm diameter hole were still only about 25 microamperes in spite of the use of curved grids and other devices in an effort to "focus" the ions on the hole in the probe. Low probe current density undoubtedly means a correspondingly insufficient ion density in the arc plasma. However, increasing the arc current (0.1 to 10 amperes) only decreased the tube current in most cases. Various sources of this general type can be made to yield several hundred microamperes through probe holes 5 mm or more in diameter with high arc pressures, but it is impracticable to provide the pump speed or the deuterium gas required if a low pressure is needed beyond the probe. To drive large ion currents through canals of great length would require voltages in excess of 10 kilovolts. Gas flow resistance increases as the first power of the canal length, and the ion current at a given voltage experimentally decreases much more rapidly than the first power after a given canal length is exceeded, perhaps due to mutual-repulsion effects on the ions.

The source arrangement with which most of our work has been done to date is similar to that shown in Figs. 11a and 12 (the grid and cylinder are connected to the filament) and has the following characteristics: Arc current 0.7 ampere; probe voltage 4500; probe current 3 to 6 milliamperes; probe canal 1.6- to 2.5-mm diameter, 26 to 48 mm long; arc pressure uncertain; tube pressure 1 to 4×10^{-5} mm; gas flow (hydrogen) 3 to 10 cc (at normal pressure and temperature) per hour; ion current into tubes 3 to 8 (15) microamperes; magnetically resolved proton current 0.5 to 12 microamperes (maximum), frequently not over 2 microamperes maximum; hydrogen ions always 55 to 90 percent atomic.

It is perhaps not flattering to ourselves but only proper to record that three separate high voltage discharge tubes intended as examples of the type of source used by Oliphant and Rutherford[21] failed to result in an ion source giving

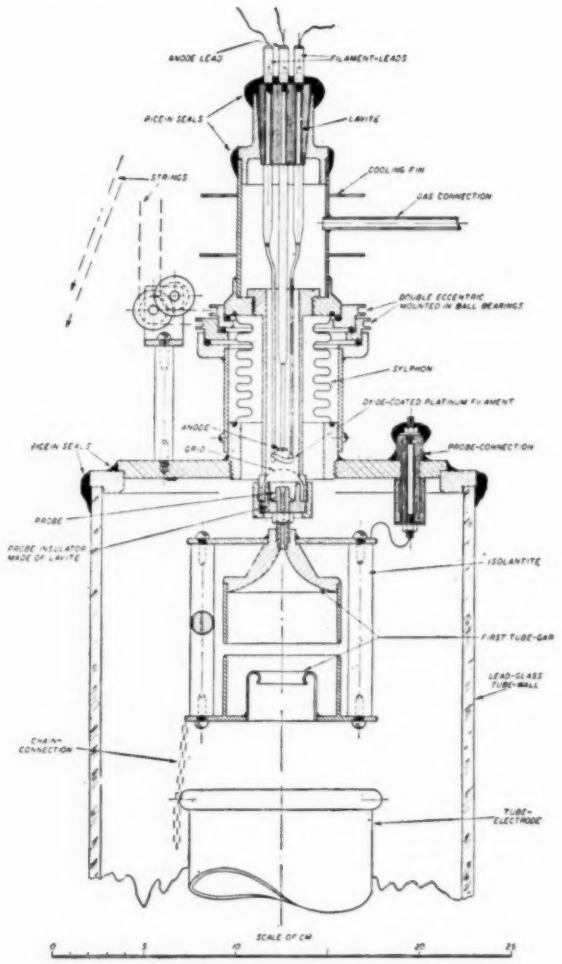

FIG. 12. Ion source.

the large currents (20 to 1000 microamperes) obtained in Cambridge. It appears from our experience and from verbal information from other workers that quite high voltages (much more than 10 kv) and large amounts of power (several kilowatts) are essential to the proper operation of a source of this type, and these requirements were difficult for us to meet. Trouble was also experienced with the insulator design at the top of the discharge tube in this design; at 10 to 15 kilovolts, 150 to 30 milliamperes, and moderate pressures only small ion currents were obtained (10 to 20 microamperes); at higher voltages and lower currents (lower available power and also lower pressures) internal sparkover gave trouble with several designs of insulators and adjoining parts. It is of course clear that this type of source gives intense ion

[21] Oliphant and Rutherford, Proc. Roy. Soc. **A141**, 259 (1933).

beams when relatively high voltage and high power are used as in Cambridge, but our experience does not encourage any belief that it might be operated with more modest equipment. Space and power, as well as artificial cooling, are at a premium inside a high voltage generator of the type we are using.

An ion source capable of supplying total currents as high as several milliamperes, with low power consumption and gas flow and with ideal flexibility of control, has recently been developed in this laboratory and is described in another paper. This new source has been used on another tube at lower voltages but has not yet been put into use with the two-meter generator since this was found to require certain minor changes in the apparatus and the original ion source was able to supply enough current for the problems immediately in hand. The original ion source and tube have been adequate for a whole series of investigations, and consequently all changes have been postponed in favor of continued operation of the present set up, although we plan to change both tube and ion source within the next several months, primarily in order to improve the steadiness of the target spot and incidentally to make available much larger currents for those problems in which they can be utilized.

E. Focusing Technique and Magnetic Analysis

A somewhat detailed description of our technique and experience in focusing the ion beam and in its analysis and steadiness on the targets may be of value to other experimentalists and also of interest in assessing the validity of transmutation results using this technique, especially in reference to the homogeneity (in energy and kind) of the ion beam bombarding the target.

Because of the dissymmetry and lack of alignment of the various tube sections, the focusing technique with this provisional tube (2-meter generator) is unnecessarily complex, as adjustment of the voltages on various tube sections (especially near the top of the tube, where the beam is slower) not only changes the size of the focal spot but also shifts its position. Major control of the focusing is accomplished by varying the voltage across each of the two tube sections which lie between the outer and inner shells of the generator. This is done by controlling the position of the two arms carrying corona points which are indicated in Fig. 6; since the charging current to the inner shell is constant (usually about 400 microamperes) and large compared to the tube current, settings of this device maintain steady controlled voltages across these two tube sections. Increasing the voltage on the first section causes the ion beam to behave exactly as a lens of variable focal length, when focused giving a spot, usually not round but with dimensions of the order of a centimeter, at some point on the quartz focusing screen shown in Fig. 10. After setting No. 1 at an underfocused voltage (divergent beam), increasing the voltage on No. 2 produces a similar behavior, but also shifts the spot to a new position perhaps 2 or 3 cm away from the position when focused with No. 1 and makes a round spot usually about 3 or 4 mm in diameter. When the tube has not been open to the air for several days and with currents of 1 microampere or less, the focal spot may be reduced to about 1-mm diameter, but with these sharp settings the spot splits into three or four adjacent spots, apparently due to a separation of ions of different mass, and these are surrounded by a diffuse spot about 10 mm in diameter. The latter aberrant ions are restored to the main spot 3 to 4 mm in diameter at the less critical settings. A third control, used to reduce the voltage and hence the arbitrary deflection produced by any of the lower sections (outside the large shell), is provided by a short length of chain inserted in a loop of silk fish-line and passing over pulleys at top and bottom so that it can be moved between any two ring shields on the outside of the tube, reducing the voltage across the selected section by corona. To facilitate the exact placing of the focal spot, in order that it shall enter the magnetic-analysis slits within 2 mm of a given position, the whole ion source is mounted on a flexible sylphon and can be shifted to any desired position in a circle 10 mm in diameter by means of a pair of eccentrics (see Fig. 12). This control has been essential also because of the slow drifts of the focal spot experienced especially during the first hour of operation with this tube; probably due to small

changes in the voltages across the various sections and to charges on the glass walls influencing the ion beam through the unnecessarily wide tube gaps between electrodes. There is a slight magnification at the focal spot of the ion source motion, but this is always less than a factor of two; a great magnification undoubtedly could be obtained by moving the ion source alone, with respect to the first lens (tube gap No. 1 at top), but to avoid large distortions (with a small diameter cylinder on the first gap) it was considered safest to mount this also on the eccentrics as shown in Fig. 12.

During the first month after its erection (autumn 1933) successful focusing of ion currents up to 7 microamperes of protons after magnetic analysis was obtained using the 4-inch electrodes shown in Fig. 9 for all tube gaps including the first one (next to the ion source). The double eccentric sylphon mount was then installed on the ion source, and to reduce the focusing voltage required on the first tube gap (which was near the maximum attainable) the four electrodes on the latter were replaced by a smaller diameter cone and cylinder arrangement similar to that described by Crane, Lauritsen and Soltan,[22] and this (see Fig. 12) has been left unchanged. An empirical investigation of the various parameters important to the focusing of a beam of ions down a high voltage tube has just been completed and is presented in a separate paper.

The arrangement of the magnetic analysis apparatus at the bottom end of the high voltage tube is shown to scale in Fig. 10. The magnet[23] gives a maximum field of 5500 gauss with a pole face separation of 3.5 cm, and this just suffices to bring the mass 5 spot (protons = mass 1) onto the target at full voltage. The focal spot is reproduced (usually with some distortion toward a linear form, due to the nonuniform edges of the magnetic deflecting field) on the quartz focusing disk in the target position, the desired ions (protons, deuterons, tritons, helium ions) being selected by adjusting the magnet current. The virtual separation of the various spots at the target distance is 4 to 7 cm; hence, there is no overlapping, and only ions of the specified mass can strike the target. The high degree of purity of resolution (absence of high speed in ions having directions other than that of the main beam, lack of scattering from slits, etc.) is clearly demonstrated by the fact that when a mixture of ordinary hydrogen and deuterium is used in the tube, whereas bombardment of carbon or quartz by the mass 2 spot gives rise to a count of several hundred particles per *second* actually recorded by a linear amplifier adjacent to a mica window near the target, shifting the magnetic field to bring the mass 1 spot on the target (roughly equal current), promptly reduces the count to the residual value (frequently 0 counts in 2 minutes, but arbitrarily assigned as 4 counts per minute to be as conservative as possible). A similar test of the purity of resolution is afforded by experiments on the induced radioactivity of carbon, where the effect at 1000 kilovolts due to deuterons is approximately 10,000 times as large as that due to a similar current of protons and the latter has been proved (by excitation functions) due to the protons alone. Tests made when 95 percent deuterium gas was flowing through the ion source showed likewise that the contamination of the mass 1 spot by deuterons was not detectable, and hence was less than one part in several thousand. When 98 percent deuterium gas flows into the ion source the mass 2 spot measures about 10 times the current of any other spot up to mass 6. A similar condition holds for the mass 1 spot when using ordinary tank hydrogen. The gas flow is usually set at a value which approximately doubles the ionization manometer reading of the residual tube pressure (1 to 5 microamperes on the ionization gauge).

It is to be pointed out that magnetic analysis (or even crossed electric and magnetic fields) for a given particle energy can only select ions of a given value of e/m, hence the mass 1 spot is the only one which is not a mixture. The mass 2 spot contains H^2 nuclei and H^1H^1 molecular ions; mass 3 spot contains H^3, H^2H^1, and $H^1H^1H^1$ ions, and the mass 4 spot contains He^4, H^3H^1 H^2H^2, $H^2H^1H^1$ and $H^1H^1H^1H^1$ ions. Thus a

[22] Crane, Lauritsen and Soltan, Phys. Rev. **45**, 507 (1934).

[23] A copy of a magnet built by Dr. L. F. Curtiss to whom we are grateful for the design details. This magnet utilizes a one-piece yoke cut from the billet by acetylene torches, kindly supplied by the American Rolling Mill Company, Middletown, Ohio.

subtractive technique, based finally on the purity of the mass 1 spot, must be followed in ascribing given results to given types and energies of ions. Since the various ions have different *velocities*, although the same energies, a separation by *range* can be effected if a homogeneous medium, air, for example, is used for stopping power. This procedure has been used for the identification of stable hydrogen atoms of mass 3 in numerous electrolytic deuterium samples.[12] The simple assumption that the composition of the ion beam from a high voltage tube is the same as the composition of the gas flowing into it is a highly erroneous practice, due to the large numerical ratios between the effects of different ions and the consequent importance of very small percentages of impurities (such as H^2 diffusing from the electrodes after use, etc.). The general effect of the input gas composition on the ion ratios is of course obvious.

The homogeneity in voltage distribution of the ion beam striking our targets is another factor of great importance, and is best demonstrated by our measurements on various resonance processes.[24] Suffice to say here that the ion beam has a spread of less than 20 kilovolts (probably considerably less) due to all causes, including both tube and generator, except at the highest voltages (above 900 kv—corona control removed) where the voltage fluctuations of the generator itself may be considerable because of small sparks to the belts, supports, control strings and out into air. A fluctuation exceeding about ± 50 kilovolts is not tolerated, even at peak voltage, the belt and strings then being dried to prevent sparking or the voltage reduced slightly by a weak corona control to give a steadier voltage.

The analytical virtues of a homogeneous ion beam are not fully realized, of course, if thick targets are bombarded, since ions of all velocities down to zero are then present in the target. For the numerous cases in which the effect under observation changes rapidly with voltage, including both the effects which show an exponential increase with voltage and those which show the familiar characteristics of a resonance response, observations with thin targets are almost essential since the thick target curve is an integral one and differentiation of an experimental curve is a procedure having a long history of defaults, valuable as an indicator when no other procedure is possible but to be avoided otherwise.

The authors take pleasure in recording their great obligation to Dr. John A. Fleming, Director of the Department of Terrestrial Magnetism, Carnegie Institution of Washington, for his sustained interest in these experiments. Without his vision of its ultimate significance and without his hearty support, this work could never have been carried out.

[24] L. R. Hafstad and M. A. Tuve, Phys. Rev. **47**, 506 (1935).

Extension of the Rh I-Like Isoelectronic Sequence to the Spectrum of Ag III

W. P. GILBERT, *Department of Physics, Cornell University*

(Received June 15, 1935)

The spark spectrum of silver has been photographed and measured in the region from 500 to 3000A. To assist in the identification of Ag III lines, the spectrum of silver from the hollow cathode discharge in an atmosphere of helium was photographed from 500 to 2600A. A spark gap placed in series with the Schüler tube served to bring out the Ag III lines in the spectrum of this discharge. With the already reported separation of 4607 cm^{-1} for the ground state, $4d^9\ ^2D_{2\frac{1}{2},1\frac{1}{2}}$, as a basis and by employing the above method of distinguishing the radiations, it has been possible to establish 55 terms originating from the $4d^9$, $4d^8 5s$, and $4d^8 5p$ configurations and to classify a total of 257 lines. Approximate term values have been obtained by extrapolation of a Moseley diagram for the elements of this sequence. The value obtained for the lowest state of Ag III with respect to the $4d^8\ ^3F_4$ state of Ag IV is 291,250 cm^{-1}, which corresponds to an ionization potential of 35.9 volts.

AN analysis of the Rh I spectrum has been given by Sommer[1] and an analysis of the Pd II spectrum has been reported by Shenstone[2] and Blair.[3] Kimura and Nakamura[4] photographed the spectrum of silver from the condensed discharge and found a few lines which they attributed to Ag III. Gibbs and White[5] have published a preliminary report on the analysis of this spectrum but the work has not been completed and published in detail. Their abstract communicates solely the separation, 4607 cm^{-1}, of the low $4d^9\ ^2D_{2\frac{1}{2},1\frac{1}{2}}$ levels. In another paper[6] the wave number of the line $4d^8(^3F)5s\ ^4F_{4\frac{1}{2}} - 4d^8(^3F)5p\ ^4G^\circ_{5\frac{1}{2}}$ has been reported.

Experimental Details

The vacuum spark spectrum of silver was photographed in the region from 500–1200A with a vacuum spectrograph equipped with a grating which gave a dispersion of about 5.2A per mm, and from 1200–2600A with a similar instrument which gave a dispersion of 11.3A per mm. The aluminum lines measured by Ekefors[7] and by Zumstein,[8] and impurity lines of carbon, nitrogen and oxygen[9] served as standards. In the region 1900–3000A the spectrum of a silver spark in air between pointed electrodes was photographed with a grating (Rowland mounting) which gave a dispersion of about 4.6A per mm. Sharp lines of Ag II[10] were used as standards. The Ag III lines could be readily recognized by their polar character.

To provide a way of distinguishing between the spectrum lines arising from various stages of ionization which appeared on the vacuum spark plates, the spectrum of silver from the hollow cathode discharge in an atmosphere of helium was photographed in the region from 500–2600A. A spark gap placed in series with the Schüler tube[11] served to bring out strongly in the discharge lines arising from transitions between the lower configurations of Ag III without exciting higher stages of ionization to any appreciable extent. Since the majority of the Ag II lines which fall in this region have been previously classified, it was thus possible, by comparing the vacuum spark and hollow cathode data, to select the Ag III lines with considerable assurance.

Term Values and Classifications

The normal $4d^9$ electron configuration of the Ag III ion gives rise to inverted ^2D terms. The present work is concerned with the identification of the terms which arise when one of the $4d$ electrons is raised to a $5s$ or $5p$ state. The terms predicted by the Hund theory for these configurations are listed in Table I together with those identified in this investigation.

By analogy with the Rh I and Pd II spectra three of the strongest lines of the Ag III spectrum should arise from the transitions: $4d^8(^3F)5s\ ^4F_{4\frac{1}{2}} - 4d^8(^3F)5p\ ^4G^\circ_{5\frac{1}{2}}$, $^4D^\circ_{3\frac{1}{2}}$ and $^4F^\circ_{4\frac{1}{2}}$. A linear extrapolation of the wave numbers for the ele-

[1] Sommer, Zeits. f. Physik **45**, 147 (1927).
[2] Shenstone, Phys. Rev. **32**, 30 (1928).
[3] Blair, Phys. Rev. **36**, 173 (1930).
[4] Kimura and Nakamura, Jap. J. Phys. **3**, 197 (1924).
[5] Gibbs and White, Phys. Rev. **32**, 318 (1928).
[6] Gibbs and White, Proc. Nat. Acad. Sci. **14**, 559 (1928).
[7] Ekefors, Zeits. f. Physik **51**, 471 (1928).
[8] Zumstein, Phys. Rev. **38**, 2214 (1931).
[9] Edlén, Zeits. f. Physik **85**, 85 (1933).
[10] Shenstone, Phys. Rev. **31**, 317 (1928).
[11] Gartlein and Gibbs, Phys. Rev. **38**, 1907 (1931).

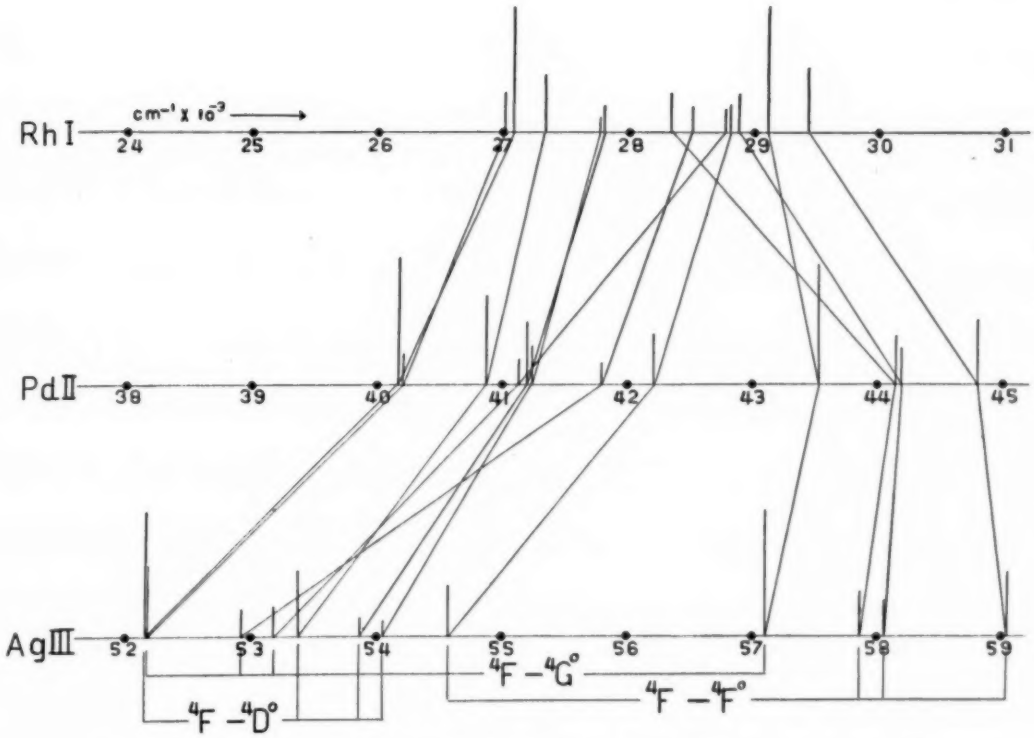

FIG. 1. Regular displacement of wave number for the electron transition $4d^9 5s - 4d^9 5p$.

TABLE I. *Predicted and observed terms of Ag III.*

ELECTRON CONFIGURATION	PREDICTED TERMS	LIMIT Ag IV	OBSERVED TERMS	REMARKS
$4d^9$	^2D		^2D	
$4d^8 5s$	^2S	(^1S)	—	
	^2D	(^1D)	^2D	
	^2G	(^1G)	^2G	
	2, ^4P	(^3P)	2, ^4P	$^4P_{\frac{1}{2}}$ questionable
	2, ^4F	(^3F)	2, ^4F	
$4d^8 5p$	$^2S°$	(^1S)	—	
	$^2(P°D°F°)$	(^1D)	$^2(P°D°F°)$	
	$^2(F°G°H°)$	(^1G)	$^2(F°H°)$	
	2, $^4(S°P°D°)$	(^3P)	2, $^4(P°D°)$	$^4D°_{\frac{1}{2}}$ missing
	2, $^4(D°F°G°)$	(^3F)	2, $^4(D°F°G°)$	

TABLE II. *Square roots of some term values of the Rh I-like isoelectronic sequence.*

TERMS	Rh I	$\Delta(\nu)^{\frac{1}{2}}$	Pd II	$\Delta(\nu)^{\frac{1}{2}}$	Ag III
$4d^9\ ^2D_{\frac{3}{2}}$	243.1	157.7	400.8	138.9	539.7
$4d^8(^3F_4)5s\ ^4F_{\frac{9}{2}}$	249.8	118.3	368.1	109.4	*477.5**
$^2F_{\frac{7}{2}}$	238.2	120.0	358.2	110.3	468.5
$4d^8(^3F_4)5p\ ^4D°_{\frac{3}{2}}$	188.0	120.8	308.8	110.5	419.3
$^4G°_{\frac{5}{2}}$	182.5	120.8	303.3	110.1	*413.4**
$^4F°_{\frac{9}{2}}$	181.6	119.6	301.2	109.9	411.1
$^2F°_{\frac{7}{2}}$	174.4	121.0	295.4	110.2	405.6

* Used in establishing the approximate absolute term values.

TABLE III. *Term values for Ag III.*

TERM SYMBOL	RELATIVE TERM VALUES (cm^{-1})	TERM SYMBOL	RELATIVE TERM VALUES (cm^{-1})	TERM SYMBOL	RELATIVE TERM VALUES (cm^{-1})	TERM SYMBOL	RELATIVE TERM VALUES (cm^{-1})
$4d^9\ ^2D_{\frac{5}{2}}$	0	$4d^8(^1G)5s\ ^2G_{\frac{9}{2}}$	85599	$^2D°_{\frac{5}{2}}$	125095	$^2D°_{1\frac{1}{2}}$	135356
$^2D_{1\frac{1}{2}}$	4607	$^2G_{\frac{7}{2}}$	85727	$^2G°_{\frac{9}{2}}$	125250	$^2D°_{\frac{3}{2}}$	135762
$4d^8(^3F)5s\ ^4F_{\frac{9}{2}}$	63250	$4d^8(^3P)5s\ ^4P_{\frac{1}{2}}$	87477	$^4F°_{\frac{3}{2}}$	126208	$4d^8(^3P)5p\ ^4D°_{1\frac{1}{2}}$	136808
$^4F_{\frac{3}{2}}$	65764	$4d^8(^3F)5p\ ^4D°_{\frac{5}{2}}$	115412	$^2F°_{\frac{5}{2}}$	126732	$4d^8(^1G)5p\ ^2H°_{\frac{9}{2}}$	136809
$^4F_{\frac{5}{2}}$	68145	$^4G°_{\frac{9}{2}}$	117931	$^2G°_{\frac{9}{2}}$	127729	$4d^8(^3P)5p\ ^4D°_{\frac{3}{2}}$	136931
$^4F_{1\frac{1}{2}}$	69351	$^4D°_{\frac{3}{2}}$	119143	$^2D°_{1\frac{1}{2}}$	127870	$^4D°_{\frac{5}{2}}$	136976
$^2F_{\frac{5}{2}}$	71691	$^4G°_{\frac{5}{2}}$	120359	$^2F°_{\frac{7}{2}}$	128804	$^2D°_{\frac{5}{2}}$	138849
$^2F_{\frac{7}{2}}$	73934	$^4G°_{\frac{7}{2}}$	121068	$4d^8(^3P)5p\ ^4P°_{\frac{1}{2}}$	129143	$^2D°_{1\frac{1}{2}}$	139322
$4d^8(^3P)5s\ ^4P_{\frac{5}{2}}$	76406	$^4D°_{1\frac{1}{2}}$	122014	$^4P°_{1\frac{1}{2}}$	129937	$4d^8(^1G)5p\ ^2H°_{\frac{9}{2}}$	139942
$^4P_{1\frac{1}{2}}$	77413	$^4F°_{\frac{9}{2}}$	122300	$^4P°_{\frac{3}{2}}$	130152	$4d^8(^3P)5p\ ^2P°_{1\frac{1}{2}}$	140078
$^4P_{\frac{1}{2}}$	79326?	$^4G°_{\frac{9}{2}}$	122532	$4d^8(^1D)5p\ ^2F°_{\frac{5}{2}}$	131875	$4d^8(^1G)5p\ ^2F°_{\frac{5}{2}}$	140881
$4d^8(^1D)5s\ ^2D_{1\frac{1}{2}}$	80131	$^4D°_{\frac{1}{2}}$	123408	$^2P°_{\frac{1}{2}}$	133467	$^2F°_{\frac{7}{2}}$	142165
$^2D_{\frac{3}{2}}$	82231	$^4F°_{\frac{3}{2}}$	123631	$^2F°_{\frac{5}{2}}$	133635	$4d^8(^3P)5p\ ^2P°_{\frac{1}{2}}$	143781
$4d^8(^3P)5s\ ^2P_{1\frac{1}{2}}$	85182	$^4F°_{1\frac{1}{2}}$	123927	$^2P°_{1\frac{1}{2}}$	134955		

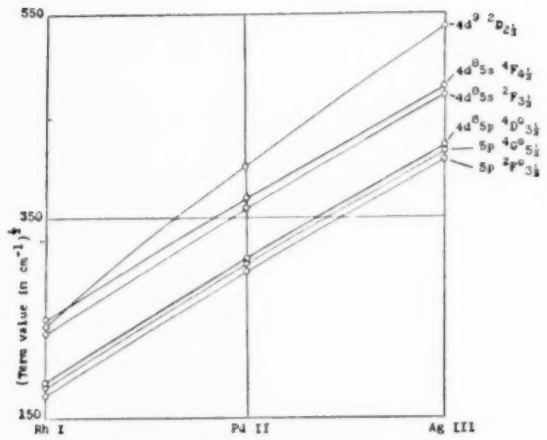

FIG. 2. Moseley diagram.

ments of this sequence (irregular doublet law) gave the approximate position in the spectrum of these Ag III lines. (Fig. 1.) The absolute term values were approximated by the extrapolation of a Moseley diagram (Fig. 2). The lines representing the terms $4d^8(^3F)5s\ ^4F_{4\frac{1}{2}}$ and $4d^8(^3F)5p\ ^4G^\circ_{5\frac{1}{2}}$ were extended to Ag III by drawing them so as to keep $\Delta(\nu)^{\frac{1}{2}}$ constant (required by the irregular doublet law) and yet choose the ordinates so that the difference in their squares is equal to the wave number of the radiated line. The data used in plotting the Moseley diagram are given in Table II. As determined by this method the absolute value of the $4d^8(^3F_4)5s\ ^4F_{4\frac{1}{2}}$ term is 228,000 cm^{-1}.[12]

The approximate position of the low $4d^9\ ^2D_{2\frac{1}{2}}$ term was likewise obtained by extrapolation on a Moseley diagram and the finding and classification of the majority of the $4d^9-4d^85p$ transitions then established accurately the relative position of the ground levels. The $4d^9\ ^2D_{2\frac{1}{2}}$ term lies 63,250 cm^{-1} below $4d^8(^3F_4)5s\ ^4F_{4\frac{1}{2}}$. Therefore the approximate absolute value of the lowest state of Ag III with respect to $4d^8\ ^3F_4$ of Ag IV is 291,250 cm^{-1}, which corresponds to an ionization potential of 35.9 volts.

A centroid diagram for the terms of the $4d^85s$ configuration is shown in Fig. 3. The $4d^8(^1S_0)5s\ ^2S_{\frac{1}{2}}$ term is omitted since it has not been found for

[12] B. V. R. Rao (Proc. Ind. Acad. Sci. **1**, 28, July (1934)), reports 237,000 cm^{-1} for the absolute value of this term. According to the abstract of Rao's article the terms $4d^8(^3F)5s\ ^{2,4}F$ and $4d^8(^3F)5p\ ^{2,4}F^\circ$ have been identified by him. Since the author has been unable to obtain a copy of Rao's paper, no detailed comparison could be made with the results reported here.

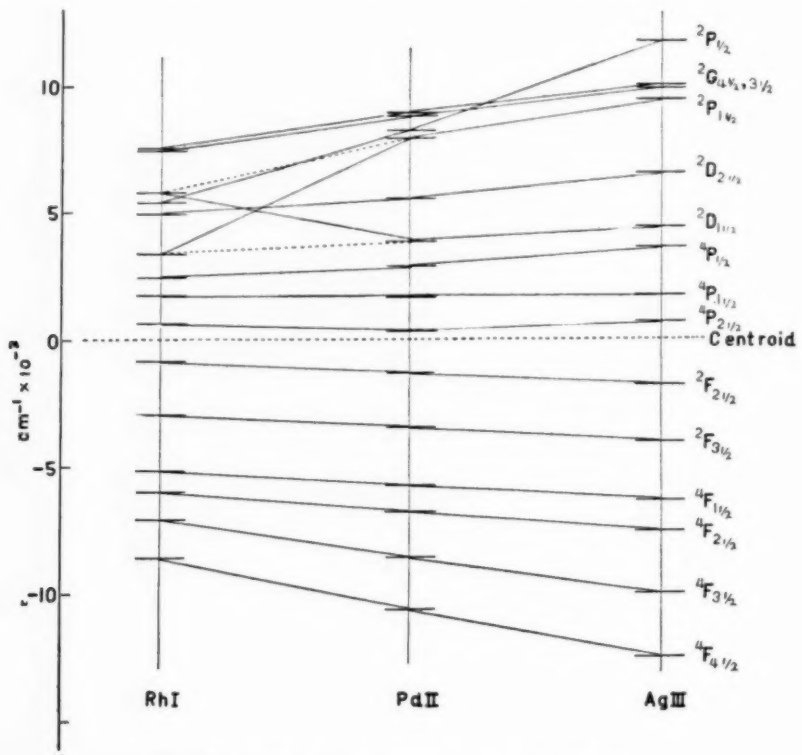

FIG. 3. Centroid diagram for $4d^85s$ configuration.

TABLE IV. *Classified lines of Ag III.*

INT.	λ VAC.	ν VAC.	CLASSIFICATION
1	3013.81	33181	$4d^8(^1D)5s\ ^2D_{2\frac{1}{2}} - 4d^8(^3F)5p\ ^4D^\circ_{3\frac{1}{2}}$
1	2992.50	33962	$(^3P)5s\ ^2P_{1\frac{1}{2}} - (^3F)5p\ ^4D^\circ_{2\frac{1}{2}}$
1	2716.98	36806	$(^1G)5s\ ^2G_{3\frac{1}{2}} - (^3F)5p\ ^4G^\circ_{3\frac{1}{2}}$
1	2709.16	36912	$(^1D)5s\ ^2D_{2\frac{1}{2}} - (^3F)5p\ ^4D^\circ_{2\frac{1}{2}}$
1	2677.44	37349	$(^3P)5s\ ^2P_{1\frac{1}{2}} - (^3F)5p\ ^4G^\circ_{2\frac{1}{2}}$
0	2638.62	37906	$(^3G)5s\ ^2G_{4\frac{1}{2}} - (^3F)5p\ ^4F^\circ_{3\frac{1}{2}}$
8	2629.32	38033	$(^1G)5s\ ^2G_{4\frac{1}{2}} - (^3F)5p\ ^4F^\circ_{4\frac{1}{2}}$
10	2563.64	39007	$(^3P)5s\ ^4P_{2\frac{1}{2}} - (^3F)5p\ ^4D^\circ_{3\frac{1}{2}}$
1	2563.30	39012	$(^1D)5s\ ^2D_{1\frac{1}{2}} - (^3F)5p\ ^4D^\circ_{2\frac{1}{2}}$
10	2470.37	40480	$(^1G)5s\ ^2G_{4\frac{1}{2}} - (^3F)5p\ ^4F^\circ_{4\frac{1}{2}}$
0	2415.53	41399	$(^1D)5s\ ^2D_{2\frac{1}{2}} - (^3F)5p\ ^4F^\circ_{3\frac{1}{2}}$
5	2410.82	41480	$(^3F)5s\ ^2F_{3\frac{1}{2}} - (^3F)5p\ ^4D^\circ_{3\frac{1}{2}}$
0	2400.01	41667	$(^3P)5s\ ^2P_{\frac{1}{2}} - (^3P)5p\ ^4P^\circ_{\frac{1}{2}}$
30	2396.42	41729	$(^3P)5s\ ^4P_{1\frac{1}{2}} - (^3F)5p\ ^4D^\circ_{2\frac{1}{2}}$
10	2387.57	41884	$(^1D)5s\ ^2D_{1\frac{1}{2}} - (^3F)5p\ ^4D^\circ_{1\frac{1}{2}}$
6	2342.62	42687	$(^3P)5s\ ^2P_{1\frac{1}{2}} - (^3F)5p\ ^2D^\circ_{1\frac{1}{2}}$
			$(^3P)5s\ ^4P_{\frac{1}{2}} - (^3F)5p\ ^4D^\circ_{1\frac{1}{2}}$
5	2339.94	42736	$(^3P)5s\ ^4P_{2\frac{1}{2}} - (^3F)5p\ ^4D^\circ_{2\frac{1}{2}}$
0	2333.00	42863	$(^1D)5s\ ^2D_{2\frac{1}{2}} - (^3F)5p\ ^2D^\circ_{2\frac{1}{2}}$
10	2287.20	43722	$(^3F)5s\ ^2F_{3\frac{1}{2}} - (^3F)5p\ ^4D^\circ_{3\frac{1}{2}}$
3	2282.92	43804	$(^1D)5s\ ^2D_{1\frac{1}{2}} - (^3F)5p\ ^4F^\circ_{1\frac{1}{2}}$
6	2273.88	43978	$(^1D)5s\ ^2D_{2\frac{1}{2}} - (^3F)5p\ ^4F^\circ_{2\frac{1}{2}}$
3	2242.06	44602	$(^3P)5s\ ^4P_{1\frac{1}{2}} - (^3P)5p\ ^4D^\circ_{1\frac{1}{2}}$
			$(^3P)5s\ ^4P_{\frac{1}{2}} - (^3F)5p\ ^4F^\circ_{1\frac{1}{2}}$
10	2239.09	44661	$(^3P)5s\ ^4P_{2\frac{1}{2}} - (^3F)5p\ ^4G^\circ_{3\frac{1}{2}}$
0	2234.41	44755	$(^3P)5s\ ^2P_{1\frac{1}{2}} - (^3P)5p\ ^4P^\circ_{1\frac{1}{2}}$
5	2223.62	44972	$(^1D)5s\ ^2D_{1\frac{1}{2}} - (^3F)5p\ ^2D^\circ_{2\frac{1}{2}}$
			$(^3P)5s\ ^2P_{1\frac{1}{2}} - (^3P)5p\ ^4P^\circ_{2\frac{1}{2}}$
15	2211.92	45210	$(^3F)5s\ ^2F_{2\frac{1}{2}} - (^3F)5p\ ^4D^\circ_{2\frac{1}{2}}$
1	2197.86	45499	$(^1D)5s\ ^2D_{2\frac{1}{2}} - (^3F)5p\ ^2G^\circ_{3\frac{1}{2}}$
5	2192.63	45607	$(^3P)5s\ ^4P_{2\frac{1}{2}} - (^3F)5p\ ^4D^\circ_{1\frac{1}{2}}$
4	2174.16	45995	$(^3P)5s\ ^4P_{1\frac{1}{2}} - (^3P)5p\ ^4D^\circ_{\frac{1}{2}}$
5	2170.25	46078	$(^1D)5s\ ^2D_{1\frac{1}{2}} - (^3F)5p\ ^4F^\circ_{2\frac{1}{2}}$
60	2162.57	46241	$(^3F)5s\ ^2F_{3\frac{1}{2}} - (^3F)5p\ ^4G^\circ_{4\frac{1}{2}}$
15	2149.87	46514	$(^3P)5s\ ^4P_{1\frac{1}{2}} - (^3F)5p\ ^4F^\circ_{1\frac{1}{2}}$
0	2121.58	47135	$(^3F)5s\ ^2F_{2\frac{1}{2}} - (^3F)5p\ ^4G^\circ_{3\frac{1}{2}}$
8	2107.39	47452	$(^3F)5s\ ^2F_{3\frac{1}{2}} - (^3F)5p\ ^4D^\circ_{2\frac{1}{2}}$
3	2104.30	47522	$(^3P)5s\ ^4P_{2\frac{1}{2}} - (^3F)5p\ ^4F^\circ_{1\frac{1}{2}}$
5	2096.13	47707	$(^1D)5s\ ^2D_{2\frac{1}{2}} - (^3P)5p\ ^4P^\circ_{1\frac{1}{2}}$
1	2094.73	47739	$(^1D)5s\ ^2D_{1\frac{1}{2}} - (^3F)5p\ ^2D^\circ_{1\frac{1}{2}}$
4	2088.54	47880	$(^1P)5s\ ^2P_{1\frac{1}{2}} - (^1D)5p\ ^2D^\circ_{1\frac{1}{2}}$
3	2086.78	47921	$(^1D)5s\ ^2D_{2\frac{1}{2}} - (^3P)5p\ ^4P^\circ_{2\frac{1}{2}}$
20	2081.70	48038	$(^1G)5s\ ^2G_{4\frac{1}{2}} - (^1D)5p\ ^2F^\circ_{3\frac{1}{2}}$
1	2071.02	48285	$(^3P)5s\ ^2P_{1\frac{1}{2}} - (^1D)5p\ ^2P^\circ_{\frac{1}{2}}$
20	2057.65	48599	$(^3F)5s\ ^2F_{2\frac{1}{2}} - (^3F)5p\ ^4G^\circ_{3\frac{1}{2}}$
15	2054.49	48674	$(^1D)5s\ ^2D_{1\frac{1}{2}} - (^3F)5p\ ^2F^\circ_{2\frac{1}{2}}$
15	2053.83	48690	$(^3P)5s\ ^4P_{2\frac{1}{2}} - (^3F)5p\ ^2D^\circ_{2\frac{1}{2}}$
0	2049.37	48796	$(^3P)5s\ ^4P_{1\frac{1}{2}} - (^3F)5p\ ^4F^\circ_{2\frac{1}{2}}$
5	2040.26	49013	$(^1D)5s\ ^2D_{1\frac{1}{2}} - (^3P)5p\ ^4P^\circ_{\frac{1}{2}}$
2	2025.25	49377	$(^3F)5s\ ^2F_{3\frac{1}{2}} - (^3F)5p\ ^4G^\circ_{3\frac{1}{2}}$
15	2014.30	49645	$(^1D)5s\ ^2D_{2\frac{1}{2}} - (^1D)5p\ ^2F^\circ_{2\frac{1}{2}}$
			$(^3F)5s\ ^4F_{3\frac{1}{2}} - (^3F)5p\ ^4D^\circ_{2\frac{1}{2}}$
20	2012.14	49698	$(^3F)5s\ ^2F_{2\frac{1}{2}} - (^3F)5p\ ^4F^\circ_{2\frac{1}{2}}$
6	2009.10	49774	$(^3P)5s\ ^2P_{1\frac{1}{2}} - (^1D)5p\ ^2P^\circ_{1\frac{1}{2}}$
6	2007.94	49802	$(^3P)5s\ ^4P_{2\frac{1}{2}} - (^3F)5p\ ^4F^\circ_{2\frac{1}{2}}$
6	2007.74	49807	$(^1D)5s\ ^2D_{1\frac{1}{2}} - (^3P)5p\ ^4P^\circ_{1\frac{1}{2}}$
60	2000.24	49994	$(^3F)5s\ ^2F_{3\frac{1}{2}} - (^3F)5p\ ^4F^\circ_{4\frac{1}{2}}$
7	1999.14	50022	$(^1D)5s\ ^2D_{1\frac{1}{2}} - (^3P)5p\ ^4P^\circ_{2\frac{1}{2}}$
20	1987.02	50327	$(^3P)5s\ ^4P_{2\frac{1}{2}} - (^3F)5p\ ^2F^\circ_{3\frac{1}{2}}$
15	1981.87	50457	$(^3P)5s\ ^4P_{1\frac{1}{2}} - (^3F)5p\ ^2D^\circ_{1\frac{1}{2}}$
50	1977.03	50581	$(^3P)5s\ ^2P_{1\frac{1}{2}} - (^1D)5p\ ^2D^\circ_{2\frac{1}{2}}$
60	1975.92	50609	$(^3F)5s\ ^2F_{3\frac{1}{2}} - (^3F)5p\ ^4F^\circ_{4\frac{1}{2}}$
			$(^3P)5s\ ^4P_{\frac{1}{2}} - (^3P)5p\ ^4P^\circ_{1\frac{1}{2}}$
40	1966.89	50842	$(^3F)5s\ ^2F_{3\frac{1}{2}} - (^3F)5p\ ^4G^\circ_{4\frac{1}{2}}$
10	1960.86	50998	$(^3F)5s\ ^4F_{3\frac{1}{2}} - (^3F)5p\ ^4D^\circ_{2\frac{1}{2}}$
70	1957.62	51082	$(^1G)5s\ ^2G_{4\frac{1}{2}} - (^1G)5p\ ^2H^\circ_{4\frac{1}{2}}$
2	1954.59	51162	$(^3F)5s\ ^2F_{3\frac{1}{2}} - (^3F)5p\ ^2D^\circ_{2\frac{1}{2}}$
4	1952.98	51204	$(^3G)5s\ ^2G_{4\frac{1}{2}} - (^3F)5p\ ^4D^\circ_{2\frac{1}{2}}$
5	1952.74	51210	$(^1G)5s\ ^2G_{4\frac{1}{2}} - (^1G)5p\ ^2H^\circ_{4\frac{1}{2}}$
10	1948.44	51323	$(^3P)5s\ ^4P_{2\frac{1}{2}} - (^3F)5p\ ^2G^\circ_{3\frac{1}{2}}$
15	1946.32	51379	$(^1G)5s\ ^2G_{4\frac{1}{2}} - (^3P)5p\ ^4D^\circ_{2\frac{1}{2}}$
5	1945.37	51404	$(^1D)5s\ ^2D_{2\frac{1}{2}} - (^1D)5p\ ^2F^\circ_{3\frac{1}{2}}$
4	1943.12	51464	$(^3P)5s\ ^4P_{2\frac{1}{2}} - (^3F)5p\ ^2D^\circ_{1\frac{1}{2}}$
4	1937.00	51626	$(^3P)5s\ ^2P_{1\frac{1}{2}} - (^3P)5p\ ^4D^\circ_{1\frac{1}{2}}$
7	1933.11	51730	$(^3P)5s\ ^4P_{1\frac{1}{2}} - (^3P)5p\ ^4P^\circ_{\frac{1}{2}}$
5	1932.53	51746	$(^1D)5s\ ^2D_{1\frac{1}{2}} - (^1D)5p\ ^2F^\circ_{2\frac{1}{2}}$
			$(^3P)5s\ ^2P_{1\frac{1}{2}} - (^3P)5p\ ^4D^\circ_{2\frac{1}{2}}$
20	1925.30	51940	$(^3F)5s\ ^2F_{3\frac{1}{2}} - (^3F)5p\ ^4F^\circ_{4\frac{1}{2}}$
60	1917.08	52163	$(^3F)5s\ ^4F_{4\frac{1}{2}} - (^3F)5p\ ^4D^\circ_{3\frac{1}{2}}$
40	1916.92	52167	$(^3F)5s\ ^4F_{3\frac{1}{2}} - (^3F)5p\ ^4G^\circ_{4\frac{1}{2}}$
6	1913.01	52274	$(^3F)5s\ ^2F_{2\frac{1}{2}} - (^3F)5p\ ^4F^\circ_{2\frac{1}{2}}$
6	1908.49	52397	$(^3P)5s\ ^4P_{2\frac{1}{2}} - (^3F)5p\ ^2F^\circ_{3\frac{1}{2}}$
0	1901.20	52598	$(^3P)5s\ ^2P_{\frac{1}{2}} - (^3P)5p\ ^2P^\circ_{1\frac{1}{2}}$
2	1898.86	52663	$(^3F)5s\ ^4F_{4\frac{1}{2}} - (^3F)5p\ ^4D^\circ_{3\frac{1}{2}}$
7	1896.69	52723	$(^1D)5s\ ^2D_{2\frac{1}{2}} - (^1D)5p\ ^2P^\circ_{1\frac{1}{2}}$
7	1894.01	52798	$(^3F)5s\ ^2F_{3\frac{1}{2}} - (^3F)5p\ ^2F^\circ_{3\frac{1}{2}}$
30	1889.57	52922	$(^3F)5s\ ^4F_{3\frac{1}{2}} - (^3F)5p\ ^4G^\circ_{3\frac{1}{2}}$
2	1882.44	53123	$(^1D)5s\ ^2D_{2\frac{1}{2}} - (^1D)5p\ ^2D^\circ_{1\frac{1}{2}}$
25	1880.36	53181	$(^3F)5s\ ^4F_{4\frac{1}{2}} - (^3F)5p\ ^4G^\circ_{5\frac{1}{2}}$
5	1874.93	53335	$(^1D)5s\ ^2D_{1\frac{1}{2}} - (^1D)5p\ ^2P^\circ_{\frac{1}{2}}$
40	1873.45	53378	$(^3F)5s\ ^4F_{3\frac{1}{2}} - (^3F)5p\ ^4D^\circ_{2\frac{1}{2}}$
10	1872.55	53403	$(^3F)5s\ ^2F_{3\frac{1}{2}} - (^3F)5p\ ^2D^\circ_{2\frac{1}{2}}$
15	1868.10	53530	$(^3P)5s\ ^4P_{2\frac{1}{2}} - (^3P)5p\ ^4P^\circ_{1\frac{1}{2}}$
			$(^1D)5s\ ^2D_{2\frac{1}{2}} - (^1D)5p\ ^2D^\circ_{2\frac{1}{2}}$
35	1867.12	53558	$(^3F)5s\ ^2F_{3\frac{1}{2}} - (^3F)5p\ ^2G^\circ_{4\frac{1}{2}}$
8	1863.39	53666	$(^3P)5s\ ^2P_{1\frac{1}{2}} - (^3P)5p\ ^2D^\circ_{2\frac{1}{2}}$
10	1860.64	53745	$(^3P)5s\ ^4P_{2\frac{1}{2}} - (^3P)5p\ ^4P^\circ_{2\frac{1}{2}}$
12	1858.91	53795	$(^3F)5s\ ^2F_{3\frac{1}{2}} - (^3F)5p\ ^2G^\circ_{4\frac{1}{2}}$
15	1856.33	53870	$(^3F)5s\ ^4F_{3\frac{1}{2}} - (^3F)5p\ ^4D^\circ_{1\frac{1}{2}}$
6	1854.04	53936	$(^3F)5s\ ^2F_{3\frac{1}{2}} - (^3F)5p\ ^2D^\circ_{1\frac{1}{2}}$
12	1849.93	54056	$(^3F)5s\ ^4F_{4\frac{1}{2}} - (^3F)5p\ ^4D^\circ_{\frac{1}{2}}$
10	1846.96	54143	$(^3P)5s\ ^2P_{1\frac{1}{2}} - (^3P)5p\ ^2D^\circ_{1\frac{1}{2}}$
40	1840.14	54344	$(^1G)5s\ ^2G_{4\frac{1}{2}} - (^1G)5p\ ^2H^\circ_{5\frac{1}{2}}$
15	1838.64	54388	$(^3F)5s\ ^4F_{4\frac{1}{2}} - (^3F)5p\ ^4G^\circ_{5\frac{1}{2}}$
25	1836.10	54463	$(^3P)5s\ ^4P_{1\frac{1}{2}} - (^1D)5p\ ^2F^\circ_{2\frac{1}{2}}$
10	1834.31	54516	$(^3F)5s\ ^2F_{3\frac{1}{2}} - (^3F)5p\ ^4F^\circ_{2\frac{1}{2}}$
25	1832.33	54575	$(^3F)5s\ ^4F_{4\frac{1}{2}} - (^3F)5p\ ^4F^\circ_{1\frac{1}{2}}$
			$(^1D)5s\ ^2D_{2\frac{1}{2}} - (^3P)5p\ ^4D^\circ_{1\frac{1}{2}}$
35	1828.83	54680	$(^3F)5s\ ^4F_{4\frac{1}{2}} - (^3F)5p\ ^4G^\circ_{4\frac{1}{2}}$
0	1828.21	54698	$(^1D)5s\ ^2D_{2\frac{1}{2}} - (^3P)5p\ ^4D^\circ_{2\frac{1}{2}}$
8	1826.61	54746	$(^1D)5s\ ^2D_{2\frac{1}{2}} - (^3P)5p\ ^4D^\circ_{3\frac{1}{2}}$
4	1823.99	54825	$(^1D)5s\ ^2D_{1\frac{1}{2}} - (^1D)5p\ ^2P^\circ_{1\frac{1}{2}}$
15	1822.45	54871	$(^3F)5s\ ^2F_{3\frac{1}{2}} - (^3F)5p\ ^2F^\circ_{3\frac{1}{2}}$
2	1821.50	54900	$(^3P)5s\ ^2P_{1\frac{1}{2}} - (^3P)5p\ ^2P^\circ_{1\frac{1}{2}}$
25	1816.83	55041	$(^3F)5s\ ^2F_{3\frac{1}{2}} - (^3F)5p\ ^2F^\circ_{2\frac{1}{2}}$
0	1813.15	55153	$(^1G)5s\ ^2G_{4\frac{1}{2}} - (^1G)5p\ ^2F^\circ_{3\frac{1}{2}}$
1	1810.74	55226	$(^1D)5s\ ^2D_{1\frac{1}{2}} - (^1D)5p\ ^2D^\circ_{1\frac{1}{2}}$
5	1808.92	55282	$(^1G)5s\ ^2G_{4\frac{1}{2}} - (^1G)5p\ ^2F^\circ_{4\frac{1}{2}}$
30	1808.23	55303	$(^3F)5s\ ^4F_{3\frac{1}{2}} - (^3F)5p\ ^4G^\circ_{3\frac{1}{2}}$
15	1802.24	55487	$(^3F)5s\ ^4F_{4\frac{1}{2}} - (^3F)5p\ ^4F^\circ_{3\frac{1}{2}}$
3	1797.64	55629	$(^1D)5s\ ^2D_{1\frac{1}{2}} - (^1D)5p\ ^2D^\circ_{2\frac{1}{2}}$
			$(^3P)5s\ ^4P_{\frac{1}{2}} - (^1D)5p\ ^2P^\circ_{1\frac{1}{2}}$
15	1793.90	55745	$(^3F)5s\ ^4F_{4\frac{1}{2}} - (^3F)5p\ ^2D^\circ_{2\frac{1}{2}}$
1	1785.59	56004	$(^3F)5s\ ^2F_{2\frac{1}{2}} - (^3P)5p\ ^4P^\circ_{1\frac{1}{2}}$
2	1784.48	56039	$(^3F)5s\ ^2F_{3\frac{1}{2}} - (^3F)5p\ ^2G^\circ_{3\frac{1}{2}}$
1	1783.93	56056	$(^3P)5s\ ^4P_{1\frac{1}{2}} - (^1D)5p\ ^2P^\circ_{\frac{1}{2}}$
5	1778.75	56219	$(^3F)5s\ ^2F_{2\frac{1}{2}} - (^3P)5p\ ^4P^\circ_{2\frac{1}{2}}$
2	1776.07	56304	$(^3P)5s\ ^2P_{\frac{1}{2}} - (^3P)5p\ ^2P^\circ_{\frac{1}{2}}$
10	1771.81	56440	$(^3F)5s\ ^2G_{4\frac{1}{2}} - (^1G)5p\ ^2F^\circ_{3\frac{1}{2}}$
15	1768.70	56536	$(^3F)5s\ ^4F_{4\frac{1}{2}} - (^3F)5p\ ^4F^\circ_{4\frac{1}{2}}$
4	1766.22	56618	$(^1D)5s\ ^2D_{2\frac{1}{2}} - (^3P)5p\ ^2D^\circ_{2\frac{1}{2}}$
7	1764.36	56678	$(^1D)5s\ ^2D_{1\frac{1}{2}} - (^3P)5p\ ^4D^\circ_{1\frac{1}{2}}$
1	1761.57	56768	$(^3F)5s\ ^4F_{3\frac{1}{2}} - (^3F)5p\ ^4G^\circ_{2\frac{1}{2}}$
10	1760.57	56800	$(^1D)5s\ ^2D_{2\frac{1}{2}} - (^3P)5p\ ^4D^\circ_{2\frac{1}{2}}$
3	1758.79	56857	$(^3F)5s\ ^4F_{3\frac{1}{2}} - (^3F)5p\ ^4F^\circ_{2\frac{1}{2}}$
4	1755.90	56951	$(^3F)5s\ ^4F_{3\frac{1}{2}} - (^3F)5p\ ^2D^\circ_{2\frac{1}{2}}$
2	1754.89	56984	$(^3P)5s\ ^2P_{1\frac{1}{2}} - (^1G)5p\ ^2F^\circ_{2\frac{1}{2}}$
75	1751.03[1]	57109	$(^3F)5s\ ^4F_{4\frac{1}{2}} - (^3F)5p\ ^4G^\circ_{4\frac{1}{2}}$
20	1747.34	57230	$(^3P)5s\ ^4P_{2\frac{1}{2}} - (^1D)5p\ ^2F^\circ_{3\frac{1}{2}}$
3	1739.52	57487	$(^3P)5s\ ^4P_{\frac{1}{2}} - (^3P)5p\ ^4D^\circ_{1\frac{1}{2}}$
1*d*	1737.92	57540	$(^3P)5s\ ^4P_{1\frac{1}{2}} - (^1D)5p\ ^2P^\circ_{1\frac{1}{2}}$
3*d*	1729.55	57819	$(^3F)5s\ ^4F_{4\frac{1}{2}} - (^3F)5p\ ^4G^\circ_{5\frac{1}{2}}$
0	1728.73	57846	$(^1D)5s\ ^2D_{2\frac{1}{2}} - (^3P)5p\ ^2P^\circ_{1\frac{1}{2}}$
25	1728.14	57866	$(^3F)5s\ ^4F_{3\frac{1}{2}} - (^3F)5p\ ^4F^\circ_{3\frac{1}{2}}$
0	1725.85	57943	$(^3F)5s\ ^2F_{2\frac{1}{2}} - (^1D)5p\ ^2F^\circ_{2\frac{1}{2}}$
20	1722.27	58063	$(^3F)5s\ ^4F_{2\frac{1}{2}} - (^3F)5p\ ^4F^\circ_{2\frac{1}{2}}$
2	1713.81	58350	$(^3P)5s\ ^4P_{1\frac{1}{2}} - (^1D)5p\ ^2D^\circ_{2\frac{1}{2}}$
1	1710.56	58460	$(^3F)5s\ ^2F_{3\frac{1}{2}} - (^3P)5p\ ^4P^\circ_{2\frac{1}{2}}$
15	1708.86	58519	$(^3F)5s\ ^4F_{4\frac{1}{2}} - (^3F)5p\ ^2D^\circ_{2\frac{1}{2}}$
0	1707.97	58549	$(^3P)5s\ ^4P_{2\frac{1}{2}} - (^1D)5p\ ^2P^\circ_{1\frac{1}{2}}$
5	1706.89	58586	$(^3F)5s\ ^4F_{2\frac{1}{2}} - (^3F)5p\ ^2F^\circ_{3\frac{1}{2}}$
5	1706.61	58596	$(^3P)5s\ ^2P_{1\frac{1}{2}} - (^3P)5p\ ^2P^\circ_{\frac{1}{2}}$
20	1705.06	58649	$(^1D)5s\ ^2D_{2\frac{1}{2}} - (^1G)5p\ ^2F^\circ_{3\frac{1}{2}}$
5	1703.04	58719	$(^1D)5s\ ^2D_{1\frac{1}{2}} - (^3P)5p\ ^2D^\circ_{2\frac{1}{2}}$
50	1693.51	59049	$(^3F)5s\ ^4F_{4\frac{1}{2}} - (^3F)5p\ ^4F^\circ_{4\frac{1}{2}}$
0	1685.46	59331	$(^3F)5s\ ^4F_{3\frac{1}{2}} - (^3F)5p\ ^2D^\circ_{2\frac{1}{2}}$
0	1684.68	59359	$(^3P)5s\ ^4P_{2\frac{1}{2}} - (^1D)5p\ ^2D^\circ_{2\frac{1}{2}}$
1*d*	1683.56	59398	$(^3P)5s\ ^4P_{1\frac{1}{2}} - (^3P)5p\ ^4D^\circ_{1\frac{1}{2}}$
0	1682.09	59450	$(^3F)5s\ ^4F_{4\frac{1}{2}} - (^3F)5p\ ^2F^\circ_{3\frac{1}{2}}$
10	1681.07	59486	$(^3F)5s\ ^4F_{3\frac{1}{2}} - (^3F)5p\ ^2G^\circ_{4\frac{1}{2}}$
0	1680.18	59517	$(^3P)5s\ ^4P_{1\frac{1}{2}} - (^3P)5p\ ^4D^\circ_{2\frac{1}{2}}$
8	1678.27	59585	$(^3F)5s\ ^4F_{3\frac{1}{2}} - (^3F)5p\ ^2G^\circ_{3\frac{1}{2}}$
6	1674.99	59702	$(^3F)5s\ ^2F_{2\frac{1}{2}} - (^1D)5p\ ^2F^\circ_{3\frac{1}{2}}$
8	1674.34	59725	$(^3F)5s\ ^4F_{3\frac{1}{2}} - (^3F)5p\ ^2D^\circ_{1\frac{1}{2}}$
1	1668.48	59935	$(^1D)5s\ ^2D_{2\frac{1}{2}} - (^1G)5p\ ^2F^\circ_{2\frac{1}{2}}$
0	1668.20	59945	$(^1D)5s\ ^2D_{1\frac{1}{2}} - (^3P)5p\ ^2P^\circ_{1\frac{1}{2}}$
0	1655.60	60401	$(^3P)5s\ ^4P_{2\frac{1}{2}} - (^3P)5p\ ^4D^\circ_{1\frac{1}{2}}$
2	1650.97	60571	$(^3P)5s\ ^4P_{2\frac{1}{2}} - (^3P)5p\ ^4D^\circ_{2\frac{1}{2}}$
2	1650.52	60587	$(^3F)5s\ ^4F_{4\frac{1}{2}} - (^3P)5p\ ^4P^\circ_{1\frac{1}{2}}$
0	1648.54	60660	$(^3F)5s\ ^4F_{3\frac{1}{2}} - (^3F)5p\ ^2F^\circ_{2\frac{1}{2}}$
2	1644.66	60803	$(^3F)5s\ ^4F_{4\frac{1}{2}} - (^3P)5p\ ^4P^\circ_{2\frac{1}{2}}$
2	1640.22	60967	$(^3F)5s\ ^4F_{4\frac{1}{2}} - (^3F)5p\ ^2F^\circ_{3\frac{1}{2}}$
1	1638.75	61022	$(^3F)5s\ ^2F_{3\frac{1}{2}} - (^1D)5p\ ^2P^\circ_{1\frac{1}{2}}$
1	1627.61	61440	$(^3P)5s\ ^4P_{1\frac{1}{2}} - (^3P)5p\ ^2D^\circ_{2\frac{1}{2}}$
1	1618.34	61792	$(^3F)5s\ ^4F_{3\frac{1}{2}} - (^3P)5p\ ^4P^\circ_{1\frac{1}{2}}$
0	1615.25	61910	$(^3P)5s\ ^4P_{1\frac{1}{2}} - (^3P)5p\ ^2D^\circ_{1\frac{1}{2}}$
3	1614.26	61948	$(^3F)5s\ ^2F_{2\frac{1}{2}} - (^1D)5p\ ^2F^\circ_{2\frac{1}{2}}$

[1] Classification by Gibbs and White.
d denotes a diffuse line.

TABLE IV—(*continued*)

INT.	λ VAC.	ν VAC.	CLASSIFICATION	INT.	λ VAC.	ν VAC.	CLASSIFICATION
1	1612.75	62006	$(^2F)5s\ ^4F_{4\frac{1}{2}} - (^3F)5p\ ^2G^\circ_{4\frac{1}{2}}$ $(^2F)5s\ ^4F_{2\frac{1}{2}} - (^3P)5p\ ^4P^\circ_{2\frac{1}{2}}$	6	826.00	121065	$^2D_{2\frac{1}{2}} - (^1F)5p\ ^4G^\circ_{2\frac{1}{2}}$
3	1611.90	62039	$(^3F)5s\ ^2D_{1\frac{1}{2}} - (^1G)5p\ ^2F^\circ_{2\frac{1}{2}}$	18	822.39	121597	$^2D_{1\frac{1}{2}} - (^3F)5p\ ^4F^\circ_{2\frac{1}{2}}$
2	1601.48	62442	$(^3P)5s\ ^4P_{2\frac{1}{2}} - (^3P)5p\ ^2D^\circ_{2\frac{1}{2}}$	3	819.59	122012	$^2D_{2\frac{1}{2}} - (^3F)5p\ ^4D^\circ_{1\frac{1}{2}}$
1	1595.69	62669	$(^1P)5s\ ^4P_{1\frac{1}{2}} - (^3P)5p\ ^2P^\circ_{1\frac{1}{2}}$	15	816.22	122531	$^2D_{2\frac{1}{2}} - (^3F)5p\ ^4G^\circ_{2\frac{1}{2}}$
1	1590.47	62875	$(^3F)5s\ ^2F_{2\frac{1}{2}} - (^3P)5p\ ^4D^\circ_{1\frac{1}{2}}$	1	811.30	123259	$^2D_{1\frac{1}{2}} - (^3F)5p\ ^2D^\circ_{1\frac{1}{2}}$
1	1587.39	62997	$(^2F)5s\ ^2F_{2\frac{1}{2}} - (^3P)5p\ ^4D^\circ_{2\frac{1}{2}}$	30	808.88	123628	$^2D_{2\frac{1}{2}} - (^3F)5p\ ^4F^\circ_{2\frac{1}{2}}$
1	1586.26	63041	$(^3F)5s\ ^4F_{3\frac{1}{2}} - (^3F)5p\ ^2F^\circ_{2\frac{1}{2}}$ $(^3F)5s\ ^2F_{2\frac{1}{2}} - (^3P)5p\ ^4D^\circ_{2\frac{1}{2}}$	5	806.93	123926	$^2D_{2\frac{1}{2}} - (^3F)5p\ ^4F^\circ_{1\frac{1}{2}}$
				1	805.18	124196	$^2D_{1\frac{1}{2}} - (^3F)5p\ ^2F^\circ_{2\frac{1}{2}}$
				0	802.99	124535	$^2D_{1\frac{1}{2}} - (^3P)5p\ ^4P^\circ_{\frac{1}{2}}$
1	1575.26	63481	$(^3F)5s\ ^4F_{4\frac{1}{2}} - (^3F)5p\ ^2F^\circ_{3\frac{1}{2}}$	40	799.41	125092	$^2D_{2\frac{1}{2}} - (^3F)5p\ ^2D^\circ_{2\frac{1}{2}}$
0d	1571.07	63651	$(^1D)5s\ ^2D_{1\frac{1}{2}} - (^3P)5p\ ^2P^\circ_{\frac{1}{2}}$	25	797.91	125327	$^2D_{1\frac{1}{2}} - (^3P)5p\ ^4P^\circ_{1\frac{1}{2}}$
1	1570.38	63679	$(^3P)5s\ ^4P_{2\frac{1}{2}} - (^3P)5p\ ^2P^\circ_{1\frac{1}{2}}$	20	796.54	125543	$^2D_{1\frac{1}{2}} - (^3P)5p\ ^4P^\circ_{2\frac{1}{2}}$
1	1569.16	63728	$(^3F)5s\ ^4F_{3\frac{1}{2}} - (^1D)5p\ ^2F^\circ_{2\frac{1}{2}}$	25	792.35	126207	$^2D_{2\frac{1}{2}} - (^3F)5p\ ^4F^\circ_{2\frac{1}{2}}$
1	1560.74	64072	$(^2F)5s\ ^2F_{2\frac{1}{2}} - (^1D)5p\ ^2D^\circ_{2\frac{1}{2}}$	20	789.08	126730	$^2D_{2\frac{1}{2}} - (^3F)5p\ ^2F^\circ_{2\frac{1}{2}}$
1	1551.44	64456	$(^3P)5s\ ^4P_{\frac{1}{2}} - (^3P)5p\ ^2P^\circ_{\frac{1}{2}}$	15	785.76	127265	$^2D_{1\frac{1}{2}} - (^1D)5p\ ^2F^\circ_{2\frac{1}{2}}$
1	1550.94	64477	$(^3F)5s\ ^4F_{4\frac{1}{2}} - (^3F)5p\ ^2G^\circ_{3\frac{1}{2}}$ $(^3P)5s\ ^4P_{2\frac{1}{2}} - (^1G)5p\ ^2F^\circ_{2\frac{1}{2}}$	20	782.91	127729	$^2D_{2\frac{1}{2}} - (^3F)5p\ ^2G^\circ_{3\frac{1}{2}}$
				35	776.38	128803	$^2D_{2\frac{1}{2}} - (^3F)5p\ ^2F^\circ_{2\frac{1}{2}}$
3d	1531.71	65287	$(^3F)5s\ ^2F_{2\frac{1}{2}} - (^3P)5p\ ^4D^\circ_{2\frac{1}{2}}$	5	776.03	128861	$^2D_{1\frac{1}{2}} - (^1D)5p\ ^2P^\circ_{\frac{1}{2}}$
1	1527.06	65485	$(^3F)5s\ ^4F_{2\frac{1}{2}} - (^1D)5p\ ^2F^\circ_{2\frac{1}{2}}$	15	769.61	129936	$^2D_{2\frac{1}{2}} - (^3P)5p\ ^4P^\circ_{1\frac{1}{2}}$
1	1512.64	66110	$(^3F)5s\ ^4F_{3\frac{1}{2}} - (^1D)5p\ ^2F^\circ_{3\frac{1}{2}}$	25	768.33	130152	$^2D_{2\frac{1}{2}} - (^3P)5p\ ^4P^\circ_{2\frac{1}{2}}$
1	1511.86	66144	$(^2F)5s\ ^2F_{2\frac{1}{2}} - (^3P)5p\ ^2P^\circ_{1\frac{1}{2}}$	20	767.19	130346	$^2D_{1\frac{1}{2}} - (^1D)5p\ ^2P^\circ_{1\frac{1}{2}}$
0	1506.74	66369	$(^3P)5s\ ^4P_{1\frac{1}{2}} - (^3P)5p\ ^2P^\circ_{\frac{1}{2}}$	3	762.43	131160	$^2D_{1\frac{1}{2}} - (^1D)5p\ ^2D^\circ_{2\frac{1}{2}}$
0	1493.69	66948	$(^3F)5s\ ^2F_{2\frac{1}{2}} - (^1G)5p\ ^2F^\circ_{2\frac{1}{2}}$	10	758.27	131879	$^2D_{2\frac{1}{2}} - (^1D)5p\ ^2F^\circ_{2\frac{1}{2}}$
0	1479.81	67576	$(^3F)5s\ ^4F_{1\frac{1}{2}} - (^3P)5p\ ^4D^\circ_{2\frac{1}{2}}$	4	756.43	132200	$^2D_{1\frac{1}{2}} - (^3P)5p\ ^4D^\circ_{1\frac{1}{2}}$
0	1473.40	67870	$(^3F)5s\ ^4F_{3\frac{1}{2}} - (^1D)5p\ ^2F^\circ_{3\frac{1}{2}}$	15	755.73	132322	$^2D_{1\frac{1}{2}} - (^3P)5p\ ^4D^\circ_{2\frac{1}{2}}$
1	1453.75	68788	$(^3F)5s\ ^4F_{2\frac{1}{2}} - (^3P)5p\ ^4D^\circ_{2\frac{1}{2}}$	20	748.30	133636	$^2D_{2\frac{1}{2}} - (^1D)5p\ ^2F^\circ_{3\frac{1}{2}}$
0	1445.34	69188	$(^2F)5s\ ^2F_{2\frac{1}{2}} - (^1G)5p\ ^2F^\circ_{2\frac{1}{2}}$	8	744.91	134244	$^2D_{1\frac{1}{2}} - (^3P)5p\ ^2D^\circ_{2\frac{1}{2}}$
1	1420.82	70382	$(^3F)5s\ ^4F_{4\frac{1}{2}} - (^1D)5p\ ^2F^\circ_{3\frac{1}{2}}$	20	742.29	134718	$^2D_{1\frac{1}{2}} - (^3P)5p\ ^2D^\circ_{1\frac{1}{2}}$
6	1405.25	71162	$(^3F)5s\ ^4F_{3\frac{1}{2}} - (^3P)5p\ ^4D^\circ_{2\frac{1}{2}}$	20	740.98	134956	$^2D_{2\frac{1}{2}} - (^1D)5p\ ^2P^\circ_{1\frac{1}{2}}$
0	1404.30	71210	$(^3F)5s\ ^4F_{2\frac{1}{2}} - (^3P)5p\ ^4D^\circ_{3\frac{1}{2}}$	10	738.13	135477	$^2D_{1\frac{1}{2}} - (^3P)5p\ ^2P^\circ_{1\frac{1}{2}}$
0	1390.17	71934	$(^3F)5s\ ^4F_{2\frac{1}{2}} - (^3P)5p\ ^2P^\circ_{1\frac{1}{2}}$	20	736.57	135764	$^2D_{2\frac{1}{2}} - (^1D)5p\ ^2D^\circ_{2\frac{1}{2}}$
0	1356.33	73728	$(^3F)5s\ ^4F_{4\frac{1}{2}} - (^3P)5p\ ^4D^\circ_{3\frac{1}{2}}$	15	730.94	136810	$^2D_{2\frac{1}{2}} - (^3P)5p\ ^4D^\circ_{2\frac{1}{2}}$
0	1308.84	76404	$(^2F)5s\ ^4F_{3\frac{1}{2}} - (^1G)5p\ ^2F^\circ_{2\frac{1}{2}}$	15	730.28	136934	$^2D_{2\frac{1}{2}} - (^3P)5p\ ^4D^\circ_{2\frac{1}{2}}$
4	873.13	114530	$4d^9\ ^2D_{1\frac{1}{2}} - 4d^8(^3F)5p\ ^4D^\circ_{2\frac{1}{2}}$	35	730.04	136979	$^2D_{2\frac{1}{2}} - (^3P)5p\ ^4D^\circ_{3\frac{1}{2}}$
0	866.47	115411	$^2D_{2\frac{1}{2}} - (^3F)5p\ ^4D^\circ_{3\frac{1}{2}}$	30	726.96	137559	$^2D_{1\frac{1}{2}} - (^1G)5p\ ^2F^\circ_{2\frac{1}{2}}$
0	851.69	117414	$^2D_{1\frac{1}{2}} - (^3F)5p\ ^4D^\circ_{1\frac{1}{2}}$	5	720.15	138860	$^2D_{2\frac{1}{2}} - (^3P)5p\ ^2D^\circ_{2\frac{1}{2}}$
5	848.00	117924	$^2D_{1\frac{1}{2}} - (^3F)5p\ ^4G^\circ_{2\frac{1}{2}}$	20	718.53	139173	$^2D_{1\frac{1}{2}} - (^3P)5p\ ^2P^\circ_{\frac{1}{2}}$
6	839.34	119141	$^2D_{2\frac{1}{2}} - (^3F)5p\ ^4D^\circ_{2\frac{1}{2}}$	10	717.73	139328	$^2D_{2\frac{1}{2}} - (^3P)5p\ ^2D^\circ_{1\frac{1}{2}}$
20	838.11	119316	$^2D_{1\frac{1}{2}} - (^3F)5p\ ^4F^\circ_{1\frac{1}{2}}$	20	713.85	140085	$^2D_{2\frac{1}{2}} - (^3P)5p\ ^2P^\circ_{1\frac{1}{2}}$
8	829.98	120485	$^2D_{1\frac{1}{2}} - (^3F)5p\ ^2D^\circ_{2\frac{1}{2}}$	20	709.80	140885	$^2D_{2\frac{1}{2}} - (^1G)5p\ ^2F^\circ_{3\frac{1}{2}}$

any of the elements of the sequence. The reinversion of the $4d^8(^1D)5s\ ^2D_{2\frac{1}{2},\ 1\frac{1}{2}}$ levels in passing from Rh I to Pd II appears as a marked irregularity. The relative position of the levels in Pd II and Ag III makes it seem probable that the $4d^8(^3P)5s\ ^2P_{1\frac{1}{2}}$ and $4d^8(^1D)5s\ ^2D_{1\frac{1}{2}}$ levels have been confused in the analysis of the Rh I spectrum. The dotted lines indicate the increase in regularity when these two levels are interchanged in Rh I.

The term values relative to $4d^9\ ^2D_{2\frac{1}{2}}$ as zero are given in Table III. The term structure shows considerable departure from L–S coupling. The multiplets in this sequence are irregular and overlap considerably especially in the $4d^85p$ configuration. Except for the multiplets $4d^8(^3F)5p\ ^4D^\circ$ and $4d^8(^3F)5s\ ^4F$, the Landé interval rule is not even approximately obeyed. There are marked departures from the usual L selection rules. Transitions involving a change in L as great as ± 3 are common and give rise to some of the strong lines of the spectrum. The term $4d^8(^3P)5s\ ^4P_{\frac{1}{2}}$ is considered questionable for two reasons. The transition $4d^8(^3P)5s\ ^4P_{\frac{1}{2}} - 4d^8(^3F)5p\ ^4D^\circ_{\frac{1}{2}}$, which should occur with an intensity of about 6 on the scale used, is entirely absent. Furthermore, the use of this term (i.e., $^4P_{\frac{1}{2}} = 79{,}326\ \text{cm}^{-1}$) results in a number of coincidences with lines used elsewhere in the analysis. However, the position of the level in the centroid diagram, and the fact that no other term value has been found which yields the observed transitions, lends some support to the assignment given here. Some terms, notably $4d^8(^1G)5p\ ^2G^\circ_{4\frac{1}{2},\ 3\frac{1}{2}}$, $4d^8(^3P)5p\ ^4S^\circ_{1\frac{1}{2}}$ and $^2S^\circ_{\frac{1}{2}}$ could not be definitely established either because of paucity, or lack of intensity, of the combinations with other terms.

The classified lines are collected in Table IV. The measurements are believed to be accurate to at least 0.05A (1.4 cm^{-1} at 1900A to 5 cm^{-1} at 1000A) for all wavelengths reported. The wavelengths and intensities are those obtained from the spectrum of the silver spark.

The author wishes to express his gratitude to Professor R. C. Gibbs for helpful advice and criticism given during the course of this investigation. Thanks are also extended to Dr. C. W. Gartlein, who suggested the problem, for assistance in carrying out some of the experimental work.

Band Spectrum of Pb_2 in Absorption and Emission

E. N. SHAWHAN, *Mendenhall Laboratory of Physics, The Ohio State University*

(Received June 10, 1935)

A band system has been observed when light is absorbed by lead vapor heated to about 1400°C. The same band system has also been found in emission. Some ninety band heads have been located between the wavelengths of 4600 and 5200A. The bands are degraded toward the red. The vibrational analysis has been made but the complexity of the isotope effect has prevented a rotational analysis. Within the error of observation the heads are represented by the formula:

$$\nu = 19{,}570.8 + 159.22(v'+\tfrac{1}{2}) - 0.882(v'+\tfrac{1}{2})^2 + 0.00518(v'+\tfrac{1}{2})^3 - 256.5(v''+\tfrac{1}{2}) + 2.96(v''+\tfrac{1}{2})^2.$$

Fairly conclusive evidence is presented for the ascription of this band system to the molecule Pb_2.

INTRODUCTION

SINCE band spectra cannot originate from single atoms, the presence of band spectra in metallic vapors is evidence for the formation of molecules of like or unlike metallic atoms. The alkali metal vapors which have been investigated from this point of view have shown extensive band spectra which may be ascribed to molecules formed from two like alkali atoms. In the case of lithium,[1, 2, 3, 4] sodium,[5, 6, 7] and potassium,[8, 9, 10] partial vibrational and rotational analyses are available. Partial vibrational analyses of several band systems of diatomic caesium[11, 12] and rubidium[12] have been made. Similar investigations carried out on the vapors of the metals of the second group[13, 14, 15, 16] have revealed bands which have been attributed to diatomic molecules but no vibrational analyses have been obtained. A study of the band spectra of metals of the fifth group shows that these metals also form diatomic molecules in the vapor state. In the case of phosphorus[17, 18] both vibrational and rotational analyses have been made. Only vibrational constants are known for arsenic,[19, 20] antimony[21] and bismuth.[21, 22]

Since it is of interest to extend this type of investigation to metals occurring in other groups of the periodic table, it was decided to investigate lead vapor in order to determine whether or not molecules of this element exist in the vapor state.

EXPERIMENTAL

Chemically pure lead was introduced into a graphite tube about 50 cm long and 2 cm in internal diameter. This tube, which was heated by means of a Hoskins electric furnace operated at 25 volts a.c. and 400 amperes, was open to air at atmospheric pressure. The temperature was maintained at about 1400°C. The carbon vapor from the interior of the graphite tube served as a reducing agent and thus decreased the rate of oxidation of the lead vapor. A five-hundred watt projection lamp or an underwater spark with magnesium electrodes provided a source of continuous radiation. When the background used in obtaining the absorption spectrum was removed the bands could be photographed in emission from the hot vapor.

The spectrum, which showed bands between 4600 and 5200A, was photographed both in absorption and emission with a Hilger E-1

[1] J. E. Vance and J. R. Duffman, Phys. Rev. **47**, 215 (1935).
[2] F. W. Loomis and R. E. Nusbaum, Phys. Rev. **38**, 1447 (1931).
[3] A. Harvey and F. A. Jenkins, Phys. Rev. **35**, 789 (1930).
[4] K. Wurm, Zeits. f. Physik **59**, 35 (1929).
[5] F. W. Loomis and R. E. Nusbaum, Phys. Rev. **40**, 380 (1932).
[6] W. R. Fredrickson, Phys. Rev. **34**, 207 (1929).
[7] W. Weizel and M. Kulp, Ann. d. Physik **4**, 971 (1930).
[8] R. E. Nusbaum and F. W. Loomis, Phys. Rev. **39**, 89 (1932).
[9] F. W. Loomis, Phys. Rev. **38**, 2153 (1931).
[10] W. O. Crane and A. Christy, Phys. Rev. **36**, 421 (1930).
[11] F. W. Loomis and P. Kusch, Phys. Rev. **46**, 292 (1934).
[12] E. Matuyama, Tôhoku Univ. Sci. Rep. **23**, 308 (1934).
[13] H. Hamada, Nature **127**, 555 (1931).
[14] J. G. Winans, Phil. Mag. **7**, 555 (1929).
[15] F. L. Mohler and H. R. Moore, J. Opt. Soc. Am. **15**, 74 (1927).
[16] J. M. Walters and S. Barratt, Proc. Roy. Soc. **A122**, 201 (1928).
[17] G. Hertzberg, Phys. Rev. **40**, 313 (1932).
[18] A. Jackowlewa, Zeits. f. Physik **69**, 548 (1931).
[19] G. M. Almy and G. D. Kinzer, Phys. Rev. **47**, 721 (1935).
[20] G. E. Gibson and Angus Macfarlane, Phys. Rev. **46**, 1059 (1934).
[21] G. Nakamura and T. Shidei, Jap. J. Phys. **10**, 11 (1935).
[22] G. M. Almy and F. M. Sparks, Phys. Rev. **44**, 365 (1933).

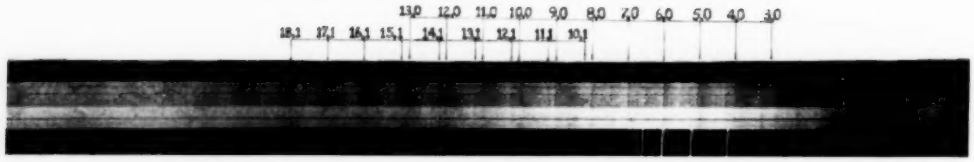

FIG. 1. Band spectrum of Pb_2 in absorption between 4600 and 5200A with iron comparison spectrum.

quartz spectrograph and with a large two-prism glass spectrograph giving a dispersion of 6 to 13A/mm in the region of the spectrum used. It was also photographed in absorption in the second order of a Littrow mounted concave grating having a radius of curvature of 10 feet and giving a dispersion of 2.7A/mm. The time of exposure ranged from 30 seconds on the E-1 spectrograph to 30 minutes on the concave grating.

Photographs of the spectrum taken through the hot graphite tube without the lead vapor in it, showed no bands in this region. Tin, which might be expected to occur as an impurity in the lead, was introduced into the tube without the lead, but only the band spectrum of tin oxide was developed. It was, however, found possible to observe the band heads associated with lead vapor when the graphite tube was replaced by an iron tube. In this case the temperature at which the bands first appear is somewhat lower—at about 1300°C. At this temperature the iron is near its melting point. The rate of oxidation of the iron is large and the lead probably oxidizes less rapidly than in the carbon tube so that the concentration of lead vapor is higher than it would be if the lead were heated to the same temperature in a graphite tube. Hence sufficient vapor is present to develop the bands at a lower temperature. The iron tube, when heated without the lead in it, did not show this band system either in absorption or emission.

Lead vapor rapidly attacks quartz and alundum tubes so that the choice of tubes that can be used at these temperatures is quite limited.

An iron arc was used as a standard of wavelengths and the bands on the several plates were measured by means of a Geneva Society comparator which could be read to ±0.001 mm. However, the diffuseness of the heads does not permit settings to be made to this accuracy.

RESULTS

Some ninety band heads in all were measured. These bands lie between 4600A and 5200A and degrade to the red. They therefore occur in the same region of the spectrum as the *A* and *B* systems of PbO which extend from 4145A to 6720A. Fig. 1 shows this band system with iron comparison spectrum as photographed on the glass spectrograph. The wave numbers of the band heads which have been measured are recorded in Table I, together with their vibrational quantum numbers and estimated intensities. These heads are represented within the observational error by the formula:

TABLE I. *Band heads of* Pb_2.

I	v'	v''	$\nu_{obs.}$	$\nu_{obs.}-\nu_{calc.}$	I	v'	v''	$\nu_{obs.}$	$\nu_{obs.}-\nu_{calc.}$
2	2	2	19337.5	−3.2	0	12	2	20806.5	−4.3
0	7	5	19396.8	0.4	2	19	6	20838.6	1.8
0	1	1	19430.6	1.0	8	9	0	20881.0	0.2
0	12	8	19466.5	−0.6	5	11	1	20911.8	−2.3
0	11	7	19533.5	−2.4	6	10	0	21023.8	−0.2
0	14	9	19536.1	−4.3	6	12	1	21054.7	0.7
7	10	6	19612.7	3.4	0	14	2	21084.9	−2.4
0	7	4	19622.2	−1.3	0	16	3	21116.3	−3.6
1	4	2	19646.6	−0.6	5	11	0	21165.1	−0.6
0	15	9	19675.1	−1.6	7	13	1	21194.9	0.6
0	9	5	19691.0	3.9	0	15	2	21224.1	0.5
0	6	3	19708.1	−0.4	5	12	0	21305.2	−0.8
0	3	1	19738.4	−1.0	7	14	1	21333.0	1.1
7	8	4	19769.5	0.1	1	16	2	21359.5	0.9
0	13	7	19815.8	0.6	0	18	3	21387.2	0.0
6	15	8	19878.5	−1.4	3	13	0	21442.2	−2.7
0	4	1	19893.4	1.6	5	15	1	21467.8	−0.4
0	17	9	19944.0	−1.5	3	17	2	21495.2	2.9
4	11	5	19967.3	−4.7	1	19	3	21515.0	−3.5
3	3	0	19988.2	−1.8	1	23	5	21571.8	−0.9
7	13	6	20032.9	2.7	3	16	1	21605.1	1.9
0	15	7	20090.5	1.4	4	18	2	21627.4	2.5
0	7	2	20094.2	−0.6	1	20	3	21648.6	−0.1
6	4	0	20143.0	0.6	0	22	4	21671.2	−0.5
0	14	6	20170.1	2.3	3	17	2	21734.1	−0.9
0	16	7	20226.5	2.4	3	19	2	21755.3	−0.9
0	8	2	20240.4	−0.6	1	21	3	21776.6	−1.2
8	5	0	20294.0	1.0	1	23	4	21796.0	−3.6
1	15	6	20306.1	2.0	1	18	1	21865.7	−3.7
3	20	9	20334.8	−4.8	1	20	2	21886.1	−0.3
3	7	1	20340.6	0.8	2	22	3	21906.9	1.4
0	17	7	20356.7	−1.1	1	24	4	21923.0	−1.4
10	6	0	20443.4	1.0	0	26	5	21946.3	0.0
1	13	4	20480.9	2.8	1	28	6	21973.9	3.6
1	8	1	20486.0	0.4	0	30	7	21995.6	1.2
0	10	2	20532.2	3.5	1	21	2	22015.7	0.2
10	7	0	20591.3	1.2	1	23	3	22029.1	−4.3
2	16	5	20661.8	1.7	1	25	4	22053.9	4.6
0	11	2	20669.9	−0.5	0	27	5	22068.1	−1.2
0	13	3	20711.8	0.9	0	31	7	22119.0	2.7
10	8	0	20736.8	0.6	1	22	2	22140.6	−2.7
0	15	4	20756.4	−4.4	1	24	3	22161.2	2.9
0	10	1	20771.9	−1.3	0	26	4	22175.9	2.7
					0	28	5	22192.7	1.4

$$\nu = 19{,}570.8 + 159.22(v'+\tfrac{1}{2}) - 0.882(v'+\tfrac{1}{2})^2 + 0.00518(v'+\tfrac{1}{2})^3 - 256.5(v''+\tfrac{1}{2}) + 2.96(v''+\tfrac{1}{2})^2.$$

There is no noticeable difference in the intensity distribution of the Pb_2 bands as observed in absorption and in emission. The system terminates abruptly at the red end with nearly all the strong bands included in two long v' progressions and with no indication of corresponding v'' progressions. It is unfortunate that data are not available to make possible the construction of accurate potential curves and permit a quantitative examination of the processes involved. However, it seems likely that the absence of v'' progressions is due to a red edge occurring near the system origin. The existence of a red edge in the spectrum of Na_2 has been discussed by Loomis and Nile[23] and is to be expected in all cases where $\omega'' > \omega'$ while $D'' < D'$. For these bands ω'' is 256.5 and ω' is 159.22. Plots of $\Delta G(v)$ against $G(v)-G(0)$ indicate that D'' is approximately 5000 cm^{-1} and D' about 20,000 cm. No explanation is offered for the apparently abnormal intensities of several bands near the red end of the spectrum. Similar anomalies have been observed in a number of cases, notably in the A system of PbS.[24]

In the absence of the $v'=0$ progression, the assignment of the values of v' from the bands observed would be somewhat uncertain. The manner of locating the system origin will be discussed in connection with the isotope effect.

The heads near the red end of the system are quite sharp but become increasingly diffuse toward the violet end. Still farther to the violet are a number of headless bands, or possibly groups of very diffuse bands which appear both in emission and in absorption.

Identification of the Emitting Molecule

We believe this band system to arise from the diatomic lead molecule Pb_2 for the following reasons:

(1) This band system appeared only when lead was present in the carbon or iron tube. Hence it cannot be ascribed to any of the constituents out of which the tubes were made or to impurities in the tube. It therefore seems evident that lead is one of the atoms forming the diatomic molecule which gives rise to this band system.

(2) Since lead was heated in tubes open to the atmosphere so that lead oxide is formed, this band system might at first thought be ascribed to PbO. It does fall in the same region of the spectrum as lead oxide (PbO). That an assignment to any system of lead oxide is impossible is evident from the fact that for these bands $\omega_e''=255.6$, while for PbO $\omega_e''=722.5$. Moreover, when lead was heated in graphite tubes no known bands of the A and B systems of PbO were observed and, when lead oxide (PbO) was heated in an alundum tube, although the A and B systems appeared there was no trace of these bands.

(3) The fact that $\omega_e''=255.6$ for this system, while $\omega_e''=428.14$ for PbS indicates that the molecule is heavier than PbS so that an element with an atomic weight greater than that of sulfur must be assumed to have united with lead. This excludes the possibility that the molecule is formed by the union of lead with such lighter elements as carbon, nitrogen, oxygen, or silicon.

(4) Microphotometer traces were made of some of the spectrograms taken in the second order of the concave grating. Although the lines due to the different isotopes of lead are not resolved, it is possible from these traces to get some information which substantiates the selection of diatomic lead as the emitting molecule.

Lead is known to consist chiefly of three isotopes of masses 208, 207 and 206 with the relative abundances 7, 3, 4. The spectrum of Pb_2 should then consist of the overlapping spectra of the molecules Pb^{208} Pb^{208} (25), Pb^{208} Pb^{207} (21), Pb^{208} Pb^{206} (29), Pb^{207} Pb^{207} (5), Pb^{207} Pb^{206} (12), and Pb^{206} Pb^{206} (8) with the approximate percent abundances indicated in parentheses. The displacements of the isotope lines from those of Pb^{208} Pb^{208} may be expressed by the usual approximation

$$\nu^i - \nu = (\rho-1)\nu_v + 2(\rho-1)\nu_r,$$

where ρ has the values 1.0012, 1.0024, 1.0024, 1.0036 and 1.0048, respectively.

The heads should therefore be fivefold with increasing separation at greater distances from the system origin, but if the isotope heads were

[23] Loomis and Nile, Phys. Rev. **32**, 873 (1928).
[24] G. D. Rochester and H. G. Howell, Proc. Roy. Soc. **A148**, 57 (1935).

obscured by overlapping fine structure the observed heads would merely appear increasingly diffuse. The extent of the diffuseness of these heads was determined by measuring the frequency differences of the positions of maximum and minimum absorption from microphotometer traces of the heads of the strong bands and found to be of the right order of magnitude. A plot of these differences against the frequencies of the heads indicates that the position of the sharpest heads and hence the location of the system origin, should be in the vicinity of 19,500 cm^{-1}.

It is evident from the values of ρ that the isotope lines will be evenly spaced with the separation $0.0012\nu_v+0.0024\nu_r$, where ν_v is positive for all the strong bands and ν_r is essentially negative. Wherever this separation matches the spacing of the lines of a branch, the fine structure should exhibit a simplified appearance. Traces of the earlier members of the $v''=0$ progression show a region in each band consisting of regularly spaced maxima with weaker maxima between them. This agrees with the expected structure if we interpret the stronger maxima as blends of the lines of Pb^{208} Pb^{208}, Pb^{208} Pb^{206}, Pb^{207} Pb^{207} and Pb^{206} Pb^{206} and the weaker maxima as due to the superimposed lines of Pb^{208} Pb^{207} and Pb^{207} Pb^{206}. The average separation of the stronger maxima in the (4,0) band with head at 20,143 cm^{-1} is 1.34 cm^{-1}. On the preceding interpretation this should be twice the spacing of the isotope lines. The center of the region where the maxima occur is about 50 cm^{-1} from the head of the band. With $\nu_r=-50$ cm^{-1}, ν_v must be 658 cm^{-1} corresponding to an origin at 19,485 cm^{-1}. Determinations of the origin made in this manner from the (5,0), (6,0) and (7,0) bands give 19,491, 19,532 and 19,595 cm^{-1}, respectively. These values agree with one another as well as can be expected. Hence all the available data on the isotope splitting are in accord with the conclusion that the emitting molecule is diatomic lead.

Grateful acknowledgment is made to Professor Alpheus W. Smith and Dr. R. V. Zumstein for their many helpful suggestions.

AUGUST 15, 1935 PHYSICAL REVIEW VOLUME 48

The Four Vector Problem and Its Application to Energies and Intensities in Platinum-Like Spectra

A. T. GOBLE, *University of Wisconsin**

(Received June 26, 1934)

The theory of two-electron systems involves both the electrostatic interaction between the electrons and the magnetic interaction between the spin and orbital moments of each electron. The inclusion of this latter effect requires the knowledge of the matrix of $a_1\mathbf{l}_1\cdot\mathbf{s}_1+a_2\mathbf{l}_2\cdot\mathbf{s}_2$. This matrix has been given by Johnson, who obtained it by the method of noncommutative vector algebra. An outline of an alternative method based on the correspondence principle is given here because of its simplicity.

Mack's data on the $5d^96s$ and $5d^96p$ configurations of Pt I, Au II, Hg III, Tl IV, Pb V and Bi VI are used to check the theory because they present a complete isoelectronic sequence in which the coupling is decidedly intermediate. We find it more convenient to use the secular determinants for the *jj* rather than the Russell-Saunders system of representation as the starting point of our perturbation calculation. These secular equations contain five electrostatic and two magnetic parameters. One of the magnetic parameters, a_1, is determined from the triplet width in $5d^96s$. The other and the five electrostatic ones are determined from six relations between the observed intervals. The intervals computed from the secular equations by using these values of the parameters are then compared with the experimental intervals. The $5/2,\ 3/2|_4$ level was used as origin. The results are quite satisfactory. A second method in which the number of electrostatic parameters is decreased to three by the use of Shortley's theory of the electrostatic interaction of almost closed shells is also used. Here the agreement, though satisfactory, is not as good as that obtained by the first method. The $5d^96s$ configurations were considered by applying the well-known equations of Houston. These results make it possible to compute the intensities in intermediate coupling of lines in the transition array, $5d^96s-5d^96p$. The intensities of $5d^{10}-5d^96p$ are also found. Comparison with the observed intensities shows as good agreement as one can expect considering the difficulties under which the experimental values were determined.

Introduction

TWO-ELECTRON systems present the most favorable cases for the experimental verification of the theory of complex spectra since they offer a decided increase in complexity over one-electron systems and on the other hand are about the most complex systems which are amenable to complete treatment. Configurations in which there are but two electrons are in most cases examples of very near Russell-Saunders coupling and therefore satisfy the simplest of multiplet theories such as give the usual interval rule.[1] Groups of electrons which lack but one of being a closed shell behave in many ways as a single electron. Configurations containing them may, therefore, be considered in many ways tantamount to two-electron systems. Such configurations frequently exhibit considerable deviations from Russell-Saunders coupling and are therefore of interest.

There have been numerous studies made which have compared the observed energy levels with those predicted by theory. Among these is the work of Laporte and Inglis and of Condon and Shortley[2] who studied the "Houston problem" concerned with configurations in which one of the two electrons is an s electron. They found reasonably good agreement for a large number of elements including actual two-electron systems and systems of a single electron plus an almost closed shell. Shortley[3] has studied the $n'p^5np$ and $n'p^5nd$ configurations of the rare gases with considerable success. Such discrepancies as he found are readily accounted for in the approximations used, for he neglected interactions between levels arising from different "parent" jj terms. (His secular equations were obtained in the jj system of representation.) Marvin[4] considered the $3d^94p$ configuration of Ni I, which is essentially equivalent to a dp configuration. He used a method similar to those used in this paper. His results do not show the desired agreement between theory and experiment but this is no doubt due to the perturbations caused by the $5d^84s4p$ configuration which is interlaced with the one considered.

It is of interest to compare the theory with experiment for configurations which definitely have intermediate coupling. Configurations containing almost closed shells are more likely to behave this way, as are the systems of the heavier elements. For these reasons the data compiled and classified by Mack[5] on the $5d^96s$ and $5d^96p$ configurations of the platinum-like elements, Pt I, Au II, Hg III, Tl IV, Pb V and Bi VI, serve as excellent tests for the theory and so will be examined in the present paper. These elements furnish a complete array of data of an isoelectronic sequence so that the effect with increasing Z can be noted. Furthermore it turns out that a variety of coupling ranging from near jj to quite intermediate behavior is manifested by these elements.

The development of the theory of complex spectra was as follows. The electrostatic interaction between electrons was first treated by Slater,[6] then by Condon and Shortley,[7] and finally extended to almost closed shells by Shortley.[8] The magnetic interaction between the spin of each electron and its orbital motion for the special case in which one of the two electrons is an s electron has been treated by Houston.[9] Finally, Johnson[10] has given the general theory involving the spin-orbit interaction for two electron systems.

These theories involve, essentially, the solution of the wave equation

$$[\mathfrak{H}^0+a_1\mathbf{l}_1\cdot\mathbf{s}_1+a_2\mathbf{l}_2\cdot\mathbf{s}_2-W]\Psi=0, \qquad (1)$$

where $\mathbf{l}_i$ and $\mathbf{s}_i$ are the orbital and spin angular momenta of the ith electron and $\mathfrak{H}^0$ is the operator

$$\mathfrak{H}^0=(h^2/8\pi^2m)(\nabla_1^2+\nabla_2^2)+V(r_1, r_2, r_{12}). \qquad (2)$$

Here $V(r_1, r_2, r_{12})$ is the potential energy function for the electrons in a self-consistent field and also includes the electrostatic interaction between the electrons. The terms $a_1\mathbf{l}_1\cdot\mathbf{s}_1+a_2\mathbf{l}_2\cdot\mathbf{s}_2$ give the magnetic interaction between the spin

---

* Now at University of Tulsa.

[1] For example see Pauling and Goudsmit, *Structure of Line Spectra*, p. 97.

[2] Laporte and Inglis, Phys. Rev. **35**, 1337 (1930); Condon and Shortley, Phys. Rev. **35**, 1342 (1930).

[3] Shortley, Phys. Rev. **44**, 666 (1933).

[4] Marvin, Phys. Rev. **44**, 818 (1933).

[5] Mack and Fromer, Phys. Rev. This issue.

[6] Slater, Phys. Rev. **34**, 1293 (1929).

[7] Condon and Shortley, Phys. Rev. **37**, 1025 (1931).

[8] Shortley, Phys. Rev. **40**, 185 (1932).

[9] Houston, Phys. Rev. **33**, 297 (1929).

[10] Johnson, Phys. Rev. **38**, 1628 (1931).

and orbital moments of each electron. Terms of the form $\mathbf{l}_i \cdot \mathbf{s}_j$ are neglected since they involve Z^3 instead of Z^4, where Ze is the effective nuclear charge.

We shall assume that we know the "Russell-Saunders" wave functions ψ^0 which satisfy

$$[\mathcal{H}^0 - W]\psi^0 = 0. \quad (3)$$

In other words we shall assume that the problem including the electrostatic interaction as treated by Slater and modified by Shortley has been solved. The characteristic values obtained from this problem are the degenerate multiplets of pure Russell-Saunders coupling. If we expand the final wave functions in terms of the "Russell-Saunders" wave functions we find for the condition that we can solve for the coefficients that

$$|H_1(nm) + [H^0(nn) - W]\delta(nm)| = 0, \quad (4)$$

where

$$H_1(nm) = \int \psi_n^{*0}(a_1\mathbf{l}_1 \cdot \mathbf{s}_1 + a_2\mathbf{l}_2 \cdot \mathbf{s}_2)\psi_m^0 dv \quad (5)$$

and $H^0(nn)$ are the characteristic values of (3). Thus it is seen that we need the matrix of $a_1\mathbf{l}_1 \cdot \mathbf{s}_1 + a_2\mathbf{l}_2 \cdot \mathbf{s}_2$ in the Russell-Saunders system of representation.

The Matrix of $a_1\mathbf{l}_1 \cdot \mathbf{s}_1 + a_2\mathbf{l}_2 \cdot \mathbf{s}_2$

Johnson[10] first published the general expression for the matrix of $a_1\mathbf{l}_1 \cdot \mathbf{s}_1 + a_2\mathbf{l}_2 \cdot \mathbf{s}_2$. He derived it by an application of noncommutative vector algebra. It has also been derived by Brinkman[11] by the use of Kramers' symbolic method of representation.

Previous to the publication of Johnson's work, the author was working on this same problem, using an application of the correspondence principle. The completion of this work was unavoidably delayed until after Johnson's results were published. Because of the simplicity of the method based on the correspondence principle, it may be well to indicate briefly here how the $\mathbf{l} \cdot \mathbf{s}$ matrix may be obtained by its use.

Kronig[12] and Wigner[13] have given expressions from which one can obtain the amplitude factors for the electric moment, $\Sigma e_i \mathbf{r}_i$, of two-electron systems having Russell-Saunders coupling. We are instead interested in the matrix elements or amplitudes for the angular momentum, $\mathbf{l}_i$. Fortunately, group theory tells us that except for a proportionality factor the amplitudes of the electric moment and angular momentum are similar for a given type of transition, in our case $l_i \rightarrow l_i$. This follows from the facts that both the electric moment and angular momentum transform like a vector, i.e., involve a representation of the rotation group of order three, and that there is only one representation of a given order. The absolute value of the amplitude factors is chosen to make the characteristic values of $|l_i|^2$ equal to $l_i(l_i+1)$. We use the transitions $l_i \rightarrow l_i$ because they correspond to the component of $\mathbf{r}$ parallel to $\mathbf{l}_i$, which is independent of the frequency or precession about $\mathbf{l}_i$. A component of $\mathbf{r}$ perpendicular to $\mathbf{l}_i$, which depends upon this precession frequency, is characterized by transitions in which $l_i \rightarrow l_i \pm 1$. There are no elements of $\mathbf{l}_i$ of the form $l_i \rightarrow l_i \pm 1$, as $\mathbf{l}_i$ has naturally no component perpendicular to itself. Part II of Kronig's paper[12] does not give the amplitudes for transitions of the form $l_i \rightarrow l_i$ so one must also make use of the results of Part I which indicate the correct form for that type of transition. The matrix elements of $\mathbf{l}_2$ are identical with those of $\mathbf{l}_1$ with the subscripts interchanged. Similarly the formulas for $\mathbf{s}_1$ and $\mathbf{s}_2$ are found by replacing l_1 by s_1, l_2 by s_2 and L by S.

The phase factors or signs of the separate elements which are needed before the matrix multiplication to obtain $a_1\mathbf{l}_1 \cdot \mathbf{s}_1 + a_2\mathbf{l}_2 \cdot \mathbf{s}_2$ can be performed are found by an application of the correspondence principle. Using the usual vector model for Russell-Saunders couplings one computes the classical expression for $\mathbf{l}_1$, etc. in terms of the precession frequencies about $\mathbf{L}$, $\mathbf{S}$, $\mathbf{J}$ and $\mathbf{M}$. By picking out the coefficients of the appropriate time factors one obtains the classical analogs of the matrix elements. Thus the coefficient of $e^{2\pi i(\omega_L - \omega_J)t}$ is associated with the transition $L, J, M \rightarrow L+1, J-1, M$. The signs of these coefficients give the correct phase factors for use in connection with the amplitudes found in the preceding paragraph. Thus one has all the information needed to compute the matrix of $a_1\mathbf{l}_1 \cdot \mathbf{s}_1 + a_2\mathbf{l}_2 \cdot \mathbf{s}_2$ in Russell-Saunders coupling.

[11] Brinkman, Zeits. f. Physik **79**, 753 (1932).
[12] Kronig, Zeits. f. Physik **31**, 885; **33**, 261 (1925).
[13] Wigner, *Gruppentheorie*, p. 298.

The Secular Equations for d^9p

Johnson[10] gives the matrix for $a_1\mathbf{l}_1\cdot\mathbf{s}_1+a_2\mathbf{l}_2\cdot\mathbf{s}_2$ for the dp configuration in the Russell-Saunders system of representation; hence there is no need of repeating it here. There will be no change for the d^9p configuration, but a_1 will be negative. Throughout this paper the subscript 1 after a or l or s will refer to the group of equivalent d electrons and the subscript 2 to the p electron. In order to obtain the secular equation, whose roots are the theoretical energy levels, one needs to add to each diagonal term the appropriate electrostatic, Russell-Saunders, energy $H^0(nn)$. It is convenient to choose the $^3F_4$ level as the origin; hence the quantity $\frac{1}{2}(2a_1+a_2)$ must also be subtracted from each diagonal element. The following notation will be used to represent the pure Russell-Saunders parameters:

$$\alpha={}^1F-{}^3F;\ \beta={}^3D-{}^3F;\ \gamma={}^1D-{}^3F;$$
$$\delta={}^3P-{}^3F;\ \epsilon={}^1P-{}^3F.$$

It happens that in the platinum-like sequence the magnetic terms play the predominant role in the energy; hence they are examples more nearly of jj than of Russell-Saunders coupling. It is therefore convenient to transform the energy matrix to the jj system of representation. This is done by finding the transformation matrix which will make the matrix of $a_1\mathbf{l}_1\cdot\mathbf{s}_1+a_2\mathbf{l}_2\cdot\mathbf{s}_2$ diagonal. Shortley[14] has also given this matrix although the phases of his wave functions differ from those used here. When one applies these to the matrix of the Hamiltonian one gets the secular equations:[15]

$J=4$

	5/2,3/2
5/2,3/2	$W=0,$

$J=3$

	5/2,3/2	5/2,1/2	3/2,3/2
5/2,3/2	$4(3\alpha+8\beta)/45-W$	$-2(5)^{\frac{1}{2}}(3\alpha-4\beta)/45$	$-2(6)^{\frac{1}{2}}(3\alpha-2\beta)/45$
5/2,1/2	$-2(5)^{\frac{1}{2}}(3\alpha-4\beta)/45$	$(3\alpha+2\beta)/9-(3/2)a_2-W$	$-30^{\frac{1}{2}}(3\alpha+\beta)/45$
3/2,3/2	$-2(6)^{\frac{1}{2}}(3\alpha-2\beta)/45$	$-30^{\frac{1}{2}}(3\alpha+\beta)/45$	$(6\alpha+\beta)/15-(5/2)a_1-W$

$=0$

$J=2$

	5/2,3/2	5/2,1/2	3/2,3/2	3/2,1/2
5/2,3/2	$7(5\beta+30\gamma+27\delta)/450-W$	$14^{\frac{1}{2}}(10\beta+15\gamma-27\delta)/225$	$21^{\frac{1}{2}}(10\beta-15\gamma+9\delta)/225$	$21^{\frac{1}{2}}(-5\beta+30\gamma-9\delta)/450$
5/2,1/2	$14^{\frac{1}{2}}(10\beta+15\gamma-27\delta)/225$	$2(40\beta+15\gamma-18\delta)/225-(3/2)a_2-W$	$6^{\frac{1}{2}}(40\beta-15\gamma-18\delta)/225$	$6^{\frac{1}{2}}(-10\beta+15\gamma+9\delta)/225$
3/2,3/2	$21^{\frac{1}{2}}(10\beta-15\gamma+9\delta)/225$	$6^{\frac{1}{2}}(40\beta-15\gamma-18\delta)/225$	$(40\beta+15\gamma+6\delta)/75-(5/2)a_1-W$	$(-10\beta-15\gamma-3\delta)/75$
3/2,1/2	$21^{\frac{1}{2}}(-5\beta+30\gamma-9\delta)/450$	$6^{\frac{1}{2}}(-10\beta+15\gamma+9\delta)/225$	$(-10\beta-15\gamma-3\delta)/75$	$(5\beta+30\gamma+3\delta)/150-(5/2)a_1-(3/2)a_2-W$

$=0$ (6)

$J=1$

	5/2,3/2	3/2,3/2	3/2,1/2
5/2,3/2	$(\beta+3\delta+6\epsilon)/10-W$	$(-\beta+2\delta-\epsilon)/5$	$5^{\frac{1}{2}}(\beta+\delta-2\epsilon)/10$
3/2,3/2	$(-\beta+2\delta-\epsilon)/5$	$(6\beta+8\delta+\epsilon)/15-(5/2)a_1-W$	$5^{\frac{1}{2}}(-3\beta+2\delta+\epsilon)/15$
3/2,1/2	$5^{\frac{1}{2}}(\beta+\delta-2\epsilon)/10$	$5^{\frac{1}{2}}(-3\beta+2\delta+\epsilon)/15$	$(3\beta+\delta+2\epsilon)/6-(5/2)a_1-(3/2)a_2-W$

$=0.$

$J=0$

	3/2,3/2
3/2,3/2	$\delta-(5/2)a_1-W=0$

Shortley and Johnson[16] have shown that the following relations should hold between the electrostatic, Russell-Saunders, parameters:

$$\alpha=-2F_2+90G_3;\ \beta=\gamma=9F_2;$$
$$\delta=-(5/9)\beta=-5F_2;\ \epsilon=-9F_2+20G_1, \quad (7)$$

where the F's and G's are certain radial integrals. Experience with other elements indicates that such relations do not hold very accurately.[17] For this reason two sets of calculations are made,

[14] Shortley, Phys. Rev. **43**, 451 (1933).

[15] The diagonal elements of the matrix of the electrostatic interaction were found by Inglis, Phys. Rev. **38**, 868 (1931).

[16] These relations were given in a private communication from Dr. Shortley. They were later published by Johnson, Phys. Rev. **43**, 632 (1933).

[17] For examples of the failure of the Slater relations see Slater, Phys. Rev. **34**, 1293 (1929) or Condon and Shortley, Phys. Rev. **37**, 1025 (1931).

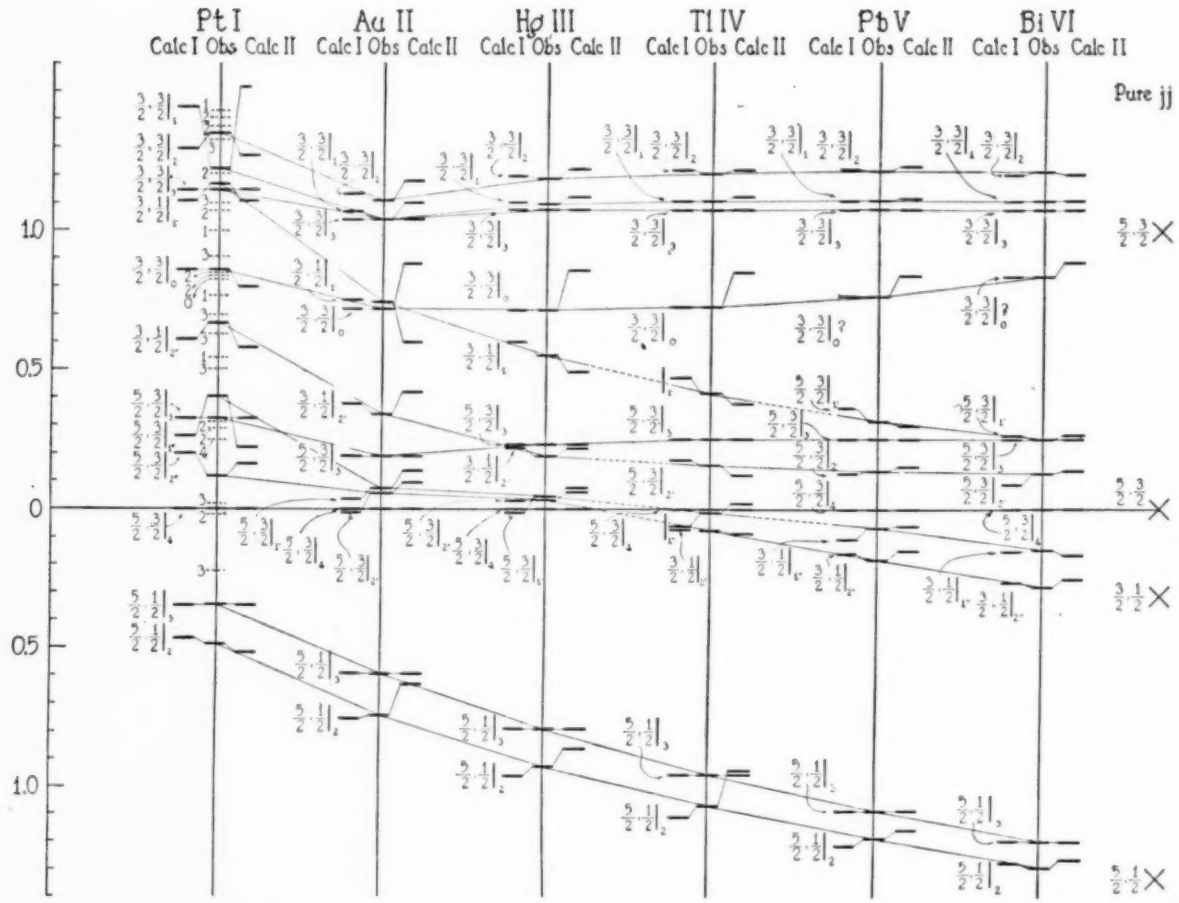

FIG. 1. Experimental and observed values of the levels of $5d^9 6p$ for all the platinum-like elements. The levels have been plotted in units of the triplet width in $5d^9 6s$ and the $5/2,3/2|_4$ levels have been chosen as origin. The experimental values are given in the middle column, the values computed by method I in the left column, and those computed by method II in the right column. The pure *jj* values for Bi VI have been indicated by crosses at the extreme right to indicate the general *jj* character of these configurations. The dotted levels in Pt I belong to the $5d^8 6s 6p$ configuration which might perturb $5d^9 6p$. ? Experimental values uncertain. *Erratum:* The uppermost pure *jj* level should be labeled 3/2,3/2.

one considering all five quantities, α, β, γ, δ and ϵ, as independent parameters to be determined, and the other making use of the relations (7). The methods used to determine all the parameters and then evaluate the theoretical intervals are as follows:

Method I

The determinant for $J=3$ involves four parameters, a_1, a_2, α and β. The calculations are simplified a great deal if one knows the value of one of these. There is good reason to believe that the value of a_1 for the d^9p configuration not greatly different from that for d^9s. For this reason, we shall take the value of a_1 as obtained from the triplet width in d^9s and use it directly in our calculations in all this work. This obviously may introduce an error and may account in part for some of the discrepancies observed between the experimental and calculated values of the intervals. The simplification afforded by this assumption is sufficient to warrant its use.

Now one can choose a_2, α and β to make the calculated intervals for $J=3$ agree exactly with those observed. To obtain these values one must solve two simultaneous quadratics in both α and β. This was done by a graphical method.

The $3/2,3/2|_0$ level gave the value for δ directly and the value of ϵ was chosen to make the sum of the roots of the equation for $J=1$ equal to the sum of the observed values for $J=1$. Similarly γ was chosen to make the sum of the

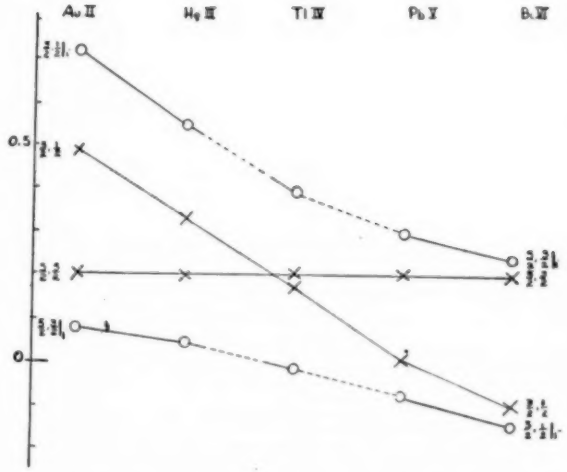

FIG. 2. To illustrate the effect of a perturbation on the roots of a secular problem where the unperturbed levels cross. The $5/2,3/2|_1$ and $3/2,1/2|_1$ levels have been plotted along with the corresponding pure jj levels. To facilitate comparison, the origin for the ordinates of the latter has been raised by an amount of 0.2 since the effect of the perturbation in this case raises the roots as well as separates them. Circles are actual roots, crosses are pure jj levels.

roots of the equation for $J=2$ equal to the sum of the experimental values of the intervals for $J=2$. The notation used above and in the rest of this paper gives the values of j_1, j_2, and J associated with a level thus, j_1, $j_2|_J$.

Method II

This method is identical with the first through the part in which a_1, a_2, α and β are obtained. The Shortley relations then give γ and δ directly. The requirement that the sum of the roots of the equation for $J=1$ equal the sum of the experimental values for $J=1$ gives the value of ϵ. Thus only four intervals or equivalent combinations of intervals are needed in the second method while the first requires six.

These schemes are not all one might ask for since they "force" the fit on some levels thus making the others bear the brunt of what variations there are.

The cubics of both methods were expanded and solved directly. Since the interaction between $3/2,3/2|_2$ level and the rest of the $J=2$ terms is small, second order perturbation theory was used to evaluate this level and thus reduce the quartic to a cubic.[18] The roots of this cubic were then found directly. The quartic was completely expanded in the case of Tl IV and the roots found. They did not differ appreciably from the results obtained by the approximate method.

[18] Jordahl, Phys. Rev. **45**, 87 (1934).

RESULTS

The comparison between the calculated and observed terms is shown in Fig. 1. For convenience in plotting and to show certain regularities, the energy levels have been plotted in units of the over-all triplet width for d^9s, i.e., $5d^9_{3/2},6s_{1/2}|_1 - 5d^9_{5/2},6s_{1/2}|_3$. The $5/2,3/2|_4$ level has been chosen as origin. For each element the middle column gives the experimental values, the left column gives the theoretical values obtained by method I, and the right those obtained by method II.

The levels have been labeled so that the jj portion of the designation corresponds to the jj wave function which predominates in the actual wave function. This causes no difficulty except in the case of the $5/2,3/2$ and $3/2,1/2$ levels for $J=2$ and $J=1$. As one goes to higher degrees of ionization the value of a_2 increases until at Tl IV the separation due to the p electron becomes almost equal to that due to the d electrons. As a result the pure jj levels cross as is shown in Fig. 2. This means that near Tl IV the upper of these two roots concerned in $J=2$ and $J=1$ change from being predominantly $3/2,1/2$ to predominantly $5/2,3/2$. This has led to the adoption of the notation in which the upper of the questionable roots has been indicated by a prime on the J value and the lower by a double prime. The change has been indicated by breaking the line connecting these roots. This well-known phenomenon in which the introduction of a perturbation, here the electrostatic interaction, separates roots which would otherwise cross is indicated in Fig. 2. The actual roots for the two levels involved for $J=1$ have been plotted along with the pure jj levels. The effect is quite apparent as the actual roots fall on curves asymptotic to the pure jj levels. The value 0.2 has been chosen as the origin for the ordinates in plotting the pure jj levels since the action of the electrostatic perturbation raises both roots as well as separates them.

Since Tl IV comes very near the transition

point it is of particular interest. The pure jj $5/2,3/2$ and $3/2,1/2$ levels are so close that the two actual wave functions share the pure jj ones nearly equally. The wave functions associated with the upper roots contain about 69 percent and 43 percent of the $5/2,3/2$ wave function for $J=2$ and $J=1$, respectively, and 27 percent and 54 percent of $3/2,1/2$. The lower levels contain 25 percent and 47 percent of $5/2,3/2$ and 72 percent and 46 percent of $3/2,1/2$. The $J=2$ levels of Tl IV have each a sufficient preponderance of one wave function to make it possible quite definitely to assign jj values to them. In the case of the $J=1$ levels of Tl IV, however, the wave functions are so completely mixed that one has no real assurance that any designation is correct. For example, a slight change in the values of the parameters might reverse the notation. The lower level does not even have a "majority" of one wave function but only a "plurality." For that reason no jj values have been indicated in the designation of these levels.

The fact that the $J=2$ roots have changed to being more like Pb V and Bi VI than Au II and Hg III while the $J=1$ roots are questionable is a result of the different manner in which the electrostatic parameters enter into the two secular equations. All the other levels are well separated and hence maintain more nearly their pure jj nature. The success with which the theory meets this peculiar situation is quite striking.

Another element which demands particular attention is Pt I. Here there is little agreement between experiment and theory. In a sense, this is desirable for the configurations involved are badly perturbed. If the theory which neglects these perturbations was able to fit the observed values, the criticism that the theory could fit any set of levels might be valid. Fortunately this is not the case.

The extra-configurational perturbations which spoil the agreement in Pt I are due to the levels of $5d^86s6p$. Those which might have an appreciable effect have been plotted in dotted lines in Fig. 1. It is barely possible that the triplet separation in $5d^96s$ might be influenced by the $5d^86s^2$ configuration thus affecting the value of a_1. However, this effect is probably small since the value of a_1 for Pt I is in keeping with that for the other elements.

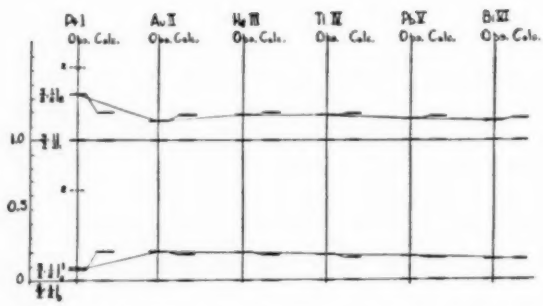

FIG. 3. Experimental and observed values of the levels of $5d^96s$ for the platinum-like spectra. The terms have been plotted in units of the triplet width. The experimental values are given in the left column and the observed values are given in the right. The dotted levels in Pt I belong to the $5d^86s^2$ configuration which might perturb the $5d^96s$ configuration.

It is of interest to note that the experimental values of the $3/2,3/2|_0$ terms for Hg III, Tl IV, Pb V and Bi VI were found after their location had been indicated by the theory. An earlier set of calculations had been made in which δ and ϵ were chosen to make the product as well as the sum of the roots of the equation for $J=1$ agree with the product and sum of the experimental term values. The location of the $3/2,3/2|_0$ term for each element was indicated by these results and a search for lines arising from these levels was made in the wavelength tables. The values given were thus obtained. Since such few transitions exist for each level, they are not well established but there are good reasons to accept these values. The regularity of the variation with Z of the values of the parameter obtained by using these terms is one of them. A complete summary of the evidence is given by Mack.[5]

The results on the whole are quite satisfactory. It should be noted that method I yields the better results. This is to be expected since there are two more parameters available for adjustment. This further indicates that the Slater-Shortley relations are not well verified in these elements.[17]

THE d^9s CONFIGURATION

The method used by Laporte and Inglis[2] to consider the Houston problem consists in determining the electrostatic parameter from each of the two $J=2$ levels. The comparison of these showed the success of the theory. For our work it is more convenient to make a slight modifica-

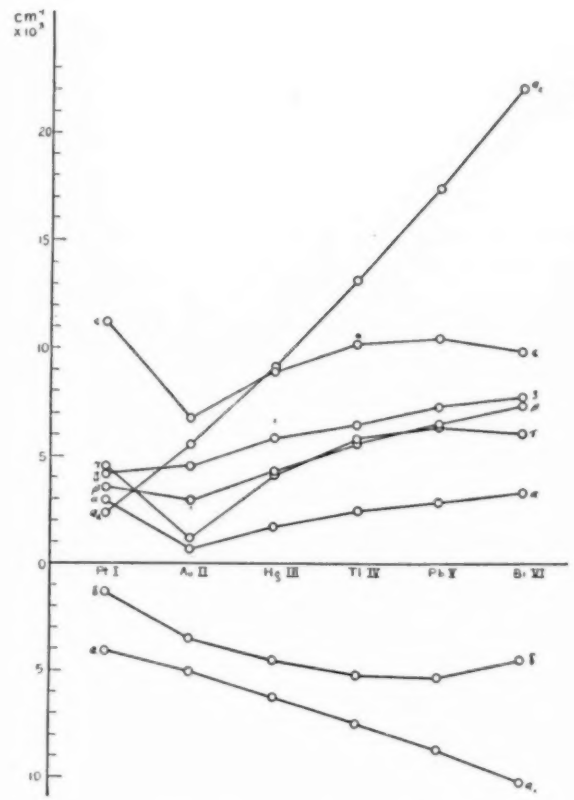

FIG. 4. The variation of the parameters with stage of ionization. These are the parameters used in method I. Note the failure of the "Slater-Shortley" relations which require that $\gamma=\beta$ and $\delta=-(5/9)\beta$.

tion in their treatment. The method used here is as follows. If one refers energies to the $J=3$ level the secular equations for this configuration are

$$\begin{aligned} &J=3, \quad W=0, \\ &J=2, \quad W^2-W[-(5/2)a_1+\zeta]+(3/2)a_1\zeta=0, \\ &J=1, \quad W=-(5/2)a_1, \end{aligned} \tag{8}$$

where $\zeta={}^1D-{}^3D$. Thus a_1 is directly determined. It was this value which was used in the calculations on the $5d^96p$ configuration. The condition that the coefficient of W in the secular equation for $J=2$ equal the sum of the observed levels having $J=2$ was used to determine ζ. The experimental and calculated terms are shown in Fig. 3. Here again the levels have been plotted in units of the triplet width.

The variation of all the parameters with stage of ionization is shown in Fig. 4. The coupling coefficients a_1 and a_2 behave regularly as one would expect. The regularity of the electrostatic parameters is quite satisfying and leads to an added confidence in the classification of the levels.

INTENSITIES

The secular equations were obtained as the condition for the solvability of the chain of equations for determining the transformation coefficients. By transformation coefficients we mean the coefficients which occur in the expansion of the actual final wave functions in terms of the original jj wave functions. These coefficients are, of course, the elements of the transformation matrices which will convert the matrix representation of any dynamical quantity from the jj system of representation to the intermediate system.

Bartlett[19] has given the values of the relative intensities for the transitions of the supermultiplet d^9s-d^9p in jj coupling. However the matrix to which the transformation should be applied is the amplitude matrix. As a matter of fact, the square roots of the values given by Bartlett may be used if one attaches appropriate phase factors to them. This results from the fact that these quantities differ from the actual amplitude factors only by quantities which are the same for all elements in a particular J group. This is equivalent to using the square roots of what Shortley[20] calls "line strengths." To these quantities one can apply the transformation, and the resulting quantities when squared are the transition probabilities.

In order to find the correct phases it is easier to start with the Russell-Saunders system of representation. The absolute values of the line strengths in this system of representation were also given by Bartlett[19] or may be found in other sources such as in Kronig's[12] paper or in Wigner.[13] The phases were found by the method discussed in connection with the $\mathbf{l}\cdot\mathbf{s}$ matrix, based on the correspondence principle. One makes an expansion of a vector perpendicular to $\mathbf{l}_2$ in terms of the various precession frequencies. The coefficients of the time factors give the classical form for the amplitude elements as described

[19] Bartlett, Phys. Rev. **35**, 229 (1930).
[20] Shortley, Phys. Rev. **47**, 295 (1935).

before and the signs determine the phases. The reason for considering a vector perpendicular to $\mathbf{l}_2$ is that the transitions considered are of the type, $l_2 \rightarrow l_2 - 1$, which corresponds to terms dependent upon the frequency of precession about $\mathbf{l}_2$. Of course, care must be taken that the same phase relations exist between the various vectors as in the determination of the phases for $\mathbf{l}$ and $\mathbf{s}$. Then to obtain the amplitude matrix in jj coupling one applies the same transformation as was used to transform the Hamiltonian function. This preserves the correct phase relations. To this matrix one then applies the final transformation matrix.

Since a second order perturbation theory was used for $3/2,3/2|_2$ in d^9p, the transformation matrix used consists of the cubic found as usual, surrounded by elements $S(n4) = II(n4)/h\nu(4n)$, $S(4n) = II(4n)/h\nu(n4)$, $S(44) = 1$. This of course introduces some error but only very little.

In each case the secular equations and roots of method I were used, as they gave the most satisfactory agreement with experiment.

The transformation coefficients are quite sensitive to the values of the parameters used and to the accuracy to which the roots were computed. As a result the amplitude factors may differ by appreciable amounts from the correct values, i.e., those that would be obtained with the best choice of the parameters and with the exact evaluation of the roots of the secular equations.

It is interesting to note that the J group rule of Harrison and Johnson[21] and the J file rule of Shortley[20] apply in this case and have been very useful in checking the values of the amplitude factors in intermediate coupling.

Comparison with Experiment

Since the experimental values for the observed intensities are visual estimates of densities on a photographic plate the following scheme was used to compute theoretical values for these. To the best of the author's knowledge the intensity scale was logarithmic to the base 2. That is, a line judged as intensity d had twice the effect on the plate of one judged as $d-1$. Therefore, if we call the visual estimate d, we have $d = \log_2 E + C$ where E is a term proportional to the "blackening power" of the line. Since we have no satisfactory theory of photographic action and since we have no evidence as to the actual spectral variation of sensitivity of the plates used, it was decided to assume that the blackening was proportional to the number of quanta incident rather than to the energy. Thus we have for the "blackening power" of a line between states r and s,

$$E_{rs} = \text{const} \cdot \nu(rs)^3 (2J+1) |q(rs)|^2,$$

where $q(rs)$ is the amplitude factor for the transition, J relates to the final state, and $\nu(rs)$ is the theoretical frequency of the line.

The values of $\log_2 E_{rs}$ were all computed. Since C is undetermined, the difference between the value of $\log_2 E_{rs}$ and the observed values of d were found and the average was added to each $\log_2 E_{rs}$ to get the theoretical value of d. Thus there was one fitted constant for each spectrum. The results are tabulated in Table I in which the experimental values are given in italics and the theoretical values in regular type.

On the whole the agreement is fair. There are several discrepancies, however, which are difficult to account for. The experimental conditions are not very good for intensity measurements, since the excitation was in a condensed spark and since no care was taken to preserve intensity relations in the photographs. Thus one should not expect too much of the results. The theoretical values of the intensities were calculated under the assumption of uniform excitation, i.e., each initial state has a number of atoms in it proportional to the statistical weight $(2J+1)$ of the level. This, of course, is not to be expected since all the lines were observed in a condensed spark. However, one should expect agreement for all lines arising from a common initial level. That is, one would expect a consistent difference between theory and experiment across a row for each element in the table, the difference indicating the degree of excitation. There is much better agreement of this sort, but there are still inconsistencies; e.g. the transition $5d^9{}_{3/2}6s_{1/2}|_2 - 5d^9{}_{5/2}6p_{1/2}|_2$ is much too strong in all observed cases. The general character of the results, however, is quite striking. Transitions from the $3/2,3/2|_2$, $3/2,3/2|_1$ and all the $J=3$ levels, which are quite pure jj, show a strong tendency

[21] Harrison and Johnson, Phys. Rev. **38**, 757 (1931).

TABLE I. *Comparison of calculated and observed intensities for $5d^96s-5d^96p$.* The observed values are given in italics. These observed values are visual estimates based on a scale most consistent with the results of the several observers from which these data were taken by Mack.

The levels in each J group are given in the order of their energies. The cross rules at thallium indicate the change of the jj notation for the 2′ and 2″ levels. The questionable character of the 1′ and 1″ levels has been indicated by the "bridge" around thallium and the cross rules have the same significance as for the $J=2$ levels.

$5d^96s$

				Pt I				Au II				Hg III				Tl IV				Pb V				Bi VI						
			j_1	3/2	3/2	5/2	5/2	3/2	3/2	5/2	5/2	3/2	3/2	5/2	5/2	3/2	3/2	5/2	5/2	3/2	3/2	5/2	5/2	3/2	3/2	5/2	5/2	j_1			
			j_2	1/2	1/2	1/2	1/2	1/2	1/2	1/2	1/2	1/2	1/2	1/2	1/2	1/2	1/2	1/2	1/2	1/2	1/2	1/2	1/2	1/2	1/2	1/2	1/2	j_2			
j_1	j_2	J		1	2	2	3	1	2	2	3	1	2	2	3	1	2	2	3	1	2	2	3	1	2	2	3	J	j_1	j_2	J
3/2	3/2	4	Calc.				7.0				10.1				9.9				8.0				9.7				9.1		5/2	3/2	4
			Obs.				*10*				*10*				*10*				*6*				*10*				*8*				
3/2	3/2	3	Calc.		6.5	1.3	2.6		9.6	5.5	1.8		9.3	7.4	0.2		7.5	3.6	0.1		9.3	3.8	1.3		8.7	3.9	−0.1		3/2	3/2	3
			Obs.		*1*	*2*	*0*		*9*	*3*	2		*8*	*5*	*2*		*6*	*5*	—		*7*	*5*	—		*7*	*3*	—				
5/2	3/2	3	Calc.		−0.9	4.6	6.2		3.1	8.1	8.9		3.1	8.1	9.1		1.2	6.2	6.2		2.3	10.5	8.8		2.0	7.5	8.2		5/2	3/2	3
			Obs.		*3a*	*2a*	*1*		*4*	*7*	*9*		*4*	*9*	*8*		*1*	*4*	*4*		*3*	*8*	*15*		*x*	*6*	*10*				
5/2	1/2	3	Calc.		−4.7	5.2	4.6		1.5	8.2	7.7		1.7	7.9	7.4		−1.1	5.9	5.4		−0.2	7.4	6.9		−1.0	5.6	6.3		5/2	1/2	3
			Obs.		—	*10*	*7*		*6*	*9R*	*8R*		*3*	*8*	*8*		*5*	*8*	*4*		*r*	*7*	*9*		—	*10*	*10*				
3/2	3/2	2	Calc.	4.8	4.5	−0.2	0.2	8.3	8.0	4.1	2.9	8.1	7.9	2.6	3.2	6.2	5.9	0.9	1.0	7.8	9.1	2.7	2.4	7.3	7.2	2.1	1.3	3/2	3/2	3/2	2
			Obs.	*1*	*1*	*0*	*0?*	*6*	*7*	*6*	*4*	*9-y*	*8*	*4*	*2*	*4*	*4*	—	*2*	*7*	*7*	*1*	*1*	*7*	*4*	*1*	*1?*				
3/2	1/2	2′	Calc.	4.7	4.1	4.3	−0.4	8.4	7.4	5.0	0.1	7.1	6.4	7.7	3.7	3.9	2.3	6.9	3.1	4.2	1.8	8.6	5.4	−1.0	−3.0	8.0	5.4	5/2	3/2	2′
			Obs.	*8*	*2*	*1*	*0*	*7*	*6*	*2*	*1*	*8*	*7*	*6*	*y*	*3*	*5*	*4*	*2*	*4*	*5*	*9*	*7*	—	*2*	*7*	*4*				
5/2	3/2	2″	Calc.	1.4	2.2	5.0	−8.1	−1.3	3.5	8.9	4.9	9.1	5.8	8.1	4.1	4.9	5.1	4.2	1.0	6.8	6.7	2.4	4.2	6.1	6.1	0.6	−0.1	3/2	1/2	2″
			Obs.	*3*	*1*	*3*	—	*x*	*1*	*9*	*4*	*6*	*6*	*8*	*5*	*5*	*6*	*5*	—	*8*	*10*	*5?*	*1*	*8*	*7?*	*5*	—				
5/2	1/2	2	Calc.	−8.1	−5.3	−0.6	5.5	−3.2	−2.6	4.9	8.5	−3.3	−0.8	7.0	8.2	−5.6	−2.8	2.1	6.0	−2.1	−1.4	4.0	7.6	−5.0	−2.0	3.6	6.8	5/2	1/2	2
			Obs.	*1*	*1*	*3*	*17*	*2*	*6*	*7-x*	*10R*	*0*	*3*	*7-x*	*8*	—	*3*	*5*	*7*	*r*	*r*	*6*	*9*	—	*r*	*4?*	*10*				
3/2	3/2	1	Calc.	2.5	5.2	3.9		8.2	5.6	5.0		8.1	5.7	5.1		6.2	4.3	2.8		7.9	5.2	4.3		7.4	4.6	3.0		3/2	3/2	1
			Obs.	*1*	*1*	*0*		*7*	*2*	*4*		*8*	*5*	*3*		*2*	*2*	*3*		*7*	*2*	*1*		*3*	*2*	*1*				
3/2	1/2	1′	Calc.	5.6	2.1	−3.0		5.8	7.6	5.4		5.8	7.1	6.2		3.6	4.8	4.9		4.9	6.0	7.1		3.7	5.4	7.0		5/2	3/2	1′
			Obs.	*0*	*1*	—		*3*	*8*	*6*		*5*	*6*	*6*		*2*	*3*	*3*		*2*	*5*	*7*		*5*	*3-x*	*5*				
5/2	3/2	1″	Calc.	−2.1	1.3	5.1		0.4	4.3	7.8		0.6	5.1	7.8		−4.1	3.7	5.6		0.8	5.8	6.9		1.9	5.6	5.0		3/2	1/2	1″
			Obs.	*3*	—	*1*		*2*	*7*	*7*		*0*	*x*	*8*		—	*5*	*4*		*1*	*6*	*7*		*1*	*6h*	*6*				
3/2	3/2	0	Calc.	3.5				6.7				6.5				4.6				6.3				5.2				3/2	3/2	0
			Obs.	*1b*				*3*				*6*				*3*				*4*				*3*						

a, Line also classified elsewhere; *b*, Line not strictly comparable with others; *c*, Masked by carbon line; *h*, Line with four hyperfine components of intensity 4 each; *r*, Line not in the range of the observer's (Arvidsson's) work; *x* and $n-x$ refer to lines of nearly the same wavelength both contributing to give an intensity n; *y* and $n-y$, same; *R*, Line reversed; *?*, Experimental uncertainty about line; —, Line missing.

to obey *jj* selection rules. At least in most cases, forbidden lines are weak compared with the allowed lines. Transitions from the other levels in which there is considerable "mixing" of *jj* properties naturally do not obey the selection rules of *jj* coupling.

The $5d^{10}-5d^96p$ Transitions

The $^1S_0$ state for the configuration $5d^{10}$ is known for all elements of this isoelectronic sequence and transitions between it and $5d^96p$ have been observed. In Russell-Saunders coupling the selection rules allow only the transition $5d^{10}\,{}^1S_0-5d^96p\,{}^1P_1$; hence no difficulty arises in obtaining the amplitude matrix in intermediate coupling. One assigns an amplitude factor 1 to this transition; one then applies the transformation leading to *jj* coupling; and finally one transforms from *jj* to intermediate coupling. These results are then treated by the scheme just discussed, to yield the theoretical values of the intensities of the three possible transitions. These along with the observed values are shown in Table II.

TABLE II. *Comparison of calculated and observed intensities for* $5d^{10}-5d^96p$. The observed values are in italics. The bridge around thallium has the same significance as in Table I. a, Not comparable with others.

			$5d^{10}\,{}^1S_0$						
			Pt I	Au II	Hg III	Tl IV	Pb V	Bi VI	
	$3/2,3/2\|_1$	Calc.	7.0	2.2	7.1	8.1	7.6	8.2	$3/2,3/2\|_1$
		Obs.	*2*	*3*	*6*	*7*	*7*	*8a*	
$5d^96p$	$3/2,1/2\|_{1'}$	Calc.	1.0	3.8	8.6	10.0	9.6	10.6	$5/2,3/2\|_{1'}$
		Obs.	*6*	*3*	*8*	*10*	10	*10*	
	$5/2,3/2\|_{1''}$	Calc.	0.1	−2.8	4.0	2.9	−0.9	6.1	$3/2,1/2\|_{1''}$
		Obs.	*1*	*2*	*8*	*4*	1	*7*	

One can finally conclude that on the whole the results on both energies and intensities indicate a satisfactory check on the theory of complex spectra of two electron systems.

Hyperfine Structure

The hyperfine structure of some of the lines of the platinum-like spectra has been observed. The data are incomplete and no direct comparison with experiment can be made at present. It is perhaps worth while to point out that there is sufficient information available to determine the various hyperfine multiplet constants. The transformation matrices determined are all that is needed to make use of the theory of hyperfine structure in intermediate coupling due to Breit and Wills.[22] The method is indicated in section 3 of their paper. However, it should be pointed out that one must pay due regard to phases. There is no assurance that the phases used in this paper agree with those of Breit and Wills since a perfectly arbitrary set of phases have been used throughout this paper.

It is possible that the agreement or disagreement of this theory with the observed hyperfine structure of the $J=1'$ and $J=1''$ levels of thallium might serve to fix their *jj* designation but it appears that the values obtained for the relative amounts of pure *jj* wave functions already obtained are more accurate than those that would be indicated by the hyperfine structure.

Because of the lack of experimental values of the hyperfine structure no calculations on this point have been made.

The author wishes to express his indebtedness to Professor Van Vleck under whose direction this work was done; he also wishes to thank Professor Mack for placing the experimental data at his disposal and for many helpful suggestions; and he wishes to thank the Wisconsin Alumni Research Association for the appointment as post-doctorate research associate which made it possible for him to make the calculations on intensities.

[22] Breit and Wills, Phys. Rev. **44**, 470 (1933).

New Energy Levels in Au II, Hg III, Tl IV, Pb V and Bi VI

J. E. MACK AND M. FROMER, *Department of Physics, University of Wisconsin*

(Received April 24, 1935)

All the previously unknown $5d^{10}$, $5d^96s$ and $5d^96p$ levels in all the stable members of the platinum-like isoelectronic sequence, and some $5d^96d$ and $5d^97s$ levels, have been identified. Several corrections are made to the literature on Au II, Hg III and Tl IV. The Pb V and Bi VI classifications verify Arvidsson's estimates of the stages of ionization for the individual lines. The $5d^96p|_0$ levels were found only in consequence of Goble's predictions from his solution of the four-vector problem. The dependence of the energy and intensity values upon the atomic number is very smooth, except for a branching effect explained by Goble. New d^9s screening numbers and Houston parameters are given. Ionization potentials are estimated, by a comparison method, up to 87.9 ± 0.7 volts for Bi VI. Analysis of the one (partly resolved) hyperfine structure pattern attributed to Bi VI yields a splitting factor $a(6s)=3.1\pm0.2$ cm^{-1}.

MODERN methods of excitation of extreme ultraviolet spark spectra are capable of stripping atoms of all kinds to stages with very simple spectra, and (except in the case of the lightest elements) to others as well, with very complicated spectra. The abundance of the lines thus excited leads to quite a high probability of fortuitous agreement in wave number differences, so that one frequently meets lines listed in the literature as belonging to ions removed by several stages of ionization from those to which they are later found to belong. A few investigations with the excitation controlled, especially by means of a variable series inductance,[1] have yielded reliable quantitative information about the stages of ionization of lines. Notable among these investigations is that of the spark spectra of lead and bismuth, by Arvidsson.[2] His success leaves no doubt as to the quantitative applicability of the method as far as the sixth spectrum at least. The first step in our investigation[3] was the completion of the classification of the $5d^{10}$, $5d^96s$ and $5d^96p$ levels of Pb V and Bi VI, except $5d^96p|_0$, whose later discovery is discussed below. The new Pb V and Bi VI levels are all derived from Arvidsson's lines, classified with few exceptions in exactly the stage of ionization to which they were assigned by Arvidsson. The exceptions never involve a discrepancy of more than one in z (where $z\equiv$Roman numeral). They occur mainly in the region of wavelengths much shorter than any heretofore classified in lead or bismuth; so they are not surprising, in view of the fact that Arvidsson's method of separation was a relative one, depending upon the presence of lines belonging to known stages.

Because of the relative excellence of the experimental material for these two elements, their platinum-like spectra were then known better than the earlier members of the isoelectronic sequence, so they presented an unusual opportunity for the verification of the levels already reported and the discovery of new ones, by interpolation, and in one lot of levels, by backward extrapolation from the fourth spark spectrum. Many of the better known rules for the classification of spectra are inapplicable in this sequence. In Pt I itself the configurations built upon the $5d^86s$ configuration of the spark spectrum are so mixed with those built upon the $5d^9$ configuration that, in general, the individual levels can scarcely be coordinated with corresponding levels in the spark spectra. (For this reason Pt I will not be considered again in this report.) In the finally verified sequence there are even instances of sharp breaks in the graph of relative energy as a function of the atomic number, within an isolated configuration. The reports up to Arvidsson's upon spectra in the sequence were all based upon experimental material considerably less modern than that given by Arvidsson. Altogether, then, it is not surprising that in extending our knowledge of the sequence it has been necessary not only to fill in the gaps, but also to make a critical examination of all the older data and rectify several misclassifications in Au II, Hg III and Tl IV. It has been found possible from a study of the existing data in the light of our new knowledge from

[1] A. Fowler, Phil. Trans. Roy. Soc. **A225**, 1 (1925); R. C. Gibbs, A. M. Vieweg and C. W. Gartlein, Phys. Rev. **34**, 406 (1929).

[2] G. Arvidsson, Ann. d. Physik **12**, 787 (1932).

[3] A. T. Goble and J. E. Mack, Phys. Rev. **42**, 909 (1932). With the revisions mentioned in the next paragraph, the irregularities pointed out in this abstract disappear.

Arvidsson[2] on the one hand, and from Goble[3, 4] on the other, to complete the identification of all the seventeen levels belonging to the configurations $5d^{10}$, $5d^96s$, and $5d^96p$ in each of the six stable elements of the sequence. In addition, the $5d^97s$ levels have been found in Pb V and Bi VI, and five possible $5d^9{}_{5/2}6d$ levels in Pb V.

Certain general properties of the spectra of this sequence are shown in the figures and tables of Goble's[4] paper just preceding this one. Except for a hyperbola-like branching effect in two pairs of levels (to be discussed below in connection with certain notational difficulties it introduces) the dependence of the energy values upon the atomic number is quite smooth. In fact, although the total spread of the $5d^96p$ configuration ranges up to almost sixty thousand units, in most cases the misplacement of a level by a hundred units would have caused a noticeable loss of regularity in the large scale original of Goble's Fig. 1.

No attempt is made in this report to interpret the energy distribution of the $5d^96p$ levels, or the intensities. The reader is referred to the Goble paper for a full treatment of these matters.

Table I, showing some other general properties, is almost self-explanatory. It includes certain values from the gold- and mercury-like sequences for comparison. In the configuration means the levels are weighted by the factor $2J+1$. Houston's[5] X's are calculated according to Laporte and Inglis'[6] Eq. (3′), where X' or X''' equals Goble's[4] $-2\zeta/a_1$. The slight negative change of the regular doublet screening number σ_{-5d} of Au II between $5d^96s$ and $5d^97s$ is probably a false effect due to the overlapping of $5d^97s$ and $5d^96d$. The discrepancy between X''' and X' in $5d^96s$ decreases regularly as $5d^86s^2$ recedes with increasing z. In Bi VI $5d^97s$ Houston's relationship is exactly fulfilled, the recorded discrepancy amounting to only 3 cm^{-1}, or less than the uncertainty in the values of the separations. This bespeaks a fortuitous balancing of perturbing effects or a remarkably weak interaction between $5d^97s$ and the neighboring (undiscovered) $5d^96d$.

The estimation of the ionization potentials (I. P., Table I) required a close study of neighboring and analogous spectra. The highest series member from which the ionization potential was estimated, and the estimating author, for the gold-like spectra, are shown in the line labeled "determined from." The hybrid method finally adopted for our sequence, which appeared to give the most plausible results there, was to calculate a first approximate Moseley ordinate $(\nu_{6s}/R)^{\frac{1}{2}}{}_{\text{Rydberg}}$ by applying the Rydberg formula to the first two members of the $5d^9{}_{5/2}ns\,|_3$ series, where possible, and to make the same slight correction, $\Delta(\nu_{6s}/R)^{\frac{1}{2}}$, to this ordinate as in the corresponding spectrum of the gold-like sequence, where the Moseley ordinates are almost identical and the corrections are known from higher terms. The absolute energies of the normal levels $5d^{10}\,|_0$, referred to the limits $5d^9|_{5/2}$, could then be evaluated directly from known spectrum lines. The method is almost tantamount to assuming the same Ritz correction in the platinum-like as in the gold-like spectrum of the same stage of ionization, but lends itself better to interpolation. The correction to the simple Rydberg value amounts to between three and four percent of the $6s$ term value. In Cu II, the only homologous spectrum where the absolute term values are known from its own series, the method yields results 0.4 percent too high. We suppose our estimates are reliable to about 1 percent.

The spectra are discussed separately below, except for the $5d^9{}_{3/2}6p_{3/2}\,|_0$ level, which is treated after Bi VI for all the spectra in common. In part A of each of the Tables II to VI there is given at the head of each column and row, the configuration with appropriate j and J values, and the relative energy, for a level. A self-explanatory jj notation is used throughout except for some notational expedients described in the next paragraph. In Au II and Hg III the energies are referred to $5d^9{}_{5/2}6s\,|_3$; in Tl IV, Pb V and Bi VI, to the normal level $5d^{10}\,|_0$. At each intersection, corresponding to a spectrum line, there is given the observed intensity, followed by the wave number discrepancy $\nu_{\text{obs}}-\nu_{\text{calc}}$. In Pb V and Bi VI, the intensity is preceded by a Roman numeral showing Arvidsson's estimate z_A, if any, of the stage of ionization to which the line belongs. In part B of each table, the experimental data for each line are taken from the author whose intensity estimate is shown farthest to the left (except where otherwise specified).

[4] A. T. Goble, Phys. Rev. this issue.
[5] W. V. Houston, Phys. Rev. **33**, 297 (1929).
[6] O. Laporte and D. R. Inglis, Phys. Rev. **35**, 1337 (1930).

TABLE I. *The x-ray doublets, Houston parameters and ionizing energy values, in the platinum-like spectra.*[1]

Spectrum	Seq.	I	II	III	IV	V	VI
	80	Hg I	Tl II	Pb III	Bi IV		
	79	Au I	Hg II	Tl III	Pb IV	Bi V	
	78	Pt I	Au II	Hg III	Tl IV	Pb V	Bi VI
Irregular doublets:							
$5d^{10}6s^2-5d^{10}6s6p_{\text{mean}}$	80	44855	61854	77875	93722		
$(6s-6p)_{80}-(6s-6p)_{79}$	—	4953	4283	3843	3532		
$5d^{10}6s-5d^{10}6p_{\text{mean}}$	79	39902	57571	74032	90190	106372	
$(6s-6p)_{79}-(6s-6p)_{78}$	—	3066	3279	3540	3946	4388	
$5d^96s_{\text{mean}}-5d^96p_{\text{mean}}$	78	[36836]	54292	70492	86244	101984	117900
Δ_1		+17456	+16200	+15752	+15740	+15916	
Δ_2			−1256	−448	−12	+176	
Regular doublets:							
$\Delta\nu_{-5d}(5d^96s^2)$	79	12274	15040				
$\sigma_{-5d}(5d^96s^2)$		43.560	42.708				
$\Delta\sigma_{-5d}(6s^2-6s)$	—	Au+0.327	Hg+0.315				
$\Delta\nu_{-5d}(5d^96s)$	78	10132	12727	15554	18624	21943	25522
$\sigma_{-5d}(5d^96s)$		44.215	43.233	42.393	41.661	41.015	40.437
Δ_1		−0.992	−0.840	−0.732	−0.646	−0.578	
$\Delta\sigma_{-5d}(6s-7s)$		[−1.95]	−0.054			+0.052	+0.071
$\Delta\nu_{-5d}(5d^97s)$		[7978]	12650			22055	25693
$\sigma_{-5d}(5d^97s)$		[46.17]	43.287			40.963	40.366
Δ_1		−2.88	←	−0.77×3	→	−0.597	
Houston parameters:							
$X'''(5d^9{}_{5/2}6s\|_2)$	78	[0.67]	2.055	2.053	1.914	1.751	1.598
$X'(5d^9{}_{3/2}6s\|_2)$		[3.02]	1.530	1.765	1.691	1.566	1.438
$X'''-X'$		[−2.35]	+0.525	+0.288	+0.223	+0.185	+0.160
Δ_1		+2.88	−0.237	−0.065	−0.038	−0.025	
$X'''(5d^9{}_{/2}7s\|_2)$		0.308	0.310			0.3076	0.2978
$X'(5d^9{}_{3/2}7s\|_2)$		[0.424]	0.285			0.3154	0.2987
$X'''-X'$		−0.116	+0.025			−0.0078	−0.0009
Ionizing energies:							
$5d^{10}6s_{1/2}-5d^{10}7s_{1/2}$	79	54485	95714	139209	185100	233346	
$(\nu_{6s}/R)^{\frac{1}{2}}_{\text{Rydberg}}$		0.8396	1.1969	1.5068	1.7945	2.0644	
$\Delta(\nu_{6s}/R)^{\frac{1}{2}}$		−0.016	−0.023	−0.026	−0.030	−0.033	
$(\nu_{6s}/R)^{\frac{1}{2}}_{\text{best}}$		0.8238	1.174	1.481	1.764	(2.031)	
determined from		7d(MM)	12g(P)	7h(M)[2]	7h(M)[2]		
$5d^96s\|_3-5d^97s\|_3$	78	52379	93132			227672	277092
$(\nu_{6s}/R)^{\frac{1}{2}}_{\text{Rydberg}}$		0.8258	1.1834			2.0447	2.2998
$\Delta(\nu_{6s}/R)^{\frac{1}{2}}$		−0.016	(−0.023)			(−0.033)	(−0.035)
$(\nu_{6s}/R)^{\frac{1}{2}}_{\text{best}}$		0.810	1.160	(1.464)	(1.746)	2.012	2.265
Δ_1		+0.350	+0.304	+0.282	+0.266	+0.253	
$10^{-2}\nu_{6s}$		720	1477	2353	3343	4442	5630
$10^{-2}\nu_{5d}$		659	1617	2781	4094	5550	7125
$(\nu_{5d}/R)^{\frac{1}{2}}$		0.775	1.214	1.592	1.932	2.249	2.548
Δ_1		+0.439	+0.378	+0.340	+0.317	+0.299	
I. P., $5d^9{}_{5/2}(6s\rightarrow\infty)$, volts		8.88					
I. P., $5d^9{}_{5/2}(5d\rightarrow\infty)$, volts			19.95 ±0.2	34.3 ±0.3	50.5 ±0.4	68.5 ±0.5	87.9 ±0.7

[ ] These values in Pt I are irregular, due to the mixture of $5d^96s$ with $5d^96s^2$, and of $5d^96p$ with $5d^96s6p$ in many of the levels.
( ) Estimated values.
[1] In this and the following tables the values given without special references are taken from sources which may be found in Bacher and Goudsmit, *Atomic Energy States*, McGraw-Hill, 1932, or from the new material in this paper, below. Authors referred to only by their initials can be identified by the bibliographical references at the appropriate points in Bacher and Goudsmit.
[2] Kindly communicated privately by Professor McLay.

For each of the J values common to the $5d^9{}_{5/2}6p_{3/2}$ and $5d^9{}_{3/2}6p_{1/2}$ groups (*viz.*, $J=1$ and $J=2$) the crossing of the pure jj roots, shown by Goble,[4] is accompanied by a hyperbola-like branching of the pair of levels, with an interchange of the formally assigned approximate j values near the vertices. (See Goble's Fig. 2.) The vertices for the $J=1$ pair are so near to Tl IV that the wave function of the lower level there, according to Goble, shows no clear majority in favor of either jj assignment. For these reasons it has been found expedient to supplement the notation by adding a prime (′) for the higher and a double prime (″) for the lower level of each of

TABLE II. *A: Energy levels and transitions in Au II (supplementary to Bacher and Goudsmit, Table I, reference 1).*

Config.		$5d^{10}\|_0$	$5d^9{}_{3/2}6s\|_1$	$5d^96s^2\|_1$	$5d^9{}_{5/2}6d\|_1$	$5d^9{}_{5/2}6d\|_1$	$5d^9{}_{3/2}7s\|_1$
J					1	5	
B & G symbol							
	$\nu(cm^{-1})$	−14023**	12726.7*	?46710.0*	101008.8*	102256.4*	105781.2*
$5d^9{}_{3/2}6p_{3/2}\|_{1''}$	58364.5*	2 +1	old	—	old	old	—
$5d^9{}_{3/2}6p_{3/2}\|_0$	66606.5†		3 0	—	3 0.0	—	1 0.0
$5d^9{}_{3/2}6p_{1/2}\|_{1'}$	66620.2*	3 +4	old	—	(see IIB)	old	old
$5d^9{}_{3/2}6p_{3/2}\|_1$	70668.0*	3 −17	old	?old	—	old	old

Several putative levels not listed here may be found in B. V. Rao, Proc. Roy. Soc. **A142**, 118 (1933).
* Old level (MM).
** Replaces (ST)[1] $5d^{10}\,{}^1S_0 = -15036$.
† Replaces (MM) $6p\,{}^3P_0 = 67574.5$.

? 46710_1 is one of a group of five (MM) levels evidently overlooked by B & G. The question mark is ours; with the repudiation of 67574.5_0 this supposed level is supported only by a single pair, and in any case one would expect the $d^9s^2|_1$ level to be near the middle $J=2$ level (probably 33471.6_2) of the configuration.

TABLE II. *B: Newly classified lines of Au II.*

BBF[2]	BB[2]	Intensity EH[3] spark	Intensity EH[3] arc	MM[4]	λ_{vac}	ν	
3					1181.00	84674	$5d^{10}\|_0 - 5d^9{}_{3/2}6p_{3/2}\|_1$
3					1239.97	80647	$5d^{10}\|_0 - 5d^9{}_{3/2}6p_{1/2}\|_{1'}$
	2				1381.44	72388	$5d^{10}\|_0 - 5d^9{}_{3/2}6p_{3/2}\|_{1''}$
	2				1852.54	53980	$5d^9{}_{3/2}6s\|_1 - 5d^9{}_{3/2}6p_{3/2}\|_0$
					λ_{air}		
		1	—		2551.90	39174.7	$5d^9{}_{3/2}6p_{3/2}\|_0 - 5d^9{}_{3/2}7s\|_1$
		3	1		2905.93	34402.3	$5d^9{}_{3/2}6p_{3/2}\|_0 - 5d^9{}_{5/2}6d\ 1\|_1$
		4	—	5	2907.07	34388.7	$5d^96s^2\|_2 - 5d^9{}_{3/2}6p_{3/2}\|_2$; $5d^9{}_{3/2}6p_{1/2}\|_{1'} - 5d^9{}_{5/2}6d\ 1\|_1$, (overlooked in (MM) line list)

[1] R. A. Sawyer and K. Thomson, Phys. Rev. **38**, 2203 (1931).
[2] L. Bloch, E. Bloch and J. Farineau, J. de phys. et rad. **3**, 437 (1932); L. Bloch and E. Bloch, J. de phys. et rad. **6**, 160 (1925).
[3] F. Exner and E. Haschek, quoted in Kayser and Konen, *Handbuch der Spectroskopie*, VII.
[4] Table I, reference 1.

these pairs throughout the sequence, and to omit the j values entirely for the 1′ and 1″ levels of Tl IV. (The $J=2$ levels exchange j values between Hg III and Tl IV. If formal j values had been assigned in the Tl IV $J=1$ pair according to the minority plurality these two levels would have exchanged j values between Tl IV and Pb V.) Doctor Goble's advice as to the nature of the phenomena to be expected in the branching region has been invaluable. Of course the assignments of the doubtful j values were made on the basis of his calculations.

Au II (*Table II*). All the published $5d^96s$, $5d^96p$ and $5d^97s$ levels are verified except $5d6p\,|_0$. An alternative value for the normal level $5d^{10}\,|_0$ is proposed. The new value for the normal level fits into the scheme of Moseley ordinates (Table I) perhaps better than the old ($(\nu_{5d}/R)^{\frac{1}{2}}_{old} = 1.218$), but this in itself is hardly conclusive, since Moseley graphs for isoelectronic sequences generally show relatively sharp departures from linearity in the neighborhood of the neutral atom. A much more serious matter is the line list of the Blochs. In a number of instances the qualitative correctness of the ultraviolet line lists of those authors has been verified, although, obtained from a low dispersion instrument, the frequency values are not necessarily especially accurate. Although the three lines establishing the new level are far apart, their wave number agreement is well within the Blochs' own estimate of their absolute accuracy. Compared with the new level's (3, 3, 2), the intensities of the three expected transitions to the previously reported $5d^{10}\,|_0$ level are (0, 4, missing); this disparity in intensities is contrary to the behavior of almost all other known $d^{10}-d^9p$ line triads. (The case of Ag II will be treated elsewhere.) Unfortunately the BBF paper gives no hint as to how BBF intensities and BB intensities are to be compared.

Hg III[7] (*Table III*). Each of the changes improves the internal consistency of the spectrum, as well as being practically inevitable from the consideration of smoothness within the sequence. Replacement of the (MMC) $^1F_3$ relieves the analysis of an ambiguity in the Hg II line $\nu 71408$. The $d^{10}-d^9p$ lines were all stronger than any other mercury lines to the violet of λ1080 on Lang's plates, which extend to about λ600. There is hardly any doubt of the presence of a mercury

TABLE III. *A: Energy levels and transitions in Hg III (supplementary to Bacher and Goudsmit, Table I, reference 1).*

Config. J		$5d^{10}\|_0$	$5d^9{}_{5/2}6s\|_2$	$5d^9{}_{5/2}6s\|_2$	$5d^9{}_{3/2}6s\|_1$	$5d^9{}_{3/2}6s\|_2$
	ν(cm^{-1})	−42862	0*	3177*	15554*	18234*
$5d^9{}_{5/2}6p_{3/2}\|_{1''}$	75754**	8 0		old	old	old
$5d^9{}_{3/2}6p_{1/2}\|_{1'}$	83704*	8O −8		old	old	old
$5d^9{}_{3/2}6p_{3/2}\|_0$	86228				6 0	
$5d^9{}_{3/2}6p_{3/2}\|_3$	91737†		3 0	5 0	out	8 0
$5d^9{}_{3/2}6p_{3/2}\|_1$	92146	6 +1		3 −7	8 +1	5 +1
$5d^9{}_{3/2}6p_{3/2}\|_2$	93627§		2 0	4 +4	9− +1	8 −1

The best values for the (MMC) levels not listed here are: 60698_2, 62775_3, 75148_4, 75695_2, 78074_2, 78750_3.
* Old level (MMC).
** This (MMC)$^3P_1$, previously questioned, is verified by this investigation.
† Formerly (MMC)$^1D_2$; replaces (MMC) 89637_3.
§ Formerly (MMC)$^3D_1$.
out The line formerly classified (MMC) as the transition, now forbidden, between these levels, appears on Lang's plates at $\nu 76173$, $\nu_{obs} - \nu_{calc} = -10$ cm^{-1}.

TABLE III. *B: Newly classified lines of Hg III.*

L[7]	Intensity MMC	C[1]	λ_{vac}	ν	Designation
6		1	740.69	135009	$5d^{10}\|_0 - 5d^9{}_{3/2}6p_{3/2}\|_1$
8O		5O	790.15	126558	$5d^{10}\|_0 - 5d^9{}_{3/2}6p_{1/2}\|_{1'}$
8		3	843.06	118616	$5d^{10}\|_0 - 5d^9{}_{5/2}6p_{3/2}\|_{1''}$
2		—	1068.04	93627	$5d^9{}_{5/2}6s\|_2 - 5d^9{}_{3/2}6p_{3/2}\|_2$
3	5	1	1090.07	91737	$5d^9{}_{5/2}6s\|_3 - 5d^9{}_{3/2}6p_{3/2}\|_3$
4	4	1	1105.53	90454	$5d^9{}_{5/2}6s\|_2 - 5d^9{}_{3/2}6p_{3/2}\|_2$
3		—	1124.08	88962	$5d^9{}_{5/2}6s\|_2 - 5d^9{}_{3/2}6p_{3/2}\|_1$
5	4	0	1129.18	88560	$5d^9{}_{5/2}6s\|_2 - 5d^9{}_{3/2}6p_{3/2}\|_3$
9	10	4	1280.83	78074	$\begin{cases} 5d^9{}_{3/2}6s\|_1 - 5d^9{}_{3/2}6p_{3/2}\|_2; \\ 5d^9{}_{5/2}6s\|_3 - 5d^9{}_{3/2}6p_{1/2}\|_{2'} \end{cases}$
8		2	1305.61	76593	$5d^9{}_{3/2}6s\|_1 - 5d^9{}_{3/2}6p_{3/2}\|_1$
8	6	3d	1326.40	75392	$5d^9{}_{3/2}6s\|_2 - 5d^9{}_{3/2}6p_{3/2}\|_2$
5		2d	1352.94	73913	$5d^9{}_{3/2}6s\|_2 - 5d^9{}_{3/2}6p_{3/2}\|_1$
8	8	2	1360.49	73503	$5d^9{}_{3/2}6s\|_2 - 5d^9{}_{3/2}6p_{3/2}\|_3$
6		4	1414.95	70674	$5d^9{}_{3/2}6s\|_1 - 5d^9{}_{3/2}6p_{3/2}\|_0$

Note: MMC have listed only their classified lines.
d Diffuse.
O (after intensity) Masked by an oxygen line (see text).
[1] J. A. Carroll, Phil. Trans. Roy. Soc. **A225**, 357 (1925).

line overlying the unresolved oxygen pair at λ790. Lang's intensities for the oxygen lines in this region on his mercury spark spectrum plates are 779 : 787 : 790 : 796 = 1 : 3 : 8 : 2*d*, while Edlén[7] gives their intensities as 9IV, 10IV : 15IV : 13IV, 16IV : 10II, respectively. Here we have placed Edlén's intensities and *z* values between the colons.

Tl IV (*Table IV*). After the classification of the $s \leftarrow p$ transitions (replacing our (Table I, reference 1) previous $5d^96s|_1$ level by Rao's (Table IV, reference 2)) and the prediction of the d^{10} level, it was our privilege to receive, in answer to our letter to Dr. Arvidsson, a list of measurements which, though not quite complete, effected a great improvement in the accuracy of our knowledge of the spectrum and tended to verify our scheme in detail. The columns headed by " A " in Table IV refer to this hitherto unpublished list, and for the lines listed in the column ν_A, the wavelengths are Arvidsson's; for the rest of the lines, the large discrepancies are no worse than might have been expected from the quality of the original data. There is a possibility that $5d^96s|_3$ and the $5d^9{}_{5/2}6p_{1/2}$ levels should be 10 or 12 cm^{-1} higher. Although no use is made in this paper of the hyperfine structure of Tl IV, the separations of some pairs are listed in Table IVA in parentheses after the wave number discrepancies, and in Table IVB in the column labeled $\delta\nu_A$, from Arvidsson's list. Of the ten to sixteen levels given in each of the three previous papers on this spectrum, not more than nine are verified in any case.

[7] We are greatly indebted to Professor Lang for generously sending us lists of readings from several mercury spark spectrum plates, which we have transformed to frequencies with respect to Paschen's Hg II and Edlén's (Zeits. f. Physik **85**, 85 (1933)) oxygen lines. The "L" in Table IIIB refers to these plates. The completeness and accuracy of the analysis presented here is due in no small measure to the availability of Lang's measurements. It is pleasing, however, to notice how closely compatible the older material of Carroll is with that of Lang. About forty of Lang's mercury spark spectrum lines of intensity more than 3, in the region λ < 2000, remain unaccounted for.

TABLE IV. *A: Energy levels and transitions in Tl IV (complete).*

Config. J	ν(cm^{-1})	$\Delta\nu$	$5d^{10}$ 0	$5d^9{}_{5/2}6s$ 3	$5d^9{}_{5/2}6s$ 2	$5d^9{}_{3/2}6s$ 1	$5d^9{}_{3/2}6s$ 2
			0	75052*	78647*	93676**	96727*
				3595	15029	3051	
$5d^9{}_{5/2}6p_{1/2}\|_2$	147635*	2206		7 − 0.9(4.7)	5 + 7	—	3 − 7
3	149841*	16584		4 − 0.4(3.4)	8 + 1(3.8)		5 − 13
$5d^9{}_{3/2}6p_{1/2}\|_{2''}$	166425†	1074		0 + 0.4	5 − 5	5 − 1.6(3.0)	6 + 2(3.4)
$5d^96p\|_{1''}$	167499† (Note)	173	4 + 1.8		4 − 4	—	5 + 3(4.7)
$5d^9{}_{5/2}6p_{3/2}\|_4$	167672*	2662		6 0.0			
$5d^9{}_{5/2}6p_{3/2}\|_{2'}$	170334*	1938		2 + 3	4 − 3	3 − 3	5 + 0.3(4.1)
$5d^9{}_{5/2}6p_{3/2}\|_3$	172272*	3018		4 − 9.0	4 + 4.5		1 + 3.1
$5d^96p\|_{1'}$	175290§ (Note)	5793	10 − 1.5		3 + 0.8	2 − 11	3 − 10(4.6)
$5d^9{}_{3/2}6p_{3/2}\|_0$	181083	6584				3 0 (4.5?)	
2	187667	566		0 calc.	5 − 6		6 + 2
1	188233†	1911	7 − 1.3		3 − 24	2 + 0.3	2 − 6
2	190144†			2 − 16	0 calc.	3 + 0.3	4 − 0.2

* Old level (M (Table I, reference 1), and sometimes one or more of P[1], R[2] and S[3]).

** This level, discovered by Rao, replaces (M) 18865 (referred to 75052_3).

† Given by Rao, in some cases with different J.

§ Designation changed from (M) $5d^9{}_{5/2}6p_{3/2}|_1$ after Goble[4].

Note: See the special discussion in the text regarding the notation for levels 1'' and 1'.

[1] P. Pattabhiramayya, Ind. J. Phys. **3**, 523 (1929).

[2] K. R. Rao, Proc. Phys. Soc. London **41**, 361 (1929).

[3] Dr. G. K. Schoepfle has courteously kept us informed of his unpublished work in Tl IV, Pb V and Bi VI (Phys. Rev. **43**, 374 (1933); **45**, 747 (1934)). His results are largely, but not entirely, in harmony with ours.

TABLE IV. *B: Classified lines of Tl IV.*

C	Intensity M	Intensity A	λ_{vac}	ν A	ν CM	$\delta\nu$ A	Designation
		7	531.260	188231.7			$5d^{10}\|_0 - 5d^9{}_{3/2}6p_{3/2}\|_1$
		10	570.488	175288.5			$5d^{10}\|_0 - 5d^96p\|_{1'}$
		4	597.012	167500.8			$5d^{10}\|_0 - 5d^96p\|_{1''}$
	2	1	868.99		115076		$5d^9{}_{5/2}6s\|_3 - 5d^9{}_{3/2}6p_{3/2}\|_2$
	—	1b	888.0	calc.			$5d^9{}_{5/2}6s\|_3 - 5d^9{}_{3/2}6p_{3/2}\|_3$
	—	3	896.9	calc.			$5d^9{}_{5/2}6s\|_2 - 5d^9{}_{3/2}6p_{3/2}\|_2$
	3	3	912.74		109560		$5d^9{}_{5/2}6s\|_2 - 5d^9{}_{3/2}6p_{3/2}\|_1$
	5	8	917.31		109014		$5d^9{}_{5/2}6s\|_2 - 5d^9{}_{3/2}6p_{3/2}\|_3$
4	6	30	1028.690	97211.0	97224		$5d^9{}_{5/2}6s\|_2 - 5d^9{}_{5/2}6p_{3/2}\|_3$
3	4	20	1034.728	96643.8	96643		$5d^9{}_{5/2}6s\|_2 - 5d^96p\|_{1'}$
3C?	4C? −	20	1036.610	96468.3	96477		$5d^9{}_{3/2}6s\|_1 - 5d^9{}_{3/2}6p_{3/2}\|_2$
2	5	10	1049.48		95285		$5d^9{}_{5/2}6s\|_3 - 5d^9{}_{5/2}6p_{3/2}\|_{2'}$
2		10	1057.56	94557.3	94557		$5d^9{}_{3/2}6s\|_1 - 5d^9{}_{5/2}6p_{3/2}\|_1$
4	5	20	1068.04	93629.5	93623		$5d^9{}_{5/2}6s\|_2 - 5d^9{}_{5/2}6p_{3/2}\|_3$
4		20	1070.471	93416.8	93416		$5d^9{}_{3/2}6s\|_2 - 5d^9{}_{3/2}6p_{3/2}\|_2$
6	6	30	1079.68	92620.0	92617		$5d^9{}_{5/2}6s\|_3 - 5d^9{}_{5/2}6p_{3/2}\|_4$
4	5		1079.70		91684		$5d^9{}_{5/2}6s\|_2 - 5d^9{}_{5/2}6p_{3/2}\|_{2'}$
2			1092.90		91500		$5d^9{}_{3/2}6s\|_2 - 5d^9{}_{3/2}6p_{3/2}\|_1$
—		4	1094.411	91373.4			$5d^9{}_{5/2}6s\|_3 - 5d^9{}_{3/2}6p_{1/2}\|_{2''}$
6			1099.60		90942		$5d^9{}_{3/2}6s\|_2 - 5d^9{}_{3/2}6p_{3/2}\|_3$
4			1125.52		88848		$5d^9{}_{5/2}6s\|_2 - 5d^96p\|_{1''}$
5			1139.30		87773		$5d^9{}_{3/2}6s\|_2 - 5d^9{}_{3/2}6p_{1/2}\|_{2''}$
3		2, 1d	1144.07		87407	4.5?	$5d^9{}_{3/2}6s\|_1 - 5d^9{}_{3/2}6p_{3/2}\|_0$
2		3, 2	1225.45		81603	4.6	$5d^9{}_{3/2}6s\|_1 - 5d^96p\|_{1'}$
3	6		1273.03		78553		$5d^9{}_{3/2}6s\|_2 - 5d^96p\|_{1'}$
3			1304.55		76655		$5d^9{}_{3/2}6s\|_1 - 5d^9{}_{5/2}6p_{3/2}\|_{2''}$
1C?	6	2	1323.660	75548.1	75542		$5d^9{}_{3/2}6s\|_2 - 5d^9{}_{5/2}6p_{3/2}\|_3$
4	7	7, 7	1337.103	74788.6	74784	3.4	$5d^9{}_{5/2}6s\|_1 - 5d^9{}_{5/2}6p_{1/2}\|_2$
5	7	3, 2	1358,56	73607.3	73606	4.1	$5d^9{}_{3/2}6s\|_2 - 5d^9{}_{5/2}6p_{3/2}\|_{2'}$
5		2, 4	1374.620	72747.4	72747	3.0	$5d^9{}_{3/2}6s\|_1 - 5d^9{}_{3/2}6p_{1/2}\|_{2''}$
7	7	7, 7	1377.750	72582.1	72582	4.7	$5d^9{}_{5/2}6s\|_3 - 5d^9{}_{3/2}6p_{1/2}\|_2$
8	7	7, 7	1404.60		71195	3.8	$5d^9{}_{5/2}6s\|_2 - 5d^9{}_{5/2}6p_{1/2}\|_3$
5		3, 2	1412.93		70775	4.7	$5d^9{}_{5/2}6s\|_2 - 5d^96p\|_{1''}$
6		3, 3	1434.72		69700	3.4	$5d^9{}_{3/2}6s\|_2 - 5d^9{}_{3/2}6p_{1/2}\|_{2''}$
5			1449.37		68995		$5d^9{}_{5/2}6s\|_2 - 5d^9{}_{5/2}6p_{1/2}\|_2$
5			1883.2		53101		$5d^9{}_{3/2}6s\|_2 - 5d^9{}_{5/2}6p_{1/2}\|_3$
3			1974.6		50901		$5d^9{}_{3/2}6s\|_2 - 5d^9{}_{5/2}6p_{1/2}\|_2$

A. Private communication from Arvidsson (see text).

C. (After intensity) masked by a carbon line.

TABLE V. *A: Energy levels and transitions in Pb V (complete).*

Config.	J	ν(cm^{-1})	$\Delta\nu$	$5d^{10}$ 0	$5d^9{}_{5/2}6s$ 3	$5d^9{}_{5/2}6s$ 2	$5d^9{}_{3/2}6s$ 1	$5d^9{}_{3/2}6s$ 2	$5d^9{}_{3/2}6p$ 4	$5d^9{}_{3/2}6p$ 3	$5d^9{}_{3/2}6p$ 2	$5d^9{}_{5/2}7s$ 3	$5d^9{}_{5/2}7s$ 2	$5d^9{}_{3/2}7s$ 1	$5d^9{}_{3/2}7s$ 2
				0	110768.0* 3937.3	114705.3* 18006.1	132711.4 3285.7	135996.9*	?327433	?329573	?329935	?332358	?332501	338440 794	339234 21261	360496 578	361073
$5d^9{}_{5/2}6p_{1/2}$	2	194803.3*			V $\begin{matrix}9+3.3\\0?-12.3\end{matrix}$	V 6 0.0	:	:00 +7		V 5 −1		—	—	V 6 0	0 0	—	—
	3	197131.2*	2328		V 9 −0.7	V 7 +0.7		:00 +1	V 7 0	VI 4 +1	VI 2 0	2 −2	1 −1	V 2 +6	V 3 +1		—
$5d^9{}_{5/2}6p_{1/2}$	2′′′	217068.4	19937		V 1 +2	V 5? −1	V 8 +0.6	V 10 −0.7		—		—	0 −1	—	0 −3	1 −1	2b+10
	1′′	219488.2	2420	V 1 −2		V 7 +1	V 1 −1.4	V 6 +1.4				—	—		—	III blend	—
$5d^9{}_{5/2}6p_{3/2}$	4	221069*	1581		V 10 0				V 1 +2	V 0 +2	0 0			V 3 0			
	2′	223908.8*	2840		V 7 0	V 9 0	V 4 +0.2	V 5 −0.6		—		V 2 −3	V 2 0	—	V 2 +1	—	—
	3	226511.0*	2602		V 15 −1	V 8 +1		V 3 0.0	V 2 −2	V 2 −1	V 1 0	0 0	0 0	V 1 0	0 +1		—
	1′	227835.2**	1324	V 10 +1		V 7 0	V 2 +0.1	V 5 0.0				IV 2 +3	V 1 0		1 +1	—	—
$5d^9{}_{3/2}6p_{3/2}$	0	237660	9825				V 4 0									V 1 −1	
	3	244661	7001		—	V 5 −1		V 7 0		—	—	—	—	—	VI 0 −1		VI 2 0
	1	245277	616	V 7 +1		VI 1 0	V 7 0	V 2 −2				V 3 +5	V 0 +2		—	1 +2	—
	2	247595	2318		1 +2	V 1 −1	V 7 −1	V 7 0		—		—	—	—	—	0 −2	0 0

* Old level (M) (Table I, reference 1). ** This level, previously question marked, is verified by this investigation. : Beyond Arvidsson's range; the lines recorded are Carroll's.

Pb V (Table V) and Bi VI (Table VI); (see below for hyperfine structure). All the previously reported levels are verified, but the values of some have been altered by a few wave numbers to fit the new data. Since the differences $5d^96s-5d^96p$ are known more accurately than the differences $5d^{10}-5d^96p$, where tenths of a unit are meaningless, the choice of d^{10} as the zero for the measurement of term values has entailed the additional arbitrary choice of a naught after the decimal point in the value of Pb V $5d^96s|_3$. The normal levels were found after the establishment of all the $5d^96p|_1$ levels. It was a most satisfactory verification of our schemes, and of the accuracy of Arvidsson's wave numbers, to find the lines $5d^{10}-5d^96p$ in each case including the strongest of the lines listed in the region $\lambda<700$A for all the spectra of the element; and moreover, to find the required differences of about 30,000 cm^{-1} among the three lines of wave number about 300,000 cm^{-1}, in each case satisfied within a total discrepancy range of 3 cm^{-1}.

The $5d^96p|_0$ level. Detailed justification is needed for our $5d^9{}_{3/2}6p_{3/2}|_0$ levels, especially because we list but one with a question mark although they give rise, in three of our five schemes, to only one line each. Previous to this investigation the level had been reported in Au II, but McLay and his collaborators had wisely omitted any attempt to place it in Hg III, and it had been proposed in Tl IV only as the result of an excessive extrapolation. It was not sought by us until Dr. Goble had kindly made a preliminary estimate of its position in Pb V from those of the other eleven levels in the configuration. The $5d^96p|_0$ energy was one of the constants wanted for his final calculation, so the product of the $J=1$ roots, referred to $5d^96p|_4$, was used in its place in the preliminary estimate. Then ν104949 was chosen as $5d^96s|_1-5d^96p|_0$, supported by the following three facts:

(1) It is the nearest Pb $V_{Arvidsson}$ line to the predicted position (below the preliminary estimate from five electrostatic parameters by 550 cm^{-1} and below that from three electrostatic parameters by 750 cm^{-1}).

(2) It leads with a discrepancy of 1 cm^{-1} to a Pb $V_{Arvidsson}$ line for $5d^96p|_0-5d^97s|_1$, the level's only other possible transition in our scheme.

(3) Since there is only one each of the levels of

TABLE V. *B: Classified lines of Pb V.*

Intensity A	Intensity M	Intensity C	λ_{vac}	ν	z_A	Designation
7			407.700	245278	V	$5d^{10}{}_0 - 5d^9{}_{3/2}6p_{3/2}\vert_1$
10			438.911	227837	V	$5d^{10}{}_0 - 5d^9{}_{3/2}6p_{3/2}\vert_{1'}$
1			455.61	219486	V	$5d^{10}{}_0 - 5d^9{}_{3/2}6p_{1/2}\vert_{1''}$
0			692.37	144431		$5d^9{}_{3/2}6p_{1/2}\vert_2 - 5d^9{}_{3/2}7s\vert_2$
2b	1		694.37	144015		$5d^9{}_{3/2}6p_{1/2}\vert_{2''} - 5d^9{}_{3/2}7s\vert_2$
6			696.20	143637	V	$5d^9{}_{3/2}6p_{1/2}\vert_2 - 5d^9{}_{3/2}7s\vert_2$
1			697.22	143427		$5d^9{}_{3/2}6p_{1/2}\vert_{2''} - 5d^9{}_{3/2}7s\vert_1$
3	2O		703.71	142014	V	$5d^9{}_{3/2}6p_{1/2}\vert_2 - 5d^9{}_{3/2}7s\vert_2$
2	1		707.64	141315	V	$5d^9{}_{3/2}6p_{1/2}\vert_2 - 5d^9{}_{3/2}7s\vert_2$
2	2		709.20	141004	III	$5d^9{}_{3/2}6p_{1/2}\vert_{1''} - 5d^9{}_{3/2}7s\vert_1$; Pb III $6s6p\ {}^3P_0 - 6s6d\ {}^3D_1$
1			730.84	136829		$5d^9{}_{3/2}6s\vert_2 - 5d^9{}_{3/2}6p_{3/2}\vert_2$
1			738.72	135369		$5d^9{}_{3/2}6p_{1/2}\vert_2 - ?332501_2$
2	1		739.51	135225		$5d^9{}_{3/2}6p_{1/2}\vert_2 - ?332358_2$
5	4		742.01	134769	V	$5d^9{}_{3/2}6p_{1/2}\vert_2 - ?329573_3$
1			752.51	132889	V	$5d^9{}_{3/2}6s\vert_2 - 5d^9{}_{3/2}6p_{3/2}\vert_2$
2	1p		752.99	132804	VI	$5d^9{}_{3/2}6p_{1/2}\vert_2 - ?329935_4$
4	4		755.05	132442	VI	$5d^9{}_{3/2}6p_{1/2}\vert_2 - ?329573_3$
1	1		765.86	130572	VI	$5d^9{}_{3/2}6s\vert_2 - 5d^9{}_{3/2}6p_{3/2}\vert_1$
7	6	0	767.45	130302	V	$5d^9{}_{3/2}6p_{1/2}\vert_2 - ?327433_4$
5	1		769.50	129955	V	$5d^9{}_{3/2}6s\vert_2 - 5d^9{}_{3/2}6p_{3/2}\vert_2$
1			814.10	122835	V	$5d^9{}_{3/2}6p_{3/2}\vert_0 - 5d^9{}_{3/2}7s\vert_1$
0			818.58	122163		$5d^9{}_{3/2}6p_{1/2}\vert_{2''} - 5d^9{}_{3/2}7s\vert_2$
3	2	00	852.00	117371	V	$5d^9{}_{3/2}6p_{3/2}\vert_4 - 5d^9{}_{3/2}7s\vert_3$
2	1		859.02	116412	VI	$5d^9{}_{3/2}6p_{3/2}\vert_2 - 5d^9{}_{3/2}7s\vert_2$
15	7	5	863.99	115742	V	$5d^9{}_{3/2}6s\vert_2 - 5d^9{}_{3/2}6p_{3/2}\vert_2$
0			866.31	115432		$5d^9{}_{3/2}6p_{1/2}\vert_{2''} - ?332501_2$
2	0		867.11	115326	V	$5d^9{}_{3/2}6p_{3/2}\vert_{2'} - 5d^9{}_{3/2}7s\vert_2$
1	0		867.90	115221		$5d^9{}_{3/2}6p_{3/2}\vert_1 - 5d^9{}_{3/2}7s\vert_1$
7	5	3	870.45	114883	V	$5d^9{}_{3/2}6s\vert_1 - 5d^9{}_{3/2}6p_{3/2}\vert_2$
0			881.23	113478		$5d^9{}_{3/2}6p_{3/2}\vert_2 - 5d^9{}_{3/2}7s\vert_2$
7	5	4	883.85	113141	V	$5d^9{}_{3/2}6s\vert_2 - 5d^9{}_{3/2}6p_{3/2}\vert_{2'}$
7			883.94	113130	V	$5d^9{}_{3/2}6s\vert_2 - 5d^9{}_{3/2}6p_{3/2}\vert_{1'}$
0			885.75	112899		$5d^9{}_{3/2}6p_{3/2}\vert_2 - 5d^9{}_{3/2}7s\vert_1$
0			887.12	112724		$5d^9{}_{3/2}6p_{3/2}\vert_2 - 5d^9{}_{3/2}7s\vert_2$
7	5	3	888.37	112566	V	$5d^9{}_{3/2}6s\vert_1 - 5d^9{}_{3/2}6p_{3/2}\vert_1$
1			893.42	111929	V	$5d^9{}_{3/2}6p_{3/2}\vert_2 - 5d^9{}_{3/2}7s\vert_2$
8	6	4	894.40	111807	V	$5d^9{}_{3/2}6s\vert_2 - 5d^9{}_{3/2}6p_{3/2}\vert_2$
7	5		896.07	111598	V	$5d^9{}_{3/2}6s\vert_2 - 5d^9{}_{3/2}6p_{3/2}\vert_2$
1			897.67	111400		$5d^9{}_{3/2}6p_{3/2}\vert_{1'} - 5d^9{}_{3/2}7s\vert_2$
10	8	7	906.61	110301	V	$5d^9{}_{3/2}6s\vert_2 - 5d^9{}_{3/2}6p_{3/2}\vert_4$
2	0		915.10	109278	V	$5d^9{}_{3/2}6s\vert_2 - 5d^9{}_{3/2}6p_{3/2}\vert_1$
9	6	3	915.72	109204	V	$5d^9{}_{3/2}6s\vert_2 - 5d^9{}_{3/2}6p_{3/2}\vert_{2'}$
0			918.56	108866		$5d^9{}_{3/2}6p_{3/2}\vert_4 - ?329935_4$
7	5	3	920.27	108664	V	$5d^9{}_{3/2}6s\vert_2 - 5d^9{}_{3/2}6p_{3/2}\vert_3$
2	1		920.87	108593	V	$5d^9{}_{3/2}6p_{3/2}\vert_{2'} - ?332501_2$
0			921.61	108506	V	$5d^9{}_{3/2}6p_{3/2}\vert_4 - ?329573_3$
2			922.12	108446	V	$5d^9{}_{3/2}6p_{3/2}\vert_{2'} - ?332358_2$
1			940.15	106366	V	$5d^9{}_{3/2}6p_{3/2}\vert_4 - ?327433_4$
1	1		940.72	106302	V	$5d^9{}_{3/2}6s\vert_2 - 5d^9{}_{3/2}6p_{1/2}\vert_{2''}$
0			943.49	105990		$5d^9{}_{3/2}6p_{3/2}\vert_2 - ?332501_2$
0		00?	944.76	105847		$5d^9{}_{3/2}6p_{3/2}\vert_2 - ?332358_2$
4	4		952.84	104949	V	$5d^9{}_{3/2}6s\vert_1 - 5d^9{}_{3/2}6p_{3/2}\vert_0$
7	6	5	954.34	104785	V	$5d^9{}_{3/2}6s\vert_2 - 5d^9{}_{3/2}6p_{1/2}\vert_{1''}$
1	1–	00?	955.42	104666	V	$5d^9{}_{3/2}6p_{3/2}\vert_{1'} - ?332501_2$
2			956.70	104526	IV	$5d^9{}_{3/2}6p_{3/2}\vert_{2'} - ?332358_2$
1			966.89	103424	V	$5d^9{}_{3/2}6p_{3/2}\vert_2 - ?329935_4$
2	1	0?	970.30	103061	V	$5d^9{}_{3/2}6p_{3/2}\vert_2 - ?329573_3$
5?	8C	4C	976.93?	102362	V?	$5d^9{}_{3/2}6s\vert_2 - 5d^9{}_{3/2}6p_{1/2}\vert_{2''}$
2			990.88	100920	V	$5d^9{}_{3/2}6p_{3/2}\vert_2 - ?327433_4$
2		0	1051.26	95123.9	V	$5d^9{}_{3/2}6s\vert_1 - 5d^9{}_{3/2}6p_{3/2}\vert_{1'}$
0			1057.40	94571.6	VI	$5d^9{}_{3/2}6p_{3/2}\vert_2 - 5d^9{}_{3/2}7s\vert_2$
5	4	2	1088.87	91838.3	V	$5d^9{}_{3/2}6s\vert_2 - 5d^9{}_{3/2}6p_{3/2}\vert_{1'}$
4	2	1d	1096.52	91197.6	V	$5d^9{}_{3/2}6s\vert_1 - 5d^9{}_{3/2}6p_{3/2}\vert_{2'}$
3	1	00	1104.80	90514.1	V	$5d^9{}_{3/2}6s\vert_2 - 5d^9{}_{3/2}6p_{3/2}\vert_2$
5	8–	5d–	1137.51	87911.3	V	$5d^9{}_{3/2}6s\vert_2 - 5d^9{}_{3/2}6p_{3/2}\vert_{2'}$
0	0		1146.45	87225.8	V	$5d^9{}_{3/2}6p_{3/2}\vert_1 - ?332501_2$
3	4	0	1148.29	87086.0	V	$5d^9{}_{3/2}6p_{3/2}\vert_1 - ?332358_2$
1			1152.40	86775.4	V	$5d^9{}_{3/2}6s\vert_1 - 5d^9{}_{3/2}6p_{1/2}\vert_{1''}$
9	8	8	1157.91	86362.5	V	$5d^9{}_{3/2}6s\vert_2 - 5d^9{}_{3/2}6p_{1/2}\vert_2$
8	6	6	1185.43	84357.6	V	$5d^9{}_{3/2}6s\vert_1 - 5d^9{}_{3/2}6p_{1/2}\vert_{2''}$
9	6	7	1189.93	84038.6	V	$5d^9{}_{3/2}6s\vert_2 - 5d^9{}_{3/2}6p_{1/2}\vert_2$
6	5	2	1197.71	83492.7	V	$5d^9{}_{3/2}6s\vert_2 - 5d^9{}_{3/2}6p_{1/2}\vert_{1''}$
7	6	5	1213.20	82426.6	V	$5d^9{}_{3/2}6s\vert_2 - 5d^9{}_{3/2}6p_{1/2}\vert_2$
10	5	3	1233.49	81070.8	V	$5d^9{}_{3/2}6s\vert_2 - 5d^9{}_{3/2}6p_{1/2}\vert_{2''}$
6	3	2	1248.47	80098.0	V	$5d^9{}_{3/2}6s\vert_2 - 5d^9{}_{3/2}6p_{1/2}\vert_2$

b Broad. C (after intensity) Uncertain; masked by a carbon line. d Diffuse. O (after intensity) Uncertain; masked by an oxygen line. – (after intensity) Unresolved blend with another line, resolved by Arvidsson.

extreme J value in each of the configurations we are considering, the intensity sum rules degenerate in this case to show that the transition $d^9s\vert_1 - d^9p\vert_0$ has one-ninth the *a priori* probability of $d^9s\vert_3 - d^9p\vert_4$, or, being in the same spectral region, a photographic magnitude roughly less by three. The experimental intensity values, using the above lines, which were chosen without regard to their intensities, form the quite satisfactory set:

$$5d^96s\vert_1 - 5d^96p\vert_0 : 5d^96s\vert_3 - 5d^96p\vert_4 :: 4 : 10;$$
$$5d^96p\vert_0 - 5d^97s\vert_1 : 5d^96p\vert_4 - 5d^97s\vert_3 :: 1 : 3.$$

The Γ-sum rule, or spur degeneracy, leads to the expectation that the difference between the line frequencies $5d^96s\vert_1 - 5d^96p\vert_0$ and $5d^96s\vert_3 - 5d^96p\vert_4$ depends especially smoothly upon the atomic number; or, in Goble's language, this difference is simply $\delta + \frac{1}{2}[5a_1(d^9s) - 5a_1(d^9p)]$, where δ is the electrostatic energy measuring in LS coupling the interval $^3P - {}^3F$, and the difference between the values of the minus d electron's ls interaction energy $5a_1/2$ in the two configurations is ordinarily neglected.

Most fortunately, Hg ν70674 was the only unclassified mercury line on Lang's plates sufficiently strong to be considered for $5d^96s\vert_1 - 5d^96p\vert_0$, within 1500 cm^{-1}. This pointed to Tl ν87407, although the less likely appearing ν87573 was not eliminated until Arvidsson reported that the former was definitely a Tl IV line, whereas a study of a reproduction of one of his plates with several exposures using different inductances, shows that the latter is a pair separated by some 30 cm^{-1}, both components probably belonging to a higher stage of ionization than IV. The Bi VI

TABLE VI. *A: Energy levels and transitions in Bi VI (complete).*

Config.	J	ν(cm⁻¹)	Δν	$5d^{10}$ 0	$5d^9_{5/2}6s$ 3	$5d^9_{5/2}6s$ 2	$5d^9_{3/2}6s$ 1	$5d^9_{3/2}6s$ 2	$5d^9_{5/2}7s$ 3	$5d^9_{5/2}7s$ 2	$5d^9_{3/2}7s$ 1	$5d^9_{3/2}7s$ 2
				0	149495*	153737*	175017	178479	426587	427483	452280	452914
					4242	21310	3462		896	24797	634	
$5d^9_{5/2}6p_{1/2}$	2	244721*	2444		VI 10_{13} 0	VI 4? 0	—	:	VI 3 +2	0 +3	—	—
	3	247165*	23438		VI 10b 0	VI 10_{20} 0		—	—	—		—
$5d^9_{3/2}6p_{1/2}$	2''	270603	3555		—	V 5 0	VI 8_{14} −0.4	VI 7? +2	—	0 +2	1 −1	VI 2 +1
	1''	274158		V 7 +1		VI 6 0	1 +0.4	VI 4 +8.7 VI 4 +4.1 VI 4 −0.6 VI 4 −6.4		—	—	00 −9
$5d^9_{5/2}6p_{3/2}$	4	277866	3708		VI 8 0				VI 3 −2			
	2'	280939*	3073		VI 4 0	VI 7 0	—	2b −1	1 −3	1 0	—	—
	1'	284036	3097	V 10 −2		VI 5 −0.5	—	V 3b−x +1		1 0	—	—
	3	284058*	22		VI 10b +3	VI 6 −0.7		V x −21	2 +2	1 0		—
$5d^9_{3/2}6p_{3/2}$	0	? 298861	14833				VI 3 0				—	
	3	305272	6381		—	V 3 −1		VI 7 0	—	—		VI 4 −1
	1	305903	630	V 8b 0		1 +4	VI 3 −1	2d −3		—	1 0	—
	2	308613	2711		1 +14?	1 0	VI 7 −1	VI 4 0	—	—	—	0 +10

* Old level (A).[2] ? (Before energy value) Existence of level is uncertain.

TABLE VI. *B: Classified lines of Bi VI.*

Intensity	λ_{vac}	ν	z_A	Designation
8b	326.901	305903	V	$5d^{10}_0 - 5d^9_{5/2}6p_{3/2}\vert_1$
10	352.070	284034	V	$5d^{10}_0 - 5d^9_{5/2}6p_{3/2}\vert_{1'}$
7	364.752	274159	V	$5d^{10}_0 - 5d^9_{3/2}6p_{1/2}\vert_{1''}$
0	547.15	182765		$5d^9_{3/2}6p_{1/2}\vert_2 - 5d^9_{3/2}7s\vert_2$
2	548.51	182312	VI	$5d^9_{3/2}6p_{1/2}\vert_{2''} - 5d^9_{3/2}7s\vert_2$
3	549.85	181868	VI	$5d^9_{5/2}6p_{1/2}\vert_2 - 5d^9_{5/2}7s\vert_3$
1	550.42	181679		$5d^9_{3/2}6p_{1/2}\vert_{2''} - 5d^9_{3/2}7s\vert_1$
00	559.45	178747		$5d^9_{3/2}6p_{1/2}\vert_{1''} - 5d^9_{3/2}7s\vert_2$
1	628.41	159132		$5d^9_{5/2}6s\vert_3 - 5d^9_{3/2}6p_{3/2}\vert_2$?
0	637.42	156882		$5d^9_{3/2}6p_{1/2}\vert_{2''} - 5d^9_{5/2}7s\vert_2$
1	645.68	154876		$5d^9_{5/2}6s\vert_2 - 5d^9_{3/2}6p_{3/2}\vert_2$
1	657.16	152170		$5d^9_{5/2}6s\vert_2 - 5d^9_{5/2}6p_{3/2}\vert_1$
3	659.92	151534	V	$5d^9_{5/2}6s\vert_2 - 5d^9_{3/2}6p_{3/2}\vert_2$
3	672.41	148719	VI	$5d^9_{5/2}6p_{3/2}\vert_4 - 5d^9_{5/2}7s\vert_3$
4	677.32	147641	VI	$5d^9_{3/2}6p_{3/2}\vert_3 - 5d^9_{3/2}7s\vert_2$
1	682.39	146544		$5d^9_{5/2}6p_{3/2}\vert_{2'} - 5d^9_{5/2}7s\vert_2$
1	683.15	146381		$5d^9_{3/2}6p_{3/2}\vert_1 - 5d^9_{3/2}7s\vert_1$
1	686.60	145645		$5d^9_{5/2}6p_{3/2}\vert_{2'} - 5d^9_{5/2}7s\vert_2$
0	692.95	144311		$5d^9_{5/2}6p_{3/2}\vert_2 - 5d^9_{3/2}7s\vert_2$
1	697.12	143447		$5d^9_{5/2}6p_{3/2}\vert_{1'} - 5d^9_{5/2}7s\vert_2$
1	697.23	143425		$5d^9_{3/2}6p_{3/2}\vert_3 - 5d^9_{3/2}7s\vert_2$
2	701.60	142531		$5d^9_{5/2}6p_{3/2}\vert_3 - 5d^9_{5/2}7s\vert_3$
10b	743.13	134566	VI	$5d^9_{3/2}6s\vert_2 - 5d^9_{5/2}6p_{3/2}\vert_3$
7	748.53	133595	VI	$5d^9_{3/2}6s\vert_1 - 5d^9_{3/2}6p_{3/2}\vert_2$
4	760.78	131444	VI	$5d^9_{5/2}6s\vert_3 - 5d^9_{5/2}6p_{3/2}\vert_{2'}$
3	764.03	130885	VI	$5d^9_{3/2}6s\vert_1 - 5d^9_{3/2}6p_{3/2}\vert_1$
6	767.340	130320.3	VI	$5d^9_{5/2}6s\vert_2 - 5d^9_{5/2}6p_{3/2}\vert_3$
5	767.468	130298.5	VI	$5d^9_{5/2}6s\vert_2 - 5d^9_{3/2}6p_{3/2}\vert_{1'}$
4	768.44	130134	VI	$5d^9_{3/2}6s\vert_2 - 5d^9_{3/2}6p_{3/2}\vert_2$
8	778.99	128371	VI	$5d^9_{5/2}6s\vert_2 - 5d^9_{5/2}6p_{3/2}\vert_4$
2d	784.80	127421		$5d^9_{3/2}6s\vert_2 - 5d^9_{3/2}6p_{3/2}\vert_1$
7	786.15	127202	VI	$5d^9_{5/2}6s\vert_2 - 5d^9_{3/2}6p_{3/2}\vert_{2'}$
7	788.69	126793	VI	$5d^9_{3/2}6s\vert_2 - 5d^9_{3/2}6p_{3/2}\vert_3$
3	807.47	123844	VI	$5d^9_{3/2}6s\vert_1 - ?\ 5d^9_{3/2}6p_{3/2}\vert_0$
6	830.42	120421	VI	$5d^9_{5/2}6s\vert_2 - 5d^9_{3/2}6p_{1/2}\vert_{1''}$
5	855.68	116866	V	$5d^9_{5/2}6s\vert_2 - 5d^9_{5/2}6p_{1/2}\vert_{2''}$
3b	947.35	105558	V	$5d^9_{3/2}6s\vert_2 - 5d^9_{5/2}6p_{3/2}\vert_3$; $5d^9_{3/2}6s\vert_2 - 5d^9_{3/2}6p_{3/2}\vert_{1'}$
2b	976.00	102459		$5d^9_{3/2}6s\vert_2 - 5d^9_{3/2}6p_{3/2}\vert_{2''}$
1	1008.66	99141.4		$5d^9_{3/2}6s\vert_1 - 5d^9_{3/2}6p_{1/2}\vert_{1''}$
10b	1023.860	97669.60	VI	$5d^9_{5/2}6s\vert_3 - 5d^9_{5/2}6p_{1/2}\vert_3$
4	1045.066	95687.7	VI	
4	1045.117	95683.1	VI	$5d^9_{3/2}6s\vert_2 - 5d^9_{3/2}6p_{1/2}\vert_{1''}$
4	1045.168	95678.4	VI	
4	1045.231	95672.6	VI	
8_{14}	1045.183	95585.6	VI	$5d^9_{3/2}6s\vert_1 - 5d^9_{3/2}6p_{1/2}\vert_{2''}$
10_{13}	1050.130	95226.3	VI	$5d^9_{5/2}6s\vert_3 - 5d^9_{5/2}6p_{1/2}\vert_2$
10_{20}	1070.34	93428.2	VI	$5d^9_{5/2}6s\vert_2 - 5d^9_{5/2}6p_{1/2}\vert_3$
7?	1085.47	92126.0	IIIa / VI	$5d^9_{3/2}6s\vert_2 - 5d^9_{3/2}6p_{1/2}\vert_{2''}$
4?	1099.09	90984.3	VI	$5d^9_{5/2}6s\vert_2 - 5d^9_{5/2}6p_{1/2}\vert_2$

a Found in the bismuth arc. b Broad. d Diffuse. ? (after designation) Wave number discrepancy casts doubt upon designation.

line chosen as $5d^96s\vert_1 - 5d^96p\vert_0$ seemed by far the most probable choice on purely experimental grounds (intensity and z_A) though unfortunately $5d^96p\vert_0 - 5d^97s\vert_1$, which might have been hoped for, is not in Arvidsson's list. A difficulty with this choice in Bi VI is treated in the next paragraph. Extrapolation back to Au II by third differences predicted $5d^96s\vert_1 - 5d^96p\vert_0$ at about ν53943 instead of MMC's ν54848. Trial with the nearest line, 37 cm⁻¹ away, led to the discovery of the $5d^96p\vert_0$ level shown in Table II. Even objectively considering the Au II spectrum alone, this level appears more convincing than the one repudiated.

TABLE VII.

Calculated:				
$F(d^9s) \leftarrow F(d^9p)$	$13/2 \leftarrow 11/2$	$11/2 \leftarrow 9/2, 11/2$	$9/2 \leftarrow 7/2, 9/2, 11/2$	$\begin{cases} 7/2 \leftarrow 7/2, 9/2 \\ 5/2 \leftarrow 7/2 \end{cases}$
$\nu - \nu_0$	0	$6\frac{1}{2}A_s - 3\frac{1}{4}A_p$	$12A_s - 34/9A_p$	$18A_s - 33/7A_p$
Intensity (energy)	(7)	(6)	(5)	(7)
$\Delta\nu$	$6.50A_s - 3.25A_p$	$5.50A_s - 0.53A_p$	$6.00A_s - 0.96A_p$	
Observed:				
Intensity (blackening)	(4)	(4)	(4)	(4)
$\Delta\nu$	5.8 cm^{-1}	4.7 cm^{-1}	4.6 cm^{-1}	
$\therefore A_s$	+0.75 cm^{-1}	+0.83 cm^{-1}	+0.72 cm^{-1}	

Goble's graph[4] (Fig. 4) of the parameters separately calculated with the aid of data from this paper shows that, although the dependence of each upon Z appears quite smooth, three of them, *viz.* γ, δ and ϵ, decrease in magnitude between Pb V and Bi VI. Though perhaps not out of the question, such a decrease is surprising. The equations used in evaluating γ and ϵ from the experimental data involved these quantities only in the sums $\delta+\gamma$ and $\delta+\epsilon$ respectively, so an increase in the magnitude of the negative quantity δ would automatically have increased the magnitudes of γ and ϵ simultaneously. The desirability of this triple change leads one to suspect that either the Bi VI $5d^96s\,|_1 - 5d^96p\,|_0$ line has somewhat ($\sim 10^3$ cm^{-1}) higher frequency than the $\nu 123844$ selected by us, or the approximation achieved in Goble's theory is insufficient to render this detail intelligible (e.g., perhaps $a_1(d^9p) \neq a_1(d^9s)$, masking the behavior of δ). The fairly strong evidence of the Bi VI data, together with the previously mentioned constancy of the differences, favors the latter alternative.

On the strength of all the above discussion, we feel justified in calling all the $5d^96p\,|_0$ levels in the sequence pretty well established except perhaps the one in Bi VI.

Hyperfine structure in Bi VI. Several of Arvidsson's Bi VI lines show noticeable breadth, as indicated by the letter *b* or by a numerical subscript giving the approximate breadth in cm^{-1}, accompanying the intensity. Only one of them, $5d^9{}_{3/2}6s\,|_2 - 5d^9{}_{3/2}6p_{1/2}\,|_{1''}$, is partly resolved, but from that one we may obtain an indication of the magnitude of the hyperfine structure splitting factor $a(6s_{1/2})$. Values in cm^{-1} of certain splitting factors in the bismuth spectra are as follows:[8,9]

	Bi I	II	III	IV	V	VI
$a(6p_{1/2})$	0.375	0.464	0.66			(1.1 ± 0.4)
$a(6s_{1/2})$		1.60	1.80	2.34	2.6	*3.1±0.2*

Assuming the $a(6p_{1/2})$ value in parentheses (which was obtained by extrapolation) and the negligibility of $a(5d^9{}_{3/2})$, we shall now derive the $a(6s)$ value shown in italics.[10] We are justified in assuming *jj* coupling, so the levels' splitting factors have the following values:

$$A(5d^9{}_{3/2}6p_{1/2}\,|_1)(\equiv A_p) = -\tfrac{1}{4}a(6p_{1/2}),$$
$$A(5d^9{}_{3/2}6s\,|_2)(\equiv A_s) = +\tfrac{1}{4}a(6s).$$

Instead of showing five components on account of the predominance of A_s, it is not surprising that the line appeared to Arvidsson in only four, for, on account of the negative value of A_p, the two closest (and faintest) groups come within $3\frac{1}{2}A_s - 10|A_p|$ of each other. Calculating the intensities of the nine individual components by the Kronig-Russell-Sommerfeld-Hönl-Dirac formulas, and assuming that Arvidsson measured the centers of gravity of the energy distributions, we have the groupings given in Table VII, measuring from the strongest (lowest frequency) component. From the data given there, we obtain:

$$a(6s_1) = 4A_s = 3.1\text{cm}^{-1} \pm \sim 6 \text{ percent.}$$

[8] R. A. Fisher and S. Goudsmit, Phys. Rev. **37**, 1057 (1931).

[9] A. B. McLay and M. F. Crawford, Phys. Rev. **44**, 986 (1933).

[10] But our results are almost independent of these assumptions. For instance, had we neglected the splitting of the d^9p term entirely ($A_p=0$, below) the mean result for $a(6s_{1/2})$ would have been 3.35 cm^{-1}. The $J=1$ levels of the interesting groups $5d^9{}_{3/2}6s^26p_{1/2}\,|_{1,2}$ and $5d^9{}_{5/2}6s^26p_{3/2}\,|_{1,2,3,4}$ in Bi IV, as identified by McLay and Crawford[9] (misled by Mack, cf. Table IV A, footnote §), show hyperfine splitting of $+1.5\pm0.4$ and -1.5 ± 0.5 cm^{-1}, respectively, which appears to lead to a negative value of $a(6p_{1/2})$. These levels, however, have a distribution strikingly (but not surprisingly) similar to that of the same groups minus the $6s^2$ shell, in Tl IV, and Goble[4] shows that just these Tl IV levels are badly intermingled. So the only conclusion we can draw about the a's from the splitting of these Bi IV levels is that $-a(6p_{1/2}) - 3a(6p_{3/2}) + 5a(5d^9{}_{3/2}) + 7a(5d^9{}_{5/2}) = 0 \pm 3.6$ cm^{-1}. The Bi VI level with which we are concerned is much more nearly pure $5d^9{}_{3/2}6p_{1/2}$.

On the Cross Section of Heavy Nuclei for Slow Neutrons

J. H. VAN VLECK, *Harvard University*

(Received June 10, 1935)

The cross section for slow neutrons is computed with the statistical model of the nucleus and neutron-proton interaction of the Majorana form. The constants in the potential are taken from Feenberg's calculations on the binding energies of light nuclei. It is rather surprising that the scattering problem is reducible to one particle form despite the fact that the Majorana operators permute the coordinates of neutrons and protons. The formulas for the cross section are applicable even when there is neutron-neutron interaction, as suggested by L. Young, provided a simple change is made in the constants. It is shown that the anomalously large cross sections in Cd and Hg cannot be interpreted on the basis of an additional node of the neutron's wave function within the nucleus for Hg as compared with Cd.

FERMI and collaborators,[1] also Dunning and Pegram,[2] have found that the cross sections of certain nuclei (notably B, Cd, W, Hg) for slow neutrons are larger than the geometrical cross section.[3] Fermi,[1] Bethe[4] and others[5] have shown that such abnormally large values are not really a mystery but can be naturally interpreted by our usual quantum mechanics. Namely, the quantum mechanical cross section for slow particles depends markedly on the phase at the edge of the nucleus, or in other words on the fractional number of de Broglie waves of centro-symmetric type ($l=0$) contained in the nucleus. The determining factor is thus the value of the expression

$$I=2\int_0^R[2M(W-V)]^{\frac{1}{2}}dr/h, \qquad (1)$$

where $V(r)$ is the potential function inside the nucleus and R is the latter's radius. Since we are considering very slow neutrons, we may equate their energy W to zero in (1). When I is a half-integer, the cross section is readily shown[4, 5] to be unusually large, of the order of the square of the de Broglie wavelength of the incident neutron outside the nucleus. This situation is presumably the cause of many of the abnormally large cross sections and is, so to speak, the opposite extreme from that in the Ramsauer effect in electron scattering, wherein I is a whole integer and the cross section hence abnormally small. The purpose of the present note is to evaluate (1) and so discover, if possible, what particular half-integers should be correlated with the observed maxima. We do not explicitly compute the cross section but this can be determined by the standard quantum mechanics of the scattering by a "potential hole" if the latter's radius and the value of the phase integral (1) are known.

The deflections of neutrons, either elastic or inelastic, presumably owe their existence mainly to neutron-proton forces, including the forces exerted by the protons bound in the alpha-particles contained in the nucleus. Consequently we shall omit neutron-neutron forces until near the end of the article. The form of the potential function $J(r_{np})$ for the interaction of neutrons with protons will be taken from the work of Feenberg.[6] Do not confuse $J(r_{np})$, which represents the coupling of one neutron and one proton, with $V(r)$, which is the potential for a neutron due to the totality of protons in the nucleus.

Wigner Theory. We shall first make the calculation under the assumption that J does not involve permutation operators and so is a potential of the ordinary or so-called Wigner type. Of course it will immediately be objected that the Wigner theory[7] is unsatisfactory since it is

[1] E. Amaldi, O. D'Agostino, E. Fermi, B. Pontecorvo, F. Rasetti and E. Segré, Proc. Roy. Soc. **A149**, 522 (1935).

[2] J. R. Dunning and G. B. Pegram, Phys. Rev. **47**, 640A (1935).

[3] The cross section may be either elastic or inelastic, as in either case the dominant question is whether or not the phase integral (1) has a value which permits the neutron to penetrate the nucleus appreciably. We throughout use the term scattering in a generalized sense to include absorption of neutrons in the nucleus as well as true scattering. The abnormally large cross section usually appears to be associated mostly with absorption (cf. Dunning, Pegram, Fink and Mitchell, Phys. Rev. **47**, 796, 970 (1935)).

[4] H. Bethe, Phys. Rev. **47**, 747 (1935).

[5] Perrin and Elsasser, Comptes rendus **200**, 450 (1935); Beck and Horsley, Phys. Rev. **47**, 510 (1935).

[6] E. Feenberg, Phys. Rev. **47**, 850 (1935).

[7] E. Wigner, Phys. Rev. **43**, 252 (1933).

known to give the wrong dependence of nuclear binding energy on atomic number. However, the calculation with the Wigner[7] form of potential is very easy and serves as an illuminating and more or less necessary introduction to the computation with the preferable Majorana theory.[8] With the former, we have simply to regard the scattered neutrons as subject to the "time-exposure charge cloud" of the totality of protons in the nucleus. We may suppose that these protons are on the time average uniformly distributed in a sphere of radius R, so that the charge cloud is centro-symmetric and of uniform density $\rho=3Z/4\pi R^3$, where Z is the number of protons in the nucleus. The relation connecting V and J is clearly

$$V=\iiint J\rho dv. \tag{2}$$

Now according to Feenberg's calculations,[6] or any others[7] devised to explain the high stability of alpha-particles as compared with deuterons, the neutron-proton forces are of short range ($\sim 1.4\times 10^{-13}$ cm) compared to the radius ($\sim 7\times 10^{-13}$ cm) of a heavy nucleus. Hence we can neglect the "edge effect," i.e., we can assume that the potential suddenly vanishes at the boundary of the nucleus. Then $V(r)$ vanishes for $r>R$, while for $r<R$ it is constant and has the value

$$V=3ZC/4\pi R^3, \tag{3}$$

$$\text{with } C=\iiint J(r_{np})dv=4\pi\int_0^\infty J(r_{np})r_{np}^2dr_{np}. \tag{4}$$

Because of the short range, it has been permissible to integrate to infinity in (4) rather than over the nucleus. If the nuclear volume is proportional to the atomic number, then one has $R^3=ZR_0^3$, where R_0 is independent of Z, and (1) becomes

$$I=Z^{\frac{1}{3}}[-6CM/\pi h^2R_0]^{\frac{1}{3}}. \tag{5}$$

If we use an exponential interaction function $J(r)=Ae^{-\alpha r^2}$, the expression (4) equals $A(\pi/\alpha)^{\frac{1}{2}}$. Feenberg's best values of A, α for the Wigner model are, respectively,

$$A=-165mc^2, \quad 1/\alpha^{\frac{1}{2}}=1.34\times 10^{-13}\text{ cm} \tag{6}$$

while Gamow's value of the radius of the lead nucleus gives $R_0=7.8\times 10^{-13}/(82)^{\frac{1}{3}}$ cm. With the constants thus evaluated, the expression (1) has the value 3.11 for Cd.

Impossibility of Attributing Successive Maxima to Additional Nodes. In view of the inaccurate status of nuclear models, especially those of Wigner type, the fact that 3.11 is closer to an integer than a half-integer, i.e., the cross section closer to a minimum than to the desired maximum need not cause concern. However, the point that we do want to make is that it does not appear possible to explain the maxima in W and Hg as due to an additional node of the wave function in the nucleus, i.e., increase of (1) by an integer, as compared with Cd. If the constants C and R_0 are adjusted so that (5) equals 3.5 in Cd, the values for W and Hg are, respectively, 4.05 and 4.15, considerably short of the next resonance value 4.5. If 2.5 rather than 3.5 is assigned to Cd the situation is even worse as the value for Hg becomes 2.97, almost exactly the wrong extreme. The corresponding value for boron is 1.18 but is less significant, since our theory is intended primarily for heavy atoms. To locate successive maxima at Cd and Hg, the value of I in Cd would have to be at least 5.5 and this is an impossibly high value since nothing like this much leeway is allowable in the choice of the parameters C, R_0, which fortunately enter in (5) only to the power one-half. Of course it is to be said that so far we have used the Wigner rather than Majorana theory but inclusion of the Majorana permutation operators makes interaction possible only where the wave functions overlap and so will reduce the magnitude of the effective potential $V(r)$. In fact, we will later see that with a Majorana potential with the same values (6) of the constants as we have used in the Wigner form, the value of I for Cd becomes 2.21 rather than 3.11. Thus with the Majorana version it is, if anything, still clearer, that the situation is quite unlike that in the Ramsauer effect in electron impact, where the periodic Ramsauer minima have been identified[9] with increasing numbers of nodes of the electron's wave function inside the atom as Z increases.

If the "additional node" hypothesis will not work, how, then, are the frequent anomalously large cross sections to be explained? A very sug-

[8] E. Majorana, Zeits. f. Physik **82**, 137 (1933).

[9] Cf. Mott and Massey, *The Theory of Atomic Collisions* (Oxford University Press, 1933), p. 142.

gestive tentative answer to this question will be given in a future paper of Bethe and Smith. They propose that sometimes the p, d, $\cdots$ partial cross sections ($l=1$, 2, $\cdots$ etc.) are effective as well as the s in causing anomalous scattering or absorption. To be sure, the centrifugal force usually keeps all but s neutrons out of the nucleus since we are dealing with slow exterior velocities. However, near resonance the behavior is somewhat exceptional, especially since we do not have rigorously a one particle system, and so p, d, $\cdots$ wave functions may acquire some s characteristics inasmuch as l is not a good quantum number. Hence many of the subsidiary maxima may be associated with other than the s cross sections which we study.[9a]

Majorana Theory. We now give the details of the calculation with the Majorana theory, which can be used without any undue difficulty provided that one applies the Thomas-Dirac statistical theory to the protons embedded in the nucleus (but not, of course, to the scattered neutron). This approximation is essentially the analog of the use of the uniform charge cloud in the Wigner form. In the Majorana theory the potential coupling the scattered neutron with the protons in the nucleus is

$$\sum_i J(r_{np^i})T(n;p^i) \quad (r_{np^i}=|\mathbf{x}_n-\mathbf{x}_{p^i}|), \quad (7)$$

where $\mathbf{x}_n$, $\mathbf{x}_{p^i}$ are, respectively, the position vectors of the neutron and a typical proton i and where $T(n;p^i)$ is a permutation operator which interchanges $\mathbf{x}_n$ and $\mathbf{x}_{p^i}$ in the arguments of the complete wave function. The wave equation is reduced, if possible, to that of one particle, the scattered neutron, by integrating over the coordinates of the protons. In this fashion one obtains the equation

$$(-h^2/8\pi^2M)\nabla^2\psi(\mathbf{x}_n)+W\psi(\mathbf{x}_n)=Q, \quad (8)$$

where

$$Q=\sum_i \int\int\int \varphi_i^*(\mathbf{x}_p)J(r_{np^i})\varphi_i(\mathbf{x}_n)\psi(\mathbf{x}_p)d\mathbf{x}_p \quad (9)$$

and where ψ denotes the wave function of the neutron, and φ_i that of the proton i. We have assumed that the complete wave function is expressible as the product $\psi(\mathbf{x}_n)\Pi\varphi_i(\mathbf{x}_{p^i})$ of the wave function of the scattered neutron and those of the individual protons in the nucleus. (To satisfy the Pauli principle, the usual antisymmetric linear combination of the protonic wave functions must be taken, but our calculation still holds with this modification.) Because of this factorization it has been possible to make the integration in (9) three rather than $3Z$ dimensional, since with any given neutron-proton potential term, the integration over $3(Z-1)$ protonic coordinates is trivial. Note especially that the integrand of (9) contains the product $\varphi_i(\mathbf{x}_n)\psi(\mathbf{x}_p)$ rather than $\varphi_i(\mathbf{x}_p)\psi(\mathbf{x}_n)$ as in the usual Wigner theory, because of the permutation operator T involved in (7).

We now use the approximate relation

$$\sum_i \varphi_i^*(x_p)\varphi_i(x_n) = (2/h^3)\int\int\int \exp\left[2\pi i\mathbf{p}\cdot(\mathbf{x}_n-\mathbf{x}_p)/h\right]d\mathbf{p}. \quad (10)$$

The left side of this equation is called the Dirac density function, which we will denote by ρ_{np} and the right side is an approximate expression which he derives[10] for it by means of the Thomas-Fermi statistical theory. The integration in (10) is over a sphere of radius P given by

$$2(4\pi P^3/3)(4\pi R^3/3)=Zh^3 \quad (11)$$

and it is supposed that the terminal point of $\frac{1}{2}(\mathbf{x}_n+\mathbf{x}_p)$ is inside the nucleus; otherwise the the density function vanishes. Since our forces are of short range compared with the nuclear diameter, it will be allowable to consider that (10) applies when the neutron is inside the nucleus and that the left side of (10) vanishes otherwise. The integration in (10) may be performed in the usual way[10] by introducing polar coordinates whose axis coincides in direction with r. Then (10) becomes

$$\rho_{np}=(-kr_{np}\cos kr_{np}+\sin kr_{np})/\pi^2r_{np}^3, \quad (12)$$

where

$$k=(9\pi Z/4R^3)^{\frac{1}{3}}. \quad (13)$$

One now assumes that the neutron's wave

[9a] Since the present paper was written, Dunning, Pegram, Fink and Mitchell find that the rare earths Sm and Tb (which lie between Cd and Hg) also have anomalously large cross sections, even greater than that of Cd (Phys. Rev. **47**, 970 (1935)). The occurrence of such frequent anomalies, also the complete absorption,[3] makes it appear somewhat doubtful whether the large cross sections are really all to be interpreted as resonance phenomena of the usual type, even when one considers the effect of states with $l>0$.

[10] See P. A. M. Dirac, Proc. Camb. Phil. Soc. **26**, 376 (1930).

function is of the usual spherical type,

$$\psi(\mathbf{x}_n)=\sin k_n r/r, \tag{14}$$

so that

$$\psi(\mathbf{x}_p)=(e^{ik_n r_p}-e^{-ik_n r_p})/2ir_p, \tag{15}$$

where

$$r_p^2=r^2+r_{np}^2-2r_{np}r\cos\theta, \tag{16}$$

$$\cos\theta=\cos(\mathbf{r}_{np},\mathbf{r}).$$

When one substitutes (15) and (16) in (9), the integration over the angular part of the volume element $d\mathbf{x}_p=r_{np}^2\sin\theta dr_{np}d\theta d\varphi$ can be performed in polar coordinates. One thus finds that

$$Q=\psi(\mathbf{x}_n)\int_0^\infty 4\pi k_n^{-1}\rho_{np}J(r_{np})(\sin k_n r_{np})r_{np}dr_{np} \tag{17}$$

with ρ_{np} as in (12). Hence the wave equation (8) has the one particle form $Q=V\psi(\mathbf{x}_n)$ provided V equals the integral in (17). An equivalent statement is that (3) and (5) are still valid provided C has the value

$$C=12\pi^3k^{-3}k_n^{-1}\int_0^\infty\rho_{np}J(r_{np})\times(\sin k_n r_{np})r_{np}dr_{np}, \tag{18}$$

instead of (4).

It must be regarded as rather surprising that *the scattering of the neutron can thus be treated by a one particle equation* despite the fact that the Majorana theory permutes the coordinates of the scattered neutron with those of the proton in the nucleus. Furthermore, Mr. C. H. Fay will prove in a later paper that this result is also true of the other partial cross sections $l>0$; the "effective potential" there, too, proves to be given by (3) and (18). One's conjecture would have been that because of the permutation effects, Q in (8) would persistently involve $\psi(\mathbf{x}_n)$ through some sort of an integral operator (cf., for instance, Fock's equation) rather than finally turning out directly proportional to $\psi(\mathbf{x}_n)$. Thus far we have not explicitly specified the value of the neutron's wavelength $2\pi/k_n$ inside the nucleus. It is, of course, that given by the relation

$$-k_n^2=8\pi^2MV/h^2=6\pi ZCM/R^3h^2 \tag{19}$$

appropriate to the effective potential V. We must emphasize that it is only because there has turned out to be an effective potential constant over the nucleus that we have been justified in assuming that the neutron's wave function is of the form (14). This assumption has been necessary in our proof of (18). Hence problems with nonconstant potentials probably would not be reducible to a one particle affair.

By eliminating C between (18) and (19) an equation is obtained for the determination of k_n. This equation must be solved by trial and error before (18) and (5) can be used to calculate (1). Eq. (18) becomes identical with (4), as we should expect, when the range of the interaction force is small compared both to $2\pi/k_n$, the neutron's wavelength while traversing the nucleus and to $2\pi/k$, the shortest wavelength of the proton embedded in the nucleus.

With the exponential form $J(r)=Ae^{-\alpha r^2}$, Eq. (18) becomes[11]

$$C=(3\pi^2/k^3)A[E(w_+)-E(w_-)+2(\alpha/\pi k_n^2)^{\frac{1}{2}}(e^{-w_+^2}-e^{-w_-^2})], \tag{20}$$

where $w_\pm=(k_n\pm k)/2\alpha^{\frac{1}{2}}$, $E(w)=(2/\pi^{\frac{1}{2}})\int_0^w e^{-x^2}dx$.

A series expansion

$$C=A\left(\frac{\pi}{\alpha}\right)^{\frac{3}{2}}e^{-k_n^2/4\alpha}\left[1-\frac{1}{10}\frac{k^2}{\alpha}\left(\frac{3}{2}-\frac{k_n^2}{4\alpha}\right)+\frac{3k^4}{224\alpha^2}\left(1-\frac{k_n^2}{3\alpha}+\frac{k_n^4}{60\alpha^2}\right)+\cdots\right] \tag{21}$$

is convenient for small values of k^2/α. With Feenberg's[6] best choice of constants for the Majorana form, *viz.*

$$A=-174mc^2,\quad \alpha^{-1}=1.29\times10^{-13}\text{ cm}, \tag{22}$$

one finds that $k_n=1.06\cdot10^{13}$ and that $I=2.21$. It makes no appreciable difference whether (6) or (22) is used.

Inclusion of Neutron-Neutron Interaction. As shown by L. Young,[12] considerations of the relative stability of nuclei with different atomic and mass numbers indicate that there must be neutron-neutron forces (and by symmetry similar proton-proton forces) besides the usual neutron-proton and Coulombic proton-proton forces. The neutron-neutron coupling is presumably small compared to the neutron-proton, but still not negligible. We shall show in the following paragraphs that inclusion of neutron-neutron inter-

[11] In deriving (20), a useful relation is obtained by integrating formula 508 of Peirce's tables with respect to the parameter b.

[12] L. Young, Phys. Rev. **47**, 972 (1935).

action is approximately equivalent merely to altering the constant A in (20) or (21).

The most general potential which depends on the relative alignment of the spins $\mathbf{s}_i$, $\mathbf{s}_j$ (measured in multiples of $h/2\pi$) of two neutrons is expressible as a linear function

$$M(r_{nn})+N(r_{nn})\mathbf{s}_i\cdot\mathbf{s}_j \tag{23}$$

of their scalar product $\mathbf{s}_i\cdot\mathbf{s}_j$ inasmuch as the latter has only two characteristic values. Eq. (23) gives the "direct" or essentially Wigner type of coupling between two neutrons. With two neutrons, however, there is exchange degeneracy, a complication not found in neutron-proton interaction. The exchange effect converts a Wigner force into one of Majorana type, or *vice versa*. (Hence the present discussion is general enough to include both the Wigner and Majorana models.) If we use the Dirac vector model,[13, 14] which shows that the exchange is formally equivalent to insertion of a spin-spin coupling factor $-\frac{1}{2}(1+4\mathbf{s}_i\cdot\mathbf{s}_j)$, we see that the exchange potential associated with (23) is

$$\begin{aligned}-\tfrac{1}{2}T_{nn}[M+N\mathbf{s}_i\cdot\mathbf{s}_j](1+4\mathbf{s}_i\cdot\mathbf{s}_j)\\ =-\tfrac{1}{2}T_{nn}\{M(1+4\mathbf{s}_i\cdot\mathbf{s}_j)+N(\tfrac{3}{4}-\mathbf{s}_i\cdot\mathbf{s}_j)\},\end{aligned} \tag{24}$$

where T_{nn} is a Majorana permutation operator. The second form of (24) follows from the first in virtue of the matrix identity[15] $16(\mathbf{s}_i\cdot\mathbf{s}_j)^2+8\mathbf{s}_i\cdot\mathbf{s}_j-3=0$. If we consider the interaction of a neutron with two other neutrons i, i' in a closed shell (i.e., in equivalent orbits with anti-parallel spin), then the part of (23) or (24) proportional to $\mathbf{s}_i\cdot\mathbf{s}_j$ disappears since $(\mathbf{s}_i+\mathbf{s}_{i'})\cdot\mathbf{s}_j=0$. Thus on the average (23) equals M and (24) equals $-\frac{1}{2}T_{nn}(M+\frac{3}{4}N)$, provided we disregard forces between neutrons, neither of which are in a closed shell, or else are in the same orbit. It is known that if the direct potential persists on the average in heavy atoms, then an excessive binding energy is obtained. (This is essentially the difficulty that Wigner terms give an energy which varies too rapidly with Z.) Hence M is zero, or at least very small, and for our purposes we can consider the neutron-neutron forces to be entirely of the Majorana type, neglecting a small correction for neutrons not in closed shells to be considered later. The effective potential is thus the sum $V+V_{nn}$ of two expressions V, V_{nn}, where V is given by (3) and (18) and where V_{nn} is given by expressions similar to (3) and (18) except that Z is replaced by Z_n, the number of neutrons in the nucleus, and that J, k must be replaced, respectively, by $-\frac{3}{8}N$ and $k'=(9\pi Z_n/4R^3)^{\frac{1}{3}}$ (cf. Eq. (13)). In the neutron-neutron version of (18) or (20) the change due to the substitution of k' for k manifests itself mainly in the factor k^{-3} (rather than in ρ_{np}) if w is moderately large. Since the neutron-neutron forces are subsidiary it will be a sufficient approximation if we ignore the distinction between k and k' except in this factor. The resulting change in (18) or (20) is then just counterbalanced by the substitution of Z_n for Z in (3). Hence to a sufficient approximation V_{nn} differs from V merely in the substitution of $-\frac{3}{8}N$ for J. Thus one may allow for neutron-neutron coupling by taking the apparent neutron-proton interaction to be $J-\frac{3}{8}N$.

Feenberg uses a neutron-neutron interaction of exponential form and of the same range as the neutron-proton, so that $J(r)=Ae^{-\alpha r^2}$, $N(r)=Be^{-\alpha r^2}$. He finds[15a] that the following choice of constants gives the proper binding energies for light atoms:

$$\begin{aligned}A=-64\ mc^2,\quad \tfrac{3}{4}B=26\ mc^2,\\ 1/\alpha^{\frac{1}{2}}=2.4\times10^{-13}\text{ cm}.\end{aligned} \tag{25}$$

Using (3) and (20), except that A is replaced by $A-\frac{3}{8}B$ in accordance with the preceding paragraph, one finds that $k=1.05\times10^{13}$, $I=2.19$. These values do not differ appreciably from those obtained with the constants (22) appropriate to a model with no neutron-neutron coupling. The similarity of the results with (22) and (25) may perhaps be a coincidence, since the constants (25), notably the range $1/\alpha^{\frac{1}{2}}$, differ considerably from (22). Still it suggests that our estimate of (1) will probably not be altered greatly by neutron-neutron complications as long as the constants are adjusted to fit the binding energies of light atoms. This fact is comforting, as the ratio of neutron-neutron to neutron-proton forces is not known at present with any precision.

Comparison with Bethe's Semi-empirical Method. Bethe[4] has estimated the value of the integral (1) by a method somewhat different from ours. He subtracts the mean kinetic energy of the neutrons bound in the nucleus, computed by the Thomas statistical method from the observed binding energy per neutron. The balance is what we may term a semi-empirical potential to be used in (1). He thus obtains the value 2.7

[13] Our rather brief treatment here assumes some familiarity with the Dirac vector model (Proc. Roy. Soc. **A123**, 714, 1929), whose use is more fully explained by the writer in Phys. Rev. **45**, 405 (1934) or in reference 15.

[14] Another and more complete discussion of neutron-neutron interaction which does not employ the language of the Dirac vector model (given here largely as an interesting alternative) will be published by Feenberg.

[15] J. H. Van Vleck, *The Theory of Electric and Megnetic Susceptibilities*, pp. 341 and 318.

[15a] These calculations of Feenberg will be published later. Since the present paper was written, he has extended them, and finds that the neutron-neutron interaction is probably smaller and in (25). This development does not matter for our purposes since even inclusion of as much neutron-neutron interaction as in (25) does not change the value of (1) materially. It is clearly to be understood that the reason the results are not affected by inclusion of neutron-neutron interaction is that the latter alters the values of A and α in such a way as largely to compensate the effect of making $B\neq0$.

for (1) in Cd.[16] That his value 2.7 is smaller than our Wigner value 3.1 is immediately intelligible, as the Wigner model gives too large an attractive potential energy for heavy atoms. It is also clear why his estimate is larger than our Majorana value 2.2. Namely, Bethe's procedure tacitly assumes forces of the Wigner type and so is not accurately applicable to the Majorana model since, in the latter, forces are effective only where the wave functions overlap and so are less potent for scattered neutrons than for the average neutron bound in the nucleus, because of the longer wavelength of the latter. Hence the effective potential for scattering is of smaller absolute magnitude than that for binding.[17]

Concluding Remarks. It would be satisfying if (1) could be estimated sufficiently accurately so that one could decide whether the resonance in Cd corresponds to the value 2.5 or 1.5 of I or whether I is really not a half integer in Cd, so that the anomaly is to be blamed on effects involving $l>0$. Unfortunately we are unable to achieve this goal. Some corrections which might be applied to our calculations are the following: The error due to considering the range of the forces as negligible compared with the radius of the nucleus and to neglecting the gradual tailing off of the nucleus may be crudely estimated by assuming that the potential decreases linearly with r from $R-L$ to $R+L$ instead of terminating suddenly at $r=R$. If $L=2\times10^{-13}$ cm, the value of (1) is raised about 10 percent.[18] A small increase of about 2 percent may be expected for each neutron of uncompensated spin in the nucleus, as such neutrons exert forces of the ordinary rather than Majorana type. On the other hand, a reduction of 10 or 15 percent in our estimates of (1) is quite conceivable because there is empirical evidence that the neutron-proton forces in scattering are smaller than those effective between bound particles. This distinction may be due either to a dependence of force on velocity, as suggested by Feenberg,[19] or to a dependence of force on spin alignment, as proposed by Massey and Mohr,[20] Wigner (unpublished) and others. The scattered neutron's spin is parallel to only half the protonic spins in heavy nuclei, whereas the situation is different in calculations made on the binding energy of the deuton, where the proton's spin and the neutron's spin are parallel.

In closing, we may mention that the effective potential given by (3) and (18), which reduces the Majorana theory to a one electron problem, will doubtless be useful in connection with other nuclear phenomena besides scattering.

The writer is much indebted to Dr. E. Feenberg for valuable suggestions and the privilege of seeing his manuscripts in advance of publication. He also wishes to thank Professor H. Bethe for interesting discussion.

[16] In comparing with Bethe's work, one must note that his integral (8) differs from our (1) by an additive constant as well as a factor π (see footnote 26b of his paper). Bethe's value of I is raised from 2.7 to 2.9 when a correction is made for the effect of the Coulombic forces on binding energy.

[17] Bethe's method suggests that a possible semi-empirical modification of our procedure is to adjust the constant A so as to obtain the right binding energy for heavy nuclei when the latter is computed by the statistical method with Gamow's empirical radius (i.e., is deduced from a calculation similar to that in Majorana's paper[8] except that the range of the forces is not assumed large compared to the wavelength). The value of I is then raised from 2.2 to 2.8 if α is given by either (22) or (25) (with neutron-neutron forces included in the latter case). One might suspect that this modified procedure had elements of truth, as the apparent A deduced from an incorrect statistical calculation of binding energies might be better for our purposes than the true A. Thus the difference between 2.2 and 2.8 may be an estimate of the error inherent in our statistical method. However, it is possible that this is an excessively pessimistic view and that with (22) or (25) the actual value of I is closer to 2.2 than 2.8, since more reliance can probably be placed in our use of the statistical method for scattering than in the calculation of binding energies, especially when the latter is performed in the worst possible way with the nuclear radius as given rather as a variable parameter. That such a calculation of binding energies is certainly bad is shown by the fact that if A is given by either (22) or (25), the absolute magnitude of the potential energy turns out to be less than that of the kinetic energy, so that nuclei cannot exist, and the proper stability is achieved only if A is multiplied by a factor $(2.8/2.2)^2$. An accurate calculation with (22) or (25) probably yields about the right binding energy for heavy as well as light atoms.

[18] The value of L can be less than $1/\alpha^{\frac{1}{2}}$, since in the Majorana theory the forces are effective only where the wave functions overlap.

[19] E. Feenberg, Phys. Rev. **47**, 857 (1935).

[20] Cf. Massey and Mohr, Proc. Roy. Soc. **A148**, 213 (1935). In the original Heisenberg theory (Zeits. f. Physik **77**, 1 (1932)), the neutron-proton forces are of opposite sign for parallel as compared with anti-parallel spins. In the Majorana form there is no dependence on spin alignment. The dependence on this alignment cannot be as drastic as in the Heisenberg theory since the latter is unable to explain the singular stability of the alpha particle and is therefore incorrect. There might, however, be a moderate dependence, so that the forces are a linear combination of the Heisenberg and Majorana types, with the latter weighted more heavily. Our calculations apply to such a modified theory if the constant A is suitably changed.

Effective Collision Cross Sections of the Alkali Atoms in Various Gases

SEYMOUR ROSIN AND I. I. RABI, *Columbia University*

(Received June 12, 1935)

The mean free paths and effective collision cross sections of neutral atoms of Li, Na, K, Rb and Cs were measured in H_2, D_2, He, Ne and A by the method of molecular beams. The beams were sufficiently narrow and the scattering gas was confined to a region sufficiently small that a resolution of one minute of arc was attained. The results show a larger collision cross section in D_2 than in H_2 for all the alkalis with the exception of Li. This effect is interpreted as a consequence of the smaller spacing of the D_2 rotational levels. The results in general are in qualitative agreement with the quantum theory of collisions.

INTRODUCTION

IN the experiments to be described, a beam of atoms was allowed to traverse a limited region containing a gas at various pressures, and the reduction of the intensity of the beam was measured. This reduction is the fraction of the atomic beam scattered out beyond a certain limiting angle, equal here to about one minute of arc. From measurements of this kind an effective mean free path and collision cross section may be calculated, as is shown below. Although the most satisfactory form of this type of experiment would be to scatter a beam of atoms homogeneous in velocity from another such beam, this is out of the question in the present state of technical development. However, experiments which measure the total scattering down to very small angles can yield important information concerning the nature of molecular collisions, since it is in this region that the predictions of various theories are most likely to differ. Such experiments have already been carried out by Mais,[1] who scattered potassium from hydrogen, helium, neon, argon, nitrogen and carbon dioxide. In the experiments described below, the method has been improved by confining the scattering gas to a small region. This has the effect of making the limiting angle smaller and more definite, and enables the utilization of higher pressures, which may be more accurately measured. Beams of lithium, sodium, potassium, rubidium and caesium were each scattered from hydrogen, deuterium, helium, neon and argon.

APPARATUS

The design of the oven (1) (Fig. 1) and the treatment of the alkali before introduction have been described by Rabi and Cohen.[2] The collimating slit which, like the oven slit, is 0.01 mm wide is situated in a holder (2) which may be removed to clean and set the slit jaws, and which is capable of slight adjustment for purposes of alignment in the large partition (3) separating the detecting chamber from the oven chamber. The defining slit holder and the slit jaws are shown in Fig. 2. The first of the stops limiting the height of the beam to 0.25 mm is placed on the oven side of the collimating slit holder. The slit jaws are fitted snugly against the back of the scattering chamber (4) so that the collimating slit itself offers high resistance to gas flow from the scattering chamber into the oven chamber, where scattering is highly undesirable. Since scattering in the collimating slit is also to be avoided, the canal is made only 0.05 mm long.

The scattering chamber is a demountable unit, fastened to the detecting side of the large partition. The back of it is a very thin sheet of

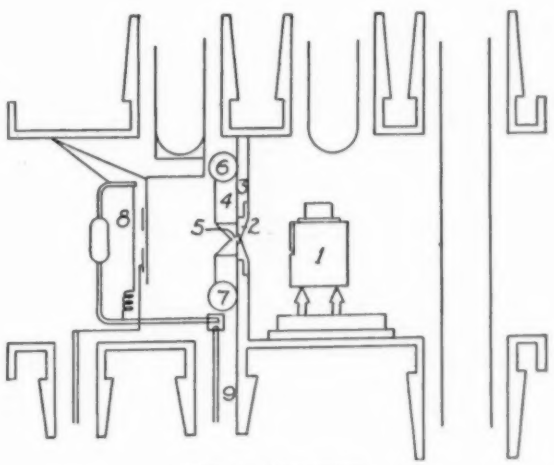

FIG. 1. Apparatus.

[1] Mais, Phys. Rev. **45**, 773 (1934).

[2] Rabi and Cohen, Phys. Rev. **46**, 707 (1934).

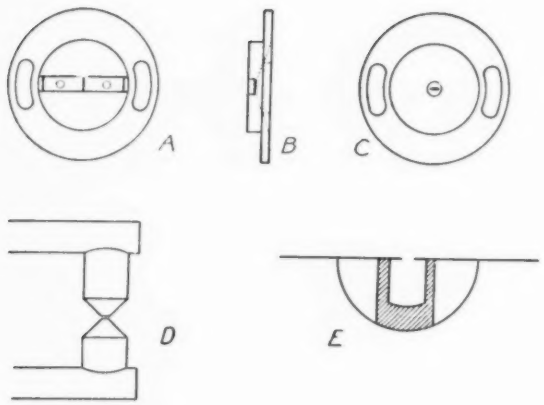

FIG. 2. *A*, Collimating slit jaws and holder, viewed from scattering chamber; *B*, holder, viewed edgewise; *C*, holder, viewed from oven chamber; *D*, scattering chamber, viewed from detecting chamber; *E*, scattering region, horizontal view. Channel is shaded.

metal pierced only by a hole 0.5 mm in diameter to let through the newly defined beam. The form of the chamber is evident from Figs. 1 and 2, consisting of two brass semicylinders soldered to the thin backing sheet and narrowed down at the region of scattering (5). The scattering chamber is connected to the exterior of the apparatus by means of two tubes, one of which, (6) serves to introduce the scattering gas, and the other (7) to lead to a calibrated McLeod gauge, which, since no net flow exists, measures the pressure at the scattering region. A trap serves to prevent mercury atoms from the McLeod from reaching the scattering chamber. The scattering gas is stored in a five liter bulb and admitted to the tube (6) through a constant leak formed by plugging the bore of a stopcock with plaster of Paris. Condensable impurities are frozen out by a Dewar placed between the leak and the scattering chamber and a one-liter bulb is inserted into the path of the gas for stability. During the course of an experiment, a dynamical equilibrium is maintained between the pressure in the five-liter bulb and that in the scattering chamber, and the pressure in the latter may be controlled to any desired value by varying the pressure in the former. The pressure measurements are reproducible to within about two percent over long periods of time. The beam enters the detecting chamber through a channel designed to offer high resistance to gas flow. A horizontal view of the scattering region (5), including the channel is shown in Fig. 2. The open space is 2 mm long, and the length of the channel is one mm and its height 0.25 mm, serving as a beam stop.

The beam is detected by means of a Langmuir-Taylor surface ionization detector[3] and an FP 54 vacuum tube electrometer[4] of sensitivity 10^{-14} amp./mm. The detector in the form of a 0.02 mm tungsten filament (8) (oxide coated when Na and Li are employed), subtends an angle of 1.7 minutes of arc at the scattering chamber. The filament may be rotated about the axis (9) of a ground joint; its position is indicated by a stage micrometer, mounted on the end of an arm 20 cm long attached to the ground joint. The stage, which is calibrated in 0.01 mm markings, is viewed through a fixed microscope. The detecting chamber is exhausted by means of an oil diffusion pump[5] of speed 40 liters/sec., in series with which is a smaller diffusion pump, and a mechanical pump. A 5-liter bulb is placed between the detecting chamber and the pumps for pumping stability.

We now consider the question of where an atom of the beam may undergo a collision. The possible regions are as follows:

(1) In the oven chamber, before the beam is defined. When the oven is hot, residual pressures ranging up to 10^{-5} mm, depending on the temperature of the oven, are measured. The effect is to broaden the beam slightly, and to reduce the intensity of the unscattered beam in the scattering chamber. Since this pressure comes to equilibrium before measurements are taken, the results are unaffected by it. It is also possible that when gas is present in the scattering chamber, enough may leak through the collimating slits to affect the beam in the oven chamber (the inverse beam of Knauer[6]). It was found in test experiments, however, that the pressure in the oven chamber is but 0.02 percent of that in the scattering chamber, and so may be neglected.

(2) In the scattering region proper.

(3) In the channel between the scattering chamber and the detecting chamber. A pressure gradient[7] exists in this region. The average

[3] Taylor, Zeits f. Physik **57**, 242 (1929).
[4] Dubridge and Brown, Rev. Sci. Inst. **4**, 532 (1933).
[5] Zabel, Rev. Sci. Inst. **6**, 54 (1935).
[6] Knauer, Zeits f. Physik **80**, 80 (1933).
[7] Clausing, Physica **9**, 1929.

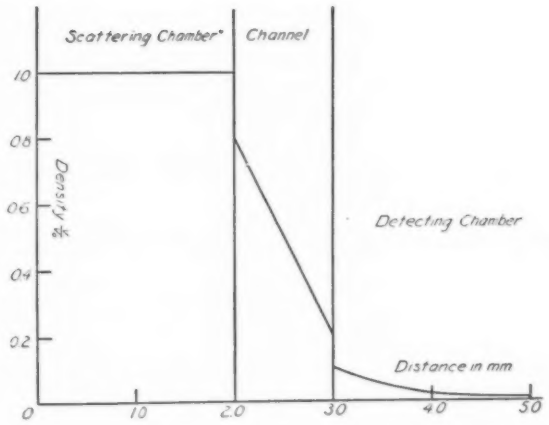

FIG. 3. Relative distribution of density in scattering chamber, channel and cloud.

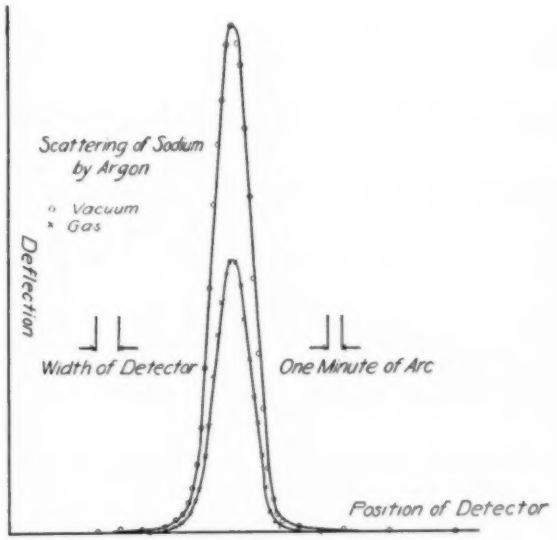

FIG. 4.

pressure is half that in the scattering chamber proper, varying linearly from 0.8 of the scattering chamber pressure to 0.2 of that quantity.

(4) In the detecting chamber where scattering may be ascribed to three sources. A cloud exists close to the scattering chamber, formed by escaping gas molecules. The density of gas escaping from a rectangular opening $2a \times 2b$ is given by

$$\rho = (8/\pi^2) N_0 (a/d) \tan^{-1} (b/d), \qquad (1)$$

where d represents the distance from the radiating rectangle, and N_0 the density on the other side of the opening. The formula is valid for d large compared to a. At the rectangle itself $\rho = N_0/2$, so that the desired function may be plotted. Secondly, residual gas from the walls may serve to reduce the beam. However, if the scattering chamber is evacuated, the McLeod reads flat, which indicates a pressure of 10^{-6} or lower; therefore no appreciable effect arises from this source. Finally, a pressure exists in the detecting chamber due to molecules escaping from the scattering chamber. In test experiments various gas pressures were established in the scattering chamber and the resulting pressure maintained by the pumps in the detecting chamber was always found to be 0.5 percent of that in the scattering chamber.

The density distribution in the scattering region, the channel and the cloud is shown in Fig. 3.

To make our measurements, the scattering chamber was evacuated and the so-called "vacuum beam" investigated by sweeping the detecting filament through the beam and noting the galvanometer deflections at the various settings. This operation was repeated after a suitable amount of some gas was introduced into the scattering chamber. Fig. 4 is a typical result, after proper corrections. The corrections consisted of subtracting the residual positive ion current from the filament, measured by cutting off the beam with a shutter, and also the background due to alkali atoms reflected from the walls of the chamber. Both of these were quite small.

CALCULATIONS AND RESULTS

A large number of curves were secured, involving the different alkalis scattered by each of the gases employed. Upon examination, it is found that the ratio of any ordinate on the gas curve to the corresponding ordinate on the vacuum curve is constant. Thus the gas curve has a form quite similar to that of the vacuum curve, and indeed is indistinguishable from a vacuum curve of lower intensity. The number of molecules scattered close to the beam must be but a small fraction of the total amount scattered, for no scattered atoms are found in this region, within the limits of detection. This result made it unnecessary to take the complete curve each time; in the later stages of the experiment only

the peak values of the gas and vacuum curves, and the pressure in the scattering chamber were measured.

To calculate the mean free paths of the atoms of the beam in the scattering gas, we write

$$P_1=e^{-s_1/\lambda_1}, \quad P_2=e^{-s_2/\lambda_2}\cdots, \tag{2}$$

where P_1, P_2, $\cdots$, etc. are the probabilities that the beam atom will pass through the regions s_1, s_2, $\cdots$, etc. without collision, and λ_1, λ_2, $\cdots$, etc. are the mean free paths. Since the mean free path is assumed to be inversely proportional to the pressure, we write

$$p\lambda=p_0\lambda_0, \tag{3}$$

where p_0 and λ_0 are constants, and p is the pressure. The probability that the atom will pass through all the regions s_1, $s_2\cdots$ etc. without collision is the product of the separate probabilities. We thus have

$$P=e^{-(1/p_0\lambda_0)\int p(s)ds}. \tag{4}$$

The scattering in the various regions is conveniently indicated in Table I. Eq. (4) may be put in a form more suitable for calculation.

$$p_0\lambda_0=0.275p/\log P^{-1}. \tag{5}$$

The mean free path λ_0 at any desired pressure p_0 may now be evaluated. P is the ratio of gas to vacuum intensities.

To test the assumption made in Eq. (3), P^{-1} was varied from 1.3 to 10, and over this large range, $p_0\lambda_0$ was constant within the experimental error. It is to be noted that where the higher pressures were employed no effect was apparent on the results in spite of the fact that the average beam atom made several collisions. Thus it is seen that once a beam atom experiences a collision, the chance it may have of striking the detector through one or more additional collisions is remote.

TABLE I. *Scattering in the various regions. (p is the pressure in the scattering chamber.)*

REGION	s (CM)	AVERAGE PRESSURE	$\int pds$	% OF TOTAL
scattering chamber	0.2	p	$0.2p$	73
channel	0.1	$p/2$	$0.05p$	18
cloud			$0.005p$	2
detecting chamber	4.0	$0.005p$	$0.02p$	7
		Total	$-0.275p$	

The results of this experiment may be expressed by giving the mean free path at some standard pressure. However, since unimportant factors such as the ratio of the masses and temperatures enter into this quantity, it is better to express the results in terms of an effective collision cross section $\pi\sigma_{AG}^2$. The number of collisions made per second by a beam atom with molecules of the scattering gas may be written[8]

$$\Theta=(\pi^{\frac{1}{2}}\nu_G\sigma_{AG}^2/h_Gm_Gc_A)\psi(c_A(h_Gm_G)^{\frac{1}{2}}),$$
$$h_G=1/2kT_G, \tag{6}$$

where the subscripts A refer to the beam atom, and the subscripts G to the scattering gas. ν is the number of molecules per cc, σ_{AG} the effective collision radius, k Boltzmann's constant, T the absolute temperature, m the molecular mass, c the molecular velocity and

$$\psi(x)=xe^{-x^2}+(2x^2+1)\int_0^x e^{-y^2}dy. \tag{7}$$

The mean free path of the atom in question is then c_A/Θ. Now the fraction of atoms striking the filament per second having speeds between c_A and c_A+dc_A is

$$f(c_A)=2(h_Am_A)^2c_A^3e^{-h_Am_Ac_A^2}dc_A. \tag{8}$$

If we average the mean free path over this distribution in the usual way, we secure for the average mean free path of the beam atoms in the scattering gas the following expression

$$\lambda_A=\frac{2}{\pi^{\frac{1}{2}}\nu_A\sigma_{AG}^2}\left(\frac{T_GM_A}{T_AM_G}\right)^2 \times\int_0^\infty \frac{x^5e^{-(T_GM_A/T_AM_G)x^2}dx}{\psi(x)} \tag{9}$$

and for the collision radius

$$\sigma_{AG}^2=\frac{3.30\times10^{-17}}{p_0\lambda_0}\alpha^2\int_0^\infty\varphi(x,\alpha)dx, \tag{10}$$

where $p_0\lambda_0$ is secured from the experimental measurements by means of Eq. (5), $\alpha=T_GM_A/T_AM_G$, and $\varphi(x,\alpha)$ is the integrand in Eq. (9). The

[8] Jeans, *Dynamical Theory of Gases*, third edition, p. 254.

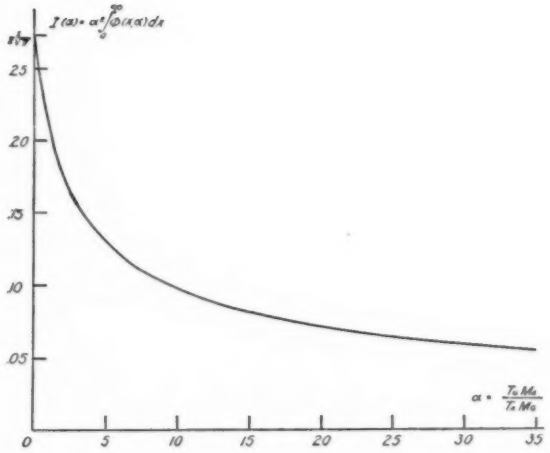

FIG. 5.

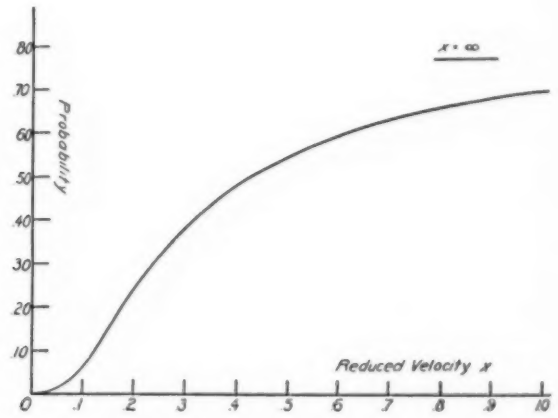

FIG. 6.

integral must be evaluated numerically; it is convenient to express it as a function of α (Eq. 10) and after evaluation at various points to plot it (Fig. 5). Inasmuch as the numerical calculations are somewhat laborious, the points are given in Table II
where

$$I(\alpha)=\alpha^2\int\varphi(x,\alpha)dx.$$

The computation of the σ_{AG}'s as outlined above is not strictly accurate. We computed the average mean free path from Eq. (9) and related this quantity to the experimental value P, the average probability that a beam atom will undergo no collision, by Eq. (5). While the latter relation is accurate for atoms of one velocity it is only an approximation for average values. A more valid procedure would be to average the probabilities.

The mean free path of a beam atom moving with velocity c_A is

$$\lambda_x=x^2/\pi^{\frac{1}{2}}\nu_G\sigma_{AG}{}^2\psi(x), \tag{11}$$

where

$$x=c_A(h_Gm_G)^{\frac{1}{2}}. \tag{12}$$

We average the probability

$$P_x=e^{-s/\lambda_x} \tag{13}$$

over the distribution

$$f(x)=2\alpha^2x^3e^{-\alpha x^2}dx,$$

which is identical with (8).

The average probability is, then,

$$P=2\alpha^2\int_0^\infty\exp\left[-\{s\pi^{\frac{1}{2}}\nu_G\sigma_{AG}{}^2/x^2\}\{xe^{-x^2}+(2x^2+1)\int_0^x e^{-y^2}dy\}-\alpha x^2\right]x^3dx. \tag{14}$$

Although more accurate, this equation is not as convenient to employ as Eq. (9) since the σ_{AG} occurs under the integral sign. Calculation shows, however, that the final results from the two methods are not appreciably different. If the σ_{AG} as found by (9) for a particular case be inserted into (13), a curve such as is shown in Fig. 6 is secured, where the probability that a beam atom will pass through the scattering gas without collision is plotted against its reduced velocity x. The upper curve in Fig. 7 is the distribution $x^3e^{-\alpha x^2}$ where the number of particles is plotted against the reduced velocity. The lower curve is the result of multiplying each of the ordinates in the upper curve by the corresponding ordinate in

TABLE II. *Values of $I(\alpha)$ for a number of values of α.*

α	$I(\alpha)$	α	$I(\alpha)$	α	$I(\alpha)$	α	$I(\alpha)$
0	$1/2\sqrt{\pi}$	0.545	0.236	3.0	0.155	10	0.094
0.05	0.275	0.8	0.221	4.0	0.140	15	0.0813
0.1	0.265	0.9	0.216	5.28	0.127	21	0.0714
0.2	0.256	1.0	0.211	7.0	0.113	25	0.0643
0.3	0.248	2.0	0.173	8.0	0.107	30	0.0589
						35	0 0548

TABLE III. *Product of mean free path and pressure, $p_0\lambda_0$ calculated from Eq. (5) (p_0 is in mm of mercury and λ_0 in cm).*

GAS	Li 860°K	Na 700°K	K 620°K	Rb 590°K	Cs 560°K
H_2	16.2×10^{-4}	8.30×10^{-4}	5.44×10^{-4}	4.24×10^{-4}	3.20×10^{-4}
D_2	18.6	8.74	5.85	4.65	3.65
He	22.6	12.52	8.32	6.50	4.89
Ne	22.5	10.94	7.77	6.65	5.41
A	11.4	5.90	4.22	3.75	3.34

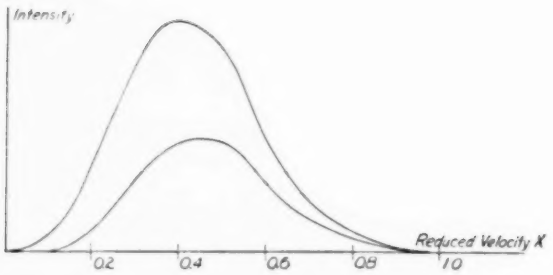

FIG. 7. Distribution of velocities in vacuum and gas beams.

Fig. 6. The upper curve gives the distribution of velocities in the vacuum beam, and the lower that in the scattered beam. Thus we see that after being scattered, the form of the original Maxwellian distribution is lost to some extent, containing a smaller proportion of low velocity atoms, and having the maximum of the distribution shifted somewhat towards the region of higher velocities. The results of previous experiments of this type may be open to the criticism that multiple scattering may have taken place, especially in the low velocity group. Owing to the low angular resolution employed by previous experimenters, the effect of multiple collisions is to give an apparent mean free path which is too large, and an effective collision radius too small.

The accuracy in the mean free path determination is estimated to be within four percent, as determined from variations in the experimental measurements. Using an apparatus with entirely different geometry, Mais obtains values of 7.20A, 6.91A, 8.74A and 11.3A* for the collision radius of potassium, respectively, with hydrogen, helium, neon and argon. Each of the first three are about 0.3–0.4A lower than the values appearing below (see Table IV), but this slight disagreement may be expected since improvement in geometry and confinement to smaller scattering angles would each tend to make the measured mean free path somewhat smaller, and collision radius larger. The precision in the σ_{AG} would be about two percent since the collision radius is proportional to the inverse square root of the mean free path; however, when $\alpha = T_G M_A / T_A M_G$ is large, the determination of σ_{AG} is very sensitive to α, and if the temperatures are not precisely known, some further error will be introduced. This corresponds to the scattering of Rb and Cs in H_2, D_2 and He and the error in σ_{AG} may be four percent. This factor is not so important in the remaining cases.

The mean free path-pressure product $p_0\lambda_0$ calculated from Eq. (5), where p_0 is in mm of mercury and λ_0 in cm, is given in Table III. The average temperature of the oven is given with each alkali; the scattering gases were all approximately at 10°C. It may be pointed out that the large increase found in the mean free path as we pass from the heavier to the lighter alkalis is to be ascribed chiefly to the increased velocity of the atoms of the latter. Furthermore, the variation of the mean free path with velocity of the beam atoms is greater in the lighter than in the heavier scattering gases (note especially the values under K, Rb and Cs); this is also predicted from the theory. The values given here for the mean free path should be useful to the molecular beam experimenter in estimating the pressures necessary for his experiment.

If we insert the values from Table III into Eq. (10), we secure the effective collision cross sections $\pi\sigma_{AG}^2$ and radii σ_{AG}. These are given in Table IV.

TABLE IV. *Values of effective collision cross sections and radii for the alkali atoms in various gases.*

GAS	LITHIUM		SODIUM		POTASSIUM		RUBIDIUM		CAESIUM	
	σ_{AG}	$\pi\sigma^2_{AG}$	σ_{AG}	$\pi\sigma^2_{AG}$	σ_{AG}	$\pi\sigma^2_{AG}$	σ_{AG}	$\pi\sigma^2_{AG}$	σ_{AG}	$\pi\sigma^2_{AG}$
H_2	6.21	122	7.01	154	7.47	175	7.38	171	7.54	179
D_2	6.32	125	7.62	182	8.54	228	8.24	213	8.34	219
He	5.82	106	6.44	130	7.25	165	6.96	152	7.18	162
Ne	6.18	120	8.24	213	9.10	259	9.23	268	9.56	287
A	9.83	303	11.3	401	13.6	580	13.5	572	13.5	572

The collision radii are expressed in Angstroms and the cross sections in square Angstroms.

DISCUSSION

The results of chief physical interest are given in Table IV. Comparison of the collision cross sections for H_2 and D_2 with the various alkalis shows D_2 to have a larger cross section in all cases except in collision with Li. In view of results[9] on the relative viscosity of H_2 and D_2, it

*The authors communicated with Dr. Mais concerning the large discrepancy in argon, and reconsideration of his original data established that this value should be raised to 13.0A.

[9] H. C. Torrey, Bull. Am. Phys. Soc., No. 1 (1935).

may be assumed that the molecular force fields are the same in both. The difference in collision cross section is therefore very likely connected with the excitation of rotational levels in the molecules. In D_2 the rotational levels are closer together, because of the larger mass.

Although the collision cross sections presented in Table IV are really lower limits, the absence of considerable small angle scattering in the region of a few minutes of arc, as shown by the fact that the beam is not appreciably broadened, implies that they are the real values such as would be obtained from an infinitely narrow beam and detector. The agreement with the results obtained by Mais with beams effectively four and a half times as broad confirms this conclusion. It is interesting in this connection to point out that classically with an attractive van der Waals force varying as r^{-5}, there would be approximately 70 percent of the total scattering above one minute of arc between one and ten minutes; and with an r^{-14} law, about 30 percent would be in this region. The absence of such scattering is, of course, in accord with the predictions of quantum theory.

We take this opportunity to thank Professor Urey and Dr. Christ of the Department of Chemistry for supplying the deuterium, Dr. Bleakney of Princeton for determining its purity on the mass spectrograph and Mr. Torrey and other members of the molecular beam laboratory for their able assistance when needed.

LETTERS TO THE EDITOR

Prompt publication of brief reports of important discoveries in physics may be secured by addressing them to this department. Closing dates for this department are, for the first issue of the month, the twentieth of the preceding month; for the second issue, the fifth of the month. The Board of Editors does not hold itself responsible for the opinions expressed by the correspondents.

The Magnetic Susceptibility of Molecular Hydrogen

The magnetic susceptibility of molecular hydrogen has been computed by Wang[1] and Van Vleck and Frank[2] using the wave function of Wang for the normal state of the hydrogen molecule, and also by Wick[3] using another simple wave function. Since then James and Coolidge[4] have obtained four new wave functions for the normal state of the hydrogen molecule, having, respectively, one, five, eleven and thirteen terms. The last three of these are much more accurate than those given by previous investigators. The writer is making calculations of the magnetic susceptibility of molecular hydrogen using the five and the eleven term functions of James and Coolidge and the following is a summary of the results obtained thus far.

For diatomic molecules in which the resulting electron spin and orbital angular momentum are zero the molar magnetic susceptibility χ_M is given by the formula[5]

$$\chi_M = -\frac{Le^2}{6mc^2}\Sigma\overline{r^2} + \tfrac{2}{3}L\sum_{n'\neq n}\frac{|m^0(n';n)|^2}{h\nu(n';n)}. \qquad (1)$$

Wang using his own wave function for the normal state of hydrogen found -4.71×10^{-6} for the value of the first term in formula (1). Van Vleck and Frank also using Wang's wave function evaluated the second term and obtained 0.51×10^{-6} which gives a final result of -4.20×10^{-6} for χ_M. Wang's wave function gives a value of the binding energy of 3.76 volts.

Wick, however, using another simple wave function obtained a value for the second term about one-ninth as great as that obtained by Van Vleck and Frank and a value for the molar susceptibility of -3.96×10^{-6}, which is in good agreement with the experimental values. But this calculation is open to the serious objection that the wave function used must be very poor, since it gives a value of the binding energy of only 2.91 electron volts. However, Wick's computation apparently leads to the conclusion that the second term is very sensitive to inaccuracies in the wave function used.

The writer has thus far evaluated the first term in formula (1) using wave functions of James and Coolidge.

TABLE I.

	BINDING ENERGY IN ELECTRON VOLTS	VALUE OF FIRST TERM IN FORMULA (1)
1 term function	2.56	-4.75×10^{-6}
5 term function	4.507	-4.02×10^{-6}
11 term function	4.682	-3.99×10^{-6}
13 term function	4.697	—
Observed	4.73 ± 0.04	—

The results are given in Table I which also gives the values of the binding energy obtained by James and Coolidge, in order to indicate the probable accuracy of the wave function. All calculations were checked. A comparison of the second and third columns in the table makes it appear probable that the true value of the first term in formula (1) differs only very slightly from the value given by the eleven term function.

The writer is now attempting to evaluate the second term in formula (1) for the five term function of James and Coolidge. According to Wick his value of the second term of formula (1) is in very much better accord with the experimental values of the magnetic moment of the rotating hydrogen molecule than Van Vleck's value. The value of the second term deduced from these experimental values of the magnetic moment of H_2 lies between 0.08×10^{-6} and 0.16×10^{-6}. If we may be permitted to combine this rather inexact value with the value of the first term given by the eleven term function we obtain the tentative result that χ_M for H_2 lies between -3.91×10^{-6} and -3.83×10^{-6}. The experimental values[6] for the molar susceptibilities of H_2 are -3.94×10^{-6} (Wills and Hector) and -3.99×10^{-6} (Soné). It seems probable therefore that the value of the second term calculated by Wick is of the right order of magnitude and that our calculation will yield a result in good agreement with the experimental values. In a future paper the writer will give a complete account of the calculation of both terms.

Honda and Hirone[7] noted that formula (1) does not take account of the paramagnetic contribution due to the thermal rotation of the molecules and therefore proceeded to evaluate this contribution to the molar susceptibility. Unfortunately it can easily be demonstrated that their work is vitiated by serious errors, since this contribution to χ_M in the case of H_2 could not exceed about 10^{-10} and is in fact negligible for all molecules.

ENOS E. WITMER

Randal Morgan Laboratory,
University of Pennsylvania,
June 21, 1935.

[1] S. C. Wang, Proc. Nat. Acad. Sci. **13**, 798 (1927); Phys. Rev. **31** 579 (1928).
[2] J. H. Van Vleck and A. Frank, Proc. Nat. Acad. Sci. **15**, 539 (1929).
[3] G. C. Wick, Zeits. f. Physik **85**, 25 (1933); Nuovo Cimento **10**, 118 (1933).
[4] H. M. James and A. S. Coolidge, J. Chem. Phys. **1**, 825 (1933); J. Chem. Phys. **3**, 129 (1935).
[5] J. H. Van Vleck, *Electric and Magnetic Susceptibilities*, p. 275.
[6] A. P. Wills and L. G. Hector, Phys. Rev. **23**, 209 (1924); L. G. Hector, ibid. **24**, 418 (1924); T. Soné, Phil. Mag. **39**, 305 (1920).
[7] K. Honda and T. Hirone, Zeits. f. Physik **84**, 208 (1933); cf. also E. C. Stoner, *Magnetism and Matter* (Metheun & Co., London, 1934), p. 277.

Near Ultraviolet Band Spectra of Iodine

The emission spectrum of iodine vapor was examined under high frequency electrodeless discharge conditions. At the minimum maintaining potential the "continuum" referred to as "3460" developed a marked maximum at λ3414. This group can be shown to be a P branch, with head at 3414 degrading to higher frequencies. $\tilde{\nu}=29{,}949+222.5\,M+28.42\,M^2+2.000\,M^3+0.0833\,M^4$ with $-J''=M=-1,\ -2$, etc.: $B'=125.42$, $B''=97.08$, $D'=0.5416$, $D''=0.4584$. Its upper level 44,893 cm^{-1} or 5.59 volts, is coincident with Sponer and Watson's rearranged Kimura and Mignishi ultraviolet bands λ2094−2511. Its lower level is coincident with 15,598.3 cm^{-1} state BO_u^+.

An adjacent band with maximum at 31,129 cm^{-1} (λ3211) was found to be a headless P branch, whose $\tilde{\nu}=31{,}760+208.83\,M+0.167\,M^3$, where $B'=B''=104.50$ and $D'=D''=0.0417$. It is proposed as a $1\rightarrow 0$ transition. Its R branch origin lies at or near 31,792 cm^{-1}. The maximum of the P branch coincides with its theoretical value. The low frequency end has a greater intensity than is expected from the rotational energy distribution in the upper state, if considered closely approximating thermal equilibrium. It was found to be the last band to disappear as the high frequency excitation potential is lowered.

Otto Stuhlman, Jr.

University of North Carolina,
Chapel Hill, N. C.,
July 15, 1935.

Scattering of High Speed Electrons of Varying Energy*

During recent years K. Lark-Horovitz and collaborators have carried out several investigations[1] on the determination of atom factors by electron diffraction. The experimental results have been compared with the theoretical expression derived from wave mechanics for the scattering of free electrons: in the first approximation the intensity of scattering as a function of $\sin\vartheta/\lambda$ is proportional to the electron form factor, E^2, given by

$$E^2=(Z-F)^2/[(\sin^4\theta/2)/\lambda^4]. \qquad (1)$$

This formula follows from the Born approximation of the wave-mechanical treatment of electron scattering as given by Bethe[2] and Mott.[3] In most cases the experimental results were in good agreement with the theoretical values derived from this formula. In the case of gold, the actual observed scattering appeared to differ from the one calculated by (1).

During a visit to this laboratory, Dr. H. A. Bethe, in a discussion of these results, pointed out that for heavy atoms the formula given above is not sufficient to calculate the scattering, but has to be replaced by the more accurate solution of the exact Schrödinger equation as given by Henneberg.[4] His investigation shows that the scattering power varies for different voltages and shows marked deviation from the simple formula, (1), with decreasing energy of the incoming electrons.

We have therefore investigated the atom factor of gold and silver at different voltages using the methods described previously.[1] The results are given in Figs. 1 and 2.

We have plotted E, in arbitrary units, as a function of $\sin\theta/\lambda$. The solid curve E_c, corrected for temperature, represents the values calculated from Eq. (1) using F, the x-ray atom factor, as calculated from the Thomas-Fermi distribution of electrons in the atoms. The observed values have been obtained from photographic intensity measurements and have been plotted (arbitrarily) so as to agree at large angles. Since only certain planes are reflecting, it is not possible to obtain the scattering for all angles but only for the Bragg angles under which the planes reflect.†

The curves show that the scattering power of the atom is not a monotonous function of the angle but shows maxima. The effect is particularly noticeable in the difference of the scattering between the (220) plane and the (311) plane. For the case of silver at a velocity of 42.5 kv, Henneberg has calculated the scattering as function

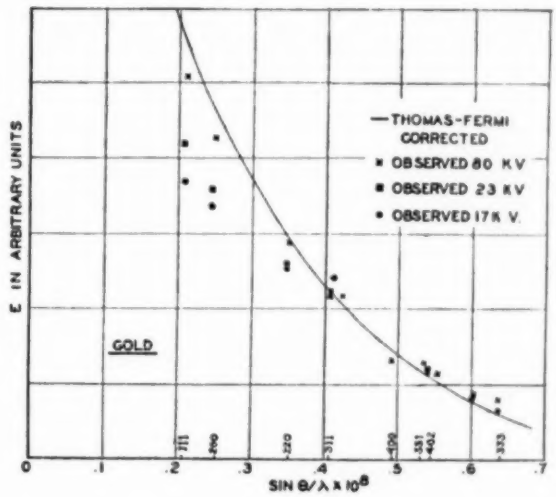

FIG. 1.

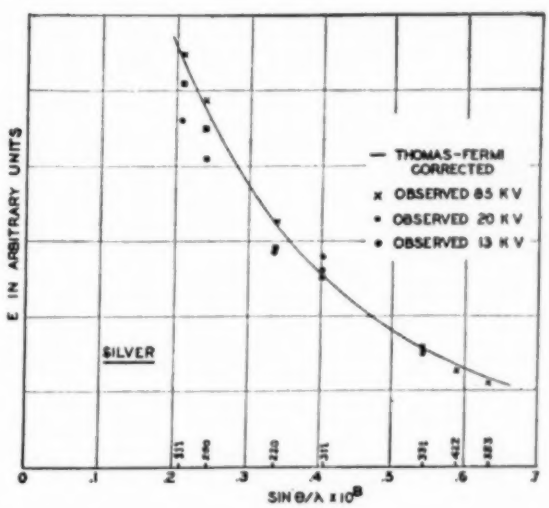

FIG. 2.

of angle. His values at this voltage already show a slight indication of the effect which we have observed much more pronounced at the still lower voltages.

It is of particular interest to note that a slight indication of the effect has been already observed by us for gold at 80 kv (the K excitation potential for gold being 80.5 kv). The effect is quite pronounced for silver at 20 kv (the K excitation potential for silver being 25.5 kv). Our results therefore show that in the calculation of the intensity in electron diffraction the solution of the exact wave equation has to be used taking into account the potential of the scattering atom. For energies great as compared with the K excitation potential the approximative formula (1) fits the experimental data.

The experiments are being continued with other materials so as to investigate more systematically the dependence of scattering upon the atomic number and are also being extended to still lower voltages. They will also be compared with values calculated from Henneberg's theory for the different scatterers and different electron energies.

We are indebted to Dr. Bethe for his suggestion and to Dr. Lark-Horovitz for his interest in this research and valuable discussions, and for the use of equipment made available by a grant-in-aid from the American Philosophical Society.

H. J. YEARIAN
J. D. HOWE

Department of Physics,
Purdue University,
July 29, 1935.

* Grateful acknowledgment is being made to the American Philosophical Society for a grant-in-aid of this research.

† Following the suggestion of K. Lark-Horovitz we are investigating now elements with lower crystal symmetry so as to obtain a greater number of reflecting angles.

[1] K. Lark-Horovitz, H. J. Yearian and J. D. Howe, Phys. Rev. **47**, 331 (1935); H. J. Yearian, Phys. Rev. **47**, 200 (1935); K. Lark-Horovitz, E. M. Purcell and H. J. Yearian, Phys. Rev. **45**, 123 (1934); K. Lark-Horovitz and H. J. Yearian, Phys. Rev. **43**, 376 (1933); K. Lark-Horovitz and H. J. Yearian, Phys. Rev. **42**, 905 (1932).
[2] H. A. Bethe, Ann. d. Physik **87**, 55 (1928).
[3] Mott, Proc. Roy. Soc. **A127**, 658 (1930).
[4] Henneberg, Zeits. f. Physik **83**, 555 (1933).

Evidence Against He^5

The expectation that He^5 should be stable, since apparently every other atomic weight in the entire range to 238 can be stable, seems still to be quite general, but a considerable body of evidence has accumulated against this view.

(1) The mass excesses of the light nuclei all fall very near (though certainly not quite on) two smooth curves, as Aston originally found (Fig. 1); curve A is for those nuclei in which the numbers of protons and nuclei are both even, and curve B for all others. (The figures are Bethe's, except that the masses of all circumnuclear electrons have been subtracted.) It is remarkable how nearly the mass excesses of all stable class B nuclei lie on one curve, however they are constituted, but the fact is evident; even though we have no explanation of it as yet, it would appear reasonable to expect He^5 to lie on the curve also; but if it did, it would certainly be violently unstable because of the

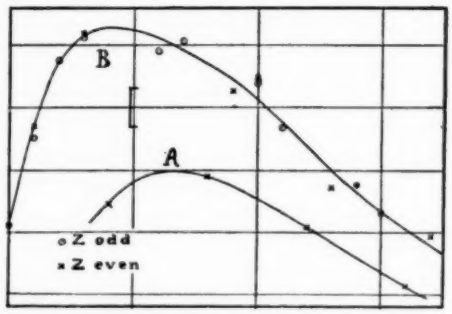

FIG. 1. Nuclear mass excess as a function of mass.

great difference between the ordinates of curves A and B in this region. The result is not much different if we confine ourselves to nuclei of the type $A=4N+1$, $Z=2N$, $(N=0, 1, \ldots)$.

(2) Since the mass excess of He^4+n is 10.77 ± 0.7, He^5 cannot be above 10.8 ± 0.7 itself; and even if we take 12.0 for its mass excess (it can scarcely be more), at least 3 nuclear reactions which ought to have produced it with appreciable energy have been studied among the lightest elements, and no He^5 was noticed. They are as follows: $Li^6.H^2\rightarrow He^5.He^3+0.3$; $Li^7.H^2\rightarrow He^5.He^4+14.7$; $B^{11}.H^2\rightarrow Be^8.He^5+5.6$. In addition the following reactions might be expected to produce it with small energy: $He^4.n\rightarrow He^5$; $He^4.H^1\rightarrow He^5.p$; $Li^6.n\rightarrow He^5.H^2$; $Li^7.n\rightarrow He^5.H^3$; $Be^9.n\rightarrow 2He^5$; $Be^9.H^2\rightarrow Li^6.He^5$; $B^{10}.H^2\rightarrow Li^7.He^5.p$; $N^{14}.H^2\rightarrow B^{11}.He^5.p$. Some of these might well be endothermic, but some at least would show if He^5 has a mass excess of 10 or less. The $He^4.n$ reaction could occur in all regular neutron-sources, if at all.

(3) In addition to the upper limit for He^5 there is a lower limit, derived from the condition that Be^9 must be stable against $He^5.He^4$, and not merely against $2He^4.n$. If we take the mass of Be^9 from the six concordant reactions listed by Bonner and Brubaker[1] we obtain for its mass excess (after deducting the extranuclear electrons) the value 11.4 ± 0.3; if we subtract the mass excess of He^4, 2.3, we find 9.0 ± 0.5 for the lower limit for He^5. There seems no very good reason to expect He^5 to hit the rather narrow range between these two limits; at least, if it does, it will not fit well onto any curve at all. Thus the evidence seems against the possibility that He^5 should be capable of existence. Since Li^5 is even less likely (it would contain more protons than neutrons), progressive synthesis from He upwards under stellar conditions apparently can occur only with the help of H^2 or H^3. The great abundance of He in the stars is thus no longer a special source of difficulty on nuclear grounds.

R. D'E. ATKINSON

Physics Department,
Rutgers University,
June 28, 1935.

[1] Bonner and Brubaker, Phys. Rev. **47**, 913 (1935).

The Intermediate Ion of the Atmosphere

In addition to the small and the large or Langevin ion in the atmosphere, there was discovered in 1909, by Pollock[1] of the University of Sydney, an ion having a mobility intermediate between that of the small ion and that of the large ion. His investigations disclosed the fact that the mean mobility of this group of ions diminishes with increasing vapor pressure of the atmosphere. He also obtained results which he interpreted as indicating that the intermediate ion consists of water vapor surrounding a solid rigid nucleus and which condenses into a liquid drop forming the large ion when the vapor-pressure reaches a certain critical value (about 15 mm) which is less than that required for saturation at the usual temperatures in summer. Additional information regarding these ions was secured by Schachl,[2] when he found that at times of Böen their number was greatly increased. Schachl interpreted this to mean that the ion was formed through the Lenard effect. Additional information regarding this ion has been secured at the Department of Terrestrial Magnetism, Carnegie Institution of Washington. These results, which will be published in detail in the *Journal of Terrestrial Magnetism and Atmospheric Electricity*, may be summarized as follows:

(1) Contrary to the findings of Pollock, intermediate ions do not diminish at any vapor pressure to form large ions through condensation of water vapor and therefore, no critical vapor pressure exists.

(2) The mobility of the intermediate ion is found to decrease with an increase in vapor pressure in strict accord with Blanc's law, just as in the case of the small ion in a gas. The mobility at zero millimeters vapor pressure is 0.5 cm per sec. per volt per cm and at 30 mm pressure is approximately a tenth of this. This result furnishes information concerning the nature of the intermediate ion.

(3) The number of intermediate ions in the atmosphere undergoes a diurnal variation, similar in character to that for the large ions and more or less opposite in character to that for the small ions of the atmosphere. Evidence indicates that the intermediate ion secures its charge from the small ion through combination with it.

(4) A value for the recombination coefficient for the intermediate ion has, for the first time, been determined, following a method which avoids an error that has occurred[3] in some of the determinations of the recombination coefficient for small ions. The value determined for the intermediate ion coefficient is 7.1×10^{-7} (a value roughly one-half that for the small ion).

(5) The intermediate ions are especially numerous during times of thunderstorms, as pointed out by Schachl, but not as a consequence of the Lenard effect. The number increases at the beginning of the storm, this increase shows a close correspondence to the increase in small ion production recently observed.[4] After the close of the storm their number gradually decreases, the decrease also having a close correspondence to the decrease in production of small ions found to occur at such times. Furthermore, the change in number of intermediate ions is associated with a change in number of small ions present rather than with the operation of the Lenard effect.

(6) As indicated under (3) above, the diurnal variation in the number of intermediate ions is opposite in character to that of the small ions, while under (5) above, it was pointed out that the number of intermediate ions increased with an increase in the number of small ions. Considering the large value found for the intermediate ion recombination coefficient, this apparent paradox is explicable with the assumption that the combination coefficient between small ions and intermediate ions is large compared with that between small ions and uncharged intermediate ion particles.

(7) The mobility spectrum for the intermediate ion appears to be a narrow band and under normal conditions, practically no ions having mobilities between that of the intermediate ion and that of the large ion was found.

(8) In small ion work, it is not customary to differentiate between small and intermediate ions, a portion of the latter being included in the count of the former. As a result, this inclusion, judged from the present results, introduces persistent errors ranging from 10 to 30 percent in small ion counts.

It is worthy of mention that the behavior of intermediate ions seems to introduce certain difficulties. According to present theory, the large ion consists of a condensation nucleus with an electric charge. It has been suggested that condensation nuclei are hygroscopic in character. Because of the similarity between the diurnal variation curves for the large and the intermediate ions as well as a similarity in their daily variation, the intermediate ion particle also might be expected to be hygroscopic. In this case the mobility of the intermediate ion would vary with the relative humidity rather than with the vapor pressure. However, the evidence indicates that the variation is in response to a variation in vapor pressure rather than to a variation in the relative humidity.

G. R. Wait

Department of Terrestrial Magnetism,
Carnegie Institution of Washington,
July 9, 1935.

[1] Pollock, Phil. Mag. **29**, 636 (1915).
[2] Schachl, Beitr. Geophysik. **38**, 202 (1933).
[3] L. B. Loeb, Trans. Am. Electrochem. Soc. **55**, 131 (1929).
[4] G. R. Wait and A. G. McNish, Mon. Weath. Rev. **62**, 1 (1934).

Absorption of Slow Neutrons in Silver

Fermi and his collaborators[1] have measured the absorption of slow neutrons in a variety of elements, using as a detector of the neutrons usually rhodium, and sometimes silver. Wide differences in absorption are found among the various elements tested, and the removal of neutrons from the beam by absorbing layers has been shown to be due to the mechanisms of capture (with emission of a gamma-ray or of a heavy particle) and elastic scattering. Of these two mechanisms, the first seems to be predominantly important in those elements exhibiting the largest cross sections for slow neutrons.[2]

It seemed desirable to measure the absorption of neutrons in a single element, using a variety of detectors, and this letter is a preliminary report of investigations of that sort. While this work was in progress, other investigators

TABLE I. *Absorption of slow neutrons in silver as measured by different detectors.*

SOURCE OF NEUTRONS	DETECTOR Element	Thickness (g/cm²)	PERCENT ACTIVITY (TRANSMISSION) WITH ABSORBER OF 0 g/cm² Ag	0.46 g/cm² Ag	0.81 g/cm² Ag	1.72 g/cm² Ag
B-Rn	Silver	1.195	100	60±1	42±3	26±4
Be-Rn	Silver	1.195	100	59±1	44±1	27±1
Be-Rn	Silver	0.094	100	46±4	30±1	17±2
Be-Rn	Copper	0.717	100	42±2	28±3	12±2
Be-Rn	Vanadium (as NH_4VO_3)	0.146	100	47±2	35±1	17±2
Be-Rn	Bromine (as NH_4Br)	0.305	100	62±1	56±1	38±1
Be-Rn	Iodine (as CH_3I)	0.143	100	57±2	48±1	36±2

have noted[3] that the cross section measured for an absorber depends strongly on the reaction whereby the slow neutrons are detected.

The geometrical conditions under which the irradiation of samples was conducted is shown in Fig. 1. The detectors of slow neutrons were disks 5 cm in diameter, the absorbers disks 7 cm in diameter. The Ag and Cu detectors were metal sheets; the I, Br and V detectors consisted of compounds (cf. Table I) held on stiff paper with thin collodion. The source of neutrons was beryllium (or boron) and radon in amounts usually between 100 and 200 millicuries. The activity of the detectors after irradiation was measured with a quartz-fiber electroscope of the Lauritsen type, provided with a window of thin aluminum. The procedure was to irradiate the detector, either bare or between two equal layers of an absorber, for a length of time standard for that detector, then to commence readings one minute after the removal of the detector from the neutron source. The reading was terminated at a time, also standard for for each detector, depending on the half-life of the activity under measurement. In Br, for example, the irradiation lasted for twenty-five minutes, and the measurement for fifteen minutes, so that only the short-lived activity was measured in these experiments. Frequent readings on the background were taken in precisely the way the measurements were made, except that the detector had not been exposed to the neutron source. The activities found were in all cases easily measurable, being from twice to about twenty-five times the background due to cosmic and local radiations.

The results are shown in Table I. The absorber was in all cases silver, and the numbers in the table under the heading Percent Activity are referred in each case to the no-absorber value for that detector as 100 percent, so that they are measures of the transmission through the absorber of neutrons having the proper energy to activate the detector.

It is known that the absorption curves obtained with such an arrangement of paraffin as was used in the present experiment are not exponential, but that the absorption decreases with increasing thickness of absorber;[1] this would seem to be the reason for the quite large difference shown in the table between the absorption measured in silver with a thin and with a thick silver detector. So long as the absorption of neutrons in the thickness of the detector can be neglected, this effect will not complicate

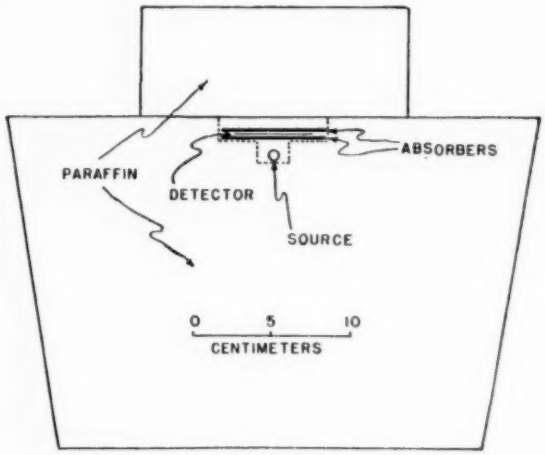

FIG. 1.

the results, and the other detectors are apparently thin enough, relative to the half-value thickness of each for slow neutron absorption,[1] so that the results obtained with them may be intercompared, and compared with those for the thin silver detector. None of the detectors employed in the present experiment has a half-value thickness of silver as large as that (1.2 g/cm²) given by Fermi for a Rh detector, but his value cannot properly be compared with the present ones because of the differences which may have been introduced by detector thickness and the disposition of paraffin about the source and detector.

The differences between Br, I and the other detectors employed in the present experiment seem necessarily to be due to the fact that neutrons captured by different detectors lie in different ranges of energy. The sense of the differences among the detectors in the energy range of neutrons most likely to be captured by each cannot be determined from these results alone, but the experiment of Moon and Tillman[3] seems to show that the neutrons activating iodine have higher energies than those activating silver, so that presumably Br is activated by faster neutrons still.

Independent experiments showed that the effect of elastic scattering of slow neutrons in the silver was not comparable with neutron capture, so that substantially all the observed absorption is due to the latter phenomenon.

We are indebted to Dr. Clyde K. Emery and the Cedars of Lebanon Hospital for their kindness in providing us with the necessary radon; to Professor C. C. Lauritsen for helpful discussions; and to Mr. K. Watanabe for assistance in taking the readings.

LOUIS N. RIDENOUR
DON M. YOST

W. K. Kellogg Radiation Laboratory
and Gates Chemical Laboratory,
California Institute of Technology,
July 29, 1935.

[1] Amaldi, D'Agostino, Fermi, Pontecorvo, Rasetti, Segrè, Proc. Roy. Soc. **A149**, 522 (1935).
[2] Dunning, Pegram, Fink and Mitchell, Phys. Rev. **47**, 970 (1935).
[3] Moon and Tillman, Nature **135**, 904 (1035); Bjerge and Westcott, Proc. Roy. Soc. **A150**, 709 (1935); Artsimovitch, Kourtschatov, Miccovskii and Palibin, Comptes rendus **200**, 2159 (1935).

THE AMERICAN INSTITUTE OF PHYSICS

INCORPORATED

GOVERNING BOARD

For The American Physical Society:

KARL T. COMPTON, *Chairman*
Massachusetts Institute of Technology

GEORGE B. PEGRAM, *Secretary*
Columbia University

JOHN T. TATE
University of Minnesota

For The Optical Society of America:

E. C. CRITTENDEN
Bureau of Standards

PAUL D. FOOTE
The Gulf Companies

F. K. RICHTMYER
Cornell University

For The Acoustical Society of America:

HARVEY FLETCHER
Bell Telephone Laboratories

VERN O. KNUDSEN
University of California at Los Angeles

WALLACE WATERFALL
The Celotex Company

For The Society of Rheology:

E. C. BINGHAM
Lafayette College

A. STUART HUNTER
du Pont Rayon Company

S. E. SHEPPARD
Eastman Kodak Company

For The American Association of Physics Teachers:

HOMER L. DODGE
University of Oklahoma

PAUL E. KLOPSTEG
Central Scientific Company

FREDERIC PALMER
Haverford College

ADMINISTRATIVE STAFF

HENRY A. BARTON, *Director* JOHN T. TATE, *Adviser on Publications*

MADELINE M. MITCHELL, *Editorial Secretary*

Office: 11 East 38th Street, New York, New York

JOURNALS

THE PHYSICAL REVIEW

REVIEWS OF MODERN PHYSICS

PHYSICS
JOHN T. TATE, *Editor*
J. W. BUCHTA, *Assistant Editor*
E. C. BINGHAM, *Rheology Editor*

THE JOURNAL OF THE OPTICAL SOCIETY OF AMERICA

THE REVIEW OF SCIENTIFIC INSTRUMENTS
WITH PHYSICS NEWS AND VIEWS
F. K. RICHTMYER, *Editor*

JOURNAL OF THE ACOUSTICAL SOCIETY OF AMERICA
F. R. WATSON, *Editor*

THE JOURNAL OF CHEMICAL PHYSICS
HAROLD C. UREY, *Editor*

THE AMERICAN PHYSICS TEACHER
DUANE ROLLER, *Editor*

The American Institute of Physics is a membership corporation of which five societies are the founding members. These five societies are the principal national societies devoted to pure and applied physics in America. Their names, and those of their representatives who form the Governing Board of the Institute, are given above. The principal work of the Institute is the publication of journals sponsored by the societies or by itself. The names and the editors of the journals are also listed above.

The broad purpose of the Institute is to represent, in all matters of wide or common interest, the five thousand or more members and subscribers associated with the Founder Societies and the journals. It aims to advance the science and profession of physics, and to promote cooperation between pure research, the applied sciences and the industries. To achieve these aims, it is greatly in need of an endowment and is empowered by law to administer grants and funds of any kind.

CONTENTS

PHYS. REV. 48 (1935) AUGUST 15

Progress of the Directional Survey of Cosmic-Ray Intensities and Its Application to the Analysis of the Primary Cosmic Radiation. . . . . THOMAS H. JOHNSON 287

Infrared Absorption Spectrum of Solid Hydrogen Chloride. PAUL E. SHEARIN 299

Inelastic Scattering of Quanta with Production of Pairs . . . . . MILTON S. PLESSET AND JOHN A. WHEELER 302

Carbon Radioactivity and Other Resonance Transmutations by Protons . . . . . L. R. HAFSTAD AND M. A. TUVE 306

High Voltage Technique for Nuclear Physics Studies . . . . . M. A. TUVE, L. R. HAFSTAD AND O. DAHL 315

Extension of the Rh I-Like Isoelectronic Sequence to the Spectrum of Ag III . . . . . W. P. GILBERT 338

Band Spectrum of Pb_2 in Absorption and Emission . . . E. N. SHAWHAN 343

Four Vector Problem and Its Application to Energies and Intensities in Platinum-Like Spectra . . . . . A. T. GOBLE 346

New Energy Levels in Au II, Hg III, Tl IV, Pb V and Bi VI. . . . . J. E. MACK AND M. FROMER 357

On the Cross Section of Heavy Nuclei for Slow Neutrons. J. H. VAN VLECK 367

Effective Collision Cross Sections of the Alkali Atoms in Various Gases. . . . . SEYMOUR ROSIN AND I. I. RABI 373

Letters to the Editor:

Magnetic Susceptibility of Molecular Hydrogen . . . . ENOS E. WITMER 380

Near Ultraviolet Band Spectra of Iodine . . . . . OTTO STUHLMAN, JR. 381

Scattering of High Speed Electrons of Varying Energy . . . . . H. J. YEARIAN AND J. D. HOWE 381

Evidence Against He^4 . . . . . R. D'E. ATKINSON 382

Intermediate Ion of the Atmosphere . . . . . G. R. WAIT 383

Absorption of Slow Neutrons in Silver . LOUIS N. RIDENOUR AND DON M. YOST 383

LANCASTER PRESS INC., LANCASTER, PA.